TARGET-TRIGGERED NANOPARTICLES FOR TUMOR DIAGNOSIS AND THERAPY

EDITED BY: Yi Hou, Jing Hao, Xiaoling Wei and Yunfeng Yan
PUBLISHED IN: Frontiers in Chemistry

frontiers Research Topics

ISSN 1664-8714
ISBN 978-2-88966-855-7
DOI 10.3389/978-2-88966-855-7

About Frontiers

Frontiers is more than just an open-access publisher of scholarly articles: it is a pioneering approach to the world of academia, radically improving the way scholarly research is managed. The grand vision of Frontiers is a world where all people have an equal opportunity to seek, share and generate knowledge. Frontiers provides immediate and permanent online open access to all its publications, but this alone is not enough to realize our grand goals.

Frontiers Journal Series

The Frontiers Journal Series is a multi-tier and interdisciplinary set of open-access, online journals, promising a paradigm shift from the current review, selection and dissemination processes in academic publishing. All Frontiers journals are driven by researchers for researchers; therefore, they constitute a service to the scholarly community. At the same time, the Frontiers Journal Series operates on a revolutionary invention, the tiered publishing system, initially addressing specific communities of scholars, and gradually climbing up to broader public understanding, thus serving the interests of the lay society, too.

Dedication to Quality

Each Frontiers article is a landmark of the highest quality, thanks to genuinely collaborative interactions between authors and review editors, who include some of the world's best academicians. Research must be certified by peers before entering a stream of knowledge that may eventually reach the public - and shape society; therefore, Frontiers only applies the most rigorous and unbiased reviews. Frontiers revolutionizes research publishing by freely delivering the most outstanding research, evaluated with no bias from both the academic and social point of view. By applying the most advanced information technologies, Frontiers is catapulting scholarly publishing into a new generation.

What are Frontiers Research Topics?

Frontiers Research Topics are very popular trademarks of the Frontiers Journals Series: they are collections of at least ten articles, all centered on a particular subject. With their unique mix of varied contributions from Original Research to Review Articles, Frontiers Research Topics unify the most influential researchers, the latest key findings and historical advances in a hot research area! Find out more on how to host your own Frontiers Research Topic or contribute to one as an author by contacting the Frontiers Editorial Office: frontiersin.org/about/contact

TARGET-TRIGGERED NANOPARTICLES FOR TUMOR DIAGNOSIS AND THERAPY

Topic Editors:
Yi Hou, Beijing University of Chemical Technology, China
Jing Hao, George Fox University Newberg, United States
Xiaoling Wei, Shanghai Institute of Microsystem and Information Technology (CAS), China
Yunfeng Yan, Zhejiang University of Technology, China

Citation: Hou, Y., Hao, J., Wei, X., Yan, Y., eds. (2021). Target-Triggered Nanoparticles for Tumor Diagnosis and Therapy. Lausanne: Frontiers Media SA. doi: 10.3389/978-2-88966-855-7

Table of Contents

frontiers in Chemistry

EDITORIAL
published: 12 April 2021
doi: 10.3389/fchem.2021.657782

Editorial: Target-Triggered Nanoparticles for Tumor Diagnosis and Therapy

Yi Hou[1]*, *Xiaoling Wei*[2,3]*, *Yunfeng Yan*[4]* and *Jing Hao*[5]*

[1]College of Life Science and Technology, Beijing University of Chemical Technology, Beijing, China, [2]Shanghai Institute of Microsystem and Information Technology, Chinese Academy of Sciences, Shanghai, China, [3]University of Chinese Academy of Sciences, Beijing, China, [4]College of Biotechnology and Bioengineering, Zhejiang University of Technology, Hangzhou, China, [5]Department of Chemistry, George Fox University, Newberg, OR, United States

Keywords: cancer theranostics, Molecular imaging, drug delivery, precision medicine, activatable nanomedicine

Editorial on the Research Topic

Target-Triggered Nanoparticles for Tumor Diagnosis and Therapy

Cancer is one of the major diseases which seriously jeopardizes the human health and life; however, there remains a lack of effective methods for early diagnosis, metastasis warning, clinical efficacy prediction, and effective treatment. Precision medicine has been heralded to bring more strategies to improve the diagnostics sensitivity and treatment efficacy of malignant tumor (Omidi, 2011; Kelkar and Reineke, 2011).

The risk of cancer is related to its malignant behaviors, including proliferation, invasion, and metastasis, which are closely associated with variations in physiological parameters, such as hypoxia, low extracellular pH, enzyme, and reducing conditions (Ma et al., 2018). These tumor-associated physiological parameters are not merely hallmarks for distinct cancer, they could also serve as targets for constructing tumor-specific medicines, especially as trigger to activate the imaging probes or antitumor drugs (Gao et al., 2017; Janib et al., 2010). In the first 2 decades of this century, many efforts have been made to develop novel theranostic reagents, and fruitful achievements have been reported (Zhang et al., 2019; Gu et al., 2019). Among these candidates, the functional nanoparticle-based drugs are considered to be promising tumor theranostic reagents because their large specific surface area offers a big room to modified functional moieties, which could respond to the stimulus in tumor microenvironments (Gao et al., 2016). The aim of this topic was to report the latest achievements in the designs of "smart" nanomedicine responding to the tumor microenvironment-related features, in order to improve the tumor imaging diagnosis and therapy.

Monitoring the tumor-associated microenvironmental physiological parameters and clarifying their relationship are critical both for tumor diagnostics and therapeutic administrations. Therefore, Hou et al. have reviewed the recent achievements in target-triggered nanoprobes for tumor theranostics, including the preparation strategies, response mechanisms, and theranostic applications of the state-of-the art activable theranostic nanoprobe. The target-triggered tumor theranostic nanoprobes have successfully associated various imaging modalities with distinct treatment approaches of tumor, including chemotherapy, chemodynamic therapy, gene therapy, immunotherapy, and physical therapy. Owing to the integration of both diagnosis and treatment of cancer, these nanoprobes are obviously superior to the conventional probes. Thus, the target-triggered nanoprobes exhibit powerful abilities to not only monitor and trace the *in vivo* behavior of themselves but also give an immediate feedback on the treatment outcome without time consumption, thereby evaluating the prognosis in real time.

The target-triggered nanoparticles have also been considered as promising delivery systems, which could realize the targeted delivery of antitumor drugs, reduced systemic toxicity, and

Edited and reviewed by:
Nasir Mahmood,
RMIT University, Australia

***Correspondence:**
Yi Hou
houyi@iccas.ac.cn
Xiaoling Wei
xlwei-jerry@mail.sim.ac.cn
Yunfeng Yan
yfyan@zjut.edu.cn
Jing Hao
jhao@georgefox.edu

Specialty section:
This article was submitted to Nanoscience, a section of the journal Frontiers in Chemistry

Received: *24 January 2021*
Accepted: *08 February 2021*
Published: *12 April 2021*

Citation:
Hou Y, Wei X, Yan Y and Hao J (2021) Editorial: Target-Triggered Nanoparticles for Tumor Diagnosis and Therapy. Front. Chem. 9:657782. doi: 10.3389/fchem.2021.657782

improved therapeutic effect. Various stimuli-responsive carriers have been developed for tumor therapeutics; among them, the enzyme-activated nanoparticles are considered as one of the most promising smart stimulus-responsive nanocarriers because the changes in the expression of specific enzymes, such as proteases, phosphatases, and glycosidases, have been observed in tumor or inflammatory regions, which can be exploited to achieve targeted accumulation of drugs at the desired biological location *via* enzyme-mediated drug release. Li et al. have reviewed the significant progress in the enzyme-responsive nanoparticles for antitumor drug delivery in the past years. They have summarized the general mechanism for controlling drug release from the enzyme-responsive carriers and highlighted the state of the art in drug delivery and disease diagnosis systems based on enzyme-responsive nanoparticles, which are organized based on different installation sites of specific enzyme bioactive functionalities on nanoparticles.

Besides enzyme, the concentrated redox species, such as glutathione (GSH), is another common phenomenon in a majority of solid tumors. Pang et al. have developed integrated nanocarriers containing FA ligands and ditelluride bonds for active tumor-targeting and GSH-responsive drug release. They synthesized a folic acid (FA)-modified PEGylated polycaprolactone (PEG-PCL) containing ditelluride linkage through a facile coupling reaction. And then, the hydrophobic doxorubicin (DOX) can be encapsulated into the polymeric micelles (F-TeNP$_{DOX}$) *via* self-assembly in aqueous solution. The nanomedicine could target tumor cells, and be efficiently internalized into the cells through FA-mediated endocytosis and achieve sufficient "active-drug" content after redox-responsive micelle dissociation.

Wang et al. introduced a redox-triggered dual-targeted liposome, CEP-LP@S/D, capable of co-delivering DOX and salinomycin (Sal) for the synergistic treatment of liver cancer. They designed CD133, and EpCAM dual-targeted Y-shaped peptide ligand, CEP, and decorated the surface of this liposome with the peptide, in order to improve both recognition and binding to cancer stem cell (CSC) subpopulations, which is believed to be associated with high chemoresistance and recurrence rates in hepatocellular carcinoma (HCC). Moreover, they endowed the CEP-LP@S/D with GSH-responsive properties to initiate anticancer drug release. The *in vitro* and *in vivo* studies indicate that their GSH-responsive co-delivery system could not only effectively enhance CSC targeting but also eliminate the non-CSC faction, thereby exhibiting high antitumor efficacy.

The external stimulus, such as photothermal effect, is considered to be employed to design precise nanomedicines. Wang et al. have developed a dual-functional micellar drug delivery system based on thermosensitive poly(N-isopropylacrylamide) (PNIPAM), poly(d,l-lactide)-poly (ethylene glycol) (PLA-PEG), and gold nanorods (GNRs). The heat generated by the GNRs under near-infrared light irradiation induces shrinking of the PNIPAM, which in turn will promote drug release and achievement of higher local drug concentration at the tumor site, leading to potent *in vivo* tumor inhibitory activity.

Photodynamic therapy (PDT) has become an alternative approach to treat tumors through reactive oxygen species (ROS) produced by the activated photosensitizers (PS). Liu et al. have reviewed the nanoparticles which could respond to tumor-associated microenvironments, mainly including pH, redox species, enzymes, and hypoxia, and highlight the applications of these smart nanomaterials as targeted delivery carriers of PS in photodynamic anticancer therapy, to further boost the development of PDT in tumor therapy.

This research topic introduces the state of the art in target-triggered tumor theranostic nanoprobes. The fruitful achievements have been gained, which exhibit great potential not only in tumor theranostics but also in other serious diseases such as Alzheimer's disease and stroke.

AUTHOR CONTRIBUTIONS

YH, XW, YY, and JH discussed and wrote the Editorial together.

REFERENCES

Omidi, Y. (2011). Smart multifunctional theranostics: simultaneous diagnosis and therapy of cancer. *Bioimpacts* 1 (3), 145–147. doi:10.5681/bi.2011.019

Kelkar, S. S., and Reineke, T. M. (2011). Theranostics: combining imaging and therapy. *Bioconjugate Chem.* 22 (10), 1879–1903. doi:10.1021/bc200151q

Ma, T., Zhang, P., Hou, Y., Ning, H., Wang, Z., Huang, J., et al. (2018). "Smart" nanoprobes for visualization of tumor microenvironments. *Adv. Health. Mater.* 7 (20), 1800391. doi:10.1002/adhm.201800391

Gao, Z., Hou, Y., Zeng, J., Chen, L., Liu, C., Yang, W., et al. (2017). Tumor Microenvironment-Triggered Aggregation of Antiphagocytosis 99mTc-Labeled Fe_3O_4 nanoprobes for enhanced tumor imaging in vivo. *Adv. Mater.* 29 (24), 1701095. doi:10.1002/adma.201701095

Janib, S. M., Moses, A. S., and MacKay, J. A. (2010). Imaging and drug delivery using theranostic nanoparticles. *Adv. Drug Deliv. Rev.* 62 (11), 1052–1063. doi:10.1016/j.addr.2010.08.004

Zhang, P., Hou, Y., Zeng, J., Li, Y., Wang, Z., Zhu, R., et al. (2019). Coordinatively unsaturated Fe3+ based activatable probes for enhanced MRI and therapy of tumors. *Angew. Chem. Int. Ed.* 58 (32), 11088–11096. doi:10.1002/anie.201904880

Gu, Z., Zhu, S., Yan, L., Zhao, F., and Zhao, Y. (2019). Graphene-based smart platforms for combined cancer therapy. *Adv. Mater.* 31 (9), 1800662. doi:10.1002/adma.201800662

Gao, Z., Ma, T., Zhao, E., Docter, D., Yang, W., Stauber, R. H., et al. (2016). Small is smarter: nano MRI contrast agents–advantages and recent achievements. *Small* 12 (5), 556–576. doi:10.1002/smll.201502309

Conflict of Interest: The authors declare that the research was conducted in the absence of any commercial or financial relationships that could be construed as a potential conflict of interest.

frontiers in Chemistry

ORIGINAL RESEARCH
published: 28 February 2020
doi: 10.3389/fchem.2020.00156

Ditelluride-Bridged PEG-PCL Copolymer as Folic Acid-Targeted and Redox-Responsive Nanoparticles for Enhanced Cancer Therapy

Zekun Pang†, *Jiayan Zhou*† *and Chunyang Sun**

Department of Radiology and Tianjin Key Laboratory of Functional Imaging, Tianjin Medical University General Hospital, Tianjin, China

The development of the nanosized delivery systems with targeting navigation and efficient cargo release for cancer therapy has attracted great attention in recent years. Herein, a folic acid (FA) modified PEGylated polycaprolactone containing ditelluride linkage was synthesized through a facile coupling reaction. The hydrophobic doxorubicin (DOX) can be encapsulated into the polymeric micelles, and such nanoparticles (F-TeNP$_{DOX}$) exhibited redox-responsive drug release under abundant glutathione (GSH) condition due to the degradation of ditelluride bonds. In addition, flow cytometric analyses showed that the FA ligands on F-TeNP$_{DOX}$ could facilitate their cellular uptake in 4T1 breast cancer cells. Therefore, F-TeNP$_{DOX}$ led to the promoted drug accumulation and enhanced growth inhibition on 4T1 tumor *in vivo*. The obtained results suggest F-TeNP$_{DOX}$ excellent potential as nanocarriers for anticancer drug delivery.

Keywords: ditelluride linkage, redox responsive, targeted nanoparticle, drug delivery, cancer therapy

OPEN ACCESS

Edited by:
Yi Hou,
Beijing University of Technology, China

Reviewed by:
Ning Zhenbo,
Beijing University of Chemical Technology, China
Xianzhu Yang,
South China University of Technology, China

***Correspondence:**
Chunyang Sun
chysunshine@gmail.com

†*These authors have contributed equally to this work*

Specialty section:
This article was submitted to Nanoscience, a section of the journal Frontiers in Chemistry

Received: *19 January 2020*
Accepted: *20 February 2020*
Published: *28 February 2020*

Citation:
Pang Z, Zhou J and Sun C (2020) Ditelluride-Bridged PEG-PCL Copolymer as Folic Acid-Targeted and Redox-Responsive Nanoparticles for Enhanced Cancer Therapy. Front. Chem. 8:156. doi: 10.3389/fchem.2020.00156

INTRODUCTION

Doxorubicin (DOX) is one of the widely used chemotherapeutic agents to treat different tumors (Rivankar, 2014). However, its clinical applications are hampered by the lack of selectivity, severe toxicity, and reduced anticancer efficacies (Olson and Mushlin, 1990; Kang et al., 1996). Over the past decades, it is found that nanoscale drug delivery vehicles can help conventional chemotherapeutic drugs to overcome this limitation (Blanco et al., 2015; Xiong et al., 2016). The nanoparticles are able to increase drug accumulation in tumors via enhanced permeability and retention (EPR) effect (Maeda et al., 2013; Wilhelm et al., 2016). Among the nanoparticles reported, most of them have been decorated by PEGylation to improve the biocompatibility and stability after the administration (Butcher et al., 2016; Huckaby and Lai, 2018; Suh et al., 2019). Although outside PEG layer can validly preserve nanoparticles from rapid clearance by the reticuloendothelial system (RES) to extend their blood circulation, its application would significantly impede cellular uptake by tumor cells and result in unsatisfactory therapeutic efficiency (Zhu et al., 2012; Fang et al., 2017; Chen et al., 2018). Accordingly, optimization of the carriers with active targeting moieties are of great interest in drug delivery field. The targeting ligands can recognize the over-expressed receptors on cancer cells, thus facilitate cell internalization via receptor-ligand mediated endocytosis (Lazarovits et al., 2015; Kosmides et al., 2017). For example, high-affinity folate receptor

is a glycosylphosphatidylinositol-linked cell surface receptor and usually expressed at elevated levels on tumoral cells. Accordingly, folic acid, which is a cheap, chemically stable and water-soluble B vitamin and could specifically recognize folate receptor, has become a commonly used ligand for convenient tumor navigation. Up to now, a series of FA modified delivery system have been developed for active targeting to cancer cells (Gabizon et al., 2004; Fathi et al., 2017; Liu et al., 2019). Following the FA decoration and attaching to the receptors, the nanocarriers would be internalized into cancer cells through the endocytotic pathway to increase intracellular drug content (Zwicke et al., 2012; Cheng et al., 2017). Additionally, other functional targeting ligands, such as arginine-glycine-aspartic acid sequences (RGD), hyaluronic acid, prostate-specific membrane antigen sequences (PSMA) have also been proven to promote drug accumulation in different types of tumor after appropriate modification on nanoparticles (Chai et al., 2019; Ma et al., 2019; Yoo et al., 2019; Zhou et al., 2019).

To amplify the therapeutic benefits, the ideal nanocarriers should boost the drug release rapidly after entering the cells (Deepagan et al., 2018; Wang et al., 2018; Sangtani et al., 2019). Unfortunately, it is difficult for conventional nanocarriers to achieve timely on-demand drug release, leading to marginal drug exposure to cancer cells. The stimuli-responsive drug release systems, which would be degraded by responding with the exogenous physicochemical stimulus (pH, reducing agent, light, temperature, etc.) in tumor microenvironment, garnered considerable attention during the last decade (El-Sawy et al., 2018; Jiménez-Balsa et al., 2018; Li et al., 2018; Qu et al., 2018). Among numerous design, disulfide linkages were widely utilized to fabricate responsive systems due to the dramatical difference of the reducing glutathione (GSH) concentration between extracellular and intracellular microenvironment (ca. 2 μM vs. ca. 10 mM) (Wu et al., 2015; Lee et al., 2016; Zhang et al., 2016). In recent years, an increasing number of studies have given importance to tellurium-containing nanoparticles. As one of the chalcogens, the chemical property of tellurium is likely to be similar to sulfur and selenium. However, because of its weaker electronegativity and stronger radius, tellurium has lower bond energy. In contrast to S–S bond (240 kJ/mol) and Se–Se bond (192 kJ/mol), the energy of Te–Te bond is only 149 kJ/mol, which reveals that the ditelluride-containing nanoparticles are more prone to be reacted by reducing stimulus (Chivers and Laitinen, 2015; Wang et al., 2016). For instance, Xu et al. proposed and synthesized a series of telluride-containing polymer which is sensitive to higher ROS concentration or gamma radiation (Cao et al., 2014, 2015a,b; Wang et al., 2015). Furthermore, Zhang's group made an effort to design another ditelluride-containing poly(ether-urethane) drug delivery system as well, suggesting the excellent potential for antitumor activity (Fang et al., 2015). Therefore, it might be a promising strategy to develop a targeted ditelluride-containing nanocarriers to achieve cascade cellular uptake and intracellular drug release for efficient cancer treatment.

Herein, we have developed an integrated nanoparticles platform containing FA ligands and ditelluride bonds for active tumor targeting and GSH-responsive drug release (**Figure 1**). It can self-assembly in aqueous solution to encapsulate the DOX, and the hydrophilic PEG shell can prolong DOX circulation in blood. Following the passive extravasation to tumor tissues via EPR effect, FA ligands bared on the surface of nanoparticles can facilitate the endocytosis for FA receptor specific expression tumor cells. Subsequently, F-TeNP$_{DOX}$ would be swelled rapidly in a reducing environment after the cleavage of bridged bonds to trigger drugs release. As a result, the enhanced inhibition on tumor growth can be achieved.

MATERIALS AND METHODS

Materials

Epsilon-caprolactone (ε-CL, 99%) was purchased from Alfa Aesar Chemical Company, Inc., and used after CaH_2 treatment and distillation. Carboxyl group modified poly(ε-caprolactone) (PCL-COOH) with 5700 average molecular weights was synthesized using aluminum isopropoxide as the initiator according to reported method (Dzienia et al., 2017). Poly(ethylene glycol) monomethylether (PEG, Mw = 5000) and 11-bromoundecanol were obtained from Sigma-Aldrich. The block copolymers of poly(ethylene glycol) monomethylether and poly(ε-caprolactone) (PEG-*b*-PCL) was synthesized as previously reported and the average molecular weights of PCL was 5930 (Han et al., 2015). FA-PEG-*b*-PCL (PEG Mw = 5000, PCL Mw = 5240) were obtained from Xi'an Ruixi Biological Technology Co., Ltd. Disodium telluride and di(1-hydroxylundecyl) ditelluride were prepared according to the previous reports (Wang et al., 2016). 3-(4,5-dimethylthiazol-2-yl)-2,5-diphenyl tetrazolium bromide (MTT) was purchased from Energy Chemical Co., Ltd. (Shanghai, China). Doxorubicin hydrochloride (DOX·HCl) was obtained from Beijing HVSF United Chemical Materials Co., Ltd. All other reagents were purchased from Shanghai Aladdin Bio-Chem Technology Co., LTD. and used as received.

Synthesis of Ditelluride-Bridged Block Copolymer With FA Ligand

The targeted diblock copolymer containing ditelluride linker (FA-PEG-*TeTe*-PCL) was synthesized via coupling reaction among FA-PEG-COOH, di(1-hydroxylundecyl) ditelluride and PCL-COOH. Initially, FA-PEG-COOH (0.37 mmol, 2.03 g) and di(1-hydroxylundecyl) ditelluride (1.1 mmol, 0.66 g) were mixed in 20 mL of anhydrous CH_2Cl_2 in a three-necked flask at 25°C, then DCC (0.56 mmmol, 115.5 mg) and DMAP (0.56 mmol, 62.8 mg) was added drop wise under nitrogen atmosphere. After reacting at rt for 24 h, the byproduct was removed by filtration. The filtrate was concentrated and precipitated into cold diethyl ether three times to obtain the FA-PEG-*TeTe*-OH. Next, the FA-PEG-*TeTe*-OH (0.19 mmol, 1.17 g), PCL-COOH (0.09 mmol, 0.4 g), DCC (0.14 mmol, 28.9 mg), and DMAP (0.14 mmol, 15.7 mg) were dissolved in 15.0 mL of anhydrous CH_2Cl_2 and reacted at 25°C under N_2. After 24 h, the mixture was filtered, concentrated and precipitated into cold diethyl ether/methanol (10:1 v/v) three times.

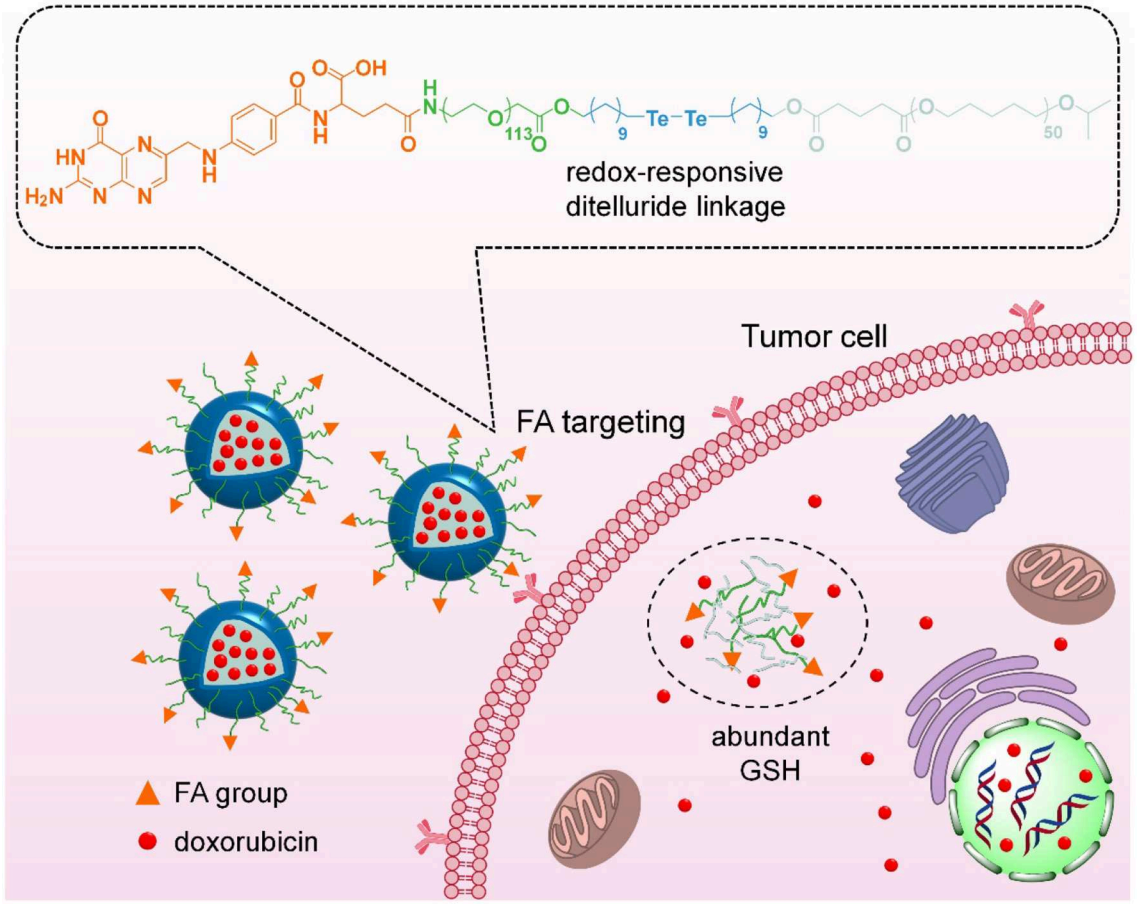

FIGURE 1 | Scheme of targeting drug delivery and GSH-responsive drug release for efficient cancer therapy.

Preparation of Drug-Loaded Nanoparticles

Briefly, 20.0 mg of PEG-*b*-PCL, FA-PEG-*b*-PCL, and FA-PEG-*TeTe*-PCL and 2.0 mg of DOX were mixed in 1.0 mL of DMSO and stirred for 30 min. Then 20.0 mL of ddH_2O was dropwise added under vigorous stirring and kept for another 2 h. The organic phase was removed by dialysis against ultrapure water in dialysis tubing (MWCO = 14000). The free DOX was further removed by centrifugation at 3,000 rpm for 5 min. The obtained nanoparticles were denoted by NP_{DOX}, F-NP_{DOX} and F-$TeNP_{DOX}$, respectively. The DOX loading content was determined by UV-vis spectrophotometer at 480 nm.

Drug Release *in vitro*

Two milliliters of NP_{DOX}, F-NP_{DOX}, and F-$TeNP_{DOX}$ (with equivalent DOX concentration at 100 μg/mL) were added into dialysis tubing (MWCO 3,500 Da). Then the tubing was immersed in the 10 mL of phosphate buffer (PB, 20 mM, pH 7.4) with or without 10 mM GSH in a shaker (120 rpm/min) at 37°C. At different time points, the external PB buffer was collected, and the tubing was immersed in fresh buffer at 37°C for further detection. The DOX content in the collected sample was measured by HPLC analysis (Ma et al., 2016).

Cellular Uptake of F-$TeNP_{DOX}$ *in vitro*

For the FACS analysis, 4T1 or NIH-3T3 cells were seeded in 12-well plates at a density of 100,000 cells per well. After culturing for 12 h, the original medium was replaced with that containing free DOX (4 μg/mL), NP_{DOX}, F-NP_{DOX} and F-$TeNP_{DOX}$ (equivalent [DOX] = 4 μg/mL). The cells were incubated for another 4 h, and then treated with cold phosphate buffered saline (PBS, 10 mM, pH 7.4) twice and trypsin (0.25%, Gibco, Canada). The cells were harvested and resuspended in paraformaldehyde (4%, 200 μL) for flow cytometry on BD FACS Verse.

In addition, cells treated with various formulations were lysed by 1% Triton X-100 (in 250 μL of PBS) after washing with cold PBS twice. The DOX content in the lysates was measured by HPLC, and the intracellular protein content was determined by a BCA Protein Assay Kit (Pierce, Rockford, IL).

To observe the subdistribution, the 4T1 cells were seeded on coverslips in 12-well plates. The cells were incubated with medium containing free DOX (4 μg/mL), NP_{DOX}, F-NP_{DOX}, and F-$TeNP_{DOX}$ (equivalent [DOX] = 4 μg/mL) for 4 h. Then, the cell nuclei was counterstained by 4′,6-diamidino-2-phenylindole (DAPI, Beyotime, China) for the cell nuclei and F-actin was counterstained by Alexa Fluor® 488 Phalloidin (Invitrogen,

Carlsbad, USA), respectively. The cells were visualized using a confocal laser scanning microscope (CLSM, LMS810, Zeiss).

Cytotoxicity of F-TeNP$_{DOX}$ *in vitro*

To determine the cytotoxicity of NP$_{DOX}$, F-NP$_{DOX}$ and F-TeNP$_{DOX}$, a MTT assay was used against 4T1 or NIH-3T3 cells. The cells were seeded in 96-well plates at 10,000 cells per well, and treated with medium containing free DOX, NP$_{DOX}$, F-NP$_{DOX}$, or F-TeNP$_{DOX}$ at different concentrations. After the incubation of 12 h, the cells were further incubated with fresh DMEM medium for another incubation of 60 h. Subsequently, DMEM medium and the MTT stock solution were added to each well. The final MTT concentration is 1 mg/mL. Following further incubation for 2 h, extraction buffer (20% sodium dodecyl sulfate in 50% DMF, pH 4.7) was added and the plate was incubated at 37°C for 4 h. The mixture absorbance was measured by a Bio-Rad 680 microplate reader at 570 nm and the cell viability was calculated according to the previously reported method. The cytotoxicity of nanoparticles without DOX loading was measured similarly.

To determine the cell apoptosis, 4T1 cells were seeded into 24-well plates and incubated for 12 h. Subsequently, the cells were treated with various DOX-loaded nanoparticles as same as the MTT assay. Thereafter, the cells were treated by Annexin V-FITC apoptosis detection kit I (BD Biosciences). The results were measured using BD Accuri® C6 flow cytometer.

Pharmacokinetics and Biodistribution of F-TeNP$_{DOX}$

Female ICR mice were divided into 4 groups ($n = 4$), and were received *i.v.* injection with DOX, NP$_{DOX}$, F-NP$_{DOX}$, or F-TeNP$_{DOX}$ ([DOX] = 10 mg/kg). After the predetermined time intervals, blood samples were collected from the retroorbital plexus of the mouse eye and the DOX content in plasma was measured via previously reported method.

To determine the DOX internalization in tumoral cells, mice bearing 4T1/GFP xenografts were administrated with DOX, NP$_{DOX}$, F-NP$_{DOX}$ or F-TeNP$_{DOX}$. At 4, 12, or 24 h, the tumor tissues were harvested and digested into single cell suspension. The quantitative distribution of DOX in GFP$^+$ cells were analyzed by both FACS and HPLC.

Anticancer Efficiency of F-TeNP$_{DOX}$ *in vivo*

The mice bearing 4T1 xenograft were randomly divided into five groups ($n = 5$). When the tumor volume was about 50 mm^3, the mice received systemic injection every week with PBS, DOX (5.0 mg/kg), NP$_{DOX}$, F-NP$_{DOX}$, or F-TeNP$_{DOX}$ ([DOX] = 5.0 mg/kg). Tumor size and body weight were monitored every 3 days. For *in vivo* biosafety assay, mice were treated daily with various formulation for 3 days ([DOX] = 5.0 mg/kg). Serum was collected for hematologic evaluation and enzyme-linked immunosorbent assay (ELISA) for alanine aminotransferase (ALT), aspartate transaminase (AST), and blood urea nitrogen (BUN).

RESULTS

Synthesis and Characterization of FA-PEG-TeTe-PCL

The synthetic route of redox-responsive ditelluride-containing copolymer was shown in **Figure 2A**. The FA-PEG-*TeTe*-PCL was synthesized by a two-step coupling reaction. The FA-PEG-COOH was first reacted with di(1-hydroxylundecyl) ditelluride (DHDT) to obtain FA-PEG-*TeTe*-OH. Then, FA-PEG-*TeTe*-OH was coupled with an carboxyl-modified poly(ε-caprolactone) (PCL-COOH), and the excess FA-PEG-TeTe-OH was removed by precipitating the product using methanol. The unimodal gel permeation chromatography (GPC) profile (**Figure 2B**) indicated an obvious shift toward higher molecular weight, suggesting successful coupling. The ^{1}H NMR spectrum in **Figure 2C** showed the molar ratio of PEG and PCL was 1:1.07, which is close to that of the desired product. Meanwhile, ^{125}Te NMR analysis in **Figure 2D** also presented a characteristic peak at 471.3 ppm, further demonstrating its chemical structure. In addition, the non-responsive FA-PEG-*b*-PCL and PEG-b-PCL were used as the control in the following experiments.

Preparation and Characterization of Redox-Sensitive Nanoparticles Containing Ditelluride Linkage

The FA-PEG-*TeTe*-PCL, FA-PEG-*b*-PCL and PEG-*b*-PCL could be self-assembled into micellar nanoparticles in aqueous solution, and then efficiently encapsulated hydrophobic DOX in the hydrophobic core. The fabricated micelles were denoted by F-TeNP$_{DOX}$, F-NP$_{DOX}$, and NP$_{DOX}$, respectively. As shown in **Figure 3A**, the average hydrodynamic diameter of F-TeNP$_{DOX}$ was found as 96.5 nm by dynamic light scattering (DLS) and polydispersity index was 0.158, whereas the nanoparticles in this size range were believed to be passively accumulated in tumors through the EPR effect (Li et al., 2010; Maruyama, 2011). Owing to the presence of hydrophilic PEG component, the size observed by transmission electron microscopy was slightly smaller than that from DLS measurement. Meanwhile, F-TeNP$_{DOX}$ with the PEG chains on the surface showed a zeta potential of −10.7 mV. The DOX loading content and encapsulation efficiency of F-TeNP$_{DOX}$ was determined by UV-vis spectra as 5.74 and 60.9%, respectively. In addition, both F-NP$_{DOX}$ and NP$_{DOX}$ exhibited comparable properties after DOX loading (**Figure S1** and **Table S1**). Due to the smaller size and the protection from the outer PEG shell, all of three nanoparticles maintained their original diameter after incubating in PBS solution for 48 h (**Figure 3B**).

According to our design, the bridged ditelluride bonds in FA-PEG-*TeTe*-PCL would be selectively cleaved in a reducing environment after cellular uptake. Considering the degradation of PEG corona lead to the nanoparticles swelling (Chen et al., 2016), we measured the size change of three nanoparticles in the presence of GSH. As shown in **Figure 3C**, the size of the F-TeNP$_{DOX}$ at 24 h was significantly raised to ∼320 nm, while the control F-NP$_{DOX}$ and NP$_{DOX}$ showed no remarkable size change. Furthermore, the size change of nanoparticles under

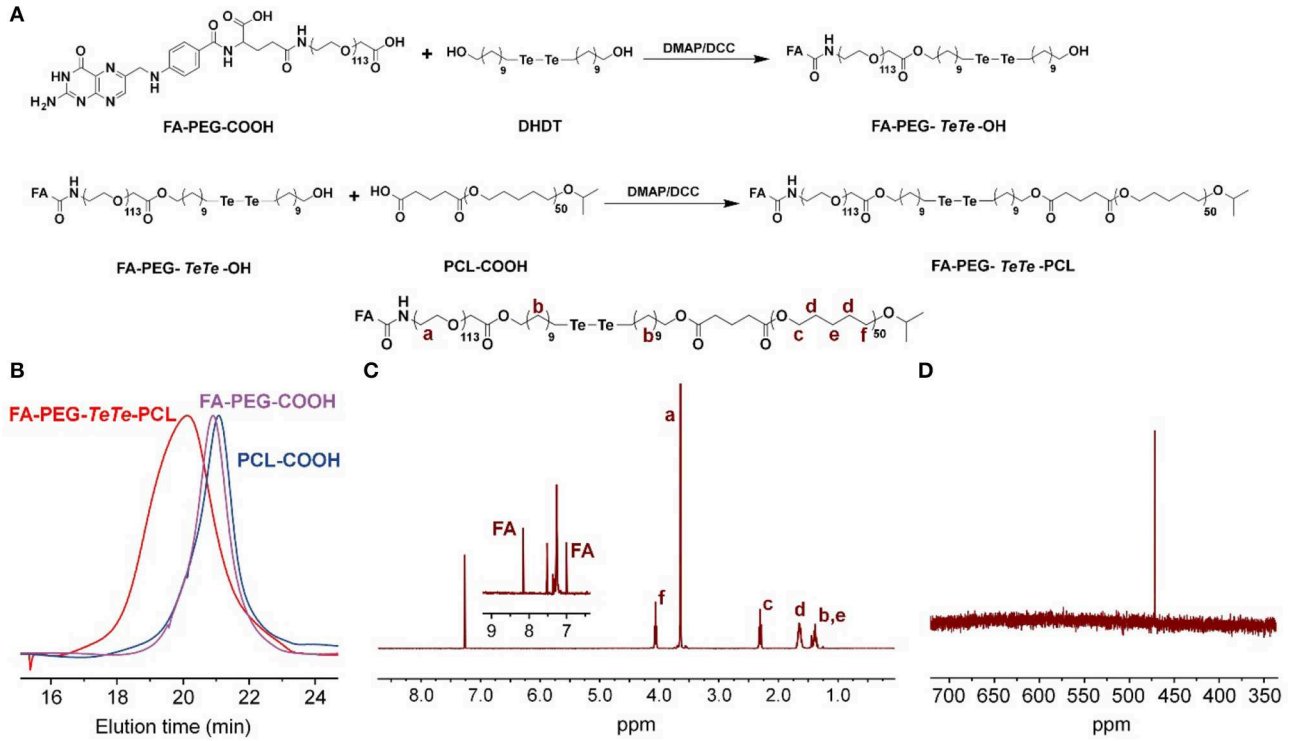

FIGURE 2 | (A) Synthetic route of FA-PEG-*TeTe*-PCL. GPC spectrum **(B)** ^{1}H NMR spectrum **(C)** and ^{125}Te NMR spectrum **(D)** of FA-PEG-*TeTe*-PCL.

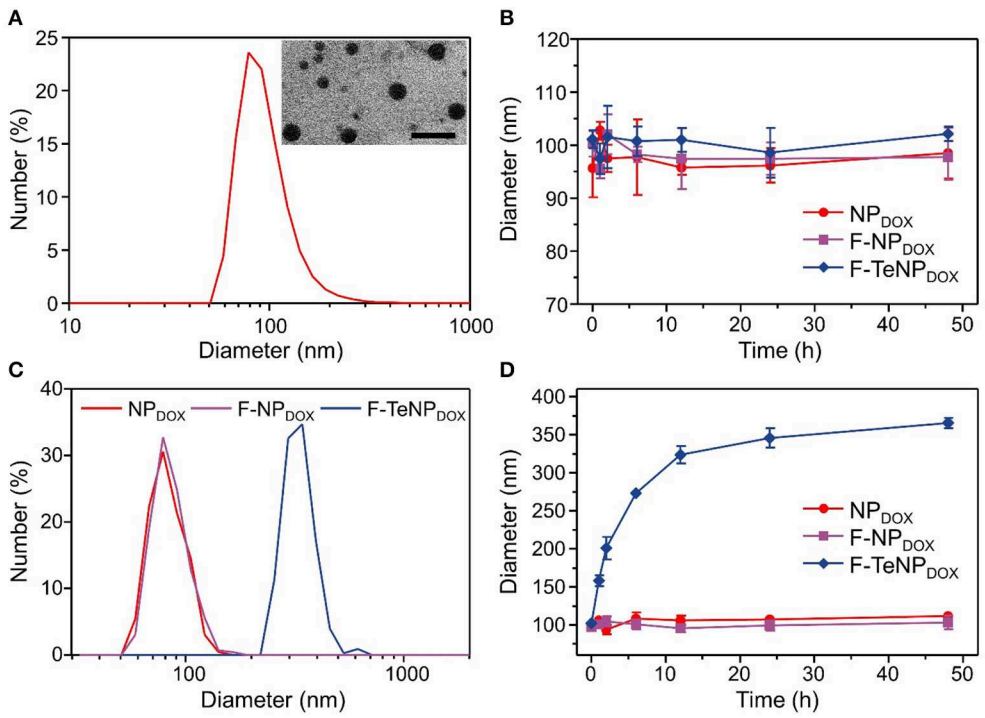

FIGURE 3 | Characterization of the redox-responsive properties of DOX-loaded micelles. **(A)** Size distribution and morphology of F-TeNP$_{DOX}$. The scale bar is 200 nm. **(B)** Change of hydrodynamic size in PBS solution (pH 7.4). **(C,D)** Diameter change of NP$_{DOX}$, F-NP$_{DOX}$, and F-TeNP$_{DOX}$ with 10 mM GSH.

abundant GSH condition was monitored during 48 h at different time intervals. As illustrated in **Figure 3D**, the aggregations of F-TeNP$_{DOX}$ was observed and the size gradually increased to approximately 365 nm. On the other hand, both control groups showed negligible size variation, in agreement with the above mentioned result. These data indicated that the ditelluride bond in F-TeNP$_{DOX}$ could be cleaved by endogenous GSH stimulus, resulting in the detachment of the PEG layer and dissociation of the F-TeNP$_{DOX}$ nanoparticle.

DOX Release *in vitro*

It is well-verified that the degradation of the PEG shell would facilitate cargo release. Therefore, the DOX would be rapidly released from F-TeNP$_{DOX}$ under redox conditions. To verify this hypothesis, quantitative drug release *in vitro* was investigated at 37°C in phosphate buffer (PB, 20 mM, pH 7.4) with or without 10 mM GSH, and the cumulative DOX release was monitored using HPLC. As shown in **Figure 4A**, the drug release rate for F-TeNP$_{DOX}$ was significantly accelerated when treated with 10 mM GSH. There was almost 76.71 ± 2.8% of DOX and was detected after 24 h, and the continual release can be observed until the end of the experiment. On the contrary, the cumulative release of DOX was merely 26.87 ± 2.06% in the absence of GSH even after 72 h. Moreover, both nanoparticles without ditelluride bonds (NP$_{DOX}$ and F-NP$_{DOX}$) showed comparable and tardy drug release pattern regardless of the reductive agent (**Figures 4B,C**). Together, the boosted drug release demonstrated that the breakage of ditelluride bond of F-TeNP$_{DOX}$ in redox condition, such as GSH, leads to a rapid destruction of nanoparticles and accelerated cargo leakage from the micelle core.

Cellular Uptake *in vitro*

For the purpose of evaluating the targeting ability of the nanoparticles modified with folic acid (FA), two types of cell lines were chosen. The 4T1 cell line is over-expressed folate receptors (FR) which can specifically bind to FA while the NIH-3T3 cells do not express the FR were used as the control cell line (Rathinaraj et al., 2015; Han et al., 2016). Furthermore, flow cytometry was performed to compare endocytosis of DOX-loaded nanoparticles (NP$_{DOX}$, F-NP$_{DOX}$, or F-TeNP$_{DOX}$). After incubation with various formulations for 4 h, the intracellular DOX fluorescence was analyzed. As shown in **Figure 5A**, it is worth noting that the intracellular fluorescence intensity of 4T1 cells treated with F-NP$_{DOX}$ or F-TeNP$_{DOX}$ was much higher than that of NP$_{DOX}$, suggesting the targeting attributes of the FA on the micelle surface. By contrast, no obvious difference can be detected among the three nanoparticles in NIH-3T3 cells, and the mean fluorescence intensity (MFI) value for three nanoparticles was apparently lower than that of 4T1 cells (**Figure 5B**). Furthermore, the promoted cellular uptake of FA-mediated nanoparticles was further confirmed by the quantitative analysis of internalized DOX content. As expected, the intracellular DOX concentration of NP$_{DOX}$ was 1.91 ± 0.18 μg per mg protein while the F-NP$_{DOX}$ and F-TeNP$_{DOX}$ achieved 3.38 ± 0.23 and 3.29 ± 0.24 μg DOX per mg protein, respectively (**Figure 5C**). Meanwhile, the drug content was significantly inhibited if adding free FA to the medium because of the competitive effect between the FA-decorated nanoparticles and the free FA. On the other hand, it is worth noting that the intracellular concentration of three nanoparticles showed a negligible difference on NIH-3T3 cells regardless of FA modification (**Figure 5D**). These results demonstrated that both F-NP$_{DOX}$ and F-TeNP$_{DOX}$ tended to be internalized into 4T1 cells via FA-mediated endocytosis, which was in agreement with previous reports.

Following the FACS and HPLC measurement, the enhanced cellular uptake of targeting nanoparticles was further corroborated using a Zeiss LMS810 confocal laser scanning microscope. The 4T1 cells were incubated with NP$_{DOX}$, F-NP$_{DOX}$, or F-TeNP$_{DOX}$ as described above for 4 h, and the cell nuclei and F-actin were labeled by 4',6-diamidino-2-phenylindole (DAPI) and Alexa Fluor® 488 Phalloidin, respectively. As displayed in **Figure 6**, a slightly weaker DOX fluorescence was observed in 4T1 cells incubated with non-targeted NP$_{DOX}$. However, a significantly stronger red fluorescence was clearly observed for the cells incubated with F-NP$_{DOX}$ or F-TeNP$_{DOX}$, suggesting the stronger internalization of nanoparticles mediated by FA ligand. Moreover, for cells treated with F-NP$_{DOX}$ or NP$_{DOX}$, the DOX signal were dominantly localized in the cytoplasm. On the contrary, broader red DOX fluorescence was detected in the nucleus of cells which were incubated with F-TeNP$_{DOX}$, indicating the intracellular abundant GSH drive the accelerated DOX release and subsequent transfer to the nucleus. These results confirmed that the ditelluride

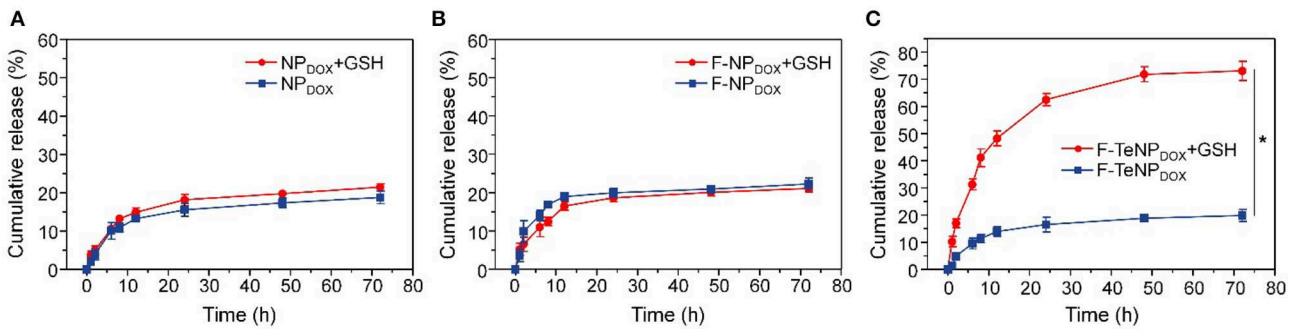

FIGURE 4 | The DOX release profile from NP$_{DOX}$ **(A)**, F-NP$_{DOX}$ **(B)**, or F-TeNP$_{DOX}$ **(C)** at different conditions ([GSH] = 10 mM). *$p < 0.05$.

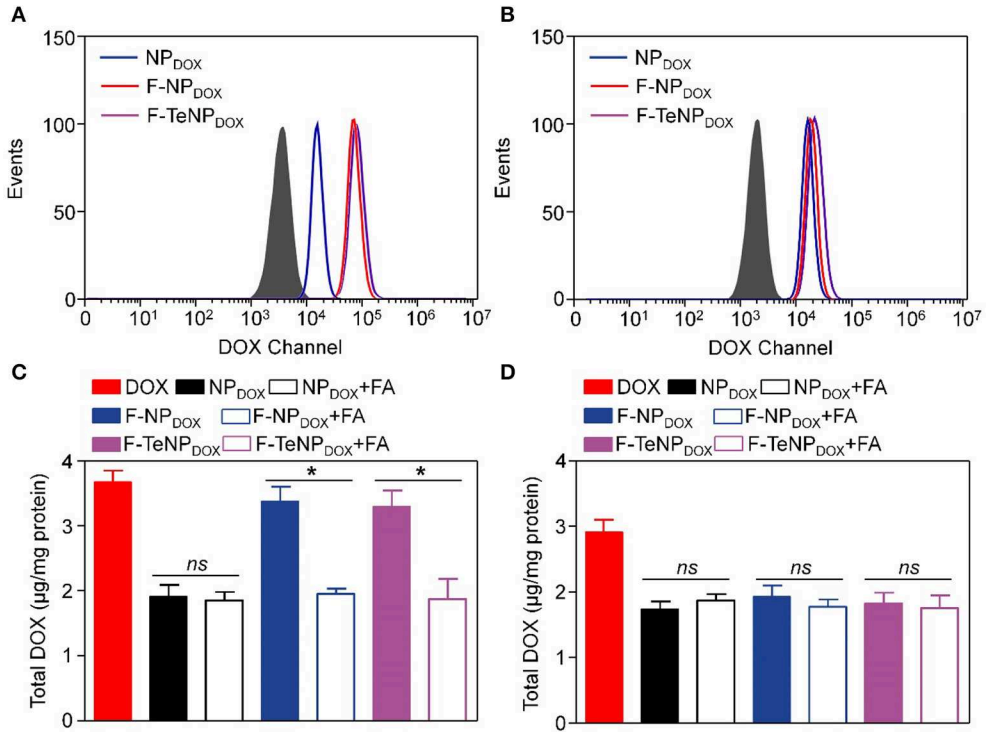

FIGURE 5 | The cellular uptake of NP_{DOX}, F-$NP_{DOX,}$ or F-$TeNP_{DOX}$ on 4T1 cells **(A)** or NIH3T3 cells **(B)**. Quantitative analyses of DOX content in 4T1 cells **(C)** or NIH 3T3 cells **(D)** after incubation with NP_{DOX}, F-$NP_{DOX,}$ or F-TeN_{PDOX} for 4 h. [DOX] = 4 μg/mL. *$p < 0.05$. ns, no significant difference.

bond of F-$TeNP_{DOX}$ could be cleaved in intracellular redox microenvironment and therefore the loaded drug can be released effectively.

Cell Killing Efficiency *in vitro*

Generally, good biocompatibility is the major prerequisite for nanoparticles to be an efficient drug delivery system. Therefore, MDA-MB-231, 4T1 and NIH-3T3 cells were used in a standard MTT assay for 72 h to evaluate the cell viability of blank FA-modified nanoparticles (F-TeNP). As shown in **Figure 7A**, the cell viabilities showed no significant difference among three cell lines and maintained above 95% even at the highest F-TeNP concentration (400 μg/mL), foreseeing the F-TeNP was biosafe in future application *in vivo*.

Thinking about the cell-killing mechanism of DOX is related to the nucleus entering and its interaction with DNA major groove, the targeted DOX delivery into 4T1 cells and subsequent GSH-triggered drug release would improve the cell growth inhibition and cell apoptosis. Next, the cancer cell-killing efficacy of F-$TeNP_{DOX}$ was studied on 4T1 cells. Following incubation with NP_{DOX}, F-NP_{DOX}, or F-$TeNP_{DOX}$ for 12 h, cells were incubated with DMEM medium for another 60 h, and the results were shown in **Figure 7B**. Although the DOX at concentrations of 0.5 μg/mL showed no noticeable cytotoxicity to 4T1 cells, the cell viability gradually decreased when the [DOX] was above 1.0 μg/mL. In comparison with the NP_{DOX}, the improved cytotoxicity of F-NP_{DOX} is probably due to the increased DOX content inside the cells via FA-mediated internalization. More importantly, it is worth noting that treatment with F-$TeNP_{DOX}$ decreased the cell viability to 50.35±1.56%, 32.57±1.59% and 23.93±3.14% when the DOX concentration is 2.0, 5.0, and 10.0 μg/mL, respectively.

To further verify the phototoxicity effect of F-$TeNP_{DOX}$, we analyzed cell apoptosis after the treatment using annexin-V-FITC and propidium iodide staining. In comparison with other groups (PBS, NP_{DOX}, and F-NP_{DOX}), 66.1% of apoptotic cells was observed in the cells treated with F-$TeNP_{DOX}$ (**Figure 7C**). These results were in agreement with the abovementioned observations, demonstrating that enhanced cell-killing efficiency of F-$TeNP_{DOX}$ is a result of FA-facilitated cellular uptake combined with GSH-responsive cargo release.

Biodistribution *in vivo*

With PEGylated shell outside the micelles, NP_{DOX}, F-NP_{DOX}, or F-$TeNP_{DOX}$ are expected to prolong drug circulation in blood. Accordingly, we then analyzed their pharmacokinetic in female ICR mice. The mice were received a systemic injection of drug-loaded nanoparticles, and free DOX was used as control. The DOX concentration in plasma at 10 min, 0.5, 1, 2, 6, 12, 24, and 48 h was measured by HPLC. In comparison with free DOX, which was cleared rapidly as previous demonstrated, NP_{DOX}, F-NP_{DOX}, or F-$TeNP_{DOX}$ exhibited a promoted DOX concentration in plasma at each

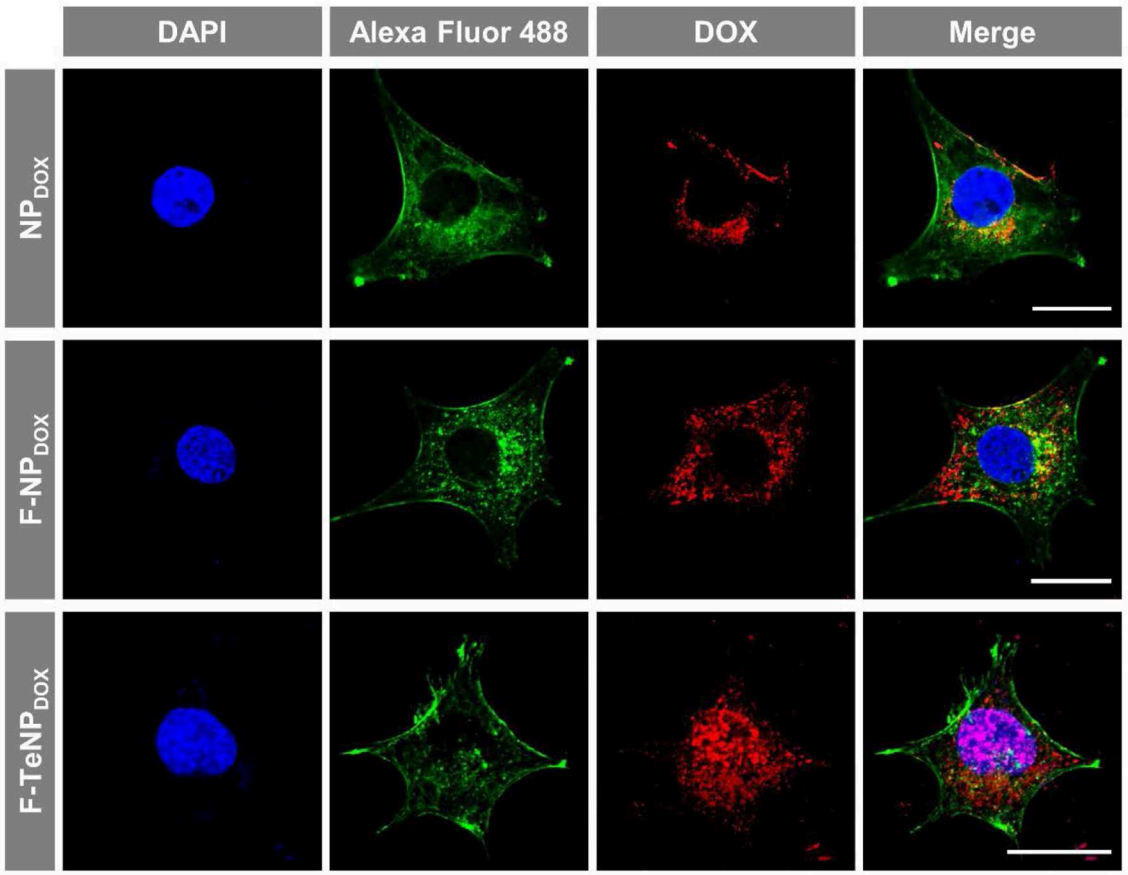

FIGURE 6 | Cellular internalization of NP_{DOX}, F-NP_{DOX}, or F-$TeNP_{DOX}$ on 4T1 cells. DAPI (blue) and Alexa Fluor 488 phalloidin (green) were used to stain cell nuclei and F-actin, respectively. The scale bar is 20 μm.

time interval (**Figure 8A**). After 48 h-post injection, the DOX concentration of NP_{DOX}, F-NP_{DOX}, or F-$TeNP_{DOX}$ was 11.40–, 7.12–, and 5.95-fold higher than that of free DOX, respectively. Moreover, all of the nanoparticular formulations showed more advanced area under curve (AUC_{0-t}) and clearance (CL) (**Table S2**), suggesting their superior retention in bloodstream.

The prolonged blood circulation of micellar nanoparticles ensured drug molecules greater opportunity to accumulate in tumor tissues via EPR effect. Following the extravasation from tumor blood vessels, FA ligand on F-NP_{DOX} or F-$TeNP_{DOX}$ would facilitate more drug into the tumoral cell (Li et al., 2015). To confirm this hypothesis, we constructed 4T1/GFP xenografts in mice and analyzed intracellular DOX content in GFP-positive tumoral cells. Following the intravenous injection with DOX, NP_{DOX}, F-NP_{DOX} or F-$TeNP_{DOX}$, the 4T1/GFP cells were isolated by flow cytometry and intracellular DOX content was quantified using HPLC at different time intervals. As shown in **Figure 8B**, mice treated with F-NP_{DOX} or F-$TeNP_{DOX}$ displayed ∼1.43, 1.95, and 3.44-fold higher DOX retention than that of NP_{DOX} at 4, 12, and 24 h, respectively. Meanwhile, there was no significant difference between the drug content of both targeted nanoparticles, indicating the ditelluride linkage was stable and would not impede micelle biodistribution in the body. These results indicated that the micellar F-TeNP with the PEGylation and FA modification substantially improved drug accumulation in tumoral cells through both passive and active targeting.

Antitumor Efficiency *in vivo*

To investigate *in vivo* tumor therapeutic efficacy, mice bearing 4T1 tumors were used as the model and randomly divided into five groups (five mice each). Each group was received with corresponding intravenous injection with PBS (200 μL), DOX (5.0 mg/kg), NP_{DOX}, F-NP_{DOX}, or F-$TeNP_{DOX}$ (equivalent DOX dose of 5.0 mg/kg). As shown in **Figure 9A**, the tumor growth of saline control group was not inhibited, reaching ∼1,750 mm^3 after 27 days. The free DOX and NP_{DOX} showed moderate inhibitory effect. On the contrary, in comparison with F-NP_{DOX} group whereas the ditelluride bond was absence, there was a remarkable growth inhibition in the F-$TeNP_{DOX}$ group, and the tumor volume was only up to 200 mm^3 at the end of the experiment. After the sacrifice of mice on day 27, the tumor

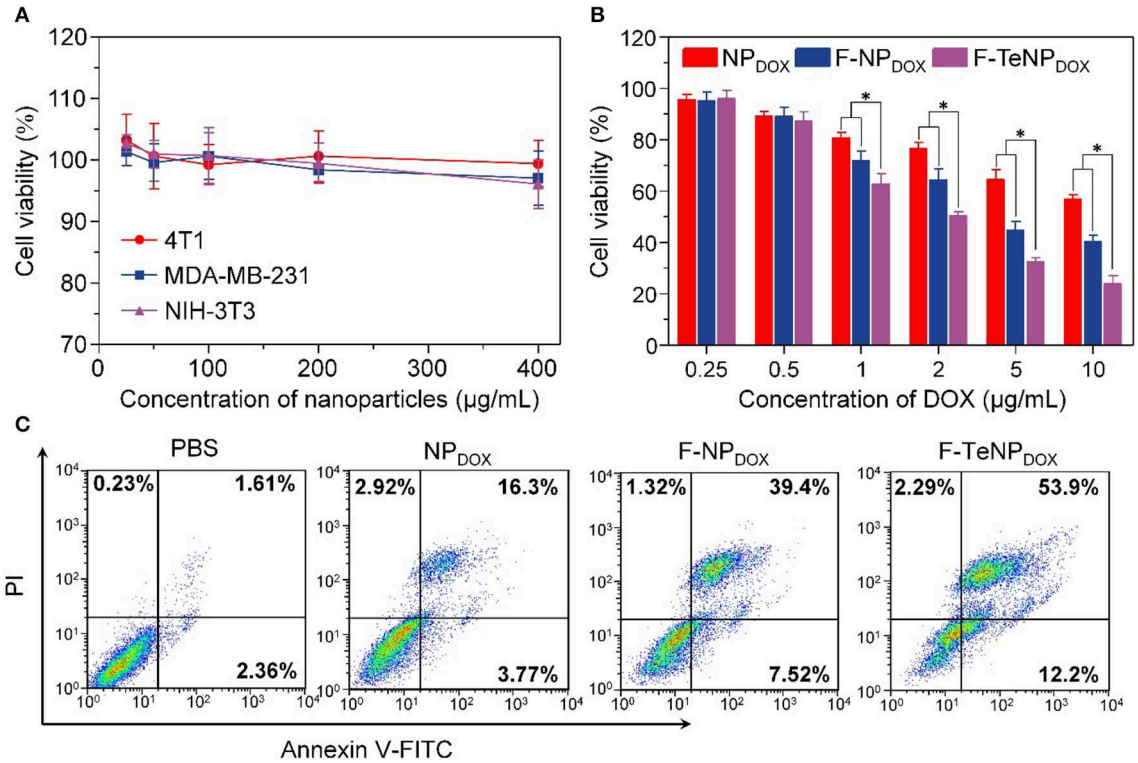

FIGURE 7 | (A) MTT assay of F-TeNP on different cell lines (MDA-MB-231, 4T1, and NIH-3T3). The cells were incubated with nanoparticles for 72 h. **(B)** Therapeutic effect of NP_{DOX}, $F\text{-}NP_{DOX}$, and $F\text{-}TeNP_{DOX}$ on 4T1 cells. $^*p < 0.05$. **(C)** 4T1 cell apoptosis induced by various formulations.

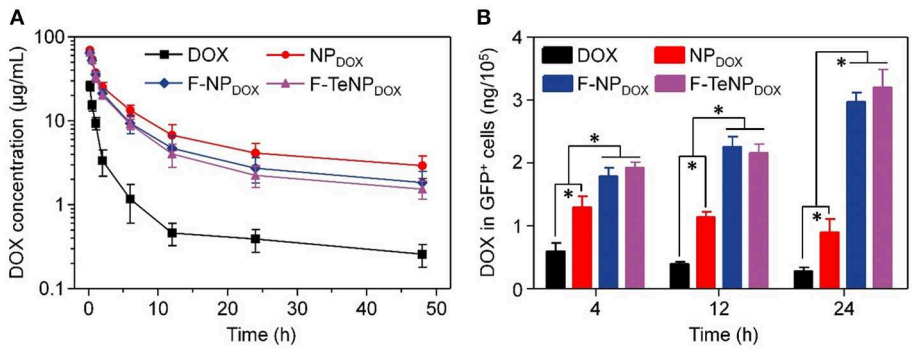

FIGURE 8 | (A) Plasma DOX concentration vs. time after *i.v.* injection of free DOX, NP_{DOX}, $F\text{-}NP_{DOX}$, or $F\text{-}TeNP_{DOX}$ ($n = 4$). **(B)** Quantitative analysis of DOX content in GFP-expressing 4T1 cells. $^*p < 0.05$.

weight analysis further demonstrated that $F\text{-}TeNP_{DOX}$ was more effective in tumor growth suppression (**Figure 9B**). In order to evaluate the biosafety of various treatments, monitoring the body weight of the mice was performed. In **Figure 9C**, the mice treated with free DOX showed a slight decline of body weight (<10%), and other groups remained relatively stable during the whole observation. In comparison with free DOX, ELISA measurements of ALT, AST, and BUN illustrated that $F\text{-}TeNP_{DOX}$ treatment induced less liver and kidney damage (**Figure 9D**). Moreover, there was no significant difference in blood routine count among PBS, NP_{DOX}, $F\text{-}NP_{DOX}$, and $F\text{-}TeNP_{DOX}$ groups (**Table S3**), further indicating its low toxicity *in vivo*.

CONCLUSIONS

In this study, we demonstrated the successful preparation of a targeting and redox-responsive delivery system for cancer therapy via FA modified PEG-PCL copolymer with

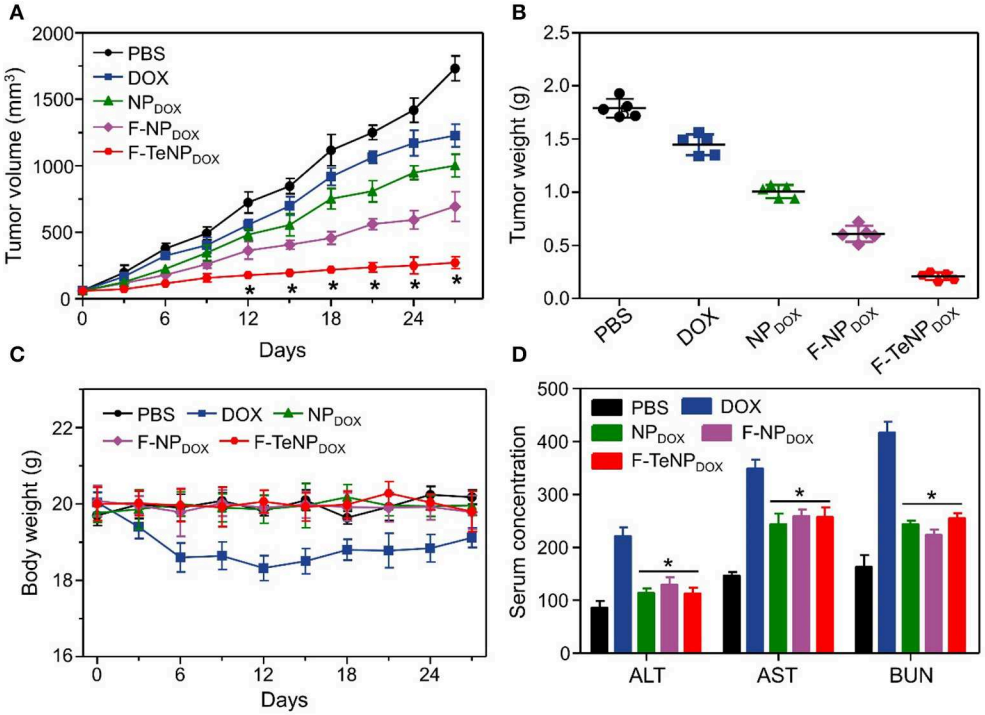

FIGURE 9 | (A) Tumor growth curve in 4T1 tumor xenograft-bearing nude mice after various treatments. The injections were performed on days 0, 7, 14, and 21. $^*p < 0.05$. **(B)** The 4T1 tumor weight after the treatment. **(C)** Body weight monitoring of the mice that received treatment with various samples. **(D)** ELISA examination of mouse ALT (U/L), AST (U/L), and BUN (10 μmol/L) in the serum after receiving different treatments. $^*p < 0.05$, vs. DOX.

ditelluride linkage. The obtained nanoparticles can efficiently load hydrophobic DOX, and showed rapid drug release triggered by intracellular GSH. Also, F-TeNP$_{DOX}$ could be efficiently internalized into 4T1 cells through FA-mediated endocytosis and achieve sufficient "active-drug" content after redox-responsive micelle dissociation. Moreover, a promoted chemotherapeutic agent accumulation in tumor tissue was observed *in vivo*, leading to a more advanced therapeutic efficiency. Therefore, our work presents a promising drug delivery system based on ditelluride-bridged copolymer, providing a new avenue toward a deeper understanding of precise drug delivery and cancer therapy.

DATA AVAILABILITY STATEMENT

All datasets generated for this study are included in the article/**Supplementary Material**.

ETHICS STATEMENT

The animal study was reviewed and approved by Tianjin Medical University Animal Care and Use Committee.

AUTHOR CONTRIBUTIONS

CS conceived the ideas, synthesized and characterized delivery system, reviewed, and edited the manuscript. ZP and JZ performed cell and animal experiments and wrote the original draft. All authors discussed the results and commented on the manuscript.

FUNDING

This research was funded by the Open Project of Key Laboratory of Biomedical Engineering of Guangdong Province (KLBEMGD201703) and Tianjin Medical University General Hospital (ZYYFY2016041).

SUPPLEMENTARY MATERIAL

The Supplementary Material for this article can be found online at: https://www.frontiersin.org/articles/10.3389/fchem.2020.00156/full#supplementary-material

REFERENCES

Blanco, E., Shen, H., and Ferrari, M. (2015). Principles of nanoparticle design for overcoming biological barriers to drug delivery. *Nat. Biotechnol.* 33, 941–951. doi: 10.1038/nbt.3330

Butcher, N. J., Mortimer, G. M., and Minchin, R. F. (2016). Drug delivery: unravelling the stealth effect. *Nat. Nanotechnol.* 11, 310–311. doi: 10.1038/nnano.2016.6

Cao, W., Gu, Y., Li, T., and Xu, H. (2015a). Ultra-sensitive ROS-responsive tellurium-containing polymers.

Chem. Commun. 51, 7069–7071. doi: 10.1039/c5cc01779c

Cao, W., Gu, Y., Meineck, M., Li, T., and Xu, H. (2014). Tellurium-containing polymer micelles: competitive-ligand-regulated coordination responsive systems. *J. Am. Chem. Soc.* 136, 5132–5137. doi: 10.1021/ja500939m

Cao, W., Wang, L., and Xu, H. (2015b). Coordination responsive tellurium-containing multilayer film for controlled delivery. *Chem. Commun.* 51, 5520–5522. doi: 10.1039/c4cc08588d

Chai, Z., Ran, D., Lu, L., Zhan, C., Ruan, H., Hu, X., et al. (2019). Ligand-modified cell membrane enables the targeted delivery of drug nanocrystals to glioma. *ACS Nano* 13, 5591–5601. doi: 10.1021/acsnano.9b00661

Chen, C., Zheng, P., Cao, Z., Ma, Y., Li, J., Qian, H., et al. (2016). PEGylated hyperbranched polyphosphoester based nanocarriers for redox-responsive delivery of doxorubicin. *Biomater. Sci.* 4, 412–417. doi: 10.1039/c5bm00440c

Chen, W. L., Yang, S. D., Li, F., Qu, C. X., Liu, Y., Wang, Y., et al. (2018). Programmed pH/reduction-responsive nanoparticles for efficient delivery of antitumor agents *in vivo*. *Acta Biomater.* 81, 219–230. doi: 10.1016/j.actbio.2018.09.040

Cheng, W., Nie, J. P., Xu, L., Liang, C. Y., Peng, Y. M., Liu, G., et al. (2017). pH-Sensitive delivery vehicle based on folic acid-conjugated polydopamine-modified mesoporous silica nanoparticles for targeted cancer therapy. *ACS Appl. Mater. Interfaces* 9, 18462–18473. doi: 10.1021/acsami.7b02457

Chivers, T., and Laitinen, R. S. (2015). Tellurium: a maverick among the chalcogens. *Chem. Soc. Rev.* 44, 1725–1739. doi: 10.1039/c4cs00434e

Deepagan, V. G., Ko, H., Kwon, S., Rao, N. V., Kim, S. K., Um, W., et al. (2018). Intracellularly activatable nanovasodilators to enhance passive cancer targeting regime. *Nano Lett.* 18, 2637–2644. doi: 10.1021/acs.nanolett.8b00495

Dzienia, A., Maksym, P., Tarnacka, M., Grudzka-Flak, I., Golba, S., Zieba, A., et al. (2017). High pressure water-initiated ring opening polymerization for the synthesis of well-defined α-hydroxy-ω-(carboxylic acid) polycaprolactones. *Green Chem.* 19, 3618–3627. doi: 10.1039/C7GC01748K

El-Sawy, H. S., Al-Abd, A. M., Ahmed, T. A., El-Say, K. M., and Torchilin, V. P. (2018). Stimuli-responsive nano-architecture drug-delivery systems to solid tumor micromilieu: past, present, and future perspectives. *ACS Nano* 12, 10636–10664. doi: 10.1021/acsnano.8b06104

Fang, R., Xu, H., Cao, W., Yang, L., and Zhang, X. (2015). Reactive oxygen species (ROS)-responsive tellurium-containing hyperbranched polymer. *Polym. Chem.* 6, 2817–2821. doi: 10.1039/C5PY00050E

Fang, Y., Xue, J., Gao, S., Lu, A., Yang, D., Jiang, H., et al. (2017). Cleavable PEGylation: a strategy for overcoming the "PEG dilemma" in efficient drug delivery. *Drug Deliv.* 24, 22–32. doi: 10.1080/10717544.2017.1388451

Fathi, M., Zangabad, P. S., Aghanejad, A., Barar, J., Erfan-Niya, H., and Omidi, Y. (2017). Folate-conjugated thermosensitive O-maleoyl modified chitosan micellar nanoparticles for targeted delivery of erlotinib. *Carbohydr. Polym.* 172, 130–141. doi: 10.1016/j.carbpol.2017.05.007

Gabizon, A., Shmeeda, H., Horowitz, A. T., and Zalipsky, S. (2004). Tumor cell targeting of liposome-entrapped drugs with phospholipid-anchored folic acid–PEG conjugates. *Adv. Drug Delivery Rev.* 56, 1177–1192. doi: 10.1016/j.addr.2004.01.011

Han, M. H., Li, Z. T., Bi, D. D., Guo, Y. F., Kuang, H. X., and Wang, X. T. (2016). Novel folate-targeted docetaxel-loaded nanoparticles for tumour targeting: *in vitro and in vivo* evaluation. *RSC Adv.* 6, 64306–64314. doi: 10.1039/C6RA04466B

Han, Q., Wang, Y., Li, X., Peng, R., Li, A., Qian, Z., et al. (2015). Effects of bevacizumab loaded PEG-PCL-PEG hydrogel intracameral application on intraocular pressure after glaucoma filtration surgery. *J. Mater. Sci. Mater. Med.* 26:225. doi: 10.1007/s10856-015-5556-6

Huckaby, J. T., and Lai, S. K. (2018). PEGylation for enhancing nanoparticle diffusion in mucus. *Adv. Drug Deliv. Rev.* 124, 125–139. doi: 10.1016/j.addr.2017.08.010

Jiménez-Balsa, A., Pinto, S., Quartin, E., Lino, M. M., Francisco, V., and Ferreira, L. (2018). Nanoparticles conjugated with photocleavable linkers for the intracellular delivery of biomolecules. *Bioconjugate Chem.* 29, 1485–1489. doi: 10.1021/acs.bioconjchem.7b00820

Kang, Y. J., Chen, Y., and Epstein, P. N. (1996). Suppression of doxorubicin cardiotoxicity by overexpression of catalase in the heart of transgenic mice. *J. Biol. Chem.* 271, 12610–12616. doi: 10.1074/jbc.271.21.12610

Kosmides, A. K., Sidhom, J. W., Fraser, A., Bessell, C. A., and Schneck, J. P. (2017). Dual targeting nanoparticle stimulates the immune system to inhibit tumor growth. *ACS Nano* 11, 5417–5429. doi: 10.1021/acsnano.6b08152

Lazarovits, J., Chen, Y. Y., Sykes, E. A., and Chan, W. C. W. (2015). Nanoparticle–blood interactions: the implications on solid tumour targeting. *Chem. Commun.* 51, 2756–2767. doi: 10.1039/C4CC07644C

Lee, B. Y., Li, Z., Clemens, D. L., Dillon, B. J., Hwang, A. A., Zink, J. I., et al. (2016). Redox-triggered release of moxifloxacin from mesoporous silica nanoparticles functionalized with disulfide snap-tops enhances efficacy against pneumonic tularemia in mice. *Small* 12, 3690–3702. doi: 10.1002/smll.201600892

Li, H., Zhou, X., Yao, D., and Liang, H. (2018). pH-Responsive spherical nucleic acid for intracellular lysosome imaging and an effective drug delivery system. *Chem. Commun.* 54, 3520–3523. doi: 10.1039/C8CC00440D

Li, Y. P., Xiao, K., Luo, J. T., Lee, J., Pan, S. R., and Lam, K. S. (2010). A novel size-tunable nanocarrier system for targeted anticancer drug delivery. *J. Control. Release* 144, 314–323. doi: 10.1016/j.jconrel.2010.02.027

Li, Z. Y., Hu, J. J., Xu, Q., Chen, S., Jia, H. Z., Sun, Y. X., et al. (2015). A redox-responsive drug delivery system based on RGD containing peptide-capped mesoporous silica nanoparticles. *J. Mater. Chem. B* 3, 39–44. doi: 10.1039/C4TB01533A

Liu, Y. X., Zong, Y. H., Yang, Z. X., Luo, M., Li, G. L., Yingsa, W., et al. (2019). Dual-targeted controlled delivery based on folic acid modified pectin-based nanoparticles for combination therapy of liver cancer. *ACS Sustain. Chem. Eng.* 7, 3614–3623. doi: 10.1021/acssuschemeng.8b06586

Ma, X., Wang, M., Wang, H., Zhang, T., Wu, Z., Sutton, M. V., et al. (2019). Development of bispecific NT-PSMA heterodimer for prostate cancer imaging: a potential approach to address tumor heterogeneity. *Bioconjugate Chem.* 30, 1314–1322. doi: 10.1021/acs.bioconjchem.9b00252

Ma, Y., Fan, X., and Li, L. (2016). pH-sensitive polymeric micelles formed by doxorubicin conjugated prodrugs for co-delivery of doxorubicin and paclitaxel. *Carbohydr. Polym.* 137, 19–29. doi: 10.1016/j.carbpol.2015.10.050

Maeda, H., Nakamura, H., and Fang, J. (2013). The EPR effect for macromolecular drug delivery to solid tumors: improvement of tumor uptake, lowering of systemic toxicity, and distinct tumor imaging *in vivo*. *Adv. Drug Deliv. Rev.* 65, 71–79. doi: 10.1016/j.addr.2012.10.002

Maruyama, K. (2011). Intracellular targeting delivery of liposomal drugs to solid tumors based on EPR effects. *Adv. Drug Deliv. Rev.* 63, 161–169. doi: 10.1016/j.addr.2010.09.003

Olson, R. D., and Mushlin, P. S. (1990). Doxorubicin cardiotoxicity: analysis of prevailing hypotheses. *FASEB J.* 4, 3076–3086. doi: 10.1096/fasebj.4.13.2210154

Qu, J., Wang, Q. Y., Chen, K. L., Luo, J. B., Zhou, Q. H., and Lin, J. (2018). Reduction/temperature/pH multi-stimuli responsive core cross-linked polypeptide hybrid micelles for triggered and intracellular drug release. *Colloids Surf. B.* 170, 373–381. doi: 10.1016/j.colsurfb.2018.06.015

Rathinaraj, P., Lee, K., Park, S., and Kang, I. (2015). Targeted images of KB cells using folate-conjugated gold nanoparticles. *Nanoscale Res. Lett.* 10:5. doi: 10.1186/s11671-014-0725-y

Rivankar, S., (2014). An overview of doxorubicin formulations in cancer therapy. *J. Cancer Res. Ther.* 10, 853–858. doi: 10.4103/0973-1482.139267

Sangtani, A., Petryayeva, E., Susumu, K., Oh, E., Huston, A. L., Lasarte-Aragones, G., et al. (2019). Nanoparticle-peptide-drug bioconjugates for unassisted defeat of multidrug resistance in a model cancer cell line. *Bioconjugate Chem.* 30, 525–530. doi: 10.1021/acs.bioconjchem.8b00755

Suh, S., Jo, A., Traore, M. A., Zhan, Y., Coutermarsh-Ott, S. L., Ringel-Scaia, V. M., et al. (2019). Nanoscale bacteria-enabled autonomous drug delivery system (NanoBEADS) enhances intratumoral transport of nanomedicine. *Adv. Sci.* 6:1801309. doi: 10.1002/advs.201801309

Wang, L., Fan, F., Cao, W., and Xu, H. (2015). Ultrasensitive ros-responsive coassemblies of tellurium-containing molecules and phospholipids. *ACS Appl. Mater. Interfaces* 7, 16054–16060. doi: 10.1021/acsami.5b04419

Wang, R., Han, Y., Sun, B., Zhao, Z., Opoku-Damoah, Y., Cheng, H., et al. (2018). Deep tumor penetrating bioparticulates inspired burst intracellular drug release for precision chemo-phototherapy. *Small* 14:e1703110. 10.1002/smll.201703110. doi: 10.1002/smll.201703110

Wang, Y., Zhu, L., Wang, Y., Li, L., Lu, Y., Shen, L., et al. (2016). Ultrasensitive GSH-responsive ditelluride-containing poly(ether-urethane) nanoparticles for

controlled drug release. *ACS Appl. Mater. Interfaces* 8, 35106–35113. doi: 10.1021/acsami.6b14639

Wilhelm, S., Tavares, A. J., Dai, Q., Ohta, S., Audet, J., Dvorak, H. F., et al. (2016). Analysis of nanoparticle delivery to tumours. *Nat. Rev. Mater.* 1:16014. doi: 10.1038/natrevmats.2016.14

Wu, J., Zhao, L., Xu, X., Bertrand, N., Choi, W. I., Yameen, B., et al. (2015). Hydrophobic cysteine poly(disulfide)-based redox-hypersensitive nanoparticle platform for cancer theranostics. *Angew. Chem. Int. Ed. Engl.* 54, 9218–9223. doi: 10.1002/anie.201503863

Xiong, H., Du, S., Ni, J., Zhou, J., and Yao, J. (2016). Mitochondria and nuclei dual-targeted heterogeneous hydroxyapatite nanoparticles for enhancing therapeutic efficacy of doxorubicin. *Biomaterials* 94, 70–83. doi: 10.1016/j.biomaterials.2016.04.004

Yoo, J., Park, C., Yi, G., Lee, D., and Koo, H. (2019). Active targeting strategies using biological ligands for nanoparticle drug delivery systems. *Cancers* 11:E640. doi: 10.3390/cancers11050640

Zhang, P., Zhang, H., He, W., Zhao, D., Song, A., and Luan, Y. (2016). Disulfide-linked amphiphilic polymer-cocetaxel conjugates assembled redox-sensitive micelles for efficient antitumor drug delivery. *Biomacromolecules* 17, 1621–1632. doi: 10.1021/acs.biomac.5b01758

Zhou, M., Wei, W., Chen, X., Xu, X., Zhang, X., and Zhang, X. (2019). pH and redox dual responsive carrier-free anticancer drug nanoparticles for targeted delivery and synergistic therapy. *Nanomedicine* 20:102008. doi: 10.1016/j.nano.2019.04.011

Zhu, L., Kate, P., and Torchilin, V. P. (2012). Matrix metalloprotease 2-responsive multifunctional liposomal nanocarrier for enhanced tumor targeting. *ACS Nano* 6, 3491–3498. doi: 10.1021/nn300524f

Zwicke, G. L., Mansoori, G. A., and Jeffery, C. J. (2012). Utilizing the folate receptor for active targeting of cancer nanotherapeutics. *Nano Rev.* 3:18496. doi: 10.3402/nano.v3i0.18496

Conflict of Interest: The authors declare that the research was conducted in the absence of any commercial or financial relationships that could be construed as a potential conflict of interest.

frontiers in Chemistry

REVIEW
published: 30 July 2020
doi: 10.3389/fchem.2020.00647

Enzyme-Responsive Nanoparticles for Anti-tumor Drug Delivery

*Mengqian Li, Guangkuo Zhao, Wei-Ke Su and Qi Shuai**

Collaborative Innovation Center of Yangtze River Delta Region Green Pharmaceuticals, Zhejiang University of Technology, Hangzhou, China

The past few decades have seen great progress in the exploration of nanoparticles (NPs) as novel tools for cancer treatments and diagnosis. Practical and reliable application of nanoparticle-based technology in clinical transformation remains nevertheless an ongoing challenge. The design, preparation, and evaluation of various smart NPs with specific physicochemical responses in tumor-related physiological conditions have been of great interests in both academic and clinical research. Of particular, smart enzyme-responsive nanoparticles can predictively and selectively react with specific enzymes expressed in tumor tissues, leading to targeted delivery of anti-tumor drugs, reduced systemic toxicity, and improved therapeutic effect. In addition, NPs interact with internal enzymes usually under mild conditions (low temperature, aqueous media, neutral or close to neutral pH) with high efficiency. In this review, recent advances in the past 5 years in enzyme-responsive nanoparticles for anti-tumor drug delivery are summarized and discussed. The following contents are divided based on the different action sites of enzymes toward NPs, notably hydrophobic core, cleavable/uncleavable linker, hydrophilic crown, and targeting ligand. Enzyme-engaged destruction of any component of these delicate nanoparticle structures could result in either targeting drug delivery or controlled drug release.

Keywords: enzyme-responsive, nanomedicine, stimuli-responsive, controlled release, cancer

OPEN ACCESS

Edited by:
Yi Hou,
Beijing University of Technology, China

Reviewed by:
Zihua Wang,
Fujian Medical University, China
Chaoyong Liu,
Beijing University of Chemical Technology, China

****Correspondence:***
Qi Shuai
qshuai@zjut.edu.cn

Specialty section:
This article was submitted to Nanoscience, a section of the journal Frontiers in Chemistry

Received: *29 April 2020*
Accepted: *22 June 2020*
Published: *30 July 2020*

Citation:
Li M, Zhao G, Su W-K and Shuai Q (2020) Enzyme-Responsive Nanoparticles for Anti-tumor Drug Delivery. Front. Chem. 8:647. doi: 10.3389/fchem.2020.00647

INTRODUCTION

Cancer is one of the leading threats to human health and one of the main causes of death worldwide (Siegel et al., 2020). Traditionally, chemotherapy has been given high priority to treat cancer due to its great potential to cure early-stage cancers, as well as its possibility to improve the life quality of patients with advanced cancers. However, conventional chemotherapeutic agents are normally distributed non-specifically in the body and both cancerous and normal cells are affected, leading to serious side effects and compromised therapeutic effects. It is true that the lack of this specificity could be overcome by developing molecular targeted drugs (Ross et al., 2004) but the rapid development of drug resistance during the treatment is still a tough nut (Morgillo and Lee, 2005). In the past few decades, cancer nanotherapeutics have been undergoing rapid development. Among them, nanoparticles (NPs), as novel drug delivery carrier, have been extensively studied to solve the limitations of conventional chemotherapeutics, such as non-specific biodistribution, poor water solubility, low therapeutic

indices, and proneness to drug resistance (Cho et al., 2008). Several therapeutic NPs have been successfully developed and launched on market, including Abraxane® and Doxil® which were, respectively approved for the treatment of metastatic breast cancer and pancreatic cancer (Poveda et al., 2005). In addition, Ontak®, Onivyde®, and DepoCyt® have also been approved by FDA for clinical use (Ventola, 2017), which indicates the bright marketing prospect of therapeutic NPs.

Various types of carriers have been used in cancer nanotherapeutics, including liposomes, polymeric NPs and micelles, metallic NPs, carbon nanotubes, solid lipid NPs, niosomes, and dendrimers (Torchilin, 2014). A wide variety of payloads, such as small molecular drugs, proteins, peptides, nucleic acids, vaccines, antibody, and so on, can be loaded and delivered through physical encapsulation, covalent conjugation, surface attachment or interception (Hans and Lowman, 2002). Diverse formulations based on versatile NPs have been successfully explored to deliver drugs to lymphatic system, brain, arterial wall, lung, liver, spleen, and other organs with long-term circulation and controlled release profile (Hans and Lowman, 2002). Usually, the size of formulated NPs ranges from a few nanometers to several 100 nm, which enables the NPs with passive targeting ability and achieves desired enrichment of payloads in tumor tissues through the enhanced permeability and retention (EPR) effect (Haley and Frenkel, 2008). In addition, with the attachment of targeting ligands or antibodies on the surface of NPs, they are potentially endowed with positive targeting ability (Kamaly et al., 2012). Both of these passive targeting ability and positive targeting ability of NPs are of great importance in reducing the side effects of anti-tumor drugs loaded and improving their therapeutic efficacy. Depending on the specific properties of drugs loaded and the desired delivery pathways, a few strategies for the design and preparation of NPs have been presented. In general, the typical structure of multifunctional, drug-loaded NPs can be roughly illustrated as follows: core (usually hydrophobic), cleavable or not linker, hydrophilic crown, and targeting ligand, as illustrated in **Figure 1**.

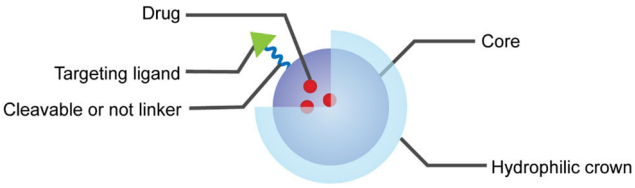

FIGURE 1 | Multifunctional and drug-loaded nanoparticles contain part or all of these components: core (usually loaded with drug), linker, hydrophilic crown, and targeting ligand.

MULTIFUNCTIONAL AND STIMULI-SENSITIVE NANOPARTICULATE DRUG DELIVERY SYSTEM

Different from traditional NPs, stimuli-responsive nanoparticles (SRNPs) have been considered as promising carriers because of their unique bio-responsive physicochemical characteristics and numerous successful applications of SRNPs have been demonstrated. These "smart" SRNPs can react in a predictable and specific way to external or internal stimuli (Karimi et al., 2016), as illustrated in **Figure 2**. In response to a range of endogenous stimuli, such as changes in pH (Lee et al., 2005; Ko et al., 2007, 2010; Lee E. S. et al., 2008; Min et al., 2010; Yang G. B. et al., 2018), hypoxia (Lin et al., 2013; Lee et al., 2017; Ihsanullah et al., 2020), enzyme-specific expression (Lee S. et al., 2008; Lee et al., 2009; Choi et al., 2011, 2014; Zhao et al., 2019), redox state (Li et al., 2012; Shi et al., 2014; Xu et al., 2018), reactive oxygen species (Kim et al., 2014; Deepagan et al., 2016; Yang Z. et al., 2018) in diseased tissues or intracellular compartments, SRNPs undergo changes in molecular structure, solubility, and surface properties, shape and self-association or dissociation behaviors, which can facilitate cellular uptake, improve endosomal escape or trigger either intracellular or extracellular drug release. In addition, SRNPs can also respond to exogenous stimuli, such as laser irradiation (Han et al., 2016) and temperature changes (Kono, 2001; Li et al., 2013; Limmer et al., 2014), to generate an off/on activation of imaging or therapeutic function. Furthermore, well-designed smart nanoparticles can even respond to combinations of multiple stimuli to further improve their specificity for targeted drug delivery and controlled drug release (Cheng et al., 2013; Chen et al., 2020; Hou et al., 2020; Yu et al., 2020). This specificity allows nanoparticles to release their payload precisely in a temporal or spatial pattern in response to specific pathological triggers present in the diseased tissues, which is supposed to reduce side effects, achieve dosing on demand, and increase therapeutic efficacy (Mura et al., 2013).

Among them, enzyme-responsive nanoparticles have been considered as one of the most promising smart stimulus-responsive nanoparticles. First of all, changes in the expression of specific enzymes, such as proteases, phosphatases, and glycosidases, can be observed in tumor or inflammatory regions, which can be exploited to achieve targeted accumulation of drugs at the desired biological location via enzyme-mediated drug release (Mura et al., 2013). For example, it is reported that the expression level of prostate-specific membrane antigen (PSMA, also known as glutamate carboxypeptidase 2) in prostatic cancer cells is 100-fold to 1000-fold to normal prostate epithelial cells (Troyer et al., 1995; Silver et al., 1997; Bostwick et al., 1998; Mannweiler et al., 2009; Maurer et al., 2015). Cathepsin B is overexpressed in various types of cancers including breast, lung, prostate, colorectum, and endometrium (Aggarwal and Sloane, 2014). Moreover, enzymes, as triggers, have many advantages, including high chemical selectivity and substrate specificity (de la Rica et al., 2012), and usually enzyme-catalyzed reactions proceed efficiently under mild conditions (low temperature, aqueous media, neutral or close to neutral pH) (Ulijn, 2006; Hu et al., 2012). For example, phospholipase A2 (sPLA2) can degrade the fatty ester group at the sn-2 position of glycerophospholipids with extremely high selectivity (Dennis et al., 2011). Plasmin can preferentially catalyze the hydrolysis of peptide bonds formed by arginine or lysine (West and Hubbell, 1999; van Dijk et al., 2010). Only at neutral pH, Cathepsin B

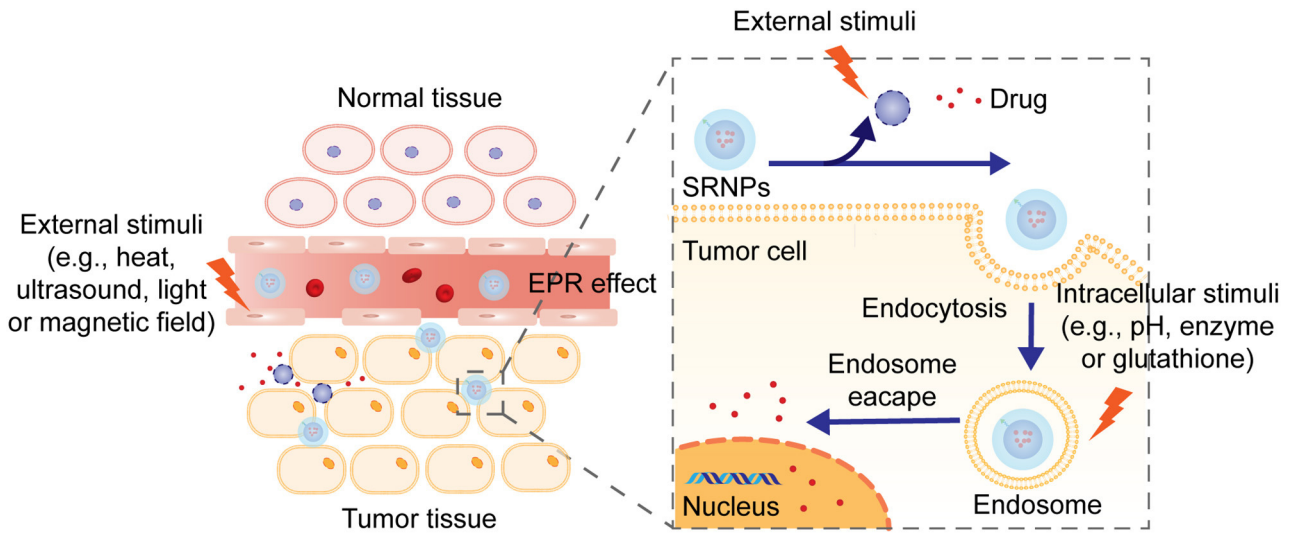

FIGURE 2 | The mechanism of drug release from stimuli-responsive nanoparticles. Nanoparticles penetrate into the tumor tissues through EFR effect or with the assistance of targeting ligands. External or internal stimuli induce structural collapsion of the nanoparticles, which prompts the release of drug at target location.

can act as an endopeptidase and catalyze the hydrolysis of large peptide substrates (Aggarwal and Sloane, 2014). Active tumor-targeting nanoparticles integrated with site-specific enzyme-triggered moieties are able to significantly achieve enhanced accumulation at the tumor site, reduced undesired uptake by non-targeted tissues, as well as site-specific controlled drug release (Allen, 2002).

In this review, we will focus on significant progress in the field of enzyme-responsive nanoparticles for anti-tumor drug delivery in the past 5 years. We will initially introduce the general mechanism for controlling enzyme-responsive drug release from nanoparticles. And then, key examples of drug delivery and disease diagnosis systems based on enzyme-responsive nanoparticles will be presented, which will be organized based on different installation sites of specific enzyme bioactive functionalities on nanoparticles. Critical discussion and an outlook for these systems will also be provided.

GENERAL MECHANISM FOR ENZYME-RESPONSIVE CONTROLLED DRUG RELEASE FROM NPs

In human body, every biological and metabolic process seriously relies on the actions of enzymes. Drug release from NPs in an enzyme-responsive way is origin from the specific enzyme-catalyzed chemical reactions which lead to degradation, dissociation, or morphological transitions of the parent NPs (Torchilin, 2014). In order to achieve controlled release profile of drugs, severe degradation of NPs exposed to enzymes, which usually leads to burst release of drugs, is neither necessary nor preferred. In tumor microenvironment with the presence of specific enzymes, controlled changes in macro-scale structure of NPs usually afford desired controlled release of drugs (Kamaly et al., 2016; Wang et al., 2019).

As we mentioned above, the delicate structure of NPs is normally consisted of four components and decomposition of any component can potentially result in the destruction of integrity of NPs, followed by the release of drugs encapsulated. This lies in the premise for the design of enzyme-responsive nanoparticles and any component is possible to be attached with enzyme-sensitive moiety which is usually a substrate or a substrate mimic of the enzyme. In addition, a second component is responsible for changes in the internal interactions, which can eventually lead to macroscopic transitions and drug release from NPs (Karimi et al., 2016). Principally, depending on the drug delivery and release demand, the action site of enzyme can be located on any component of NPs carriers, as long as it bears enzyme-sensitive functionality. Therefore, the examples in this review will be divided into the following four patterns and discussed in detail.

ENZYME-RESPONSIVE NANOPARTICLES

Nanoparticles With Enzyme-Responsive Core

Within the core of NPs are located the active drugs, which are entrapped via physical interactions or chemical covalent conjugation. Upon the action of enzymes toward functionality installed in the core, the release of drugs can be triggered by changes in structure, such as disintegration, macroscopic deformation, charge switching, breakage of covalent bonds, and so on (Zhou et al., 2019).

One of the most common methods of preparing nanoparticles with enzyme-responsive core is by self-assembly of peptides with enzyme-cleavable sequences or covalent conjugation of proteinase-sensitive peptides to therapeutic or diagnostic agents.

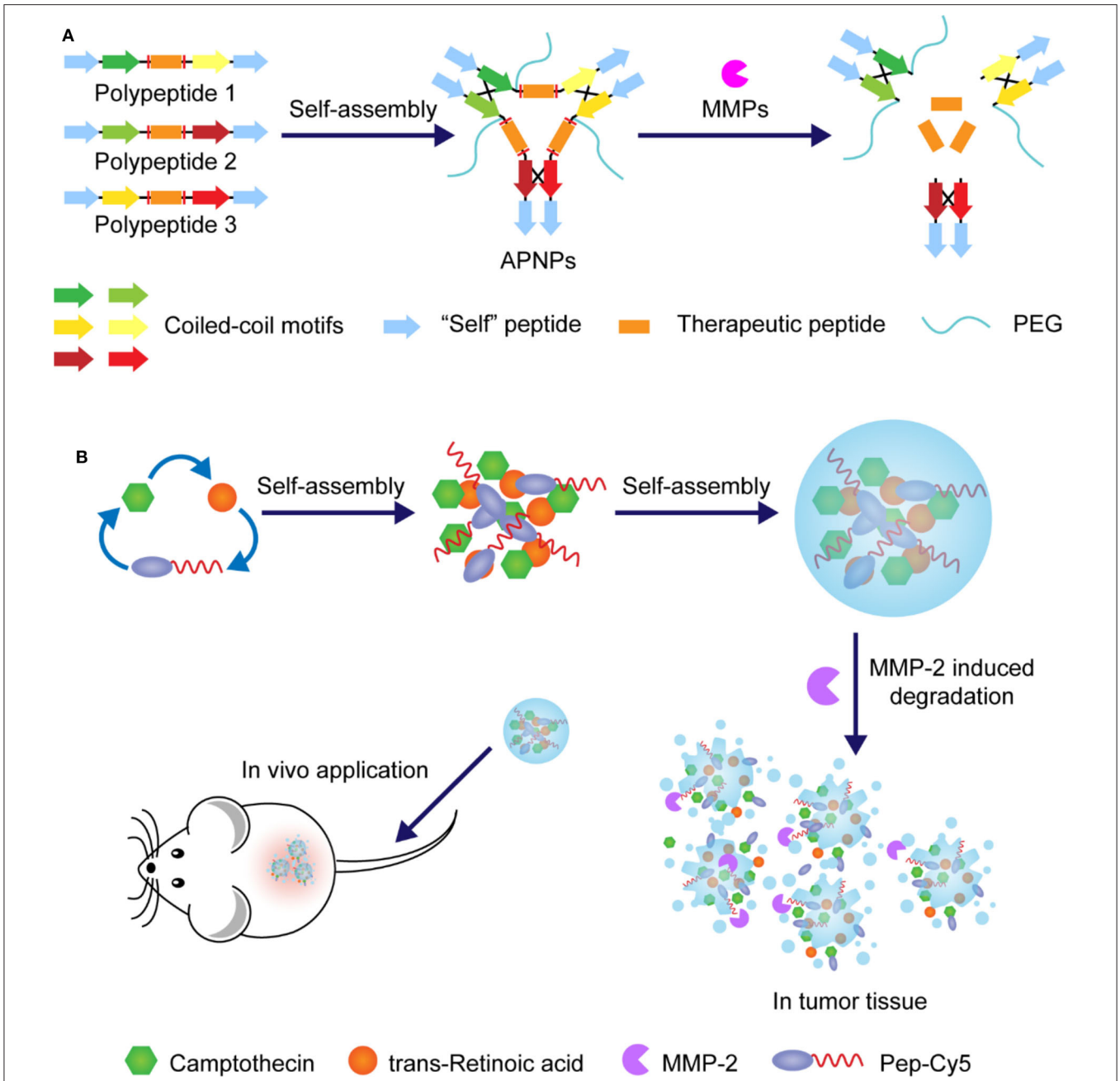

FIGURE 3 | (A) Schematic illustration and action mechanism of APNPs which were self-assembled from protease-sensitive peptides. Therapeutic peptide was released with the hydrolysis of substrate peptides. **(B)** Schematic illustration of preparation of nanoparticles through assembly of amphipathic Pep-Cy5 with two hydrophobic drugs and disintegration under the action of MMP-2.

In this case, matrix metalloproteinases (MMPs), a family of over 20 calcium-dependent zinc-containing proteinases, have been demonstrated the ability to catalyze the core degradation of peptide-based NPs. Among them, MMP-2 and MMP-9 are of particular importance for the development of enzyme-responsive anti-tumor drug delivery systems due to their proved correlation with cancer cell invasion and metastasis formation (Egeblad and Werb, 2002; Yoon et al., 2003). For example, Zhou and coworkers developed novel enzyme-responsive activatable protein nanoparticles (APNPs) for the targeting delivery of therapeutic peptides (Yu et al., 2018). In this study, the core of these PEG-coated APNPs was constructed by self-assembly of peptides embedded with therapeutic peptides and activatable toward proteases with high expression levels in the microenvironment of diseased tissues, as illustrated in **Figure 3A**. It was designed to achieve extended circulation time *in vivo*,

reduced systemic toxicity, targeted delivery, and controlled release of therapeutic peptides. Melittin (Mel), a promising anticancer agent as cargo, was used to evaluate this delivery platform, in which the peptides were specifically engineered with MMP-responsive PLGLAG sequences. It was demonstrated that, compared with free melittin, these finely tuned Mel-APNPs exhibited limited toxicity. However, desired comparable cytotoxicity was observed after exposure to MMP-2 due to the enzyme-triggered release of active melittin from Mel-APNPs. These delicate Mel-APNPs were further upgraded to TfR-Mel-APNPs with targeting ability. Targeted delivery and controlled release of melittin *in vivo* were successfully achieved, making clinical transformation of these therapeutic peptides possible.

Similarly, in one case, the MMP-2 cleavable peptide sequence GPLGVRGE was attached to hydrophobic near-infrared dye Cy5, affording an amphiphilic multifunctional molecule Pep-Cy5 (Yang et al., 2016). Through self-assembling, this belt-shaped amphiphilic molecule would form water-soluble nanoparticles with hydrophobic anti-tumor drugs that could be a combination of different drugs, making it potential for synergistic administration, as illustrated in **Figure 3B**. In this study, anti-tumor drugs camptothecin and trans-retinoic acid were cooperatively entrapped in enzyme-responsive NPs, which exhibited a desired MMP-2-triggered degradation process and achieved reduced side effects, enhanced intertumoral accumulation, and improved anti-tumor efficacy.

In another case, Zhang et al. reported an immunotherapy strategy for triple-negative breast cancer based on enzyme-responsive and structure-transformable nanoparticles, as illustrated in **Figure 4A** (Xu et al., 2019). Firstly, peptides containing anti-tumor agents cisplatin (Pt) and adjudin (ADD) and MMP-2-recognizable sequences were synthesized and then self-assembled into spherical nanoparticles with diameters less than 100 nm. It was demonstrated that after accumulation in the tumor bed with overexpressed MMP-2, these spherical nanoparticles underwent structural transformation into rod-like nanoparticles with prolonged drug retention time and deep tumor penetration capability. In addition, by adding WKYMV (a kind of FPR-1 agonist), further development of MMP-2-responsive NPs with three active components and additional hydrophilic PEG chains was realized, and similar structural changes from sphere to rod were observed. Remarkably, this enhanced version of nano-platform exhibited further improved antitumor immunity by synergistic activation and promotion of immunogenic cell death.

Like MMP, overexpression of proteinase for albumin catabolism in tumors has also been approved, which can be utilized to design proteinase-responsive NPs for antitumor drug delivery. For example, Zhang N. et al. (2016) developed a proteinase K involved multi-triggered nanoparticles based on human serum albumin, which was successfully applied for photodynamic tumor ablation. In this study, human serum albumin was used with synthetic polypeptide poly-L-lysine to prepare nanoparticles via electrostatic assembly and PEG was attached onto the surface of NPs, as illustrated in **Figure 4B**. The *in vitro* triggered release profile of photosensitizer Chlorin e6 from these NPs was evaluated in PBS solutions, which indicated that, compared with other stimuli, proteinase K significantly promoted the release of Chlorin e6 due to the accelerated degradation of NPs. Interestingly, the presence of combined multiple triggers including pH, glutathione (GSH) and proteinase K exhibited the fast release rate of Chlorin e6.

As a number of strategies have emerged to explore enzymes closely associated with specific diseases for biomedical applications, together with the high intrinsic complexity of enzyme-responsive NPs and subtle interactions between these delivery systems and diseased cells, it is quite necessary to establish a general mode for the rational design of enzyme-responsive delivery systems. As we mentioned above, MMPs are among those enzymes with top interest to researchers. Especially, MMP-9 was drawn from a cross-section of MMPs by Ulijn (2006), who presented guidance for the design of a customizable peptide-based NPs with excellent therapeutic effects (Son et al., 2019). They started with the design of peptide amphiphiles with ionic hydrophilic section, MMP-9-cleavable section and hydrophobic section. And then, they systemically studied the compatibility of the cleavable section with the entire nanoparticle system, the susceptibility of the nanoparticle to the scissor MMP-2, and the relationships between the morphology of the nanoparticle pre- and post-cleavage and its pharmacodynamic effects. Eventually, they demonstrated that surface charge, supramolecular organization and enzyme specificity of peptide-based nanoparticles could be customized by switching a few amino acids in the peptide sequences.

Nanoparticles With Enzyme-Responsive Crown

Surface modification of nanoparticles with hydrophilic moieties is usually essential for its applications in drug delivery, in order to increase water-solubility, prevent drug leakage, avoid reorganization by the reticuloendothelial system (RES), improve interactions with cells, and facilitate cellular uptake. A wide range of materials with high hydrophilicity have been investigated, among which proteins or peptides, hyaluronic acid (HA), and synthetic polymers cross-linked by peptides are of great interest for the development of NPs with enzyme-responsive crown. Ideally, this hydrophilic auxiliary of NPs is supposed to slip off after the NPs reach the targeting action sites and facilitate the release of active drugs encapsulated. In this way, it will be highly desired for the development of enzyme-triggered deshielding approaches due to the close association of enzymes with specific diseases, especially tumors.

Enzyme-cleavable peptides are of high priority for this consideration. For example, Callmann et al. (2015) successfully constructed amphiphilic block copolymers via ring-opening polymerization of norbornene analogs, which were functionalized with hydrophobic paclitaxel and hydrophilic MMP-responsive peptide (GPLGLAGGERDG) via biodegradable ester bonds and amide bonds, respectively. The resulting amphiphilic block copolymers assembled into micellar nanoparticles coated with hydrophilic peptides which were cleaved upon exposure to MMP presented in the diseased tissue, as illustrated in **Figure 5A**. As a result, the open hydrophobic

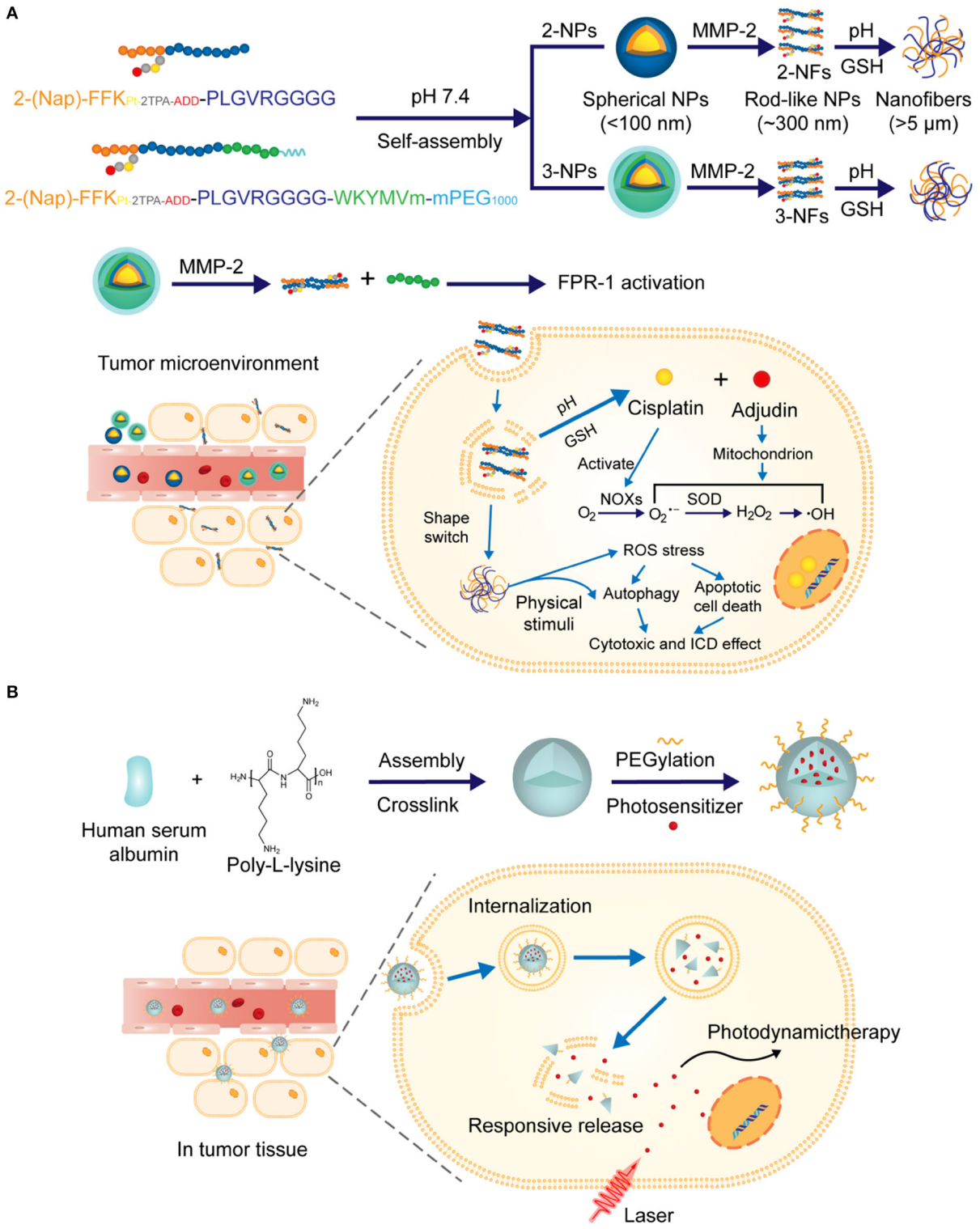

FIGURE 4 | (A) Schematic illustration of the construction of nanoparticles capable of structural transformation activated by MMP-2 in tumor microenvironment. Rod-shaped particles were uptaken by the cell and drugs were released under the trigger of pH change and GSH. **(B)** Schematic illustration of construction of the nanoparticles via electrostatic assembly from proteinase substrate human serum albumin and poly-L-lysine. Photosensitizer was released under combined multiple triggers including proteinase K.

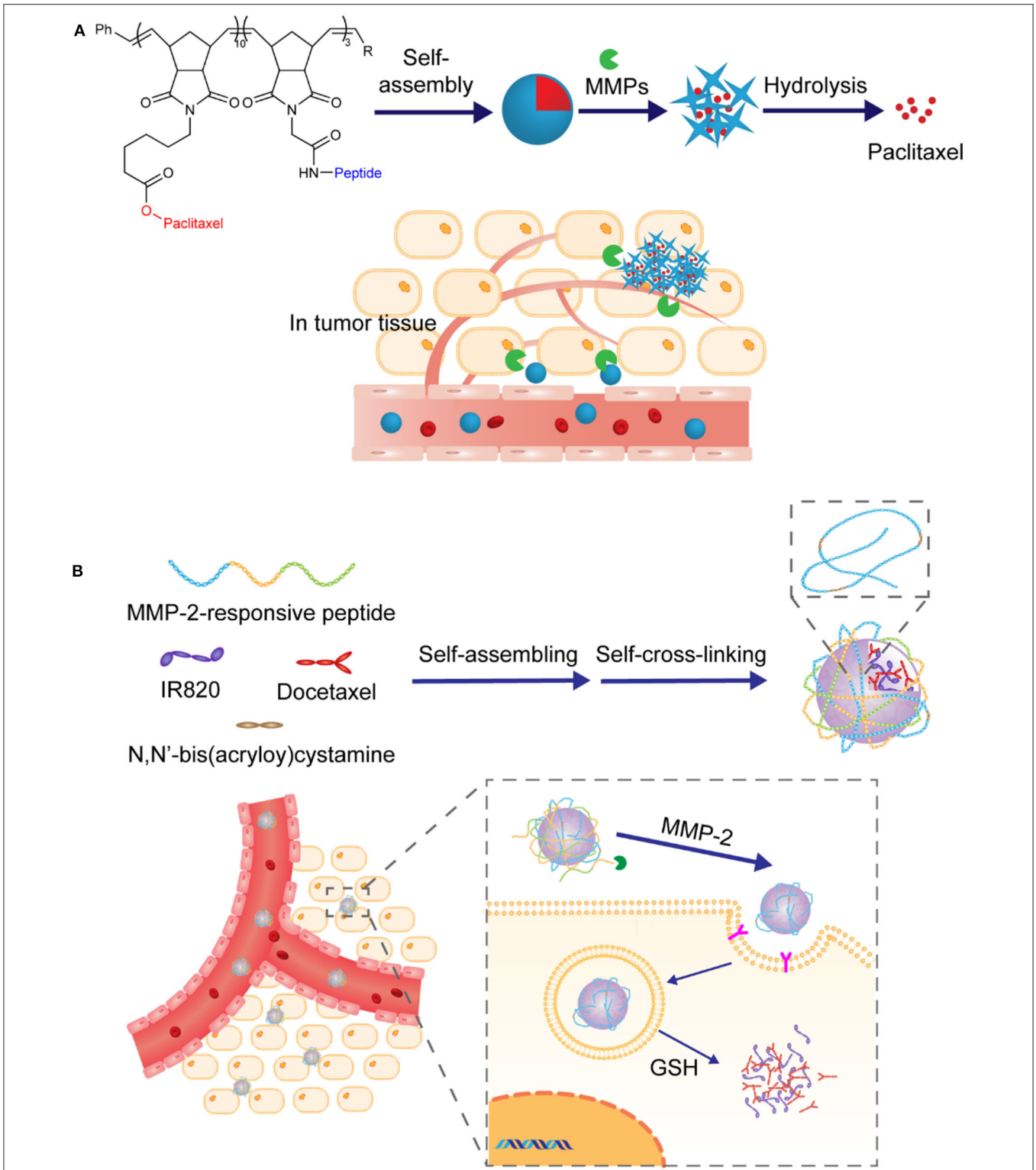

FIGURE 5 | (A) Schematic illustration of nanoparticles prepared via self-assembling of amphiphilic block copolymers and drug release in response to MMPs. **(B)** Schematic illustration of the preparation of hybrid nanoparticles via assembly and self-cross-linking formation. Drugs were released in response to MMP-2 and GSH-triggered degradation of crown.

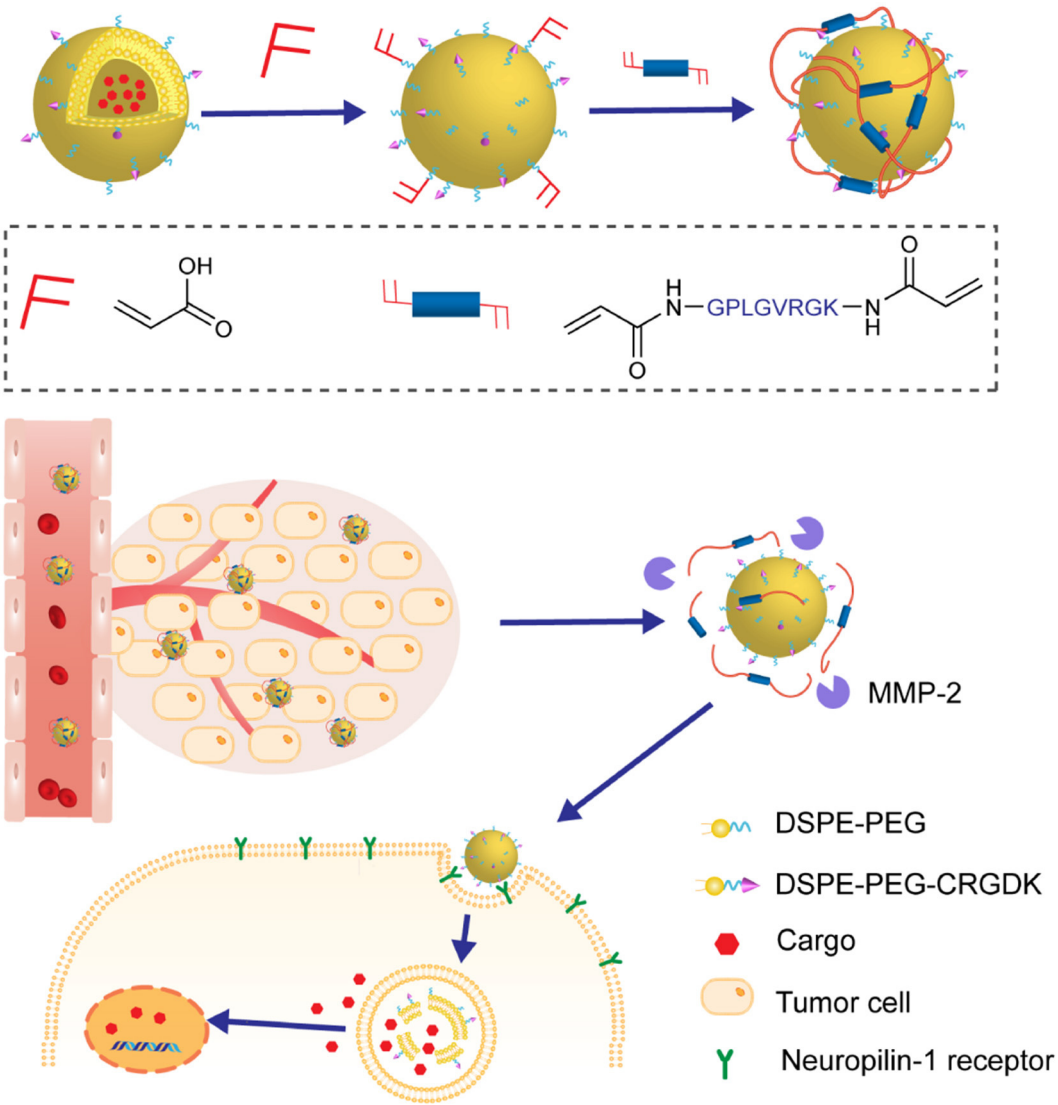

FIGURE 6 | The nanoparticles were composed of nanovesicles as core and MMP-2 responsive polymeric network as crown. The crown disassembled in the tumor microenvironment, enhancing the penetration and internalization of nanovesicles.

core turned accessible to hydrolysis and the active paclitaxel was effectively released, leading to enhanced accumulation of drugs and improved therapeutic efficacy. Moreover, in another case, the peptide-based crown was further stabilized by forming a cross-linking network structure without interference of its enzyme-sensitivity (Peng et al., 2019). In this study, the peptides with MMP-2-cleavable sequence in the middle were cross-linked by *N, N′*-bis (acryloyl) cystamine, as shown in **Figure 5B**. This was proved to be crucial for high drug loading capacity of these NPs and enhanced penetration due to the presence of additional GSH-responsive disulfide bonds.

Instead of being composed entirely of peptides, the crown can also be consisted of synthetic hydrophilic polymers cross-linked by enzyme-cleavable peptides. In this way, triggered-release of drugs could be achieved via partial degradation of polymeric crown. Chen et al. reported a delivery platform based on nanoparticles bearing synthetic PEGs as hydrophilic crown. It was further functionalized with MMP-2 responsive peptides GPLGVRGK and tumor-targeting ligand CRGDK peptides, as illustrated in **Figure 6** (Liu et al., 2015). The presence of PEGs was supposed to extend the circulation time in blood and the installation of GPLGVRGK peptides was designed to provide additional prevention from undesired drug leakage and enzyme-triggering sites. The nanoparticles accumulated in the tumor location through the EPR effect, followed by the breakage of the crown in response to the over-expressed MMP-2 in the tumor microenvironment. With the navigation effect of the tumor-targeting ligand CRGDK peptide, enhanced deep-tissue penetration and cellular internalization were achieved, which significantly improved the therapeutic efficacy.

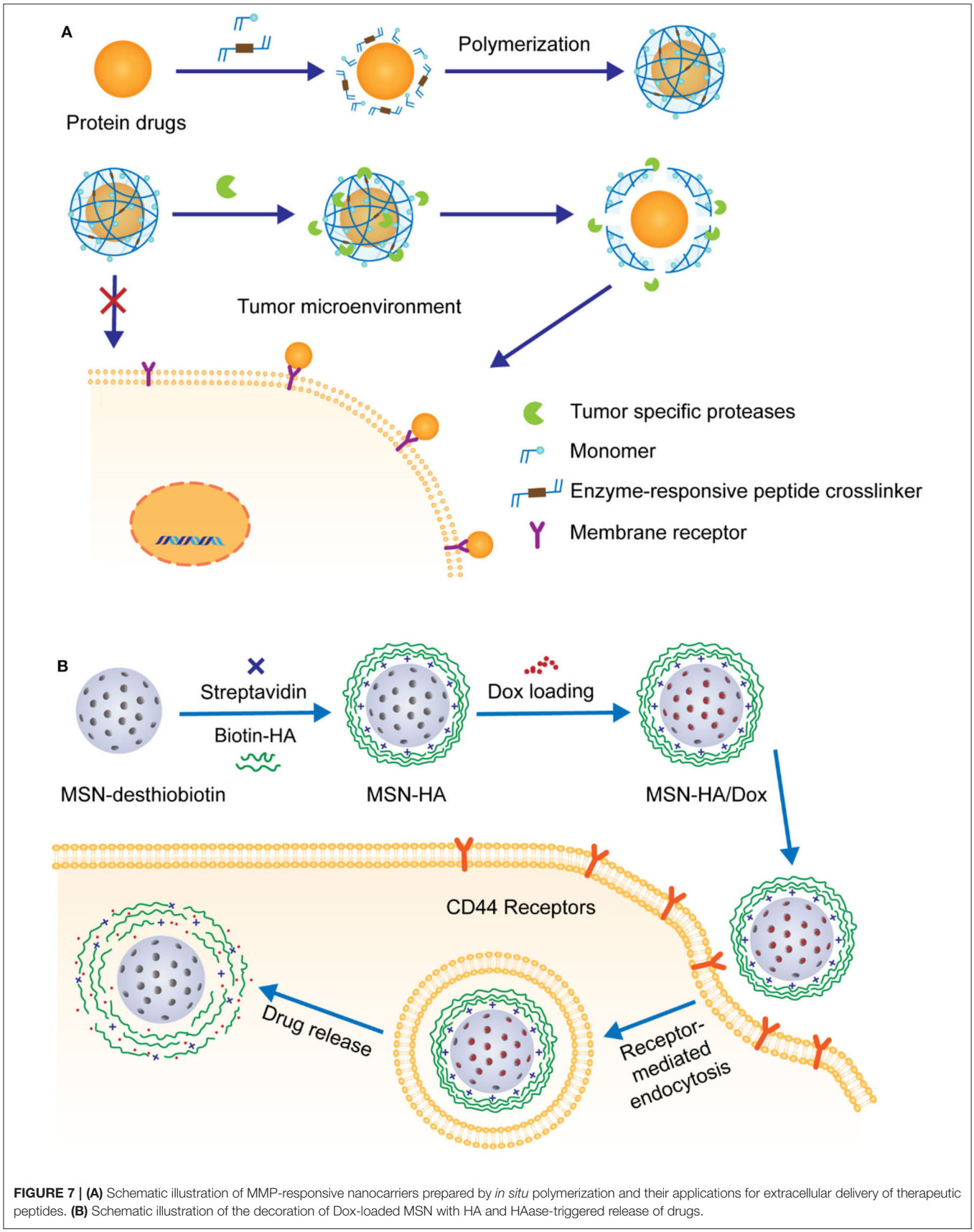

FIGURE 7 | (A) Schematic illustration of MMP-responsive nanocarriers prepared by *in situ* polymerization and their applications for extracellular delivery of therapeutic peptides. **(B)** Schematic illustration of the decoration of Dox-loaded MSN with HA and HAase-triggered release of drugs.

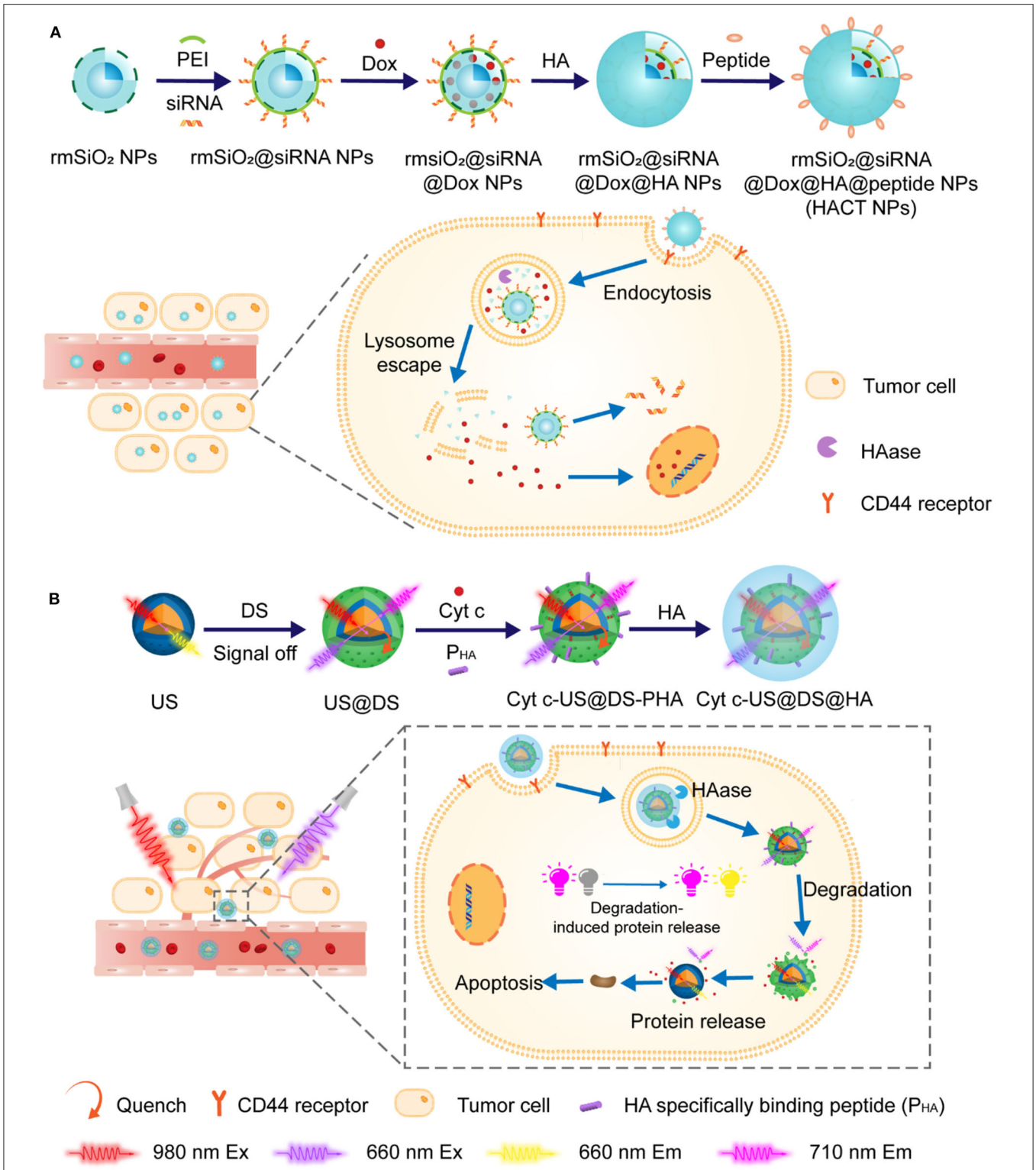

FIGURE 8 | (A) Schematic illustration of the construction of HACT NPs through "layer-by-layer assembly" strategy. HA crown decorated with peptides allowed pinpointed delivery of siRNAs along with Dox. **(B)** Schematic strategy of using outer-frame-degradable nanovehicles with NIR dual luminescence to monitor the biological distribution of nanoparticles and the release of therapeutic proteins.

Different from being active in diseased cells, extracellularly functional protein drugs with high safety and excellent specificity have recently emerged as important alternatives for clinical applications. However, like other protein-based drugs, the intrinsic fragility and susceptibility of these drugs to complex *in vivo* conditions make their clinical practice formidable. And thus, it is highly desirable to develop weakly cell-interacted, nanosized, and enzyme-responsive NPs. Lu and coworkers have developed a mild *in situ* polymerization process to construct nano delivery platforms of protein drugs with controllable enzyme-response capabilities, as shown in **Figure 7A**. In 2015, they reported the fabrication of nanocapsules with plasmin-responsive crown via *in situ* polymerization (Zhu et al., 2015). The monomers contained peptide linkages made from different enantiomers of amino acids. Spatiotemporal control of these nanocapsules in response to plasmin could be achieved by changing the chirality of peptide linkages in the crown. In their follow-up study, MMP-2-responsive peptides with highly hydrophilic zwitterionic phosphorylcholine were utilized to modify the crown of NPs (Li et al., 2019). By optimizing the filling rate of phosphorylcholine in crown, the interaction between NPs and cells could be effectively weakened and thus the undesired internalization by tumor cells and the loss of enzyme-recognizable peptides could be avoided. Recently, this platform was further improved to deliver monoclonal antibodies for brain tumor treatment (Han et al., 2019). In this case, the crown of nanocapsules was constructed via *in situ* polymerization of 2-methacryloyloxyethyl phosphorylcholine (MPC) and MMP-2-cleavable peptide crosslinker.

Recently, HA has been frequently reported due to its potential multiple roles in the development of anti-tumor therapy. First of all, similar as PEG, the high hydrophilicity, non-toxicity, and biodegradability of HA make it ideal for the coating of anti-tumor drug delivery NPs. In addition, it has been demonstrated that HA is of strong and specific targeting ability toward CD44, a transmembrane glycoprotein overexpressed on various tumor cells. Furthermore, HA is composed of enzyme-degradable N-acetylglucosamine and D-glucuronic acid disaccharide units, rendering it a good candidate for fabricating NPs with hyaluronidase (HAase)-responsive crown. For example, Zhang and coworkers prepared mesoporous silica nanoparticle (MSN)-based delivery vehicles coated with biotin-modified HA, achieving targeted delivery and controlled release of anti-tumor agent doxorubicin hydrochloride (Dox) in the tumor cells with overexpression of HAase, as shown in **Figure 7B** (Zhang M. Z. et al., 2016). The benefit of this enzyme-responsive strategy was approved by *in vitro* analyses, which showed that the simultaneous

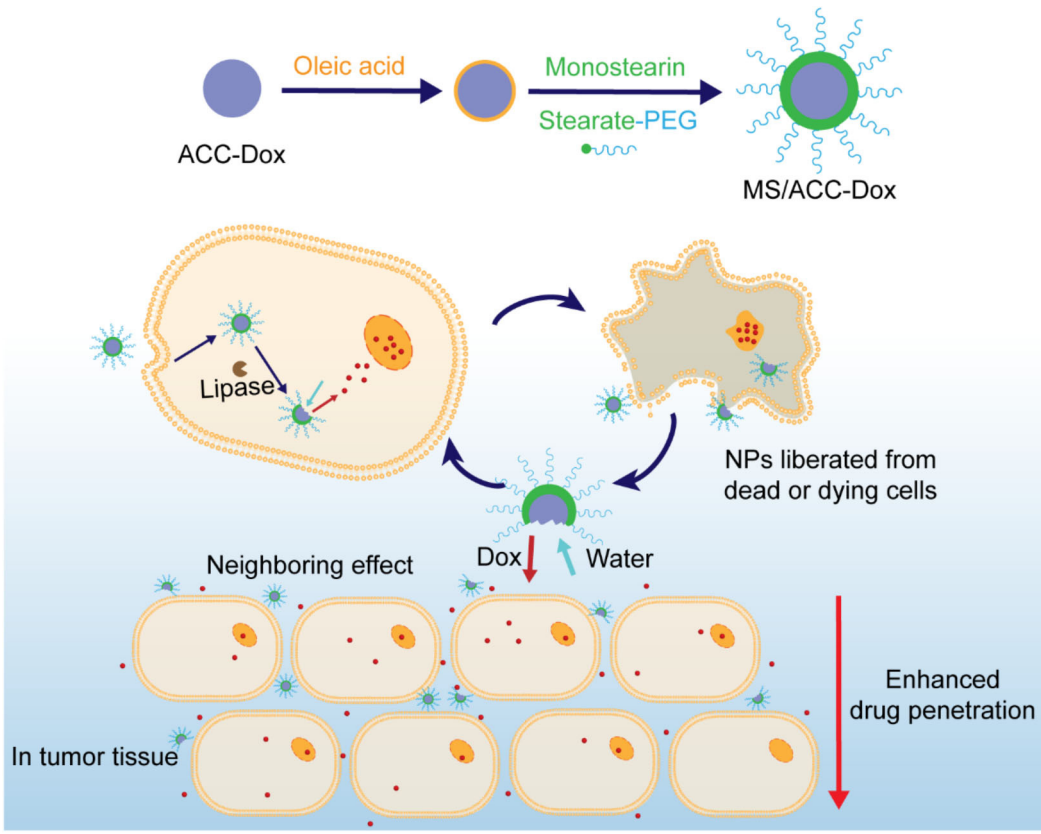

FIGURE 9 | Schematic illustration of the decoration of water-sensitive and Dox-loaded ACC with lipase-responsive monostearin. Drugs were released under the trigger of lipase and water.

presence of biotin and HAase significantly facilitated the release of Dox.

In another study by Min group, similar MSN with a hallow and rattle structure ($rmSiO_2$ NPs) were utilized for the codelivery of siRNAs and Dox in an enzyme-responsive fashion (Ding et al., 2017). In order to effectively load both hydrophilic negatively charged siRNAs and hydrophobic Dox, a "layer-by-layer assembly" strategy was adapted for the fabrication of NPs with HA on the top surface. These NPs were further functionalized with breast tumor cell homing and penetrating-peptide PEGA-pVEC, as illustrated in **Figure 8A**. The resulting novel NPs with cascade targeting capabilities showed enhanced selective accumulation in tumor microenvironment and HAase-triggered controllable release of drugs in the targeted tumor cells. As more and more NPs with therapeutic proteins or peptides as payloads have been exploited for tumor treatment, it is urgent to fully reveal the mechanism and pharmacological efficacies in tumor therapy via real-time tracking of therapeutic proteins. For this reason, the same group artfully designed and prepared an outer-frame-degradable nanovehicle by coupling upconversion nanoparticles (UNCPs) with fluorophore-doped macroporous silica (DS). It was finally coated with enzyme-responsive HA crown, as illustrated in **Figure 8B** (Zhang et al., 2019). As expected, *in vitro* and *in vivo* evaluation demonstrated that both biodistribution of nanovehicles and the HAase-induced release of protein could be visually monitored at different NIR fluorescence channels. Interestingly, in addition to be a monitoring platform, this nanovehicles with cytochrome loaded also showed excellent anti-tumor therapeutic efficacy.

Quite similar to HAase-responsive HA/MSN nanodelivery systems discussed above, lipase-triggered monostearin/amorphous calcium carbonate (MS/ACC) NPs loaded with Dox have been reported by Wang et al. (2018), as shown in **Figure 9**. In this case, a new kind of enzyme-responsive combination MS/lipase has been introduced, along with protein or peptide/protease and HA/HAase. It is noteworthy that the MS/ACC NPs exhibited additional water-sensitivity due to the high degradability of ACC in aqueous media, which proved to be crucial to induce a neighboring effect and enhance drug penetration. With Dox loaded, MS/ACC-Dox nanoparticles showed a significant effect on inhibiting tumor growth on SKOV3 xenografted nude mice.

Nanoparticles With Enzyme-Responsive Linker

Normally, cleavable linkers are an essential component of NPs. They can be utilized to attach drugs to the hydrophobic core, or connect hydrophobic core with hydrophilic crown, or modify the hydrophilic surface with targeting ligands. Ideal cleavable linkers should ensure the auxiliary of NPs remains attached

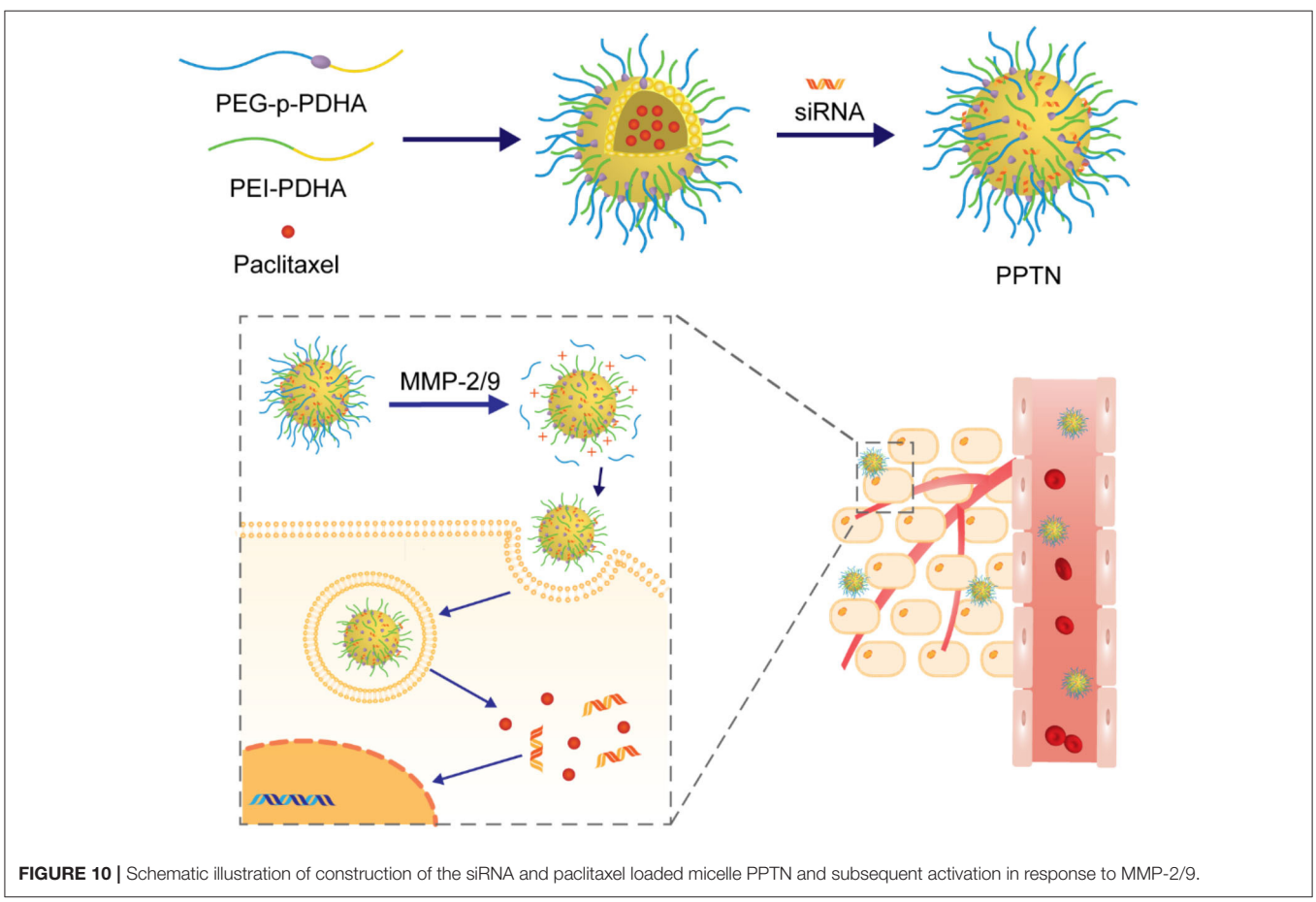

FIGURE 10 | Schematic illustration of construction of the siRNA and paclitaxel loaded micelle PPTN and subsequent activation in response to MMP-2/9.

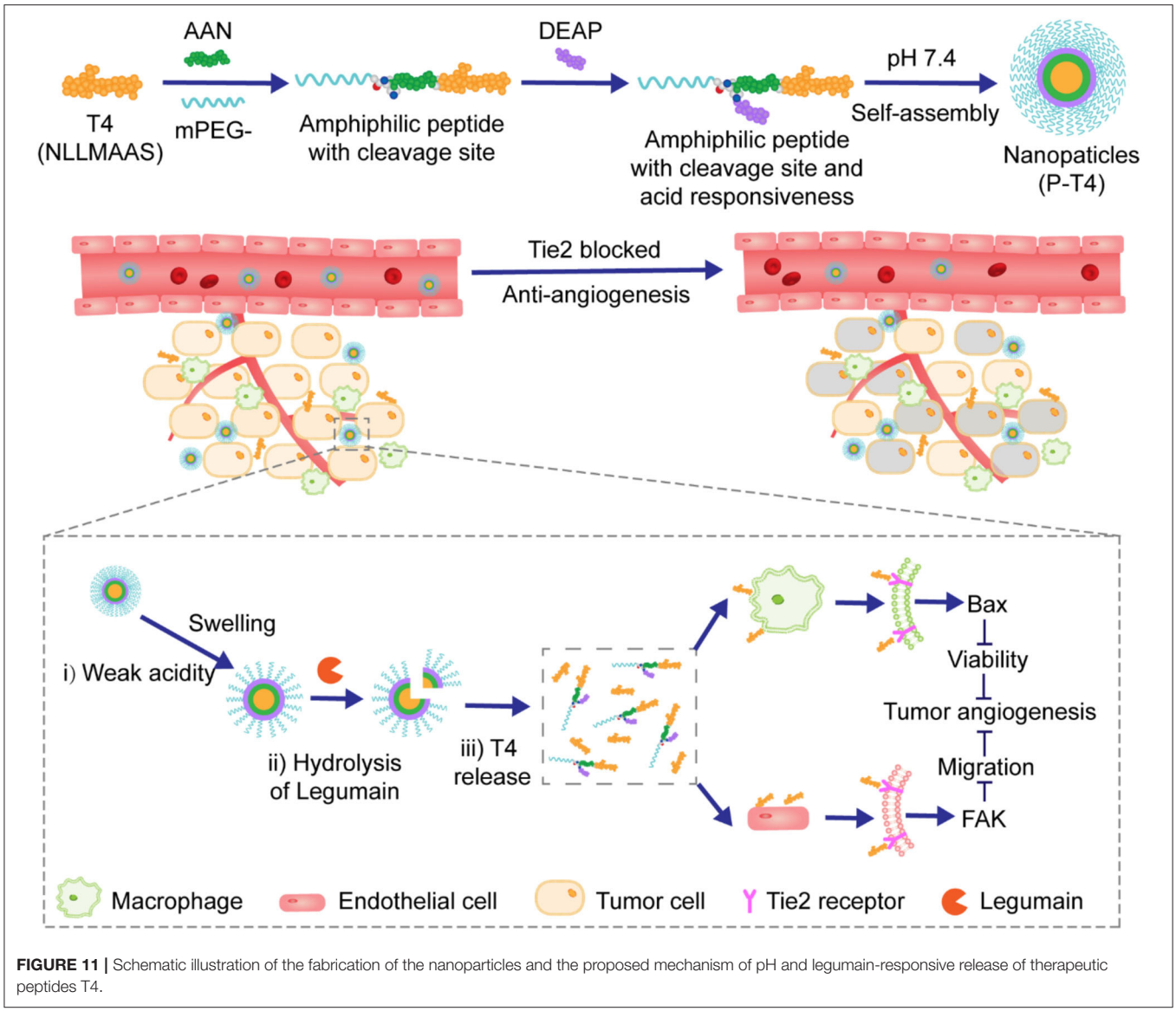

FIGURE 11 | Schematic illustration of the fabrication of the nanoparticles and the proposed mechanism of pH and legumain-responsive release of therapeutic peptides T4.

during circulation but cleaves rapidly after NPs reach the targeting action sites. It is desirable if the cleavable-linker can be endowed with enzyme-responsive capability (Bohme and Beck-Sickinger, 2015). In this context, peptides with specific protease responsibility are considered as the most common candidates for fabricating NPs with enzyme-responsive linkers.

MMPs are among the most studied proteases for applications in antitumor drug delivery systems and some cases with MMP-degradable peptides as linkers have been reported. For example, Yin and coworkers designed and prepared a nanoparticle with highly hydrophilic PEG as cationic charge shielding surface. It was attached to active agents-loaded core via an MMP-degradable peptide linker Pro-Leu-Gly-Leu-Ala-Gly (PLGLAG), as illustrated in **Figure 10** (Tang et al., 2016). In this study, it was demonstrated that these long circulating NPs could be passively localized in the tumor tissues via the EPR effect. In the presence of PLGLAG-sensitive MMP-2/9, the PEG layer fell off and the resulting exposure of positive charges promoted the uptake of NPs by the tumor cells. In another study, NPs fabricated in a similar way was reported by Zhang et al. (2019). In this approach, fragile hydrophobic therapeutic small peptides T4 (NLLMAAS) were rationally modified with PEG via an enzyme-responsive linker of amino acid sequence AAN, as illustrated in **Figure 11**. The linker is cleavable in tumor cells and tumor-related microenvironment with overexpression of cysteine protease legumain.

Like silica-and calcium carbonate-based nanoparticles, inorganic quantum dots (QDs) have also been explored as platforms for drug delivery, for which surface modification with hydrophilic motifs are deemed essential. Jin et al. reported CdSe/ZnS QDs-based NPs for the delivery of anti-pancreatic cancer therapeutic gemcitabine (GEM) (Han et al., 2017). In

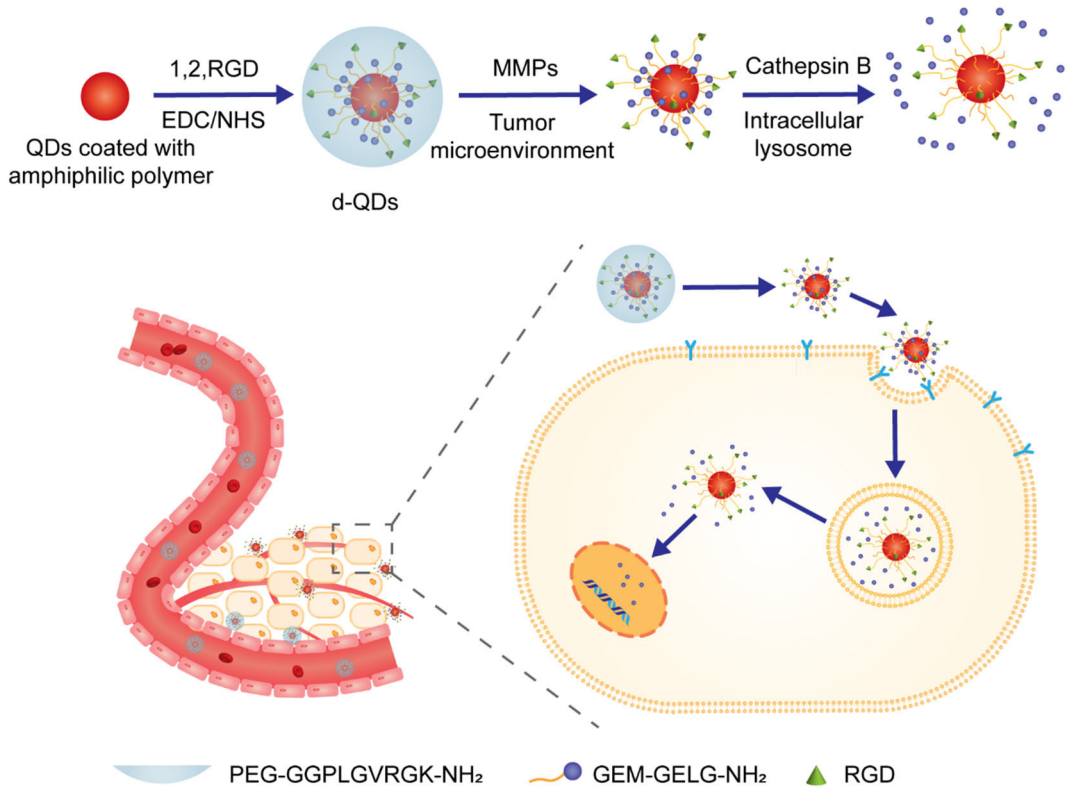

FIGURE 12 | Schematic illustration of preparation of QDs-based nanoparticles and their enzyme-triggered behavior.

this study, commonly used PEG was utilized to decorate the surface of QDs through the linkage of MMP-9 substrate peptide GGPLGVRGK. In addition, a second cathepsin B-sensitive peptide linker GFLG was installed between QDs and GEM, as illustrated in **Figure 12**. It is well demonstrated that MMP-9 is overexpressed in the pancreatic tumor microenvironment while cathepsin B is up-regulated in the pancreatic tumor cells. This novel NPs delivery system with two sequential enzyme-responsive linkers showed enhanced accumulation of the activated form of GEM, reduced side effects, and superior tumor suppression ability.

MSN-based drug delivery systems have also been successfully modified with enzyme-responsive peptide linkers. van Rijt et al. developed a novel approach for controllable release of anti-tumor therapeutics mediated by MMP-9 (van Rijt et al., 2015). Firstly, the external surface of the MSNs was coated with biotins via heptapeptide linkers, which bear MMP-9-recognizable and cleavable sequence RSWMGLP. After loading therapeutics, the outer surface of the NPs was readily covered with hydrophilic avidins which are of high affinity for biotins, as shown in **Figure 13A**. The resulting well-armed NPs induced significant apoptosis of tumor cells in lung tumor regions of mice, while showing non-toxicity in tumor-free tissues or in healthy mice.

Another interesting example involving MSNs was presented by Gayam et al. (2016). In this study, a new kind of enzyme-responsive combination quinone/quinone oxidoreductase 1 (NQO1) was introduced and utilized for the design of enzyme-triggered drug delivery system, because overexpression of NQO1 in several human tumor cells has been demonstrated. Strictly speaking, it is not the enzyme-stimuli cleavage of linker that directly leads to the release of drugs. In this case, as illustrated in **Figure 13B**, the Dox loaded in MSNs was capped by an α-cyclodextrin with a stalk going through. The end of the stalk was functionalized with a benzoquinone, which acts both as a stopper to lock the α-cyclodextrin and a reactive site toward NQO1/NADH. Interestingly, in the presence of NQO1, the stopper benzoquinone was reduced to hydroquinone, followed by self-cleavage from the stalk. As a result, the gatekeeper α-cyclodextrin was freed and thus DOX was released. This delicate drug delivery system successfully avoided the premature release of drugs.

Nanoparticles With Enzyme-Responsive Ligand

In order to achieve precise delivery of anti-tumor drugs and provide with personalized medicine due to the high heterogeneity degree of tumor cells, the strategy to arm the delivery vehicle with a targeting ligand has been accepted and implemented. The design and selection of targeting ligands mostly depend on the receptors overexpressed in diseased tissues. In current clinical studies, a wide variety of targeting ligands have emerged. Peptides

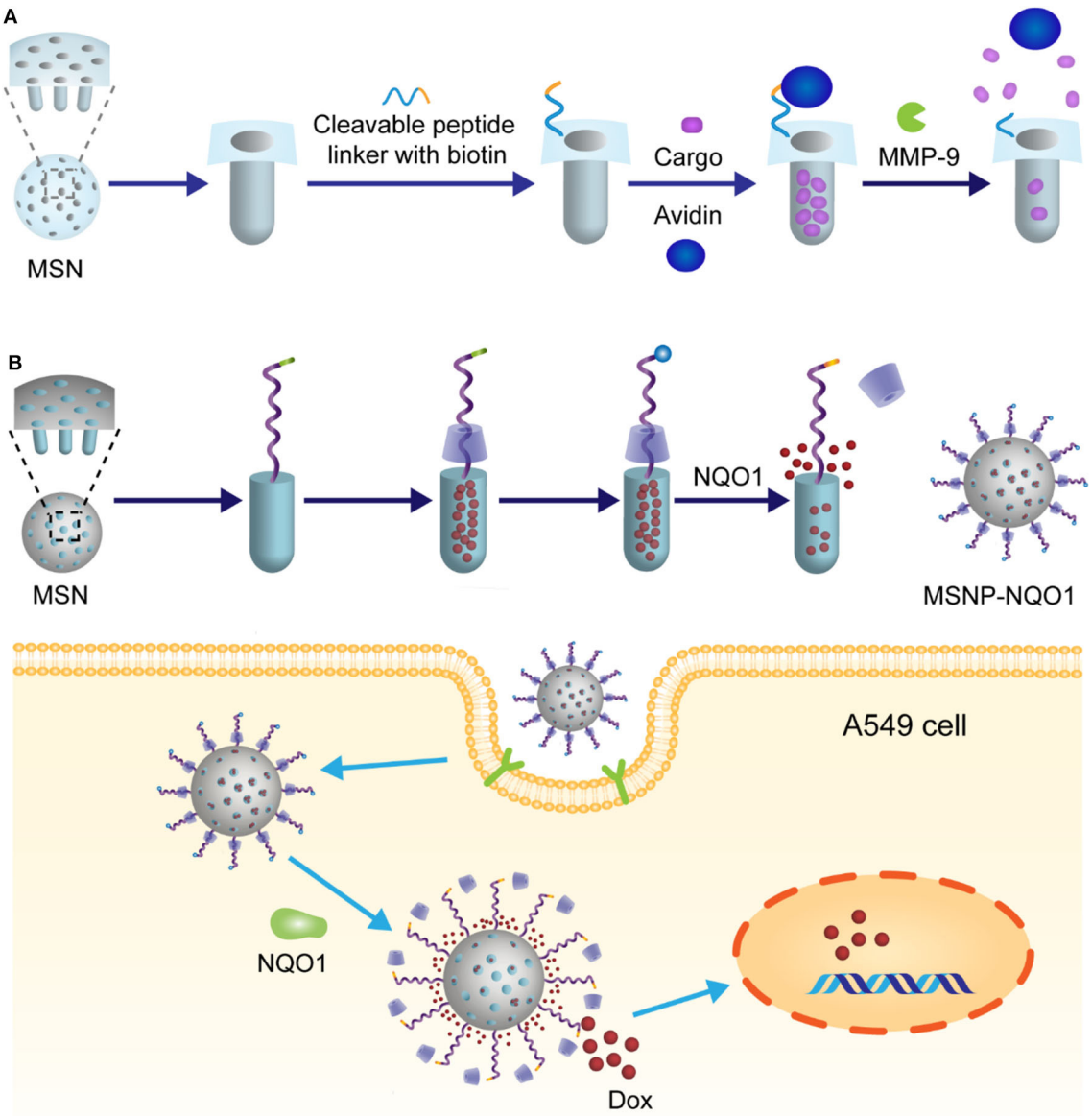

FIGURE 13 | (A) Schematic illustration of MMP-9 mediated release of MSN nanoparticles. In this system, controlled release of the drug was achieved through avidin linker which was used to cover the surface with MMP-9 substrate peptides. **(B)** Schematic illustration of MSN nanoparticles and their NQO1 triggered release mechanism.

and HA play important roles in the development of targeting ligands with enzyme-responsive ability.

Non-specific interactions of NPs with healthy tissues can be largely avoided by using enzyme-responsive materials as targeting ligands, as ligand-guided dynamic activities will occur only when NPs are exposed to specific tumor microenvironments. The aggregation guided by enzyme-responsive ligand has great importance in facilitating the penetration of NPs through the blood-brain barrier and enhancing retention of NPs in brain tumors. For example, Gao et al. developed gold nanoparticles (AuNPs) capable of aggregating in brain tumor cells with overexpression of legumain (Ruan et al., 2016). This nanoplatform was comprised of two kinds of AuNPs with different ligands, as illustrated in **Figure 14**. One ligand was designed to be legumain-specific substrate which could expose its 1,2-thiolamino groups via legumain-catalyzed hydrolysis. The other one bearing cyano groups would readily react with the 1,2-thiolamino groups via click cycloaddition, leading to the formation of AuNPs aggregates. As a result, the newly formed AuNPs with expanded size could effectively block nanoparticle exocytosis and minimize nanoparticle backflow to the bloodstream.

Not only for the delivery of intracellular active drugs, this strategy of enzyme-induced NPs aggregation is also applicable

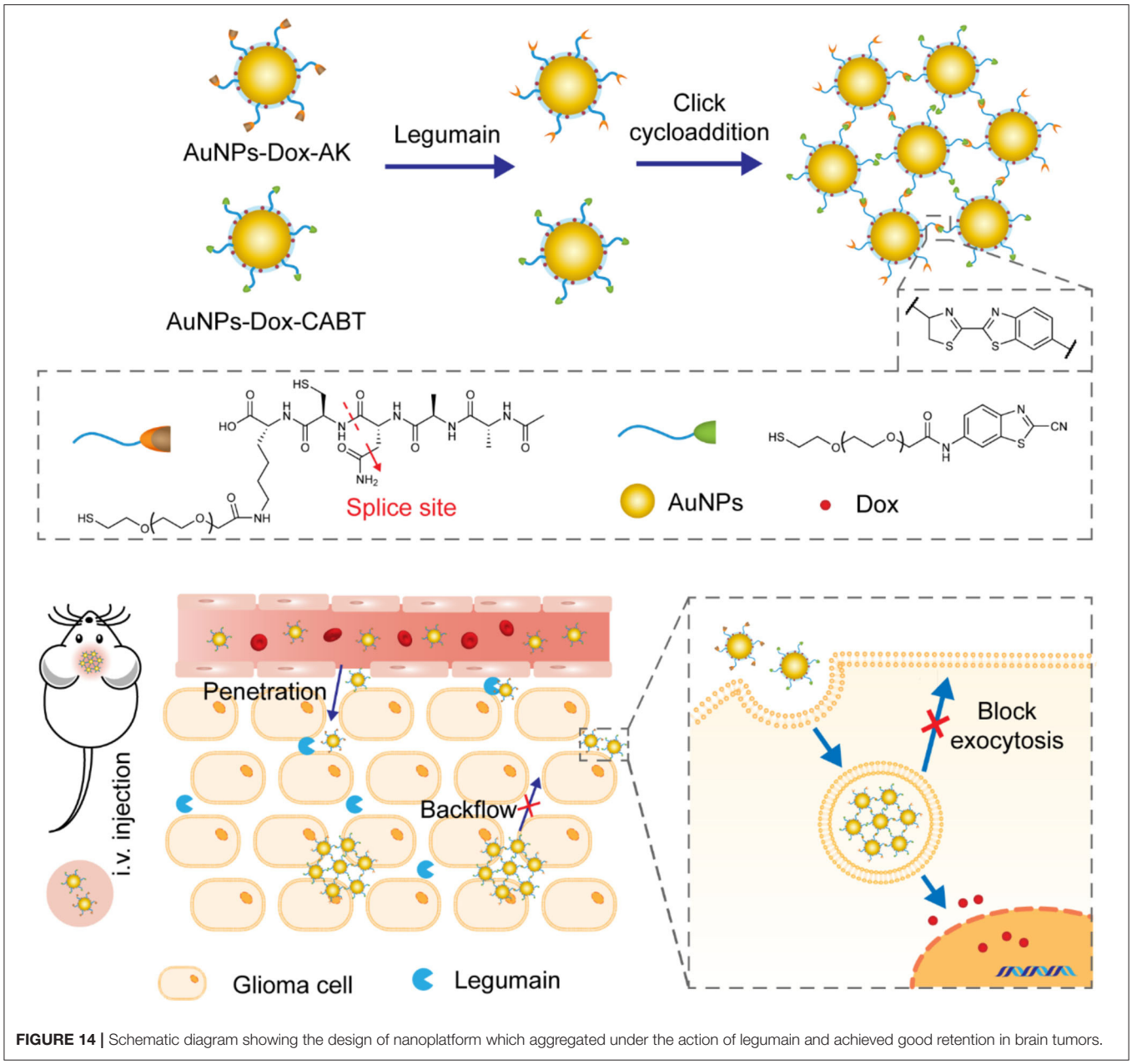

FIGURE 14 | Schematic diagram showing the design of nanoplatform which aggregated under the action of legumain and achieved good retention in brain tumors.

for the delivery and continuous release of extracellular active proteins/peptides in tumor tissues since the aggregated NPs as depots are not easy to be internalized by the cells. Gu group designed a nanoplatform (CS-NG) which could assemble into microsized extracellular depots via transglutaminase-catalyzed cross-linking of human serum albumin (Hu et al., 2016), as showed in **Figure 15**. HA matrix loaded with transglutaminase as an enzyme-responsive ligand and human serum albumin were collectively coated on the surface of glycerol dimethacrylate-based core preloaded with therapeutics. After NPs accumulated in tumor tissues with overexpression of HAase, transglutaminase was released from HA matrix, which further triggered the cross-linking of HA and formed microscale "drug-delivery depots" as reservoir to continuously release therapeutics.

CONCLUSIONS

Aberrantly high expression of tumor-associated enzymes is a feature of the tumor microenvironment, which can be utilized to design anti-tumor drug delivery systems based on nanoparticles with enzyme-response capability. In this review, four types of enzyme-responsive NPs were introduced depending on the different components of NPs on which an enzyme takes action. Different effects, such as better tissue or membrane penetration, reduced toxicity, extended circulation time, improved accumulation, and controllable release of active therapeutics, can be achieved by fabricating NPs with enzyme-responsive sites. NPs with enzyme-responsive crown are the most common carriers for antitumor drug delivery because of their

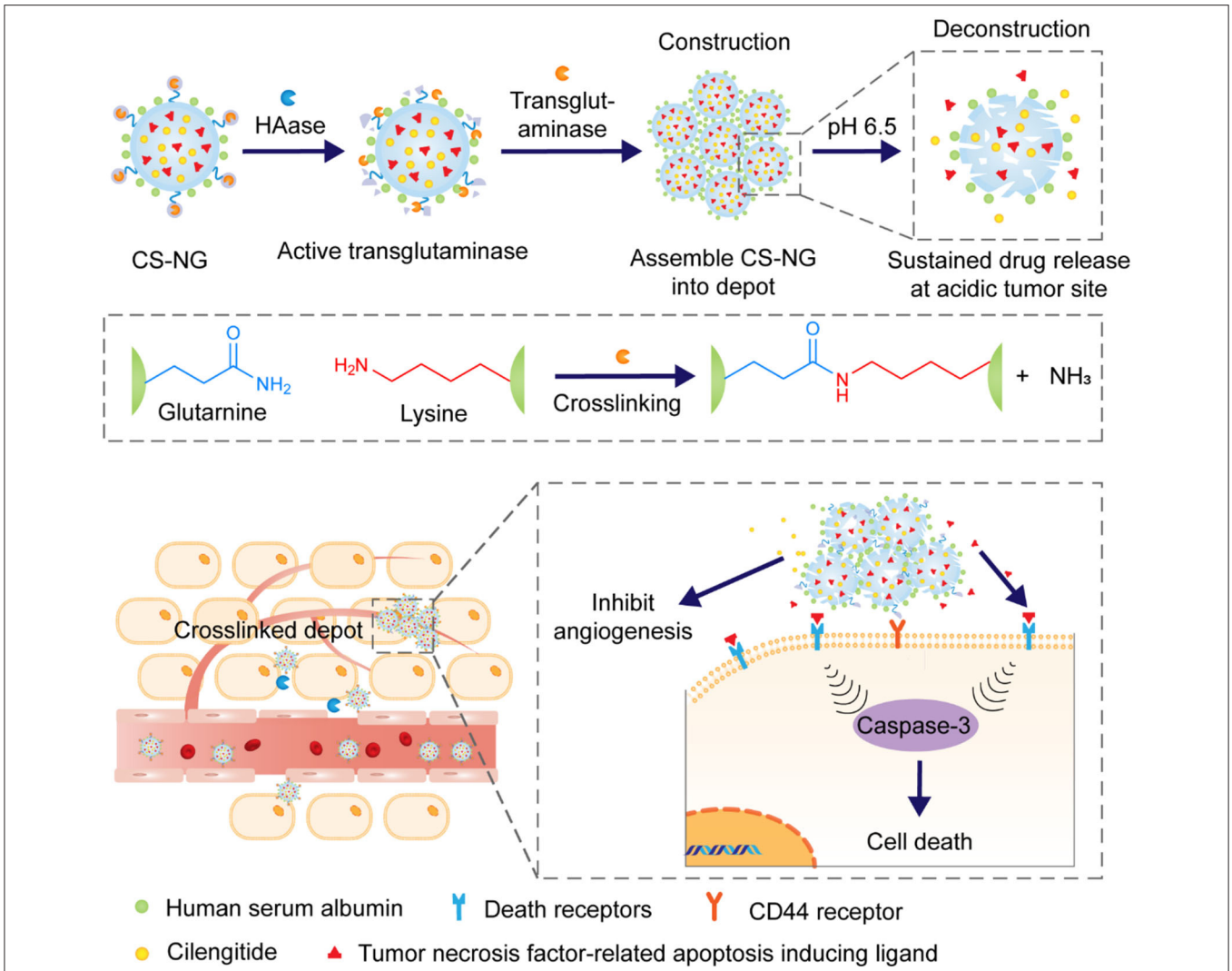

FIGURE 15 | Schematic diagram depicting the tumor microenvironment-mediated construction and deconstruction of extracellular drug depots for sustained drug release.

relatively simple structure, easy preparation, and short response time. More attention should be paid to these NPs due to their great potential for clinical applications in the future. Among the enzymes explored and evaluated, proteases with versatile response abilities toward different enzyme-sensitive components of NPs have been frequently investigated. Besides as therapy for tumor treatment, enzyme-responsive NPs have also been used for tumor monitoring and localization as they can target diseased tissues and accumulate in tumor microenvironments with desired sensitivity. In addition, it has been well demonstrated that codelivery of multiple payloads by these enzyme responsive systems is quite achievable. For all of these reasons, the exploration and clinical applications of the enzyme-responsive NPs applications will undergo considerable expansion.

Although great progress has been made in the design and application of enzyme-responsive nanoparticles, there are still many challenges that need to be addressed. First of all, considering the high complexity of tumor microenvironment, there is a tremendous variety of enzyme activity dysregulation in different cancers and even the same cancer at different stages of progress. It is really difficult to build a general enzyme-responsive nano delivery platform for anti-tumor therapeutics. And due to the high heterogeneity degree of cancer, even more difficulty could be envisioned.

Secondly, targeted and controlled release of drugs from enzyme-responsive NPs relies on the high reactivity of enzymes for their substrates with exceptional selectivity. This exclusive one-to-one relationship between enzyme-responsive NPs and tumor microenvironment with overexpression of the exact enzyme is not as solid as assumed. Take MMPs for example, this family of over 20 proteinases have similar catalytic mechanisms and thus substrate preferences. NPs modified with short peptide substrates could be sensitive to various tumor microenvironments. Therefore, rational chemistry design of

enzyme-specific substrates for fabricating NPs with precise enzyme-response ability is required.

Thirdly, compared with improved anti-tumor efficacy of enzyme-responsive NPs clearly illustrated *in vitro* investigations, there is still limited information about the underlying action mechanism of enzyme-responsive NPs *in vivo*. In addition, although positive results have been obtained in animal models, therapy based on enzyme-responsive NPs is still far away from being available for clinical use. Rational animal models should be developed and closer correlation between developed xenotransplantation models and clinical trials should be established.

Finally, a wide variety of enzyme-responsive NPs with sophisticated structures have been developed and some of them are undergoing clinical trials. Concern about their biosafety should be the key issue. Furthermore, due to their high structural complexity and multiple functionalities, enzyme-responsive NPs in development, especially those with high potential in clinical applications, might meet standards of homogeneity and the corresponding formulation techniques should be reproducible.

In summary, enzyme-responsive NPs hold great potential for more precise diagnosis and more effective treatment of cancers. There is a long way to go before we, with the assistance of enzyme-responsive NPs, eventually find a cure for cancer.

AUTHOR CONTRIBUTIONS

QS conceived the review topic and modified the manuscript. ML wrote the manuscript and arranged all the figures. All authors contributed to the final manuscript.

FUNDING

This work was supported by the National Natural Science Foundation of China (U1932164).

REFERENCES

Aggarwal, N., and Sloane, B. F. (2014). Cathepsin B: multiple roles in cancer. *Proteomics Clin. Appl.* 8, 427–437. doi: 10.1002/prca.201300105

Allen, T. M. (2002). Ligand-targeted therapeutics in anticancer therapy. *Nat. Rev. Cancer* 2, 750–763. doi: 10.1038/nrc903

Bohme, D., and Beck-Sickinger, A. G. (2015). Drug delivery and release systems for targeted tumor therapy. *J. Pept. Sci.* 21, 186–200. doi: 10.1002/psc.2753

Bostwick, D. G., Pacelli, A., Blute, M., Roche, P., and Murphy, G. P. (1998). Prostate specific membrane antigen expression in prostatic intraepithelial neoplasia and adenocarcinoma: a study of 184 cases. *Cancer* 82, 2256–2261. doi: 10.1002/(SICI)1097-0142(19980601)82:11<2256::AID-CNCR22>3.0.CO;2-S

Callmann, C. E., Barback, C. V., Thompson, M. P., Hall, D. J., Mattrey, R. F., and Gianneschi, N. C. (2015). Therapeutic enzyme-responsive nanoparticles for targeted delivery and accumulation in tumors. *Adv. Mater.* 27, 4611–4615. doi: 10.1002/adma.201501803

Chen, X. H., Gao, H. Q., Deng, Y. Y., Jin, Q., Ji, J., and Ding, D. (2020). Supramolecular aggregation-induced emission nanodots with programmed tumor microenvironment responsiveness for image-guided orthotopic pancreatic cancer therapy. *ACS Nano* 14, 5121–5134. doi: 10.1021/acsnano.0c02197

Cheng, R., Meng, F. H., Deng, C., Klok, H. A., and Zhong, Z. Y. (2013). Dual and multi-stimuli responsive polymeric nanoparticles for programmed site-specific drug delivery. *Biomaterials* 34, 3647–3657. doi: 10.1016/j.biomaterials.2013.01.084

Cho, K. J., Wang, X., Nie, S. M., Chen, Z., and Shin, D. M. (2008). Therapeutic nanoparticles for drug delivery in cancer. *Clin. Cancer. Res.* 14, 1310–1316. doi: 10.1158/1078-0432.CCR-07-1441

Choi, K. Y., Silvestre, O. F., Huang, X. L., Min, K. H., Howard, G. P., Hida, N., et al. (2014). Versatile RNA interference nanoplatform for systemic delivery of RNAs. *ACS Nano* 8, 4559–4570. doi: 10.1021/nn500085k

Choi, K. Y., Yoon, H. Y., Kim, J. H., Bae, S. M., Park, R. W., Kang, Y. M., et al. (2011). Smart nanocarrier based on PEGylated hyaluronic acid for cancer therapy. *ACS Nano* 5, 8591–8599. doi: 10.1021/nn202070n

de la Rica, R., Aili, D., and Stevens, M. M. (2012). Enzyme-responsive nanoparticles for drug release and diagnostics. *Adv. Drug Delivery Rev.* 64, 967–978. doi: 10.1016/j.addr.2012.01.002

Deepagan, V. G., Kwon, S., You, D. G., Nguyen, V. Q., Um, W., Ko, H., et al. (2016). *In situ* diselenide-crosslinked polymeric micelles for ROS-mediated anticancer drug delivery. *Biomaterials* 103, 56–66. doi: 10.1016/j.biomaterials.2016.06.044

Dennis, E. A., Cao, J., Hsu, Y. H., Magrioti, V., and Kokotos, G. (2011). Phospholipase A(2) enzymes: physical structure, biological function, disease implication, chemical inhibition, and therapeutic intervention. *Chem. Rev.* 111, 6130–6185. doi: 10.1021/cr200085w

Ding, J., Liang, T. X. Z., Zhou, Y., He, Z. W., Min, Q. H., Jiang, L. P., et al. (2017). Hyaluronidase-triggered anticancer drug and siRNA delivery from cascaded targeting nanoparticles for drug-resistant breast cancer therapy. *Nano Res.* 10, 690–703. doi: 10.1007/s12274-016-1328-y

Egeblad, M., and Werb, Z. (2002). New functions for the matrix metalloproteinases in cancer progression. *Nat. Rev. Cancer* 2, 161–174. doi: 10.1038/nrc745

Gayam, S. R., Venkatesan, P., Sung, Y. M., Sung, S. Y., Hu, S. H., Hsu, H. Y., et al. (2016). An NAD(P)H: quinone oxidoreductase 1 (NQO1) enzyme responsive nanocarrier based on mesoporous silica nanoparticles for tumor targeted drug delivery *in vitro* and *in vivo*. *Nanoscale* 8, 12307–12317. doi: 10.1039/C6NR03525F

Haley, B., and Frenkel, E. (2008). Nanoparticles for drug delivery in cancer treatment. *Urol. Oncol. Semin. Orig. Investig.* 26, 57–64. doi: 10.1016/j.urolonc.2007.03.015

Han, H. J., Valdeperez, D., Jin, Q., Yang, B., Li, Z. H., Wu, Y. L., et al. (2017). Dual enzymatic reaction-assisted gemcitabine delivery systems for programmed pancreatic cancer therapy. *ACS Nano* 11, 1281–1291. doi: 10.1021/acsnano.6b05541

Han, H. S., Choi, K. Y., Lee, H., Lee, M., An, J. Y., Shin, S., et al. (2016). Gold-nanoclustered hyaluronan nano-assemblies for photothermally maneuvered photodynamic tumor ablation. *ACS Nano* 10, 10858–10868. doi: 10.1021/acsnano.6b05113

Han, L., Liu, C. Y., Qi, H. Z., Zhou, J. H., Wen, J., Wu, D., et al. (2019). Systemic delivery of monoclonal antibodies to the central nervous system for brain tumor therapy. *Adv. Mater.* 31:1805697. doi: 10.1002/adma.201805697

Hans, M. L., and Lowman, A. M. (2002). Biodegradable nanoparticles for drug delivery and targeting. *Curr. Opin. Solid State Mat. Sci.* 6, 319–327. doi: 10.1016/S1359-0286(02)00117-1

Hou, B., Zhou, L., Wang, H., Saeed, M., Wang, D. G., Xu, Z., et al. (2020). Engineering stimuli-activatable boolean logic prodrug nanoparticles for combination cancer immunotherapy. *Adv. Mater.* 32:1907210. doi: 10.1002/adma.201907210

Hu, J. M., Zhang, G. Q., and Liu, S. Y. (2012). Enzyme-responsive polymeric assemblies, nanoparticles and hydrogels. *Chem. Soc. Rev.* 41, 5933–5949. doi: 10.1039/c2cs35103j

Hu, Q. Y., Sun, W. J., Lu, Y., Bomba, H. N., Ye, Y. Q., Jiang, T. Y., et al. (2016). Tumor microenvironment-mediated construction and deconstruction of extracellular drug-delivery depots. *Nano Lett.* 16, 1118–1126. doi: 10.1021/acs.nanolett.5b04343

Ihsanullah, K. M., Kumar, B. N., Zhao, Y. Y., Muhammad, H., Liu, Y., Wang, L., et al. (2020). Stepwise-activatable hypoxia triggered nanocarrier-based

photodynamic therapy for effective synergistic bioreductive chemotherapy. *Biomaterials* 245:119982. doi: 10.1016/j.biomaterials.2020.119982

Kamaly, N., Xiao, Z. Y., Valencia, P. M., Radovic-Moreno, A. F., and Farokhzad, O. C. (2012). Targeted polymeric therapeutic nanoparticles: design, development and clinical translation. *Chem. Soc. Rev.* 41, 2971–3010. doi: 10.1039/c2cs15344k

Kamaly, N., Yameen, B., Wu, J., and Farokhzad, O. C. (2016). Degradable controlled-release polymers and polymeric nanoparticles: mechanisms of controlling drug release. *Chem. Rev.* 116, 2602–2663. doi: 10.1021/acs.chemrev.5b00346

Karimi, M., Ghasemi, A., Zangabad, P. S., Rahighi, R., Basri, S. M. M., Mirshekari, H., et al. (2016). Smart micro/nanoparticles in stimulus-responsive drug/gene delivery systems. *Chem. Soc. Rev.* 45, 1457–1501. doi: 10.1039/C5CS00798D

Kim, H., Kim, Y., Kim, I. H., Kim, K., and Choi, Y. (2014). ROS-responsive activatable photosensitizing agent for imaging and photodynamic therapy of activated macrophages. *Theranostics* 4, 1–11. doi: 10.7150/thno.7101

Ko, J., Park, K., Kim, Y. S., Kim, M. S., Han, J. K., Kim, K., et al. (2007). Tumoral acidic extracellular pH targeting of pH-responsive MPEG-poly (beta-amino ester) block copolymer micelles for cancer therapy. *J. Control. Release* 123, 109–115. doi: 10.1016/j.jconrel.2007.07.012

Ko, J. Y., Park, S., Lee, H., Koo, H., Kim, M. S., Choi, K., et al. (2010). pH-sensitive nanoflash for tumoral acidic ph imaging in live animals. *Small* 6, 2539–2544. doi: 10.1002/smll.201001252

Kono, K. (2001). Thermosensitive polymer-modified liposomes. *Adv. Drug Delivery Rev.* 53, 307–319. doi: 10.1016/S0169-409X(01)00204-6

Lee, E. S., Gao, Z. G., Kim, D., Park, K., Kwon, I. C., and Bae, Y. H. (2008). Super pH-sensitive multifunctional polymeric micelle for tumor pH(e) specific TAT exposure and multidrug resistance. *J. Control. Release* 129, 228–236. doi: 10.1016/j.jconrel.2008.04.024

Lee, E. S., Na, K., and Bae, Y. H. (2005). Super pH-sensitive multifunctional polymeric micelle. *Nano Lett.* 5, 325–329. doi: 10.1021/nl0479987

Lee, J., Oh, E. T., Yoon, H., Kim, C. W., Han, Y., Song, J., et al. (2017). Mesoporous nanocarriers with a stimulus-responsive cyclodextrin gatekeeper for targeting tumor hypoxia. *Nanoscale* 9, 6901–6909. doi: 10.1039/C7NR00808B

Lee, S., Cha, E. J., Park, K., Lee, S. Y., Hong, J. K., Sun, I. C., et al. (2008). A near-infrared-fluorescence-quenched gold-nanoparticle imaging probe for *in vivo* drug screening and protease activity determination. *Angew. Chem. Int. Ed.* 47, 2804–2807. doi: 10.1002/anie.200705240

Lee, S., Ryu, J. H., Park, K., Lee, A., Lee, S. Y., Youn, I. C., et al. (2009). Polymeric nanoparticle-based activatable near-infrared nanosensor for protease determination *in vivo*. *Nano Lett.* 9, 4412–4416. doi: 10.1021/nl902709m

Li, J., Huo, M. R., Wang, J., Zhou, J. P., Mohammad, J. M., Zhang, Y. L., et al. (2012). Redox-sensitive micelles self-assembled from amphiphilic hyaluronic acid-deoxycholic acid conjugates for targeted intracellular delivery of paclitaxel. *Biomaterials* 33, 2310–2320. doi: 10.1016/j.biomaterials.2011.11.022

Li, L., ten Hagen, T. L. M., Hossann, M., Suss, R., van Rhoon, G. C., Eggermont, A. M. M., et al. (2013). Mild hyperthermia triggered doxorubicin release from optimized stealth thermosensitive liposomes improves intratumoral drug delivery and efficacy. *J. Control. Release* 168, 142–150. doi: 10.1016/j.jconrel.2013.03.011

Li, S. D., Chen, L. Y., Huang, K., Chen, N., Zhan, Q., Yi, K. K., et al. (2019). Tumor microenvironment-tailored weakly cell-interacted extracellular delivery platform enables precise antibody release and function. *Adv. Funct. Mater.* 29:1903296. doi: 10.1002/adfm.201903296

Limmer, S., Hahn, J., Schmidt, R., Wachholz, K., Zengerle, A., Lechner, K., et al. (2014). Gemcitabine treatment of rat soft tissue sarcoma with phosphatidyldiglycerol-based thermosensitive liposomes. *Pharm. Res.* 31, 2276–2286. doi: 10.1007/s11095-014-1322-6

Lin, Q. N., Bao, C. Y., Yang, Y. L., Liang, Q. N., Zhang, D. S., Cheng, S. Y., et al. (2013). Highly discriminating photorelease of anticancer drugs based on hypoxia activatable phototrigger conjugated chitosan nanoparticles. *Adv. Mater.* 25, 1981–1986. doi: 10.1002/adma.201204455

Liu, Y., Zhang, D., Qiao, Z. Y., Qi, G. B., Liang, X. J., Chen, X. G., et al. (2015). A peptide-network weaved nanoplatform with tumor microenvironment responsiveness and deep tissue penetration capability for cancer therapy. *Adv. Mater.* 27, 5034–5042. doi: 10.1002/adma.201501502

Mannweiler, S., Amersdorfer, P., Trajanoski, S., Terrett, J. A., King, D., and Mehes, G. (2009). Heterogeneity of prostate-specific membrane antigen (PSMA) expression in prostate carcinoma with distant metastasis. *Pathol. Oncol. Res.* 15, 167–172. doi: 10.1007/s12253-008-9104-2

Maurer, T., Weirich, G., Schottelius, M., Weineisen, M., Frisch, B., Okur, A., et al. (2015). Prostate-specific membrane antigen-radioguided surgery for metastatic lymph nodes in prostate cancer. *Eur. Urol.* 68, 530–534. doi: 10.1016/j.eururo.2015.04.034

Min, K. H., Kim, J. H., Bae, S. M., Shin, H., Kim, M. S., Park, S., et al. (2010). Tumoral acidic pH-responsive MPEG-poly(beta-amino ester) polymeric micelles for cancer targeting therapy. *J. Control. Release* 144, 259–266. doi: 10.1016/j.jconrel.2010.02.024

Morgillo, F., and Lee, H. Y. (2005). Resistance to epidermal growth factor receptor-targeted therapy. *Drug Resist. Updates* 8, 298–310. doi: 10.1016/j.drup.2005.08.004

Mura, S., Nicolas, J., and Couvreur, P. (2013). Stimuli-responsive nanocarriers for drug delivery. *Nat. Mater.* 12, 991–1003. doi: 10.1038/nmat3776

Peng, J. R., Yang, Q., Xiao, Y., Shi, K., Liu, Q. Y., Hao, Y., et al. (2019). Tumor microenvironment responsive drug-dye-peptide nanoassembly for enhanced tumor-targeting, penetration, and photo-chemo-immunotherapy. *Adv. Funct. Mater.* 29:1900004. doi: 10.1002/adfm.201900004

Poveda, A., Lopez-Pousa, A., Martin, J., Del Muro, J. G., Bernabe, R., Casado, A., et al. (2005). Phase II clinical trial with pegylated liposomal doxorubicin [CAELYX (R)/Doxil (R)] and quality of life evaluation (EORTC QLQ-C30) in adult patients with advanced soft tissue sarcomas: a study of the spanish group for research in sarcomas (GEIS). *Sarcoma* 9, 127–132. doi: 10.1080/13577140500287024

Ross, J. S., Schenkein, D. P., Pietrusko, R., Rolfe, M., Linette, G. P., Stec, J., et al. (2004). Targeted therapies for cancer 2004. *Am. J. Clin. Pathol.* 122, 598–609. doi: 10.1309/5CWPU41AFR1VYM3F

Ruan, S. B., Hu, C., Tang, X., Cun, X. L., Xiao, W., Shi, K. R., et al. (2016). Increased gold nanoparticle retention in brain tumors by *in situ* enzyme-induced aggregation. *ACS Nano* 10, 10086–10098. doi: 10.1021/acsnano.6b05070

Shi, C. L., Guo, X., Qu, Q. Q., Tang, Z. M., Wang, Y., and Zhou, S. B. (2014). Actively targeted delivery of anticancer drug to tumor cells by redox-responsive star-shaped micelles. *Biomaterials* 35, 8711–8722. doi: 10.1016/j.biomaterials.2014.06.036

Siegel, R. L., Miller, K. D., and Jemal, A. (2020). Cancer statistics, 2020. *CA Cancer J. Clin.* 70, 7–30. doi: 10.3322/caac.21590

Silver, D. A., Pellicer, I., Fair, W. R., Heston, W. D. W., and CordonCardo, C. (1997). Prostate-specific membrane antigen expression in normal and malignant human tissues. *Clin. Cancer Res.* 3, 81–85.

Son, J., Kalafatovic, D., Kumar, M., Yoo, B., Cornejo, M. A., Contel, M., et al. (2019). Customizing morphology, size, and response kinetics of matrix metalloproteinase-responsive nanostructures by systematic peptide design. *ACS Nano* 13, 1555–1562. doi: 10.1021/acsnano.8b07401

Tang, S., Meng, Q. S., Sun, H. P., Su, J. H., Yin, Q., Zhang, Z. W., et al. (2016). Tumor-microenvironment-adaptive nanoparticles codeliver paclitaxel and siRNA to inhibit growth and lung metastasis of breast cancer. *Adv. Funct. Mater.* 26, 6033–6046. doi: 10.1002/adfm.201601703

Torchilin, V. P. (2014). Multifunctional, stimuli-sensitive nanoparticulate systems for drug delivery. *Nat. Rev. Drug Discovery* 13, 813–827. doi: 10.1038/nrd4333

Troyer, J. K., Beckett, M. L., and Wright, G. L. (1995). Detection and characterization of the prostate-specific membrane antigen (PMSA) in tissue-extracts and body-fluids. *Int. J. Cancer* 62, 552–558. doi: 10.1002/ijc.2910620511

Ulijn, R. V. (2006). Enzyme-responsive materials: a new class of smart biomaterials. *J. Mater. Chem.* 16, 2217–2225. doi: 10.1039/b601776m

van Dijk, M., van Nostrum, C. F., Hennink, W. E., Rijkers, D. T. S., and Liskamp, R. M. J. (2010). Synthesis and characterization of enzymatically biodegradable PEG and peptide-based hydrogels prepared by click chemistry. *Biomacromolecules* 11, 1608–1614. doi: 10.1021/bm1002637

van Rijt, S. H., Bolukbas, D. A., Argyo, C., Datz, S., Lindner, M., Eickelberg, O., et al. (2015). Protease-mediated release of chemotherapeutics from mesoporous silica nanoparticles to *ex vivo* human and mouse lung tumors. *ACS Nano* 9, 2377–2389. doi: 10.1021/nn5070343

Ventola, C. L. (2017). Progress in nanomedicine: approved and investigational nanodrugs. *P T* 42, 742–755.

Wang, C., Chen, S. Q., Wang, Y. X., Liu, X. R., Hu, F. Q., Sun, J. H., et al. (2018). Lipase-triggered water-responsive "Pandora's Box" for cancer therapy:

toward induced neighboring effect and enhanced drug penetration. *Adv. Mater.* 30:1706407. doi: 10.1002/adma.201706407

Wang, Z. H., Wang, Y. H., Jia, X. Q., Han, Q. J., Qian, Y. X., Li, Q., et al. (2019). MMP-2-controlled transforming micelles for heterogeneic targeting and programmable cancer therapy. *Theranostics* 9, 1728–1740. doi: 10.7150/thno.30915

West, J. L., and Hubbell, J. A. (1999). Polymeric biomaterials with degradation sites for proteases involved in cell migration. *Macromolecules* 32, 241–244. doi: 10.1021/ma981296k

Xu, C. F., Yu, Y. L., Sun, Y., Kong, L., Yang, C. L., Hu, M., et al. (2019). Transformable nanoparticle-enabled synergistic elicitation and promotion of immunogenic cell death for triple-negative breast cancer immunotherapy. *Adv. Funct. Mater.* 29:1905213. doi: 10.1002/adfm.201905213

Xu, J. T., Han, W., Cheng, Z. Y., Yang, P. P., Bi, H. T., Yang, D., et al. (2018). Bioresponsive and near infrared photon co-enhanced cancer theranostic based on upconversion nanocapsules. *Chem. Sci.* 9, 3233–3247. doi: 10.1039/C7SC05414A

Yang, G. B., Xu, L. G., Xu, J., Zhang, R., Song, G. S., Chao, Y., et al. (2018). Smart nanoreactors for pH-responsive tumor homing, mitochondria-targeting, and enhanced photodynamic-immunotherapy of cancer. *Nano Lett.* 18, 2475–2484. doi: 10.1021/acs.nanolett.8b00040

Yang, Y. M., Yue, C. X., Han, Y., Zhang, W., He, A. N., Zhang, C. L., et al. (2016). Tumor-responsive small molecule self-assembled nanosystem for simultaneous fluorescence imaging and chemotherapy of lung cancer. *Adv. Funct. Mater.* 26, 8735–8745. doi: 10.1002/adfm.201601369

Yang, Z., Dai, Y. L., Yin, C., Fan, Q. L., Zhang, W. S., Song, J., et al. (2018). Activatable semiconducting theranostics: simultaneous generation and ratiometric photoacoustic imaging of reactive oxygen species *in vivo*. *Adv. Mater.* 30:1707509. doi: 10.1002/adma.201707509

Yoon, S. O., Park, S. J., Yun, C. H., and Chung, A. S. (2003). Roles of matrix metalloproteinases in tumor metastasis and angiogenesis. *J. Biochem. Mol. Biol.* 36, 128–137. doi: 10.5483/BMBRep.2003.36.1.128

Yu, Q. W., Qiu, Y., Li, J. P., Tang, X., Wang, X. H., Cun, X. L., et al. (2020). Targeting cancer-associated fibroblasts by dual-responsive lipid-albumin nanoparticles to enhance drug perfusion for pancreatic tumor therapy. *J. Control. Release* 321, 564–575. doi: 10.1016/j.jconrel.2020.02.040

Yu, X., Gou, X. C., Wu, P., Han, L., Tian, D. F., Du, F. Y., et al. (2018). Activatable protein nanoparticles for targeted delivery of therapeutic peptides. *Adv. Mater.* 30:1705383. doi: 10.1002/adma.201705383

Zhang, L. J., Qi, Y. Q., Min, H., Ni, C., Wang, F., Wang, B., et al. (2019). Cooperatively responsive peptide nanotherapeutic that regulates angiopoietin receptor Tie2 activity in tumor microenvironment to prevent breast tumor relapse after chemotherapy. *ACS Nano* 13, 5091–5102. doi: 10.1021/acsnano.8b08142

Zhang, M. Z., Xu, C. L., Wen, L. Q., Han, M. K., Xiao, B., Zhou, J., et al. (2016). A hyaluronidase-responsive nanoparticle-based drug delivery system for targeting colon cancer cells. *Cancer Res.* 76, 7208–7218. doi: 10.1158/0008-5472.CAN-16-1681

Zhang, N., Zhao, F. F., Zou, Q. L., Li, Y. X., Ma, G. H., and Yan, X. H. (2016). Multitriggered tumor-responsive drug delivery vehicles based on protein and polypeptide coassembly for enhanced photodynamic tumor ablation. *Small* 12, 5936–5943. doi: 10.1002/smll.201602339

Zhao, X. X., Li, L. L., Zhao, Y., An, H. W., Cai, Q., Lang, J. Y., et al. (2019). *In situ* self-assembled nanofibers precisely target cancer-associated fibroblasts for improved tumor imaging. *Angew. Chem. Int. Ed.* 58, 15287–15294. doi: 10.1002/anie.201908185

Zhou, Q., Shao, S. Q., Wang, J. Q., Xu, C. H., Xiang, J. J., Piao, Y., et al. (2019). Enzyme-activatable polymer-drug conjugate augments tumour penetration and treatment efficacy. *Nat. Nanotechnol.* 14, 799–809. doi: 10.1038/s41565-019-0485-z

Zhu, S. W., Nih, L., Carmichael, S. T., Lu, Y. F., and Segura, T. (2015). Enzyme-responsive delivery of multiple proteins with spatiotemporal control. *Adv. Mater.* 27, 3620–3625. doi: 10.1002/adma.201500417

Conflict of Interest: The authors declare that the research was conducted in the absence of any commercial or financial relationships that could be construed as a potential conflict of interest.

frontiers in Chemistry

ORIGINAL RESEARCH
published: 11 August 2020
doi: 10.3389/fchem.2020.00649

A Novel CD133- and EpCAM-Targeted Liposome With Redox-Responsive Properties Capable of Synergistically Eliminating Liver Cancer Stem Cells

Zihua Wang[1]*, *Mengqi Sun*[1,2], *Wang Li*[3], *Linyang Fan*[2], *Ying Zhou*[1] and *Zhiyuan Hu*[1,2,4]*

[1] Key Laboratory of Brain Aging and Neurodegenerative Diseases of Fujian Provincial Universities and Colleges, School of Basic Medical Sciences, Fujian Medical University, Fuzhou, China, [2] CAS Key Laboratory of Standardization and Measurement for Nanotechnology, CAS Key Laboratory for BiomedicalEffects of Nanomaterials and Nanosafety, CAS Center for Excellence in Nanoscience, National Center for Nanoscience and Technology of China, Beijing, China, [3] Key Laboratory of Colloid Interface and Chemical Thermodynamics, Institute of Chemistry Chinese Academy of Sciences, Beijing, China, [4] School of Nanoscience and Technology, Sino-Danish College, University of Chinese Academy of Sciences, Beijing, China

OPEN ACCESS

Edited by:
Yi Hou,
Beijing University of Technology, China

Reviewed by:
Jianfeng Zeng,
Soochow University, China
Lihong Jing,
Institute of Chemistry (CAS), China

***Correspondence:**
Zihua Wang
wangzh@iccas.ac.cn
Zhiyuan Hu
huzy@nanoctr.cn

Specialty section:
This article was submitted to Nanoscience, a section of the journal Frontiers in Chemistry

Received: *05 May 2020*
Accepted: *22 June 2020*
Published: *11 August 2020*

Citation:
Wang Z, Sun M, Li W, Fan L, Zhou Y and Hu Z (2020) A Novel CD133- and EpCAM-Targeted Liposome With Redox-Responsive Properties Capable of Synergistically Eliminating Liver Cancer Stem Cells. Front. Chem. 8:649. doi: 10.3389/fchem.2020.00649

Cancer stem cells (CSCs) are a small subset of cells that sit atop the hierarchical ladder in many cancer types. Liver CSCs have been associated with high chemoresistance and recurrence rates in hepatocellular carcinoma (HCC). However, as of yet, no satisfactorily effective liver CSC-targeted treatment is available, which drove us to design and investigate the efficacy of a liposome-based delivery system. Here, we introduce a redox-triggered dual-targeted liposome, CEP-LP@S/D, capable of co-delivering doxorubicin (Dox) and salinomycin (Sal) for the synergistic treatment of liver cancer. This system is based on the association of CD133- and EpCAM-targeted peptides to form Y-shaped CEP ligands that were anchored to the surface of the liposome and allowed the selective targeting of $CD133^+$ $EpCAM^+$ liver CSCs. After arriving to the CSCs, the CEP-LP@S/D liposome undergoes endocytosis to the cytoplasm, where a high concentration of glutathione (GSH) breaks its disulfide bonds, thereby degrading the liposome. This then induces a rapid release of Dox and Sal to synergistically inhibit tumor growth. Notably, this effect occurs through Dox-induced apoptosis and concurrent lysosomal iron sequestration by Sal. Interestingly, both *in vitro* and *in vivo* studies indicated that our GSH-responsive co-delivery system not only effectively enhanced CSC targeting but also eliminated the non-CSC faction, thereby exhibiting high antitumor efficacy. We believe that the smart liposome nanocarrier-based co-delivery system is a promising strategy to combat liver cancer, which may also lay the groundwork for more enhanced approaches to target other cancer types as well.

Keywords: targeting peptide, glutathione responsive, liver cancer stem cell, targeted drug delivery, synergistic therapy

INTRODUCTION

Hepatocellular carcinoma (HCC) is one of the most common malignant tumors in China with high mortality and incidence rates. Despite advances in diagnostic techniques and treatment approaches, most patients with advanced HCC have a poor prognosis, which may be partly attributed to a high ratio of cancer stem cells (CSCs). CSCs are a rare subset of cells that are involved in tumor maintenance, metastasis, drug resistance, and relapse (Wang et al., 2015a). Unfortunately, conventional chemotherapy and radiotherapy approaches are ineffective against CSCs and are prone to tumor recurrence, treatment failure, and ultimately death (Yarchoan et al., 2019). Salinomycin (Sal) is a potent drug that has been recently shown to selectively inhibit CSCs in various types of cancers, including liver CSCs (Gupta et al., 2009; Mai et al., 2017). However, Sal possesses unfavorable properties, such as hydrophobicity and nerve and muscle toxicity, that greatly hinder its clinical application (Wang et al., 2017). In the past decades, CD133 and EpCAM have been widely studied as stem cell markers in liver cancer (Mikhail and He, 2011). These surface markers serve not only as tools for identifying and isolating liver CSCs but also as therapeutic targets for eradicating these cells (Chan et al., 2014; Jiang et al., 2015; Saygin et al., 2019). Therefore, targeting these CSC-specific markers by optimized drug combinations would be an ideal method for overcoming the stemness of liver CSCs and ameliorating the disease (Clevers, 2011). Considering the importance of CSCs and the shortcomings of conventional anticancer therapies, dual-targeted CSC-specific delivery systems can possibly overcome this dilemma and leave an impact on the clinical setting (Dianat-Moghadam et al., 2018; Guo et al., 2019).

One way to address this issue is by using multifunctional nanoparticle (NP) systems, such as polymeric NPs, liposomes, and micelles, that can simultaneously deliver multiple therapeutic agents to induce a synergistic effect on CSCs (Zhao et al., 2014; Rao et al., 2015; Shen et al., 2015). Liposomes are an FDA-approved drug delivery system that can be loaded with both hydrophilic and hydrophobic drugs in amphiphilic lipid bilayers (Kim et al., 2015; Dianat-Moghadam et al., 2018). Peptide ligands are widely recognized as the surface modification elements in targeted-delivery therapeutic approaches (Zhang et al., 2012; Mao et al., 2015). Our previous studies have demonstrated that peptide-conjugated liposomes can facilitate drug accumulation at tumor sites and improve the anticancer effect of different drugs (Wang et al., 2019). Recently, the use of pro-drug-loaded stimuli-responsive drug delivery systems to facilitate the delivery of anticancer drugs has become a notable trend (Jia et al., 2018; Yang et al., 2018). Notably, stimuli-responsive NPs can respond to external stimuli (e.g., redox, reactive oxygen species, pH, and enzymes) to release drugs in a controlled manner (Ling et al., 2019; Liu et al., 2019). Glutathione (GSH) is a major antioxidant involved in many physiological processes that is abundant in cancer cells (Yu et al., 2019). Therefore, it is no surprise that numerous GSH-responsive nanocarriers have been developed to deliver drugs and as imaging agents for better diagnostic and therapeutic efficacy (Li et al., 2020). Nonetheless, this technology still has ways to go, as developing more efficient and smarter nanocarriers that can overcome the current challenges associated with CSCs is crucial (Shen et al., 2016; Tan et al., 2018; Reda et al., 2019).

Herein, we aimed to develop a redox-responsive liposome, hereafter known as CEP-LP@S/D, that is capable of potentially targeting both liver CSCs and bulk cancer cells. The basis of this approach was the incorporation of Sal, a hydrophobic drug, into the lipid layers of the liposome and of doxorubicin (Dox), a hydrophilic drug, into the aqueous cavity of the liposome. Considering that biomarkers are heterogeneously expressed in HCC, a CD133, and EpCAM dual-targeted Y-shaped peptide ligand, CEP, was employed to decorate the surface of this liposome in order to improve both recognition and binding to CSC subpopulations. Moreover, we went further and endowed CEP-LP@S/D with GSH-responsive properties to initiate anticancer drug release in an intracellular manner once the liposomes have made contact with the tumor cells and investigated the effects both *in vitro* and *in vivo* (**Scheme 1**).

MATERIALS AND METHODS

Materials

We obtained 1-palmitoyl-2-oleoyl-*sn*-glycero-3-phosphocholine (POPC) from A.V.T. Pharmaceutical Co., Ltd. (Shanghai, China), and phosphoethanolamine-*N*-[methoxy(polyethylene glycol)-2000] (DSPE-SS-PEG-2000) from Xi'an ruixi Biological Technology Co., Ltd. (Xi'an, China). Meanwhile, we acquired 1,1′-dioctadecyl-3,3,3′,3′-tetramethylindotricarbocyanine iodide (DiR), LysoTracker Green, and 3-(4,5)-dimethylthiahiazol(-z-y1)-3,5-di-phenytetrazoliumbromide (MTT) from Sigma-Aldrich. We purchased Dulbecco's modified Eagle's medium (DMEM) and fetal bovine serum (FBS) from Gibco (USA) and Sal from Selleck Chemicals (USA). Moreover, we obtained FITC-EpCAM and PE-CD133 antibodies from BioLegend (Shanghai, China).

Preparation and Characterization of CEP-Liposome NPs

In our previous work, we screened EP1 (YEVHTYYLD) and CY (CYIVFYDSPLE) as specific peptides toward EpCAM and CD133, respectively, using a high-throughput library (Wang et al., 2015b). These two peptide ligands were connected via a GG linker, leading to the formation of Y-shape peptides (CEP), which was synthesized by the Fmoc solid-phase synthesis technique. The CEP was then covalently conjugated to DSPE-SS-PEG2000-Mal by adding thiol groups and maleimide (Michael addition). Liposomes were fabricated according to the literature (Guo et al., 2019). Briefly, POPC/DSPE-SS-PEG2000-CEP (molar ratio 19:1) was mixed and dissolved in chloroform/methanol (v/v, 2:1). Next, a certain amount of Sal and Dox (mole ratio 1:1.5) was dissolved in 1 ml of methanol at room temperature and mixed with the lipid solution. The mixed solvent was then dried by rotary evaporation at 45°C to form a lipid film. After that, the dried film was hydrated with 5 ml of phosphate-buffered saline (PBS; pH 7.4) for 30 min and sonicated for 10 min. Finally, the prepared drug-loaded liposome, CEP-LP@S/D, was filtered through a 200-nm

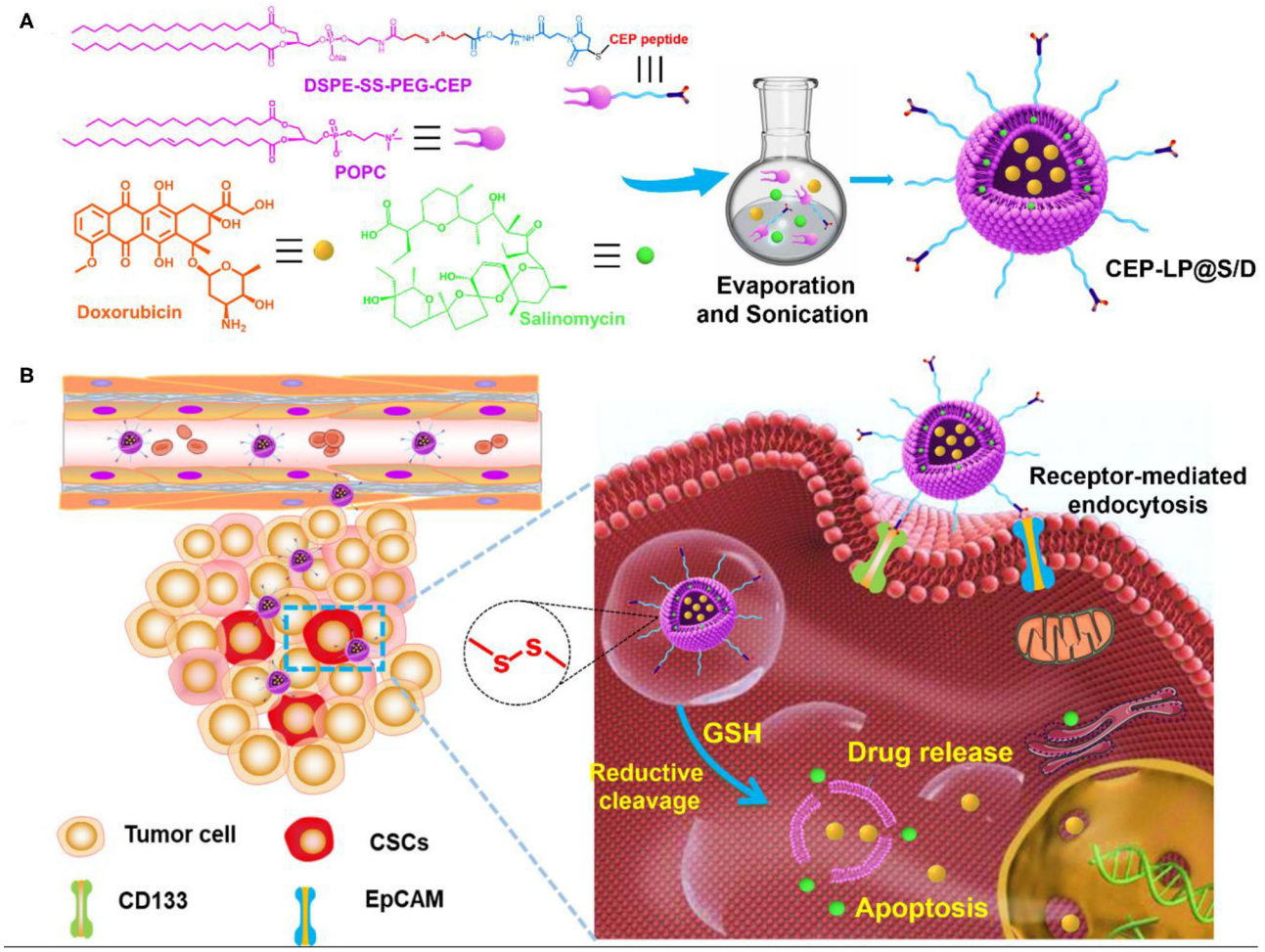

SCHEME 1 | Schematic illustration of glutathione (GSH)-responsive CEP-LP@S/D liposome for controlled drug delivery. **(A)** Schematic illustration of the structure and formation of the CEP-LP@S/D liposome. **(B)** Schematic illustration of the CEP-LP@S/D *in vivo* mechanism of action and transport.

membrane filter to remove any precipitates. As for our *in vivo* imaging studies, we used DiR as the fluorescent probe; thus, DiR-loaded CEP-LP@S/D liposomes were prepared following the same procedures as above. The morphology and size of CEP-LP@S/D were measured by transmission electron microscopy (TEM), while their hydrodynamic size and polydispersity (PDI) were further measured in aqueous solutions by dynamic light scattering (DLS).

In vitro Encapsulation and Release Profiles

The amount of Sal encapsulated in CEP-LP@S/D was detected at 392 nm by high-performance liquid chromatography (HPLC), and Dox fluorescence (λ_{Ex}: 480 nm; λ_{Em}: 590 nm) was measured using a fluorescence spectrometer. The drug encapsulation efficiency (EE) and the loading efficiency (LE) were then calculated according to the equations established by Zhang et al. (2012). Next, *in vitro* drug release from the liposomes was investigated by using a dialysis method. In short, the CEP-LP@S/D liposomes were dispersed in 1 ml of PBS (pH 7.4) and transferred to a dialysis device (MWCO: 10 kDa); they were then immersed in a GSH-containing PBS solution at 37°C and gently stirred. The Dox or Sal content released in the medium was determined by fluorescence spectrometry and HPLC at different time points as described above.

Cytotoxicity and Mammosphere Formation Assays

To evaluate the efficacy of the combination therapy *in vitro*, Huh-7 cells, or human HCC cells, were seeded in 96-well plates (5×10^3 cells per well) at 37°C for 12 h. After that, the cells were incubated with various concentrations of Dox, Sal, LP@S/D, or CEP-LP@S/D for 48 h, and cell viability was assessed by the MTT assay.

We further performed the mammosphere formation assay to assess treatment-induced changes in the stemness of these cells, that is, the CSC self-renewal ability. Thus, $EpCAM^+$ $CD133^+$ Huh-7 single-cell suspensions were sorted and seeded in ultralow-attachment six-well plates at a density of 5×10^3

cells per well. Then, various concentrations of free Sal, LP@S/D, or CEP-LP@S/D were added, and the cells were incubated at 37°C for 24 h. Thereafter, the cells were washed with 1 × BS and cultured in a serum-free DMEM/F12 medium, supplemented with 1 × B27 (Invitrogen), 20-ng/ml recombinant human epidermal growth factor (PeproTech), and 20-ng/ml basic fibroblast growth factor (PeproTech). After that, the cells were cultured in a 5% CO_2 incubator at 37°C for 7 days. The formed mammospheres in each treatment condition were counted and visualized under an optical microscope. Furthermore, to determine whether CEP-LP@S/D could induce a durable mammosphere inhibitory response, the primary mammospheres were trypsinized, prepared into single-cell suspensions, and then cultured in ultralow-adherent six-well plates as previously described. After 5 days, the number and morphology of the secondary mammospheres in each treatment condition were monitored and imaged under a microscope. The saline-treated group was considered as the control.

Cellular Uptake and Localization

The cellular internalization of LP@S/D and CEP-LP@S/D was studied by confocal laser scanning microscopy (CLSM). Huh-7 cells were cultured into glass-bottom dishes and incubated for 24 h, after which the cells were incubated with either CEP-LP@S/D or LP@S/D (20 μg/ml) as described above. After 4–8 h of incubation, the cells were washed and stained with 4′,6-diamidino-2-phenylindole (DAPI), a cell-permeant fluorescent nuclear dye, for 15 min and then rinsed with PBS. Finally, the cells were examined using a Zeiss 710 confocal microscope. In addition, we investigated the intracellular distribution of CEP-LP@S/D in the dissociated mammosphere cells via CLSM. Briefly, $CD133^+$ $EpCAM^+$ Huh-7 mammosphere cells were seeded into 24-well plates in a DMEM/F12 medium. After 24 h of incubation, they were treated with CEP-LP@S/D or LP@S/D at a concentration of 50 μg/ml for 8 h. Finally, the cells were collected and stained, as described above, and visualized using CLSM.

The Expression of Stemness-Associated Genes

To assess the stemness of $CD133^+$ $EpCAM^+$ Huh-7 tumorspheres, we extracted total RNA from the tumorspheres using TRizol (Invitrogen Inc., USA). Total RNA was converted into cDNA by using the PrimeScript™ RT Reagent Kit (Takara, China). Next, SYBR Green PCR Master Mix was added to the obtained cDNA, which was then quantified using the ABI PRISM 7,700 real-time polymerase chain reaction (PCR) platform. The mRNA expression levels of *Sox-2*, *Oct-4*, *ABCG2,* and *CD133* were normalized against that of *GAPDH* and those of PBS-treated cells.

In vivo Imaging to Evaluate the Biodistribution of CEP-LP@S/D

Tumor-bearing mice were intravenously injected with (i) PBS, (ii) LP@S/D, or (iii) CEP-LP@S/D. After 2 h, the mice were imaged using an *in vivo* imaging system (IVIS). DiR-containing CEP-LP@S/D were detected by the appearance of a fluorescent signal at 748/780 nm ($\lambda_{Ex}/\lambda_{Em}$), and images were acquired using the IVIS. At the end point of the experiment, the mice were euthanized, and their major organs were harvested and analyzed to assess the biodistribution of CEP-LP@S/D in each organ.

In vivo Antitumor Efficacy

For *in vivo* studies, BALB/C mice (6 weeks old) were subcutaneously (s.c.) injected with 1 × 10^6 sorted $CD133^+$ $EpCAM^+$ Huh-7 liver CSCs in their left flanks. When the tumor volume reached about 60–80 mm^3, the mice were randomly distributed into four groups ($n = 3$), and each group received one of the following treatments: PBS control, Sal, LP@S/D, or CEP-LP@S/D; all the formulations were administered via tail vein injection (6 mg/kg) every other day. The body weight of the mice was monitored every 3 days, and tumor volumes were calculated using the following formula: (width^2 × length)/2; measurements were obtained using a vernier caliper every other day. The mice were sacrificed to harvest their tumors and main organs for further histological examination, namely, hematoxylin–eosin (H&E) staining and terminal deoxynucleotidyl transferase-mediated dUTP nick end labeling (TUNEL) analysis according to the manufacturer's instructions. In addition, we analyzed the CSC fraction in the tumor mass tissues to assess the effectiveness of the treatments in targeting CSCs and associated stemness features; in short, the tumor tissues were cut into small pieces and the extracted RNA was analyzed by real-time quantitative PCR (qPCR) as described above.

RESULTS AND DISCUSSION

Characterization of Drug-Loaded CEP-LP@S/D Liposomes

Herein, we introduce a Y-shaped surface modification-based material, CEP-DSPE-SS-PEG, that bears two targeting peptides EpCAM and CD133, one in each head (**Supplementary Figure 1**). CEP-DSPE-SS-PEG was synthesized through covalent conjugation between the thiolated peptide CY-EP1 and DSPE-SS-PEG2000-Mal as confirmed by matrix-assisted laser desorption/ionization time-of-flight mass spectrometry (MALDI-TOF-MS) (**Supplementary Figure 2**; Belhadj et al., 2017). The anticancer drug Dox and the newly categorized anticancer agent Sal were loaded into CEP-LP@S/D and LP@S/D via the solvent evaporation method. The measurements showed that CEP-LP@S/D and LP@S/D were within a similar size range diameter-wise (**Figures 1a,b**). The average particle size for all liposome systems was around 115 nm with a small PDI value of <0.28 and good dispersion (**Figure 1c**). Notably, the particle size was not significantly affected by the CEP peptide modification. Moreover, the TEM images (**Supplementary Figure 3**) illustrated that the nanostructure of CEP-LP@S/D was disrupted in a GSH-rich surrounding after 8 h. To further confirm the capability of CEP-LP@S/D to simultaneously deliver two drugs, we tested the encapsulation efficiencies of Sal and Dox in CEP-LP@S/D using HPLC (for Sal) and a fluorescence spectrometer (for Dox). The liposomal EE for both Dox and Sal was higher than 86%. Furthermore, the drug-loading capacities of CEP-LP@S/D and LP@S/D were determined to be 2.4 and 2.2%, respectively. Additionally, the drug-release behaviors of CEP-LP@S/D were

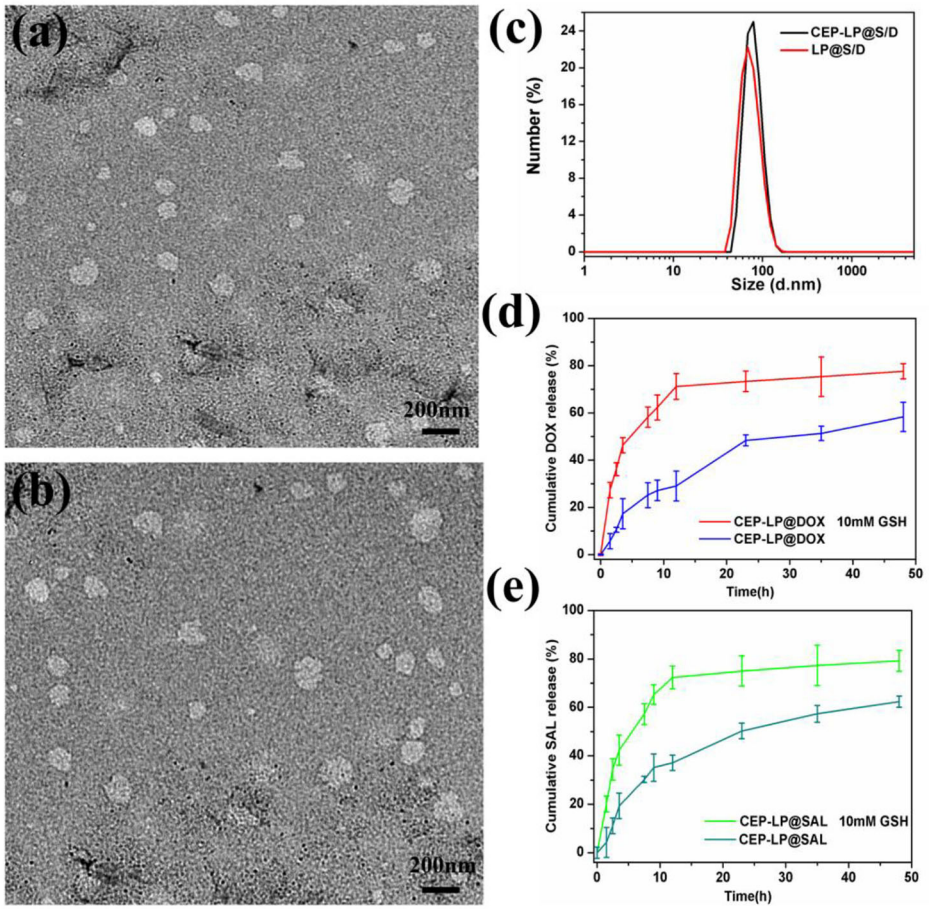

FIGURE 1 | Characterization of CEP-LP@S/D. **(a)** Transmission electron microscopy (TEM) image of LP@S/D. **(b)** TEM image of CEP-LP@S/D. **(c)** Hydrodynamic diameters of CEP-LP@S/D and LP@S/D measured by dynamic light scattering (DLS). **(d)** The *in vitro* release profiles of doxorubicin (Dox) in phosphate-buffered saline (PBS; pH 7.4) in the presence or absence of 10 mM glutathione (GSH). **(e)** The *in vitro* release profiles of salinomycin (Sal) in PBS (pH 7.4) in the presence or absence of 10 mM GSH.

investigated with or without GSH (10 mM) in PBS (pH = 7.4) at 37°C. As shown in **Figures 1d,e**, CEP-LP@S/D exhibited the ability of controlled release, as only about 37 and 29% of the Sal and Dox, respectively, were released from the drug-loaded CEP-LP@S/D after 12 h without the presence of GSH. However, a markedly enhanced drug release rate was detected in the presence of GSH (10 mM). Evidently, the GSH could effectively break the disulfide bonds of the CEP-LP@S/D lipid layers, thereby inducing the disassociation of the liposomal nanostructure; notably, more than 77.6 ± 1.4% of the loaded Dox and 79.2 ± 1.7% of the loaded Sal were released within 48 h in this case. We believe that the accelerated rate of Dox and Sal release by CEP-LP@S/D in the presence of GSH may be attributed to intracellular reducing environment-induced drug release.

Cellular Uptake and Localization

The intracellular accumulation and distribution of CEP-LP@S/D in Huh7 cells were studied using confocal microscopy. As shown in **Figure 2A**, after 4 h incubation, CEP-LP@S/D-treated cells displayed more fluorescent signals in their cytoplasms than did their LP@S/D-treated counterparts (**Supplementary Figure 4**). As time went by, red fluorescent signals indicated that Dox could diffuse into cell nuclei, indicating that the EpCAM and CD133 peptides allowed for receptor-mediated endocytosis, thereby increasing the CEP-LP@S/D uptake and internalization by CSCs. In contrast, CEP-LP@S/D-treated 293T cells showed weak red fluorescence (**Supplementary Figure 5**). On another note, these results strongly demonstrate that CEP-LP@S/D could respond to the intracellular redox environment, leading to the disruption of the disulfide bonds in the lipid membranes, which consequently enabled the highly hydrophobic Dox to readily penetrate into the cells and, thus, exhibit greater cellular accumulation. Additionally, to evaluate the CSC-targeted effect, we established $CD133^{+}EpCAM^{+}$ tumorspheres as CSC models; of course, we confirmed the stemness of these *in vitro* spheroids beforehand by analyzing the widely known stem cell markers *Oct-4*, *Sox-2*, and *CD133*, which were all overexpressed in these spheres (**Supplementary Figure 6**). As shown in **Figure 2B**,

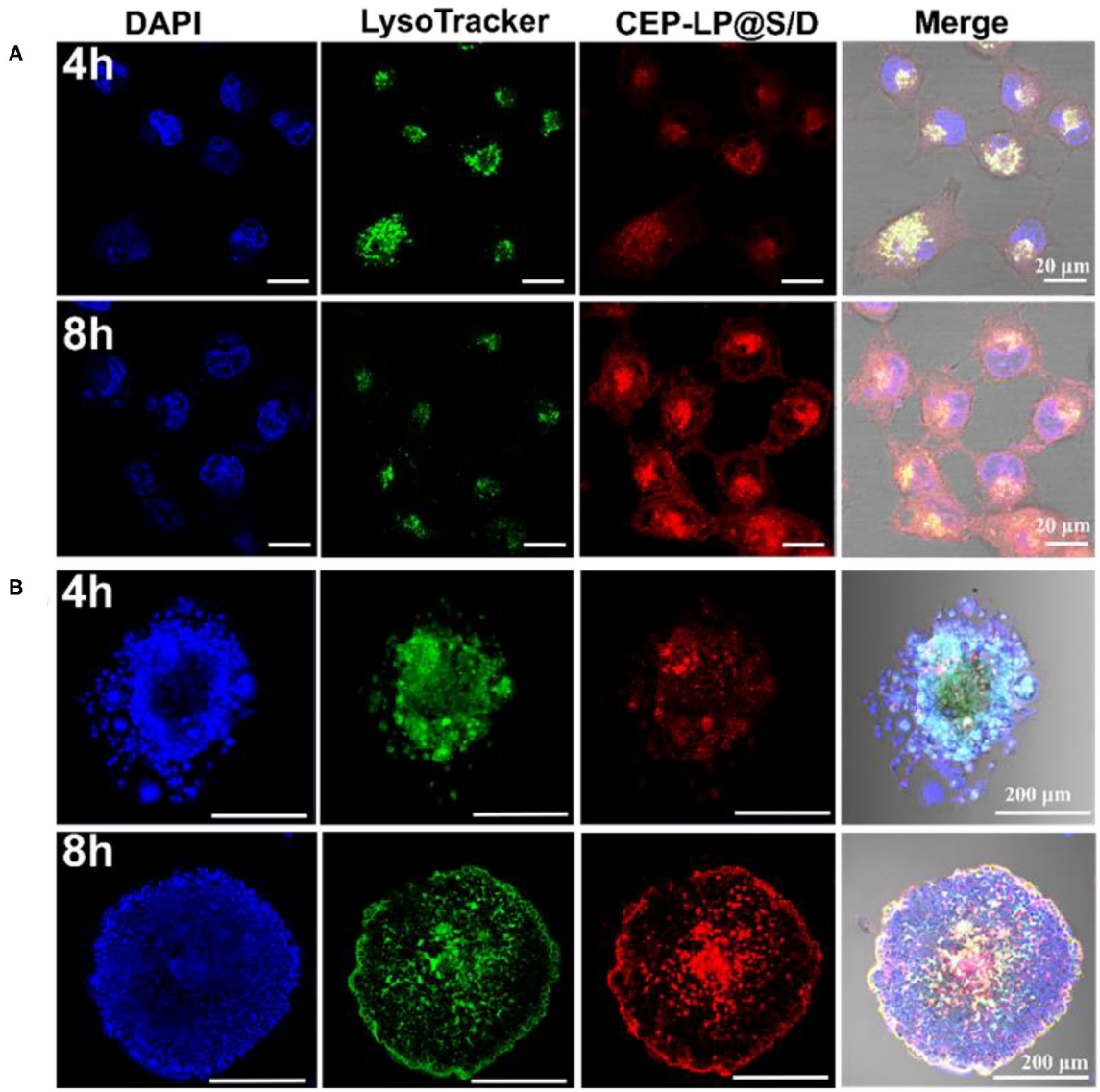

FIGURE 2 | CEP-LP@S/D uptake by confocal laser scanning microscopy (CLSM) imaging. **(A)** CLSM images of Huh-7 cells incubated with CEP-LP@S/D for 4 and 8 h. Three fluorescent dyes were used to evaluate CEP-LP@S/D uptake; the red signal represents doxorubicin (Dox), the green signal indicates lysosomes (LysoTracker Green), and the blue signal (4′,6-diamidino-2-phenylindole, DAPI) reveals the nuclei. **(B)** CLSM images of tumorsphere cells incubated with CEP-LP@S/D for 4 and 8 h.

fluorescently labeled CEP-LP@S/D (red) were obviously notable in the CSC tumorspheres and had a high intensity. Furthermore, after 8 h incubation, the red fluorescence was significantly higher and could be detected in the nuclei. These results indicate that the Y-shaped peptide modification not only led to effective targeting of CSCs but could also facilitate the permeability of liposomal NPs to the inner part of the tumorspheres. Notably, CEP-LP@S/D was efficiently accumulated in the tumors and could effectively recognize and eradicate the CSC faction.

Cytotoxicity and CSC Elimination *in vitro*

The cytotoxicity of the CEP-LP@S/D liposomes was evaluated by the MTT assay. Huh-7 cells were treated with Dox, Sal, LP@S/D, or CEP-LP@S/D at concentrations ranging from 0.01 to 0.5 mg/ml for 48 h. As shown in **Figure 3A**, CEP-LP@S/D exhibited higher cytotoxicity than did LP@S/D and the free drugs; notably, both Dox and Sal exhibited low cytotoxicity alone. This likely suggests that the dual-targeted peptide-mediated cellular uptake and GSH-triggered intracellular reductive cleavage improved the release of the loaded drugs. As expected, the tumorsphere formation assay revealed that CEP-LP@S/D induced a dramatic decrease in the number of formed tumorspheres than did the LP@S/D- and Sal-treated groups (**Figure 3B**). Moreover, as shown in **Figure 3C**, PBS (the vehicle) did not affect the tumorsphere-forming ability of Huh-7 cells. Interestingly, although the percentage of formed tumorspheres was marginally

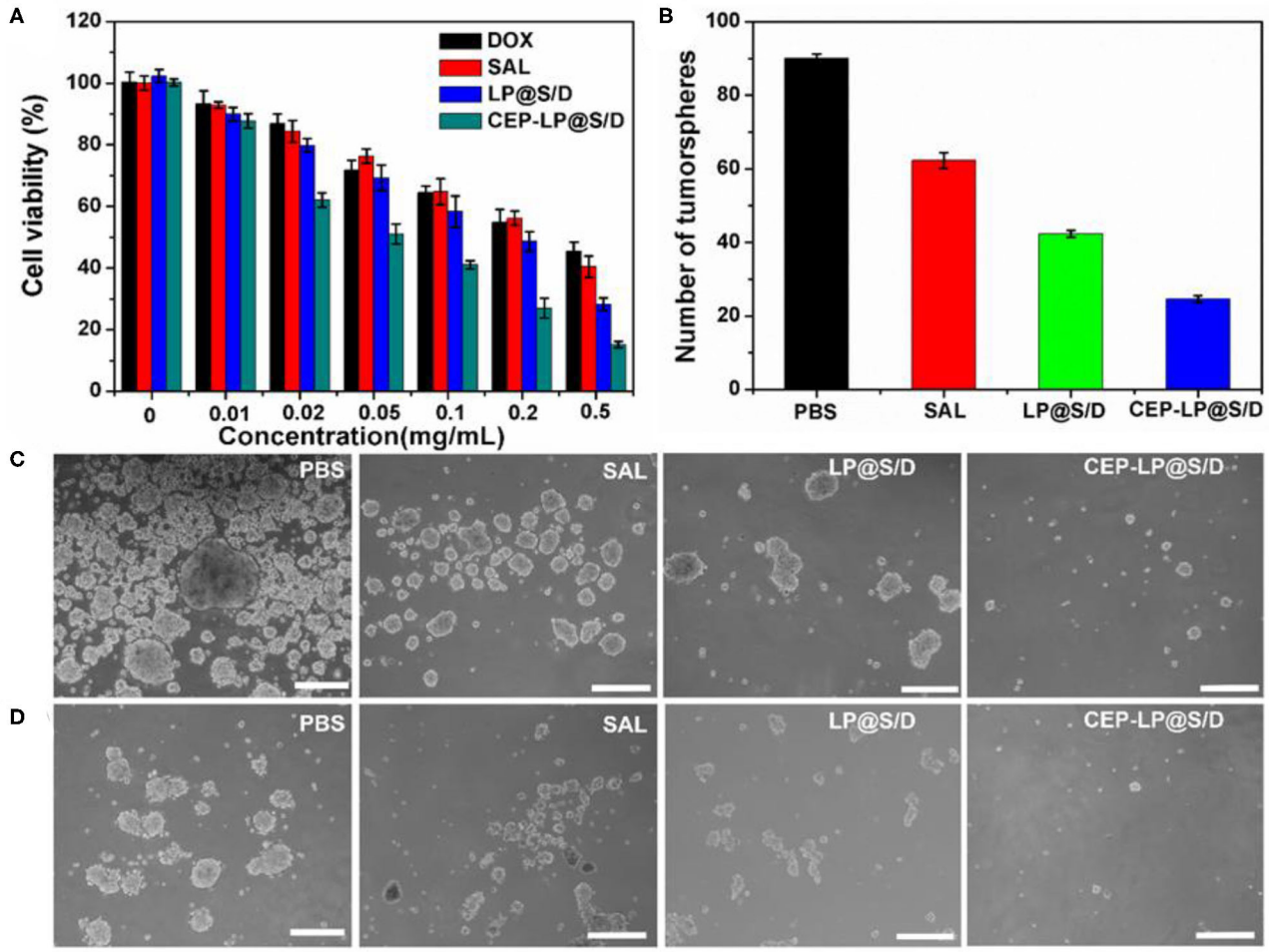

FIGURE 3 | The inhibitory effect of various groups on the tumorsphere-forming ability of Huh-7 cells. **(A)** Viability of Huh-7 cells treated with free doxorubicin (Dox), Sal, LP@S/D, or CEP-LP@S/D for 48 h. **(B)** Quantification of tumorsphere formation efficiency in Huh-7 cells treated with Sal, LP@S/D, or CEP-LP@S/D. **(C)** Images of tumorsphere formation of untreated Huh-7 cells (phosphate-buffered saline, PBS) and those treated with salinomycin (Sal), LP@S/D, or CEP-LP@S/D for 5 days. **(D)** Images of second-generation tumorsphere formation (secondary formation after dissociation of initial spheres) under PBS, Sal, LP@S/D, or CEP-LP@S/D treatment. Scale bar = 300 μm.

reduced by Sal and LP@S/D treatment, the size of the spheroids remained largely unaltered. However, the size of the tumorspheres in the CEP-LP@S/D treatment group was notably the smallest among all the groups, which suggests synergistic effects between the two drugs. To determine whether CEP-LP@S/D could induce a durable tumorsphere inhibitory response, CEP-LP@S/D-treated primary tumorspheres were dissociated into single-cell suspensions, and their propensity to form secondary tumorspheres was assessed (**Figure 3D**). It was shown that the CEP-LP@S/D group had a maximum of 89.2% inhibition rate. Once again, single-cell suspensions of Sal- and LP@S/D-treated primary tumorspheres produced more secondary tumorspheres than did those of the free Sal-treated group; however, their CEP-LP@S/D-treated counterparts exhibited non-clonogenic properties (Suntharalingam et al., 2014). It is worth mentioning that tumorsphere cells are much more resistant to free Sal, a problem that can be effectively overcome by using the liposomal construct prepared in this study. Taken together, these data show that CEP-LP@S/D inhibits the self-renewal of Huh-7 tumorspheres by eliminating the CSC population (CD133- and EpCAM-positive) and that this effect is maintained upon serial passages. Therefore, these results support the use of CEP-LP@S/D for the efficient internalization of drugs into CSC tumorspheres and preferentially inhibiting the proliferation of CSCs.

Tumor Accumulation of CEP-LP@S/D *in vivo*

The ability of CEP-LP@S/D to home toward tumors was examined by the IVIS. The CEP-LP@S/D liposomes were loaded with DiR dye prior to being injected into tumor-bearing mice. As shown in **Figure 4a**, DiR fluorescent signals were obviously detected in the tumor sites 2 h after the injection and gradually increased with time. Notably, CEP-LP@S/D-DiR signals peaked

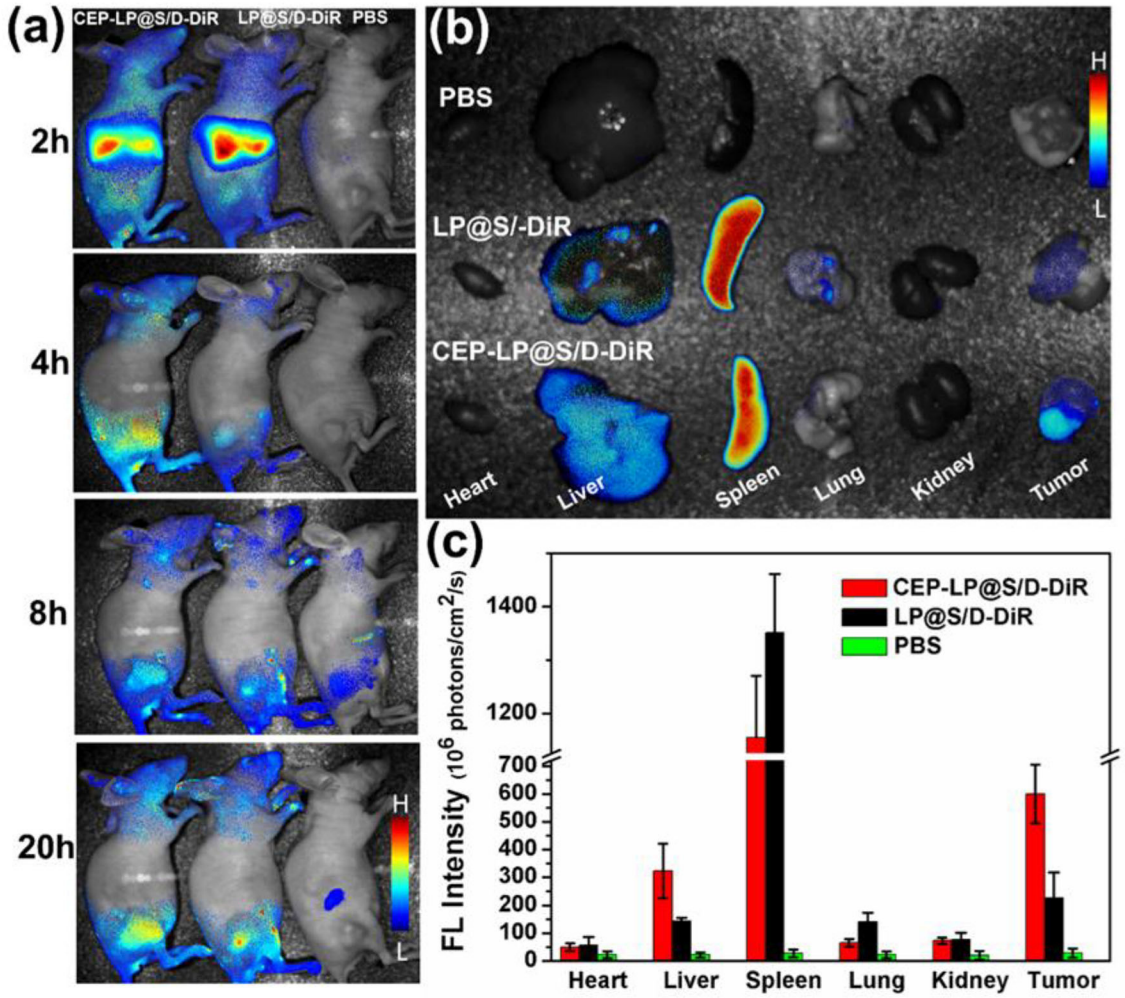

FIGURE 4 | The *in vivo* imaging distribution of CEP-LP@S/D. **(a)** *In vivo* image of Huh-7 xenograft tumor-bearing nude mice at different time points after injection with DiR-loaded CEP-LP@S/D liposomes. **(b)** *Ex vivo* image of tumors and main organs 24 h post injection of the different formulations. **(c)** The quantified biodistribution of CEP-LP@S/D in the major organs 24 h post injection.

after 20 h and gradually disappeared after the 24-h mark; moreover, they were markedly higher than those of LP@S/D-DiR. These findings clearly demonstrate that the CEP-LP@S/D liposomes remain in the tumors for a satisfactory amount of time (good retention time) and prove that they can efficiently and effectively target the tumor site in both passive and active manners. These characteristics are possible due to the Y-shaped CD133 and EpCAM ligand surface modification, which led to the enhanced permeability and retention (EPR) effect. The *ex vivo* histological analysis (biodistribution study) showed that the fluorescent CEP-LP@S/D-DiR signals were mostly detected in the tumors and spleens of the mice (**Figure 4b**). However, these signals were weaker in other organs, which exhibited only background or moderate signals, suggesting the preferable accumulation of the liposome in tumor tissues (**Figure 4c**). This result indicates that the CEP-LP@S/D liposomes favorably accumulate in the tumors, where they have a notable penetration capacity that could significantly increase the possibility of CEP-LP@S/D to eradicate CSCs *in vivo*.

In vivo Antitumor Efficacy of CEP-LP@S/D

To further verify whether CEP-LP@S/D could facilitate the accumulation of Sal and Dox in the xenograft-induced tumors, different formulations, with equivalent Dox and Sal doses of 6 mg/kg, were administered via tail vein injection every other day. As shown in **Figures 5A,B**, CEP-LP@S/D liposomes exhibited the best antitumor effect than did the other two groups. However, free Sal also showed a slight tumor inhibitory effect at the same time points, although this variation was not statistically significant. This suggests that the Y-shaped peptidic construct led to more extensive intracellular delivery via receptor-mediated targeting of $EpCAM^{+}CD133^{+}$ liver CSCs. In accordance with our *in vitro* results, CEP-LP@S/D disulfide bond breakage in response to elevated GSH levels in the cytosol explains the

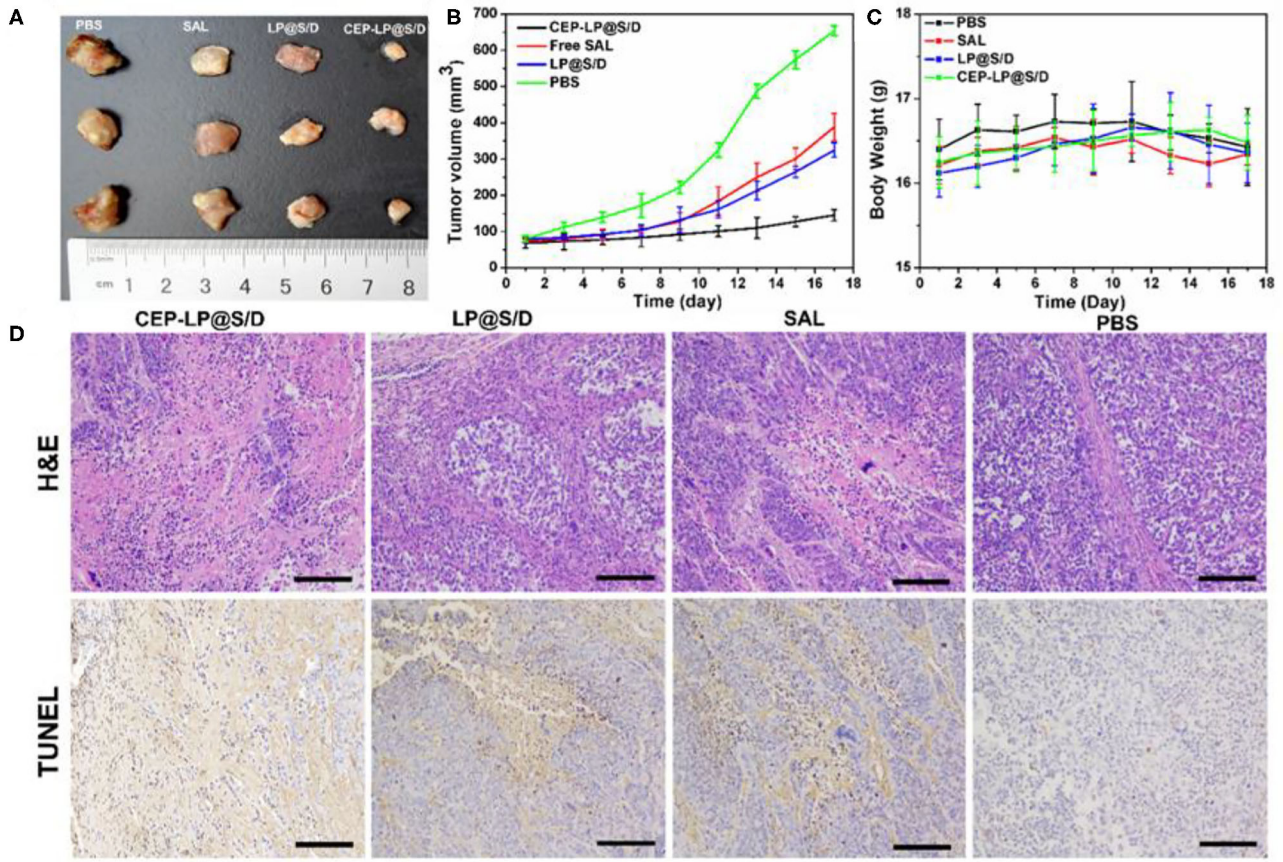

FIGURE 5 | *In vivo* antitumor activity of the different formulations on Huh-7-bearing nude mice. **(A)** The photographs of tumors in the differently treated Huh-7-bearing nude mice 18 days after tumor excision and experiment end point. **(B)** A curve representing the tumor growth of the differently treated mice. **(C)** The weight of the mice during the treatment. **(D)** Hematoxylin–eosin (HandE) and terminal deoxynucleotidyl transferase-mediated dUTP nick end labeling (TUNEL) analyses of tumor tissues after treatment with various formulations. Scale bar = 0.1 cm.

enhanced release of Dox and Sal, which in turn induce a synergistic cytotoxic effect against bulk tumor cells and CSCs. It is worth noting that none of the mice had any noticeable weight change in any of the treatment groups, suggesting there was no obvious systemic toxicity from CEP-LP@S/D (**Figure 5C**). A number of studies have indicated that *Sox-2* and *Oct-4* represent strong stemness characteristics that are crucial for the tumor initiation and self-renewal of CSCs (Ma et al., 2010). As shown in **Supplementary Figure 7**, the expression level of *Sox-2* was markedly suppressed by CEP-LP@S/D. Moreover, CEP-LP@S/D treatment also induced significant downregulation of other stemness-associated (*CD133*, *Oct-4*, and *Sox-2*) and drug efflux (*ABCG2*) genes than did the free Sal-treated group. This indicates that the CEP-LP@S/D liposome was capable of downregulating stemness-associated genes and synergistically enhancing drug cytotoxicity toward CSCs. We went further to assess the antitumor efficacy as well as the potential side effects; histological analysis of tumor slides demonstrated that CEP-LP@S/D was the most effective in inhibiting cell proliferation and inducing cell apoptosis, with only a few side effects (**Figure 5D**). In contrast, free Sal and LP@S/D did not significantly inhibit cell proliferation and showed a comparable effect to that of PBS, as demonstrated by TUNEL. Apart from these, H&E staining indicated that there is no obvious toxicity in the major organs, including the heart, liver, spleen, lung, and kidney (**Supplementary Figure 8**). As shown in **Supplementary Figure 9**, CEP-LP@S/D significantly improved the survival rate of the mice compared to other groups. Taken together, our results indicate that co-delivery of Dox and Sal via CEP-LP@S/D induced a significant synergistic anticancer effect as it combined the ability of Dox to eliminate bulk cancer cells with that of Sal to suppress the CSC population and went further to enhance their absorption and targeting abilities.

CONCLUSIONS

To reiterate, in this study, we successfully developed a new redox-responsive liposomal platform for targeted anticancer drug delivery that allows the synergistic amelioration of liver cancer. Our results indicate that the CEP-LP@S/D co-delivery system could enhance the accumulation of drugs in the tumor tissues and target CSCs via the specific peptide recognition receptors CD133 and EpCAM, which are over-expressed on

these cells. After cellular uptake, the high concentration of GSH in the cytoplasm is sufficient to break the disulfide bonds in the structure of these liposomes, thereby inducing the fast release of Dox and Sal and leading to the synergistic inhibition of tumor growth and reduction in CSC stemness. We believe that this co-delivery nano-platform could be used as an effective tool for delivering combinatorial therapeutics to synergistically inhibit liver CSCs and tumor cells. This study provides a new perspective for designing specifically responsive drug delivery systems to target CSCs and may lay the groundwork for similar approaches customized for other cancer types.

DATA AVAILABILITY STATEMENT

The original contributions presented in the study are included in the article/**Supplementary Material**, further inquiries can be directed to the corresponding authors.

ETHICS STATEMENT

The animal study was reviewed and approved by Peking University Animal ethics Committee.

AUTHOR CONTRIBUTIONS

ZW performed the experiments and wrote the manuscript. WL, MS, and YZ helped to perform *in vitro* experiments. LF helped to characterize materials and incubate cells. ZH revised the manuscript and supervised all the works. All authors contributed to the article and approved the submitted version.

FUNDING

This work was supported financially by the National Natural Science Foundation of China (Grant Nos. 81801766, 31870992, and 21775031), Science and Technology Service Network Initiative of the Chinese Academy of Sciences (Grant No. KFJ-STS-ZDTP-079), CAS-JSPS (Grant No. GJHZ2094), Fujian Medical University Foundation for the Introduction of Talents (Grant No. XRCZX2019018).

SUPPLEMENTARY MATERIAL

The Supplementary Material for this article can be found online at: https://www.frontiersin.org/articles/10.3389/fchem.2020.00649/full#supplementary-material

REFERENCES

Belhadj, Z., Ying, M., Cao, X., Hu, X., Zhan, C., Wei, X., et al. (2017). Design of Y-shaped targeting material for liposome-based multifunctional glioblastoma-targeted drug delivery. *J. Control. Release* 255, 132–141. doi: 10.1016/j.jconrel.2017.04.006

Chan, A. W. H., Tong, J. H. M., Chan, S. L., Lai, P. B. S., and To, K.-F. (2014). Expression of stemness markers (CD133 and EpCAM) in prognostication of hepatocellular carcinoma. *Histopathology* 64, 935–950. doi: 10.1111/his.12342

Clevers, H. (2011). The cancer stem cell: premises, promises and challenges. *Nat. Med.* 17, 313–319. doi: 10.1038/nm.2304

Dianat-Moghadam, H., Heidarifard, M., Jahanban-Esfahlan, R., Panahi, Y., Hamishehkar, H., Pouremamali, F., et al. (2018). Cancer stem cells-emanated therapy resistance: implications for liposomal drug delivery systems. *J. Control. Release* 288, 62–83. doi: 10.1016/j.jconrel.2018.08.043

Guo, P., Yang, J., Liu, D., Huang, L., Fell, G., Huang, J., et al. (2019). Dual complementary liposomes inhibit triple-negative breast tumor progression and metastasis. *Sci. Adv.* 5:eaav5010. doi: 10.1126/sciadv.aav5010

Gupta, P. B., Onder, T. T., Jiang, G., Tao, K., Kuperwasser, C., Weinberg, R. A., et al. (2009). Identification of selective inhibitors of cancer stem cells by high-throughput screening. *Cell* 138, 645–659. doi: 10.1016/j.cell.2009.06.034

Jia, X., Zhang, Y., Zou, Y., Wang, Y., Niu, D., He, Q., et al. (2018). Dual intratumoral redox/enzyme-responsive NO-releasing nanomedicine for the specific, high-efficacy, and low-toxic cancer therapy. *Adv. Mater.* 30:1704490. doi: 10.1002/adma.201704490

Jiang, J., Chen, H., Yu, C., Zhang, Y., Chen, M., Tian, S., et al. (2015). The promotion of salinomycin delivery to hepatocellular carcinoma cells through EGFR and CD133 aptamers conjugation by PLGA nanoparticles. *Nanomedicine* 10, 1863–1879. doi: 10.2217/nnm.15.43

Kim, Y. J., Liu, Y., Li, S., Rohrs, J., Zhang, R., Zhang, X., et al. (2015). Co-eradication of breast cancer cells and cancer stem cells by cross-linked multilamellar liposomes enhances tumor treatment. *Mol. Pharm.* 12, 2811–2822. doi: 10.1021/mp500754r

Li, S., Saw, P. E., Lin, C., Nie, Y., Tao, W., Farokhzad, O. C., et al. (2020). Redox-responsive polyprodrug nanoparticles for targeted siRNA delivery and synergistic liver cancer therapy. *Biomaterials* 234:119760. doi: 10.1016/j.biomaterials.2020.119760

Ling, X., Tu, J., Wang, J., Shajii, A., Kong, N., Feng, C., et al. (2019). Glutathione-responsive prodrug nanoparticles for effective drug delivery and cancer therapy. *ACS Nano* 13, 357–370. doi: 10.1021/acsnano.8b06400

Liu, D., Chen, B., Mo, Y., Wang, Z., Qi, T., Zhang, Q., et al. (2019). Redox-activated porphyrin-based liposome remote-loaded with indoleamine 2,3-dioxygenase (IDO) inhibitor for synergistic photoimmunotherapy through induction of immunogenic cell death and blockage of IDO pathway. *Nano Lett.* 19, 6964–6976. doi: 10.1021/acs.nanolett.9b02306

Ma, S., Tang, K. H., Chan, Y. P., Lee, T. K., Kwan, P. S., Castilho, A., et al. (2010). miR-130b promotes CD133+liver tumor-initiating cell growth and self-renewal via tumor protein 53-induced nuclear protein 1. *Cell Stem Cell* 7, 694–707. doi: 10.1016/j.stem.2010.11.010

Mai, T. T., Hamaï, A., Hienzsch, A., Cañeque, T., Müller, S., Wicinski, J., et al. (2017). Salinomycin kills cancer stem cells by sequestering iron in lysosomes. *Nat. Chem.* 9, 1025–1033. doi: 10.1038/nchem.2778

Mao, X., Liu, J., Gong, Z., Zhang, H., Lu, Y., Zou, H., et al. (2015). iRGD-conjugated DSPE-PEG2000 nanomicelles for targeted delivery of salinomycin for treatment of both liver cancer cells and cancer stem cells. *Nanomedicine* 10, 2677–2695. doi: 10.2217/nnm.15.106

Mikhail, S., and He, A. R. (2011). Liver cancer stem cells. *Int. J. Hepatol.* 2011:486954. doi: 10.4061/2011/486954

Rao, W., Wang, H., Han, J., Zhao, S., Dumbleton, J., Agarwal, P., et al. (2015). Chitosan-decorated doxorubicin-encapsulated nanoparticle targets and eliminates tumor reinitiating cancer stem-like cells. *ACS Nano* 9, 5725–5740. doi: 10.1021/nn506928p

Reda, A., Hosseiny, S., and El-Sherbiny, I. M. (2019). Next-generation nanotheranostics targeting cancer stem cells. *Nanomedicine* 14, 2487–2514. doi: 10.2217/nnm-2018-0443

Saygin, C., Matei, D., Majeti, R., Reizes, O., and Lathia, J. D. (2019). Targeting cancer stemness in the clinic: from hype to hope. *Cell Stem Cell* 24, 25–40. doi: 10.1016/j.stem.2018.11.017

Shen, S., Sun, C.-Y., Du, X.-J., Li, H.-J., Liu, Y., Xia, J.-X., et al. (2015). Co-delivery of platinum drug and siNotch1 with micelleplex for

enhanced hepatocellular carcinoma therapy. *Biomaterials* 70, 71–83. doi: 10.1016/j.biomaterials.2015.08.026

Shen, S., Xia, J. X., and Wang, J. (2016). Nanomedicine-mediated cancer stem cell therapy. *Biomaterials* 74, 1–18. doi: 10.1016/j.biomaterials.2015.09.037

Suntharalingam, K., Lin, W., Johnstone, T. C., Bruno, P. M., Zheng, Y.-R., Hemann, M. T., et al. (2014). A breast cancer stem cell-selective, mammospheres-potent osmium(VI) nitrido complex. *J. Am. Chem. Soc.* 136, 14413–14416. doi: 10.1021/ja508808v

Tan, T., Wang, H., Cao, H., Zeng, L., Wang, Y., Wang, Z., et al. (2018). Deep tumor-penetrated nanocages improve accessibility to cancer stem cells for photothermal-chemotherapy of breast cancer metastasis. *Adv. Sci.* 5:1801012. doi: 10.1002/advs.201801012

Wang, M., Xie, F., Wen, X., Chen, H., Zhang, H., Liu, J., et al. (2017). Therapeutic PEG-ceramide nanomicelles synergize with salinomycin to target both liver cancer cells and cancer stem cells. *Nanomedicine* 12, 1025–1042. doi: 10.2217/nnm-2016-0408

Wang, W., Wang, Z., Bu, X., Li, R., Zhou, M., and Hu, Z. (2015b). Discovering of tumor-targeting peptides using bi-functional microarray. *Adv. Healthcare Mater.* 4, 2802–2808. doi: 10.1002/adhm.201500724

Wang, Y., He, L., Du, Y., Zhu, P., Huang, G., Luo, J., et al. (2015a). The long noncoding RNA lncTCF7 promotes self-renewal of human liver cancer stem cells through activation of Wnt signaling. *Cell Stem Cell* 16, 413–425. doi: 10.1016/j.stem.2015.03.003

Wang, Y., Jia, F., Wang, Z., Qian, Y., Fan, L., Gong, H., et al. (2019). Boosting the theranostic effect of liposomal probes toward prominin-1 through optimized dual-site targeting. *Anal. Chem.* 91, 7245–7253. doi: 10.1021/acs.analchem.9b00622

Yang, H., Wang, Q., Li, Z., Li, F., Wu, D., Fan, M., et al. (2018). Hydrophobicity-adaptive nanogels for programmed anticancer drug delivery. *Nano Lett.* 18, 7909–7918. doi: 10.1021/acs.nanolett. 8b03828

Yarchoan, M., Agarwal, P., Villanueva, A., Rao, S., Dawson, L. A., Llovet, J. M., et al. (2019). Recent developments and therapeutic strategies against hepatocellular carcinoma. *Cancer Res.* 79, 4326–4330. doi: 10.1158/0008-5472.can-19-0803

Yu, L.-Y., Shen, Y.-A., Chen, M.-H., Wen, Y.-H., Hsieh, P.-I., and Lo, C.-L. (2019). The feasibility of ROS- and GSH-responsive micelles for treating tumor-initiating and metastatic cancer stem cells. *J. Mater. Chem. B* 7, 3109–3118. doi: 10.1039/C8TB02958J

Zhang, Y., Zhang, H., Wang, X., Wang, J., Zhang, X., and Zhang, Q. (2012). The eradication of breast cancer and cancer stem cells using octreotide modified paclitaxel active targeting micelles and salinomycin passive targeting micelles. *Biomaterials* 33, 679–691. doi: 10.1016/j.biomaterials.2011.09.072

Zhao, P., Dong, S., Bhattacharyya, J., and Chen, M. (2014). iTEP nanoparticle-delivered salinomycin displays an enhanced toxicity to cancer stem cells in orthotopic breast tumors. *Mol. Pharm.* 11, 2703–2712. doi: 10.1021/mp5002312

Conflict of Interest: The authors declare that the research was conducted in the absence of any commercial or financial relationships that could be construed as a potential conflict of interest.

The reviewer LJ declared a shared affiliation with authors MS, WL, LF, and ZH to the handling editor at the time of review.

frontiers in Chemistry

MINI REVIEW
published: 29 September 2020
doi: 10.3389/fchem.2020.00758

Tumor Microenvironment-Responsive Nanomaterials as Targeted Delivery Carriers for Photodynamic Anticancer Therapy

Houhe Liu[1], Jiwen Yao[1], Huanhuan Guo[1], Xiaowen Cai[1], Yuan Jiang[1], Mei Lin[1], Xuejun Jiang[1], Wingnang Leung[2] and Chuanshan Xu[1]**

[1] Key Laboratory of Molecular Target and Clinical Pharmacology, State Key Laboratory of Respiratory Disease, School of Pharmaceutical Science & Fifth Affiliated Hospital, Guangzhou Medical University, Guangzhou, China, [2] Asia-Pacific Institute of Aging Studies, Lingnan University, Hong Kong, China*

Photodynamic therapy (PDT), as an alternative approach to treat tumors through reactive oxygen species (ROS) produced by the activated photosensitizers (PS) upon light irradiation, has attracted wide attention in recent years due to its low invasive and highly efficient features. However, the low hydrophilicity and poor targeting of PS limits the clinical application of PDT. Stimuli-responsive nanomaterials represent a major class of remarkable functional nanocarriers for drug delivery. In particular, tumor microenvironment-responsive nanomaterials (TMRNs) can respond to the special pathological microenvironment in tumor tissues to release the loaded drugs, that allows them to control the release of PS within tumor tissues. Recent studies have demonstrated that TMRNs can achieve the targeted release of PS at tumor sites, increase the concentration of PS in tumor tissues, and reduce side effects of PDT. Hence, in the present paper, we review TMRNs, mainly including pH-, redox-, enzymes-, and hypoxia-responsive smart nanomaterials, and focus on the application of these smart nanomaterials as targeted delivery carriers of PS in photodynamic anticancer therapy, to further boost the development of PDT in tumor therapy.

Keywords: photodynamic therapy, photosensitizer, drug delivery, tumor microenvironment, stimuli-responsive nanomaterials

OPEN ACCESS

Edited by:
Yi Hou,
Beijing University of Technology, China

Reviewed by:
Zonghai Sheng,
Chinese Academy of Sciences (CAS), China
Raghvendra Ashok Bohara,
National University of Ireland Galway, Ireland

****Correspondence:***
Chuanshan Xu
xcshan@163.com
Wingnang Leung
awnleung@gmail.com

Specialty section:
This article was submitted to Nanoscience, a section of the journal Frontiers in Chemistry

Received: *28 April 2020*
Accepted: *22 July 2020*
Published: *29 September 2020*

Citation:
Liu H, Yao J, Guo H, Cai X, Jiang Y, Lin M, Jiang X, Leung W and Xu C (2020) Tumor Microenvironment-Responsive Nanomaterials as Targeted Delivery Carriers for Photodynamic Anticancer Therapy. Front. Chem. 8:758. doi: 10.3389/fchem.2020.00758

INTRODUCTION

Photodynamic therapy (PDT) is a promising approach to treat malignancies and other non-neoplastic lesions including condyloma acuminata, acne, and port wine stains (Rkein and Ozog, 2014). For decades, safe and effective PDT in the management of cancer has attracted extensive attention in clinical settings (Kelly et al., 1975; Chang et al., 2018; Feng et al., 2018; Sun et al., 2019). However, poor targeting and low solubility of most photosensitizers (PS) limits the clinical application of PDT (Panagopoulos et al., 1989; Haddad et al., 2000; Dolmans et al., 2003; Chatterjee et al., 2008). Recently, nanomaterials have shown great promise for improving the solubility and targeting of PS (Lieber, 2003; Roco, 2003a,b). Nanoformulations can not only reduce the side effects of PS, but also increase the therapeutic effect of PDT through controlling the delivery of PS in the tumor tissues. However, it is very difficult for conventional

nanomaterials such as liposomes, micelles, dendrimers, and polymeric nanoparticles to deliver PS precisely to tumor lesions via the enhanced permeability and retention effect (EPR) (Marcucci et al., 2016). It is well-known that tumor tissues are a complex system consisting of tumor cells and their surrounding cellular and extracellular materials. The tumor microenvironment (TME) is composed of tumor cells and tumor stroma (Ramamonjisoa and Ackerstaff, 2017). In TME, there are diverse cell types including fibroblasts, pericytes, endothelial cells, dendritic cells, smooth muscle cells, inflammatory cells, and cancer stem cells (CSCs). The TME-forming cells interact with tumor cells to create a unique pathological TME over the normal tissues, including hypoxia, low pH, overexpressed enzymes, and redox conditions (Liu and Huskens, 2015; Tian et al., 2017). The unique features of TME motivate many researchers to develop tumor microenvironment-responsive nanomaterials (TMRNs) as drug carriers for precisely delivering the loaded drugs to enhance drug concentrations in tumor cells through responding to the specific pathological microenvironment in tumor tissues (Muthu et al., 2009; Wei et al., 2013; Karimi, 2015; Paris et al., 2015; Nazemi et al., 2016). Most recently, TMRNs as delivery carriers of PS have been widely researched and developed in PDT on tumors. In the present article, we focus on reviewing the application of TMRNs as targeted delivery carriers for photodynamic anticancer therapy, including its principle and defect and update new research progress to enrich and promote the development of PDT.

PRINCIPLE OF PDT

PDT is based on a reactive oxygen species (ROS) generated from light-activated PS to kill cancer cells (Pervaiz and Olivo, 2006; Li et al., 2019). When PS is irradiated by light at a specific wavelength, the excited PS transfers from a single-electron state to a low-lying or high-lying electronic singlet state, and then reaches the excited triplet state by intersystem crossing. Triplet PS becomes a ground state by collision with ground-state triplet molecular oxygen, and triplet molecular oxygen is excited into a singlet electronically excited state, which in turn produces singlet oxygen and other ROS, including superoxide anions (O_2^-), hydroxyl radicals, and hydrogen peroxide (H_2O_2). These ROS can damage most types of biomolecules. ROS are the direct effectors that PDT kills tumor cells with (Oleinick et al., 2002; Jain et al., 2017; Dobson et al., 2018; Jiang et al., 2019), however, most PS lack targeting capability and induce cytotoxicity on neighbor normal cells by releasing ROS during photodynamic anticancer therapy. Thus, there is an urgent need to precisely control the production of ROS in target cells for improving the clinical outcome of PDT.

TMRNs AS TARGETED DELIVERY CARRIERS FOR PHOTODYNAMIC ANTICANCER THERAPY

A TME has unique pathological conditions over normal tissues, including low pH, high GSH, hypoxia, and some specific enzymes highly expressed in tumor tissues (Upreti et al., 2013). On the basis of the unique features in TME, TMRNs have been developed as a novel smart nanoplatform that can intelligently respond to special pathological conditions in TME, such as pH-responsive, redox-responsive, hypoxia-responsive, enzyme-responsive, and multiple stimuli-responsive nanomaterials, for specifically delivering PS to tumor tissues (Zhu et al., 2017). As shown in **Figure 1**, after the TMRNs reach the tumor site and enter the tumor tissue due to the EPR effect. Then, the photosensitizer is released inside or outside the tumor cells in response to the TME stimuli. When the photosensitizer is irradiated by excitation light, ROS will be generated by electron transfer or energy transfer. The detailed information of the reaction principles and reaction sites of several stimulus response nanomaterials mentioned below are shown in **Table 1**.

pH-Responsive Nanomaterials

Under normal circumstances, the pH of extracellular tissues and blood is usually maintained at around 7.4. Due to the high rate of glycolysis, the pH in solid tumors reduces to around 5.0–6.8 (Park et al., 2007; Chen et al., 2016; Liu et al., 2016). In addition, the pH in lysosomes is also lower than other organelles in tumor cells. Therefore, pH can be widely used as a stimuli approach for the precise delivery of PS. Currently, the design strategy for pH-responsive nanomaterials used in PDT is mainly based on chemical bond breaking in the low pH environment. Han et al. (2017) found shape-switched tumor extracellular pH-responsive chimeric peptide (named DEAK-DMA)-based nanoparticles to enhance tumor uptake of PS on the basis of acidic condition-induced detachment of the dimethylmaleic anhydride group. DEAK-DMA could self-assemble into spherical nanoparticles under physiological conditions. In the acidic microenvironment in tumor tissues, DEAK-DMA undergoes disruption of the acid-sensitive 2,3-dimethylmaleic anhydride group. Then the restoration of ionic complementarity between the DEAK-DMA induced the formation of rod-shaped nanoparticles, thereby enhancing uptake of PS in the tumor cells. The protonation of certain groups in an acidic environment can also affect the physical and chemical properties of the entire molecule (Yang X. D. et al., 2019), which also provides an alternative strategy for designing pH-responsive nanomaterials. Liang et al. (2018) designed a biocompatible pH-responsive nanoparticle (named DAA) by the self-assembly approach to exhibit effective PDT/photothermal anticancer activities due to the protonation of diethylaminophenyl. In addition, the anti-vascular drug 5,6-dimethylxanthine-4-acetic acid was combined in the DAA nanoparticles for targeting the vascular endothelial growth factor and was found to release from the weakly acidic endocytic organelles of endothelial cells by hydrolysis of the ester bond, and effectively prevent the spread and metastasis of tumors. Yang et al. (2018) used tamoxifen to fabricate a pH-responsive nanoparticle (named HSA–Ce6/TAM) for PDT via the self-assembly of the human serum albumin (HSA) modified with Chlorin e6 (Ce6). The protonated tamoxifen dissociated it from HSA–Ce6/TAM in the acidic condition to push the HSA–Ce6/TAM nanoparticles (≈130 nm) to break down into smaller nanoparticles (≈10 nm), which promoted Ce6 uptake into target cells.

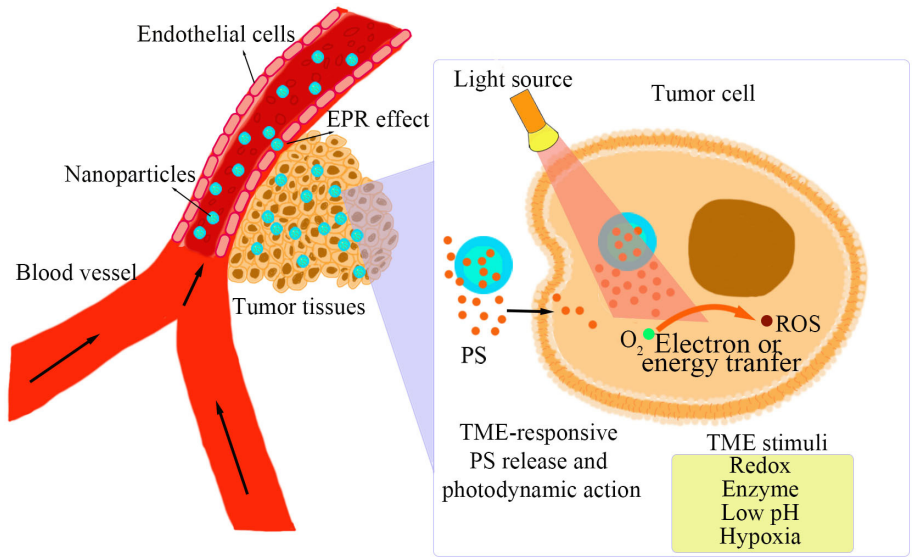

FIGURE 1 | TME-responsive PS release and photodynamic action.

In situ burst releases of tumor antigens induced by PDT significantly initiated the immune response (Ng et al., 2018; Meng et al., 2019a; Wang et al., 2019). Yang et al. (2020) prepared the pH-responsive double load nanovesicles (named PEG-b-cPPT) by self-assembly of block copolymer polyethylene glycol-b-cationic polypeptide. In the acidic environment, the double-loaded nanoparticles released the PS and indoximod into the cytoplasm because of the protonation of the tertiary amine in the cationic polypeptide. The nanovesicles were not only the carriers of PS, but also induced immunogenic cell death upon light irradiation, providing a novel strategy for the combination of PDT and immunotherapy.

Redox-Responsive Nanomaterials

Redox-responsive nanomaterials can effectively deliver and release loaded drugs to target cells because the glutathione (GSH) concentration in tumor tissues is four times that in normal tissues (Mo and Gu, 2016). In addition, the intracellular GSH level is usually higher compared with the extracellular environment. Thus, redox-responsive nanomaterials are also expected to be used for targeted delivery (Fukino et al., 2017; Raza et al., 2018). The disulfide bonds are converted into sulfhydryl groups after being reduced by the action of GSH, which leads to the destruction of the nanoparticles. Meanwhile, due to the stability of the disulfide bonds in the external environment, the redox-responsive nanomaterials can protect the loaded drugs from premature release (Iqbal and Keshavarz, 2018). Deng et al. (2020) synthesized a nanoparticle (named Ds-sP/TCPP-T^{ER}) containing disulfide reduction-sensitizer and an endoplasmic reticulum targeting PS, which could induce endoplasmic reticulum stress through ROS in the endoplasmic reticulum and enhance immunogenic cell death to activate immune activity. Wang et al. (2017) constructed a powerful and intelligent "all in one" protoporphyrin-based polymer nanoplatform (named DPPSC) that had the ability to enhance chemotherapy-PDT by gradually and intelligently responding to low pH in lysosomes and high concentration GSH in cytoplasm. The polymer consisted of dextran grafted by protoporphyrin IX as a hydrophilic segment and the anticancer drug camptothecin was coupled to dextran through a disulfide bond containing a pH-sensitive linker as a hydrophobic segment. The use of photochemical internalization enhanced nanoparticles in tumor cells and subsequently released PS and camptothecin through pH and GSH responses, achieving the synergistic therapy of PDT and chemotherapeutic drugs.

Hypoxia-Responsive Nanomaterials

Hypoxia is the most common phenomenon in a majority of solid tumors, which provides opportunities for tumor-specific diagnosis and treatment triggered by hypoxia-responsive nanomaterials (Vordermark, 2010; McKeown, 2014). Growing evidence shows that azobenzene derivatives can be reduced to aniline derivatives by various reductases in the hypoxia environment (Mirabello et al., 2018). Owing to excellent hypoxia sensitivity, azobenzene derivatives have widely been used to detect hypoxia levels as hypoxia-reactive fluorescent probes as well as deliver drug or genes to hypoxic cancer cells for anticancer therapy (Perche et al., 2014; Dong et al., 2020). Yang G. et al. (2019) cross-linked the hypoxia-sensitive azophenyl group between the HSA coupled with the Ce6 and the HSA combined with the oxaliplatin prodrug to prepare a unique hypoxia-responsive nanosystem (named HCHOA). HCHOA was stable under normal tissue. In a hypoxic tumor, the azobenzene group in HCHOA nanoparticles will be cleaved by reductase and dissociated into small particle size complexes (Ho and HC) with diameters of <10 nm, which can significantly improve the penetration ability of the nanoparticles and enhance the

TABLE 1 | Summary of tumor microenvironment-responsive nanomaterials for PDT.

Types of stimuli-responsive nanomaterials	Nanomaterials	Photosensitizer	Responsive site	Principle of response	Application	References
pH-responsive	DEAK-DMA	Protoporphyrin IX	2,3-dimethylmaleic anhydride	Amide bond breaks	PDT for hela cells and H22 tumors	Han et al., 2017
	DAA	Diketopyrrolopyrrole	Diethylaminop-henyl	The protonation of Diethylaminop-henyl	PDT for hela cells / PDT for hela tumors	Liang et al., 2018
	HSA–Ce6/TAM	Ce6	Tamoxifen	The protonation of tamoxifen	PDT for 4T1 cells / PDT for 4T1 tumors	Yang et al., 2018
	PEG-b-cPPT	2-(1-hexyloxyethyl)-2-devinyl pyropheophorbide-a	Tertiary amines	The protonation of tertiary amines	PDT for B16F10 cells and MC38 tumors	Yang et al., 2020
Redox-responsive	Ds-sP/TCPP-T^{ER}	4,4′,4′′,4′′′-(porphyrin-5,10,15,20-tetrayl)tetrakis(N-(2-((4-methylphenyl) sulfonamido)ethyl)benzamide	Disulfide bond	GSH causes Disulfide reduction	PDT for 4T1, MDA-MB-435, MDA-MB-231 and MCF-7 cells / PDT for 4T1 tumors	Deng et al., 2020
	DPPSC	Protoporphyrin IX	Disulfide bond	GSH causes Disulfide reduction	PDT for PANC-1 cells / PDT for PANC-1 tumor	Wang et al., 2017
Hypoxia-responsive	HCHOA	Ce6	Azobenzene group	Azobenzene derivatives reduce to aniline derivatives	PDT for 4T1 cells / PDT for 4T1 tumors	Yang G. et al., 2019
	TENAB	ENAB	TPZ	Hypoxia-responsive to produce (OH•)	PDT for hela cells / PDT for hela tumors	Chen et al., 2019
	PA/HA-Ce6@TPZ	Ce6	Alkylated 2-nitroimidazole	Alkylated 2-nitroimidazole reduced to alkyl-2-aminoimidazole	PDT for 4T1 and L929 cells/PDT for 4T1 tumors	Zhu et al., 2019
Enzyme-responsive	DBHA	Diiodo-styryl-BODIPY	HA	Hyaluronidase causes HA degradation	PDT for HCT-116 cells/PDT for HCT-116 tumors	Shi et al., 2016
	BCPs	coumarin and Nile blue	Quinone trimethyl	NQO1 enzyme triggers self-immolative cleavage of quinone	PDT for A549 cells/PDT for A549 tumors	Yao et al., 2020
Multiple stimuli-responsive	Ce6-Ns	Ce6	HSA and disulfide bond	Proteases causes HSA dissociate. Low pH reduced the electrostatic adsorption of HAS. GSH causes Disulfide reduction	PDT for HeLa, B16, and MCF-7 cells / PDT for MCF-7 tumors	Zhang et al., 2016
	$pSiO_2$ -ss-HA/CHI	Carbon quantum dots	Disulfide bonds, hydrogen bonds and HA	Hyaluronidase causes HA dissociate. Low pH causes swelling or shedding of the HA/CHI layer. GSH causes Disulfide reduction	PDT for HCT-116 cells	Chen et al., 2020

accumulation of photosensitizers and drugs in tumor tissues. Tirapazamine (TPZ) is a promising hypoxic-specific prodrug that can be activated under hypoxic conditions to produce hydroxyl radicals (HO•). Chen et al. (2019) encapsulated TPZ and aza-BODIPY derivatives in eutectic materials by the use of oleic acid and linoleic acid to prepare a near infrared activated and hypoxia-responsive nanomaterial (named TENAB) for the combined treatment of PDT and chemotherapy. The release of TPZ is triggered by the hyperthermia generated by aza-BODIPY derivatives under laser irradiation at 808 nm. Meanwhile, when activated at pH 5.0, aza-BODIPY derivatives in molten TENAB NPs will switch the charge transfer (CT) state to produce ROS and consume oxygen to aggravate the hypoxic environment. TPZ was reduced to its cytotoxic form, producing hydroxyl radical (HO•) to enhance PDT efficiency. Zhu et al. (2019) designed tumor-targeted, low-oxygen dissociable nanoparticles (named PA/HA-Ce6@TPZ) for the delivery of Ce6 and low-oxygen activating drug TPZ. After irradiation with Ce6 light, tumor cells enter endocytosis and produce high concentration of ROS, which leads to apoptosis and a local hypoxia environment.

Enzyme-Responsive Nanomaterials

Compared with normal tissues, certain enzymes such as matrix metalloproteinase, hyaluronidase, β-glucuronidase, and esterase

are usually overexpressed in the tumor microenvironment (Lopez-Otin and Bond, 2008; McAtee et al., 2014). The selectivity and effectivity of enzymatic reactions endow enzyme-responsive nanomaterials with an extensive prospect in the targeted delivery and precise release of PS. Hyaluronic acid (HA) is a negatively charged natural glycosaminoglycan, widely distributed in the human body. HA has good biocompatibility and can target the CD44 receptor overexpressed in many types of cancer cells (Toole, 1990). When reaching the tumor tissues, hyaluronidase within tumor tissues can degrade HA (Choi et al., 2019). Shi et al. (2016) used diiodo-styryl-BODIPY as a PS, and then conjugated HA to prepare hyaluronidas-responsive nanoparticles (named DBHA) as activatable photodynamic theranostics for treating cancer. In normal tissues, because of the aggregation of diiodo-styryl-BODIPY in DBHA, they limit the production of ROS. However, after endocytosis of tumor cells, HA of DBHA was degraded by hyaluronidase in lysosome, and then diiodo-styryl-BODIPY was released and induced the PDT activity in tumor cells.

NADPH: quinone oxidoreductase isoenzyme 1 (NQO1) is a very special enzyme, which can catalyze the two-electron reduction of quinone (Oh and Park, 2015). Numerous studies have shown that NQO1 is upregulated in breast cancer, pancreatic cancer, colorectal cancer, cervical cancer, and lung cancer (Ma et al., 2014; Yang et al., 2014). Yao et al. (2020) reported that NQO1-responsive multifunctional polymer vesicles (named BCPs) covalently conjugated with PS (coumarin and Nile Blue). In the absence of NQO1, due to the "dual quenching" effect, that is to say, the quenching caused by aggregation caused by photoinduced electron transfer (PET) and the quenching of quinone production, the fluorescence emission and PDT efficiency were in the "off" state. After the NQO1-responsive nanovesicles entered into the tumor cells, the NQO1 in the tumor cells triggered the self-immolative cleavage of the quinone trimethyl lock, the release of the PS, and the simultaneous NIR emission and PDT activation.

Multiple Stimuli-Responsive Nanomaterials

Due to the unique characteristics of the tumor microenvironment, stimuli-responsive nanomaterials are extensively accepted as targeted delivery and precise release carriers in photodynamic anticancer therapy (Yang et al., 2018; Ma et al., 2019). Many new advances have been made in developing stimuli-responsive nanomaterials in PDT, however, most stimuli-responsive nanomaterials are only responsive to a single stimulation (Zhang et al., 2017). Tumor tissues are actually very complex biological systems with low pH, hypoxia, redox, and enzymes overexpressed in the microenvironment (Klaikherd et al., 2009). Multiple stimuli-responsive nanomaterials could respond to two or more types of stimuli in the tumor environment simultaneously, which show great promise in more precise delivery and release of drugs to target sites (Zhang et al., 2016). Zhang et al. (2016) used HSA and poly-l-lysine with surface modification by polyethylene glycol to design and prepare a multiple stimuli-responsive nanomaterial (named Ce6-Ns) according to an electrostatic assembly strategy. Then Ce6, protoporphyrin IX, or verteporfin were loaded in the nanomaterials to prepare a pH/redox/enzyme-responsive protein nanospheres for photodynamic tumor ablation. When the nanoparticles reached the tumor tissues, the proteases overexpressed by the tumor cells decomposed HSA and caused the HSA to dissociate. Under the influence of the HSA isoelectric point, the acidic condition in the tumor tissues reduced the electrostatic adsorption of HSA, and the disulfide bonds in HSA were reduced by the overexpressed GSH in tumor cells. Therefore, Ce6-Ns can effectively enhance the accumulation of Ce6 in tumor sites and improve the efficiency of PDT. Chen et al. (2020) prepared a triplet responsive porous silica carrier (named pSiO2 -ss-HA/CHI) to load carbon quantum dots and doxorubicin for photodynamic / chemotherapy. Firstly, an amino-functional porous silica nanoparticles with central radial pores were prepared using an emulsion method, and then succinic acid and cystamine were successively grafted onto the surface of the nanoparticles via amide bonds as linkers. Subsequently, doxorubicin and carbon quantum dots were loaded in the nanoparticles. Finally, the surface of the carrier was coated with HA and chitosan to block the drug-loading holes. Due to the presence of disulfide bonds, amino bonds, and hydrogen bonds in the nanoparticles, the nanomaterials showed pH-, redox-, and enzyme-responsive features.

SUMMARY AND OUTLOOK

With the development of laser medicine and material science in recent years, PDT has become a promising treatment for combating malignancies. However, poor targeting and low water solubility of the conventional PS limit the application of PDT in clinical settings. TMRNs, including pH-, redox-, hypoxia-, and enzyme-responsive nanoparticles, have been proposed as targeted delivery carriers of PS to enhance the therapeutic efficacy of PDT. Moreover, a tumor is a complex and refractory disease. Single therapy is often difficult to cure it. Combined therapy has become a main strategy in the management of malignancies using multiple approaches such as chemotherapy, immunotherapy, and PDT (Liu et al., 2017; Cheng et al., 2019; Meng et al., 2019b). TMRNs as a smart delivery carrier could be a favorable "bridge" to load PS, chemotherapeutic drugs, and immune-enhancing drugs together to precisely deliver and release multiple drugs to target cells, achieving synergistic treatment of PDT, chemotherapy, and immunotherapy. As of now TMRNs have been confirmed as targeted delivery carriers of PS for PDT in *in-vitro* and *in-vivo* models. However, few clinical trials have investigated the precise delivery of PS for PDT on tumors using TMRNs. A main challenge is the complexity of TMRNs such as tedious preparation, complicated characterization, and uncertainty of the *in-vivo* fate of TMRNs. Thus, addressing these shortcomings should be an important task for translating TMRNs as a

targeted delivery carrier of PS for the clinical application of PDT.

AUTHOR CONTRIBUTIONS

HL: principal writer. CX and WL: article revision and review before submission. JY, HG, XC, YJ, ML, and XJ: provide written suggestions. All authors contributed to the article and approved the submitted version.

FUNDING

This work was supported by Funds of Talents for High-level University in the Construction of Guangzhou Medical University (no. B195002009025).

REFERENCES

Chang, Y., Cheng, Y., Feng, Y., Jian, H., Wang, L., and Ma, X., et al. (2018). Resonance energy transfer-promoted photothermal and photodynamic performance of Gold-copper sulfide yolk-shell nanoparticles for chemophototherapy of cancer. *Nano. Lett.* 18, 886–897. doi: 10.1021/acs.nanolett.7b04162

Chatterjee, D. K., Fong, L. S., and Zhang, Y. (2008). Nanoparticles in photodynamic therapy: An emerging paradigm. *Adv. Drug. Deliver. Rev.* 60, 1627–1637. doi: 10.1016/j.addr.2008.08.003

Chen, D., Tang, Y., Zhu, J., Zhang, J., Song, X., and Wang, W., et al. (2019). Photothermal-pH-hypoxia responsive multifunctional nanoplatform for cancer photo-chemo therapy with negligible skin phototoxicity. *Biomaterials* 221:119422. doi: 10.1016/j.biomaterials.2019.119422

Chen, Q., Liu, X., Zeng, J., Cheng, Z., and Liu, Z. (2016). Albumin-NIR dye self-assembled nanoparticles for photoacoustic pH imaging and pH-responsive photothermal therapy effective for large tumors. *Biomaterials* 98, 23–30. doi: 10.1016/j.biomaterials.2016.04.041

Chen, Y., Li, X., Zhao, Y., Zhang, X., and Sun, L. (2020). Preparation of triple-responsive porous silica carriers and carbon quantum dots for photodynamic-/chemotherapy and multicolor cell imaging. *Chem. Nano. Mat.* 6, 648–656. doi: 10.1002/cnma.201900777

Cheng, H., Fan, G. L., Fan, J. H., Zheng, R. R., Zhao, L. P., and Yuan, P., et al. (2019). A self-delivery chimeric peptide for photodynamic therapy amplified immunotherapy. *Macromol. Biosci.* 19:e1800410. doi: 10.1002/mabi.201800410

Choi, K. Y., Han, H. S., Lee, E. S., Shin, J. M., Almquist, B. D., and Lee, D. S., et al. (2019). Hyaluronic acid–based activatable nanomaterials for stimuli-responsive imaging and therapeutics: beyond CD44-mediated drug delivery. *Adv. Mater.* 31:e1803549. doi: 10.1002/adma.201803549

Deng, H., Zhou, Z., Yang, W., Lin, L., Wang, S., and Niu, G., et al. (2020). Endoplasmic reticulum targeting to amplify immunogenic cell death for cancer immunotherapy. *Nano. Lett.* 20, 1928–1933. doi: 10.1021/acs.nanolett.9b05210

Dobson, J., de Queiroz, G. F., and Golding, J. P. (2018). Photodynamic therapy and diagnosis: Principles and comparative aspects. *Vet. J.* 233, 8–18. doi: 10.1016/j.tvjl.2017.11.012

Dolmans, D. E., Fukumura, D., and Jain, R. K. (2003). Photodynamic therapy for cancer. *Nat. Rev. Cancer* 3, 380–387. doi: 10.1038/nrc1071

Dong, X., Mu, L. L., Liu, X. L., Zhu, H., Yang, S. C., and Lai, X., et al. (2020). Biomimetic, hypoxia-responsive nanoparticles overcome residual chemoresistant leukemic cells with Co-targeting of therapy-induced bone marrow niches. *Adv. Funct. Mater.* 30:2000309. doi: 10.1002/adfm.202000309

Feng, L., Gai, S., Dai, Y., He, F., Sun, C., and Yang, P., et al. (2018). Controllable generation of free radicals from multifunctional heat-responsive nanoplatform for targeted cancer therapy. *Chem. Mater.* 30, 526–539. doi: 10.1021/acs.chemmater.7b04841

Fukino, T., Yamagishi, H., and Aida, T. (2017). Redox-responsive molecular systems and materials. *Adv. Mater.* 29:1603888. doi: 10.1002/adma.201603888

Haddad, R., Kaplan, O., Greenberg, R., Siegal, A., Skornick, Y., and Kashtan, H. (2000). Photodynamic therapy of murine colon cancer and melanoma using systemic aminolevulinic acid as a photosensitizer. *Int. J. Surg. Investig.* 2, 171–178.

Han, K., Zhang, J., Zhang, W., Wang, S., Xu, L., and Zhang, C., et al. (2017). Tumor-triggered geometrical shape switch of chimeric peptide for enhancedin vivo tumor internalization and photodynamic therapy. *ACS. Nano.* 11, 3178–3188. doi: 10.1021/acsnano.7b00216

Iqbal, H. M. N., and Keshavarz, T. (2018). "14 - Bioinspired polymeric carriers for drug delivery applications," in *Stimuli Responsive Polymeric Nanocarriers for Drug Delivery Applications, Volume 1*, eds. A.S.H. Makhlouf & N.Y. (Abu-Thabit: Woodhead Publishing),377–404. doi: 10.1016/B978-0-08-101997-9.00018-7

Jain, M., Zellweger, M., Wagnières, G., van den Bergh, H., Cook, S., and Giraud, M. (2017). Photodynamic therapy for the treatment of atherosclerotic plaque: Lost in translation? *Cardiovasc. Ther.* 35:e12238. doi: 10.1111/1755-5922.12238

Jiang, Y., Xu, C., Leung, W., Lin, M., Cai, X., and Guo, H., et al. (2019). Role of exosomes in photodynamic anticancer therapy. *Curr. Med. Chem.* doi: 10.2174/0929867326666190918122221. [Epub ahead of print].

Karimi, M. (2015). *Smart Internal Stimulus-Responsive Nanocarriers for Drug and Gene Delivery*. San Rafael California (40 Oak Drive, San Rafael, CA, 94903, USA); Bristol England (Temple Circus, Temple Way, Bristol BS1 6HG, UK): Morgan & Claypool Publishers. doi: 10.1088/978-1-6817-4257-1

Kelly, J. F., Snell, M. E., and Berenbaum, M. C. (1975). Photodynamic destruction of human bladder carcinoma. *Br. J. Cancer* 31, 237–244. doi: 10.1038/bjc.1975.30

Klaikherd, A., Nagamani, C., and Thayumanavan, S. (2009). Multi-stimuli sensitive amphiphilic block copolymer assemblies. *J. Am. Chem. Soc.* 131, 4830–4838. doi: 10.1021/ja809475a

Li, X., Zheng, B., Peng, X., Li, S., Ying, J., and Zhao, Y., et al. (2019). Phthalocyanines as medicinal photosensitizers: Developments in the last five years. *Coordin. Chem. Rev.* 379, 147–160. doi: 10.1016/j.ccr.2017.08.003

Liang, P., Huang, X., Wang, Y., Chen, D., Ou, C., and Zhang, Q., et al. (2018). Tumor– microenvironment-responsive nanoconjugate for synergistic antivascular activity and phototherapy. *ACS. Nano.* 12, 11446–11457. doi: 10.1021/acsnano.8b06478

Lieber, C. M. (2003). Nanoscale science and technology: Building a big future from small things. *MRS. Bull.* 28, 486–491. doi: 10.1557/mrs2003.144

Liu, J., and Huskens, J. (2015). Bi-compartmental responsive polymer particles. *Chem. Commun. (Camb).* 51, 2694–2697. doi: 10.1039/C4CC08413F

Liu, L., Fu, L., Jing, T., Ruan, Z., and Yan, L. (2016). pH-triggered polypeptides nanoparticles for efficient BODIPY imaging-guided near infrared photodynamic therapy. *ACS. Appl. Mater. Interfaces* 8, 8980–8990. doi: 10.1021/acsami.6b01320

Liu, W., Wang, Y. M., Li, Y. H., Cai, S. J., Yin, X. B., and He, X. W., et al. (2017). Fluorescent imaging-guided chemotherapy-and-photodynamic dual therapy with nanoscale porphyrin metal-organic framework. *Small* 13:1603459. doi: 10.1002/smll.201603459

Lopez-Otin, C., and Bond, J. S. (2008). Proteases: multifunctional enzymes in life and disease. *J. Biol. Chem.* 283, 30433–30437. doi: 10.1074/jbc.R800035200

Ma, Y., Kong, J., Yan, G., Ren, X., Jin, D., and Jin, T., et al. (2014). NQO1 overexpression is associated with poor prognosis in squamous cell carcinoma of the uterine cervix. *BMC. Cancer* 14:414. doi: 10.1186/1471-2407-14-414

Ma, Z., Hu, P., Guo, C., Wang, D., Zhang, X., and Chen, M., et al. (2019). Folate-mediated and pH-responsive chidamide-bound micelles encapsulating photosensitizers for tumor-targeting photodynamic therapy. *Int. J. Nanomed.* 14, 5527–5540. doi: 10.2147/IJN.S208649

Marcucci, F., Stassi, G., and De Maria, R. (2016). Epithelial-mesenchymal transition: a new target in anticancer drug discovery. *Nat. Rev. Drug. Discov.* 15, 311–325. doi: 10.1038/nrd.2015.13

McAtee, C. O., Barycki, J. J., and Simpson, M. A. (2014). Emerging roles for hyaluronidase in cancer metastasis and therapy. *Adv. Cancer. Res.* 123, 1–34. doi: 10.1016/B978-0-12-800092-2.00001-0

McKeown, S. R. (2014). Defining normoxia, physoxia and hypoxia in tumours-implications for treatment response. *Br. J. Radiol.* 87:20130676. doi: 10.1259/bjr.20130676

Meng, Z., Zhou, X., Xu, J., Han, X., Dong, Z., and Wang, H., et al. (2019a). Light-triggered in situ gelation to enable robust photodynamic-immunotherapy by repeated stimulations. *Adv. Mater.* 31:e1900927. doi: 10.1002/adma.201900927

Meng, Z., Zhou, X., Xu, J., Han, X., Dong, Z., and Wang, H., et al. (2019b). Light-triggered in situ gelation to enable robust photodynamic-immunotherapy by repeated stimulations. *Adv. Mater.* 31:e1900927.

Mirabello, V., Cortezon-Tamarit, F., and Pascu, S. I. (2018). Oxygen sensing, hypoxia tracing and in vivo imaging with functional metalloprobes for the early detection of non-communicable diseases. *Front. Chem.* 6:27. doi: 10.3389/fchem.2018.00027

Mo, R., and Gu, Z. (2016). Tumor microenvironment and intracellular signal-activated nanomaterials for anticancer drug delivery. *Mater. Today* 19, 274–283. doi: 10.1016/j.mattod.2015.11.025

Muthu, M. S., Rajesh, C. V., Mishra, A., and Singh, S. (2009). Stimulus-responsive targeted nanomicelles for effective cancer therapy. *Nanomedicine* 4, 657–667. doi: 10.2217/nnm.09.44

Nazemi, A., Boott, C. E., Lunn, D. J., Gwyther, J., Hayward, D. W., and Richardson, R. M., et al. (2016). Monodisperse cylindrical micelles and block comicelles of controlled length in aqueous media. *J. Am. Chem. Soc.* 138, 4484–4493. doi: 10.1021/jacs.5b13416

Ng, C. W., Li, J., and Pu, K. (2018). Recent progresses in phototherapy-synergized cancer immunotherapy. *Adv. Funct. Mater.* 28:1804688. doi: 10.1002/adfm.201804688

Oh, E. T., and Park, H. J. (2015). Implications of NQO1 in cancer therapy. *BMB. Rep.* 48, 609–617. doi: 10.5483/BMBRep.2015.48.11.190

Oleinick, N. L., Morris, R. L., and Belichenko, I. (2002). The role of apoptosis in response to photodynamic therapy: what, where, why, and how. *Photoch. Photobio. Sci.* 1, 1–21. doi: 10.1039/b108586g

Panagopoulos, J. A., Svitra, P. P., Puliafito, C. A., and Gragoudas, E. S. (1989). Photodynamic therapy for experimental intraocular melanoma using chloroaluminum sulfonated phthalocyanine. *Arch. Ophthalmol-Chic.* 107:886. doi: 10.1001/archopht.1989.01070010908039

Paris, J. L., Cabanas, M. V., Manzano, M., and Vallet-Regi, M. (2015). Polymer-grafted mesoporous silica manoparticles as ultrasound-responsive drug carriers. *ACS. Nano.* 9, 11023–11033. doi: 10.1021/acsnano.5b04378

Park, C., Oh, K., Lee, S. C., and Kim, C. (2007). Controlled release of guest molecules from mesoporous silica particles based on a pH-responsive polypseudorotaxane motif. *Angew. Chem. Int. Edit.* 46, 1455–1457. doi: 10.1002/anie.200603404

Perche, F., Biswas, S., Wang, T., Zhu, L., and Torchilin, V. P. (2014). Hypoxia-targeted siRNA delivery. *Angew. Chem. Int. Edit.* 53, 3362–3366. doi: 10.1002/anie.201308368

Pervaiz, S., and Olivo, M. (2006). Art and science of photodynamic therapy. *Clin. Exp. P.* 33, 551–556. doi: 10.1111/j.1440-1681.2006.04406.x

Ramamonjisoa, N., and Ackerstaff, E. (2017). Characterization of the tumor microenvironment and Tumor-Stroma interaction by non-invasive preclinical imaging. *Front Oncol.* 7:3. doi: 10.3389/fonc.2017.00003

Raza, A., Hayat, U., Rasheed, T., Bilal, M., and Iqbal, H. M. N. (2018). Redox-responsive nano-carriers as tumor-targeted drug delivery systems. *Eur. J. Med. Chem.* 157, 705–715. doi: 10.1016/j.ejmech.2018.08.034

Rkein, A. M., and Ozog, D. M. (2014). Photodynamic Therapy. *Dermatol. Clin.* 32, 415–425. doi: 10.1016/j.det.2014.03.009

Roco, M. C. (2003a). Converging science and technology at the nanoscale: opportunities for education and training. *Nat. Biotechnol.* 21, 1247–1249. doi: 10.1038/nbt1003-1247

Roco, M. C. (2003b). Nanotechnology: convergence with modern biology and medicine. *Curr. Opin. Biotech.* 14, 337–346. doi: 10.1016/S0958-1669(03)00068-5

Shi, H., Sun, W., Liu, C., Gu, G., Ma, B., and Si, W., et al. (2016). Tumor-targeting, enzyme-activated nanoparticles for simultaneous cancer diagnosis and photodynamic therapy. *J. Mater. Chem. B.* 4, 113–120. doi: 10.1039/C5TB02041G

Sun, Y., Liang, Y., Dai, W., He, B., Zhang, H., and Wang, X., et al. (2019). Peptide-drug conjugate-based nanocombination actualizes breast cancer treatment by maytansinoid and photothermia with the assistance of fluorescent and photoacoustic images. *Nano. Lett.* 19, 3229–3237. doi: 10.1021/acs.nanolett.9b00770

Tian, K., Jia, X., Zhao, X., and Liu, P. (2017). Biocompatible reduction and pH dual-responsive core cross-linked micelles based on multifunctional amphiphilic linear-hyperbranched copolymer for controlled anticancer drug delivery. *Mol. Pharm.* 14, 799–807. doi: 10.1021/acs.molpharmaceut.6b01051

Toole, B. P. (1990). Hyaluronan and its binding proteins, the hyaladherins. *Curr. Opin. Cell. Biol.* 2, 839–844. doi: 10.1016/0955-0674(90)90081-O

Upreti, M., Jyoti, A., and Sethi, P. (2013). Tumor microenvironment and nanotherapeutics. *Transl. Cancer. Res.* 2, 309–319. doi: 10.3978/j.issn.2218-676X.2013.08.11

Vordermark, D. (2010). Hypoxia-specific targets in cancer therapy: role of splice variants. *BMC. Med.* 8:45. doi: 10.1186/1741-7015-8-45

Wang, H., Han, X., Dong, Z., Xu, J., Wang, J., and Liu, Z. (2019). Hyaluronidase with pH-responsive dextran modification as an adjuvant nanomedicine for enhanced photodynamic-immunotherapy of cancer. *Adv. Funct. Mater.* 29:1902440. doi: 10.1002/adfm.201902440

Wang, Y., Wei, G., Zhang, X., Xu, F., Xiong, X., and Zhou, S. (2017). A step-by-step multiple stimuli-responsive nanoplatform for enhancing combined chemo-photodynamic therapy. *Adv. Mater.* 29:1605357. doi: 10.1002/adma.201605357

Wei, H., Zhuo, R., and Zhang, X. (2013). Design and development of polymeric micelles with cleavable links for intracellular drug delivery. *Prog. Polym. Sci.* 38, 503–535. doi: 10.1016/j.progpolymsci.2012.07.002

Yang, G., Phua, S. Z. F., Lim, W. Q., Zhang, R., Feng, L., and Liu, G., et al. (2019). A hypoxia-responsive albumin-based nanosystem for deep tumor penetration and excellent therapeutic efficacy. *Adv. Mate.* 31:1901513. doi: 10.1002/adma.201901513

Yang, W., Zhang, F., Deng, H., Lin, L., Wang, S., and Kang, F., et al. (2020). Smart nanovesicle-mediated immunogenic cell death through tumor microenvironment modulation for effective photodynamic immunotherapy. *ACS. Nano.* 14, 620–631. doi: 10.1021/acsnano.9b07212

Yang, X. D., Zhu, R., Yin, J. P., Ma, S., Cui, J. W., and Zhang, J. (2019). Synergy of electron transfer and charge transfer in the control of photodynamic behavior of coordination polymers. *Chem–Eur. J.* 25, 13152–13156. doi: 10.1002/chem.201902300

Yang, Y., Zhang, Y., Wu, Q., Cui, X., Lin, Z., and Liu, S., et al. (2014). Clinical implications of high NQO1 expression in breast cancers. *J. Exp. Clin. Cancer. Res.* 33:14. doi: 10.1186/1756-9966-33-14

Yang, Z., Chen, Q., Chen, J., Dong, Z., Zhang, R., and Liu, J., et al. (2018). Tumor-pH-responsive dissociable albumin–tamoxifen nanocomplexes enabling efficient tumor penetration and hypoxia relief for enhanced cancer photodynamic therapy. *Small* 14:e1803262. doi: 10.1002/smll.201803262

Yao, C., Li, Y., Wang, Z., Song, C., Hu, X., and Liu, S. (2020). Cytosolic NQO1 enzyme-activated near-infrared fluorescence imaging and photodynamic therapy with polymeric vesicles. *ACS. Nano.* 14, 1919–1935. doi: 10.1021/acsnano.9b08285

Zhang, D., Zheng, A., Li, J., Wu, M., Cai, Z., and Wu, L., et al. (2017). Tumor microenvironment activable self-assembled DNA hybrids for pH and redox dual-responsive chemotherapy/PDT treatment of hepatocellular carcinoma. *Adv. Sci.* 4:1600460. doi: 10.1002/advs.201600460

Zhang, N., Zhao, F., Zou, Q., Li, Y., Ma, G., and Yan, X. (2016). Multitriggered tumor-responsive drug delivery vehicles based on protein and polypeptide coassembly for enhanced photodynamic tumor ablation. *Small* 12, 5936–5943. doi: 10.1002/smll.201602339

Zhu, H., Fang, Y., Miao, Q., Qi, X., Ding, D., and Chen, P., et al. (2017). Regulating near-infrared photodynamic properties of semiconducting polymer nanotheranostics for optimized cancer therapy. *ACS. Nano.* 11, 8998–9009. doi: 10.1021/acsnano.7b03507

Zhu, R., He, H., Liu, Y., Cao, D., Yan, J., and Duan, S., et al. (2019). Cancer-selective bioreductive chemotherapy mediated by dual hypoxia-responsive nanomedicine upon photodynamic therapy-induced hypoxia aggravation. *Biomacromolecules* 20, 2649–2656. doi: 10.1021/acs.biomac.9b00428

Conflict of Interest: The authors declare that the research was conducted in the absence of any commercial or financial relationships that could be construed as a potential conflict of interest.

frontiers in Chemistry

ORIGINAL RESEARCH
published: 05 January 2021
doi: 10.3389/fchem.2020.599740

Design of DOX-GNRs-PNIPAM@PEG-PLA Micelle With Temperature and Light Dual-Function for Potent Melanoma Therapy

Na Wang[1†], *Jing Shi*[2†], *Cong Wu*[2], *Weiwei Chu*[2], *Wanru Tao*[2], *Wei Li*[2*] *and Xiaohai Yuan*[1*]

[1] *Department of Cosmetics, Shanghai Skin Disease Hospital, Shanghai, China,* [2] *Laboratory of Nano Biomedicine & Intentional Joint Cancer Institute, Second Military Medical University, Shanghai, China*

Objective: The aim of this study was to construct light and temperature dual-sensitive micellar carriers loaded with doxorubicin (DOX) and gold nanorods (DOX-GNRs-PNIPAM@PEG-PLA, DAPP) for melanoma therapy.

Methods: The DAPP self-assembled using fine-tuned physicochemical properties in water. The DAPP structure, temperature- and photo-sensitivity, drug-release, *in-vitro* serum stability, and cytotoxicity against melanoma B16F10 cells were evaluated in detail. The corresponding *in-vitro* and *in-vivo* therapeutic mechanisms were then evaluated using a B16F10-melanoma bearing BALB/c nude mouse model (B16F10).

Results: The light and temperature sensitive micellar drug-delivery system assembled from block copolymer and gold nanorods exhibited a narrow particle size and size distribution, good biocompatibility, well-designed photo-temperature conversion, controlled drug release, and high serum stability. Compared with the free DOX- and PBS-treated groups, the cell endocytosis-mediated cytotoxicity and intra-tumor accumulation of DAPP was markedly enhanced by the NIR-light exposure and induced potent *in-vivo* tumor inhibitory activity.

Conclusion: The design of DAPP, a dual-functional micellar drug-delivery system with temperature- and light-sensitive properties, offers a new strategy for skin-cancer therapy with a potent therapeutic index.

Keywords: doxorubicin, gold nanorods, thermosensitive, photothermal therapy, melanoma, B16F10

OPEN ACCESS

Edited by:
Yi Hou,
Beijing University of Technology, China

Reviewed by:
Jinyao Liu,
Shanghai Jiao Tong University, China
Zihua Wang,
Fujian Medical University, China

***Correspondence:**
Xiaohai Yuan
seagullyuan@126.com
Wei Li
liwei_dds@163.com

[†]*These authors have contributed equally to this work*

Specialty section:
This article was submitted to Nanoscience, a section of the journal Frontiers in Chemistry

Received: *28 August 2020*
Accepted: *19 November 2020*
Published: *05 January 2021*

Citation:
Wang N, Shi J, Wu C, Chu W, Tao W, Li W and Yuan X (2021) Design of DOX-GNRs-PNIPAM@PEG-PLA Micelle With Temperature and Light Dual-Function for Potent Melanoma Therapy. Front. Chem. 8:599740. doi: 10.3389/fchem.2020.599740

INTRODUCTION

Skin cancer is one of the most common aggressive malignancies with an insidious and high morbidity (Siegel et al., 2019). Early melanoma is largely curable with surgery. However, most patients are in the advanced stages when they are diagnosed and lesions are difficult to fully excise due to a series of complications (Yang et al., 2016; Smith et al., 2018). The current treatment approach includes surgery, radiotherapy, chemotherapy, and immunotherapy (Ma et al., 2018; Pinho et al., 2019). Conventional chemotherapy drugs, especially doxorubicin (DOX), are widely

used in clinical practice and have good therapeutic efficiency. However, the poor bioavailability and poor tumor targeting of DOX produces a series of side effects, such as nausea, vomiting, bone marrow suppression, and cardiac toxicity, which limits its clinical merit in the treatment of melanoma. Therefore, it is an urgent unmet need to find novel strategies to reduce the clinical limitations of DOX treatment of melanoma.

Nano-based formulations have offered new hope to overcome the abovementioned shortcomings in DOX treatment of melanoma through strategies that involve the protection of therapeutic agents from degradation, improvement of drug bioavailability, and prolonged intratumoral retention (Hou et al., 2015; Pautu et al., 2017; Zhang et al., 2019b). Many nanoformulations have been developed recently for melanoma therapy. Chen et al. synthesized pH-responsive micelles to improve DOX-release when stimulated by the acidic tumor microenvironment of melanoma. The micelles proved to be stable at blood pH (∼7.4) and drug release was promoted at an acidic pH (Chen et al., 2013). A new immune gold nanoparticle (AuNP) with photodynamic therapeutic potential was generated against melanoma B16F10 cells, which induced hyperthermal therapy and stimulated an anti-tumor immune response (Zhang et al., 2019a). Other functional and targeted nanodrug delivery systems have also been extensively developed recently against solid melanoma and metastases with a potent therapeutic index and clinical applicability (Long et al., 2018). All these newly developed nanomedicines have illustrated the exciting potential for treatment of melanoma.

Conversely, Chan et al. reported that the intertumoral accumulation of nanotherapeutics was equal or lower than 0.7%, which differed from that expected from previously reported studies (Wilhelm et al., 2016). Subsequently, different nano-based formulations have been designed to improve the intratumoral accumulation of drugs, promote *in-vivo* bioavailability, enhance circulation time and drug release at the tumor site. The unique composition and properties of the melanoma tumor microenvironment (TME) is characterized by hypoxia, acidosis, and high temperature (Li et al., 2011b, 2012b; Deng et al., 2017). The TME plays a major role in the occurrence, invasion, and metastasis of tumors and has provided a rationale for in the development of multifunctional nanoparticles (Li et al., 2012a,c; Yang and Gao, 2017). An interesting study by Guangjun et al. designed a nanoparticle carrying the anti-platelet antibody R300 and chemotherapeutic drug DOX. The formulation could locally deplete tumor-related platelets, which consequently enhanced vascular permeability with a high enhanced permeability and retention (EPR) effect and drug accumulation at the tumor sites (Li et al., 2017). In contrast, the strategies of *in-situ* destruction of tumor tissue and enhancing the EPR may also lead to damage to normal cells and tissues with their associated undesired side effects. This indicates the importance of promoting intertumoral drug release without any *in-vivo* blood or non-tumor tissue damage through physical stimulation, such as using gold nanorods (GNRs) with a strong photothermal conversion effect (Zhang et al., 2016, 2017). In our previous studies, we found that the intratumoral drug accumulation was enhanced by temperature-sensitive passive targeting (TSPT) micelles composed of thermosensitive poly(N-isopropylacrylamide) (PNIPAM)(Li et al., 2011a, 2012d). Tumor accumulation can be enhanced further by the fine-tuning of the carrier based on the "Li-Teruo" plot (Li et al., 2011a,b). This indicates the potential for potent tumor accumulation of drugs by combining the photothermal conversion of GNRs with micelles having a PNIPAM-based core.

Herein, a dual-functional micellar drug delivery system based on PNIPAM, poly (d, l-lactide)-poly (ethylene glycol) (PLA-PEG), and GNRs was constructed by incorporating of DOX, GNRs, and PNIPAM into the core of PEG-PLA micelles (DAPP), equipped with temperature, and light dual-sensitive properties. The heat generated by the GNRs in the DAPP induces shrinking of the PNIPAM, which in turn will promote drug release and achievement of higher local drug concentration at the tumor site controlled by *in-situ* near-infrared (NIR)-light stimulation. The thermo-enhanced synergistic treatment against B16F10 cells by GNRs and DOX will result in no damage to off-target normal cells.

MATERIALS AND METHODS

Main Chemicals and Apparatus

Doxorubicin hydrochloride (DOX·HCl) was purchased from Dalian Meilun Biotechnology Co., Ltd. Bovine serum albumin (BSA) was purchased from J&K Scientific Ltd. GNRs, PNIPAM, and PEG-PLA were previously synthesized by our colleagues. Human melanoma cells B16F10 were purchased from the American Type Culture Collection. Dulbecco's Modified Eagle's Medium (DMEM) and fetal bovine serum (FBS) were purchased from Gibco Co, United States. The Cell Counting Kit-8 was purchased from Dojindo Laboratories (Kumamoto, Japan). The apparatus mainly consisted of a UV-VIS spectrophotometer (Cary300, Varian, CA, United States), a freeze dryer (VirTis AdVantage, United States), a dynamic light-scattering device (DLS, ALV/CGS-3, Germany), an infrared light source (IRS-S6, Shanghai, China), a transmission electron microscope (TEM) (Hitachi, H-7000 Electron Microscope), an inverted fluorescence microscope (Olympus IX71, Japan), and an enzyme-labeling instrument (Power Wave XS, Bio-TEK, United States).

Preparation of DAPP

The PNIPAM aqueous solution (2 mL) was mixed with 2.0 mg DOX and 2.0 mg GNRs. After thorough mixing, the DOX and GNRs were stirred for 4 h at room temperature in the dark, so that the DOX and GNRs were fully incorporated with the PNIPAM (Han et al., 2017a; Chen et al., 2020). The mixture was then dried by freeze-drying to form solid powder (Li et al., 2012d). Subsequently, 4 mg/mL PEG-PLA amphiphilic block copolymer solution (DMAC) was mixed with the PNIPAM/DOX/GNRs powder and stirred at room temperature to form the nanoparticles (Gong et al., 2019). After a 6-h reaction time, the solution was dialyzed with a dialysis bag (MW cut off 3500) against phosphate belanced solution (PBS) for 12 h in order to obtain the DAPP solution and to remove any unreacted polymer (Su et al., 2017).

Characterization of DAPP

GNRs and DAPP were diluted with pure Milli-Q water at a concentration ∼0.1 mg/mL. Next, the hydrodynamic diameter and particle size distribution of GNRs, DAPP, and DAPP in the presence of a NIR-light solution was evaluated by DLS at the scattering angle of 90°. The morphology of GNRs and DAPP particles was detected by TEM and the conventional TEM images were obtained at 200 kV with a magnification of 80,000 times. The photothermal conversion efficiency of GNRs and DAPP at different times and concentration of 10, 50, and 100 μg/mL was tested by infrared system at the power of 1,200 mV (Cao M. et al., 2015; Cabral et al., 2018).

Temperature-Sensitive Properties

The temperature-sensitive properties of PNIPAM and DAPP micelles was measured by DLS with temperature-controller (Li et al., 2011a). The radius of the PNIPAM and DAPP solution (∼1 mL, concentration ∼0.1 mg/mL) at different temperatures were detected at the scattering angle of 90° (Zhu et al., 2017).

Serum Stability of DAPP

BSA was used as a protein in the simulated systemic circulation to detect serum stability of DAPP. The solutions of BSA (50 mg/mL) mixed with DAPP micelles (0.1 mg/mL) in PBS were measured by DLS at the scattering angle of 90° at the time of 24 and 48 h.

In-vitro Drug Release

The evaluation of *in-vitro* drug release was conducted using the dialysis method. One set of DAPP was illuminated with NIR-light for 5 min before sampling at certain time intervals while the other received no NIR-light. A volume of 4 mL of DAPP micelles solution was added to the dialysis bag. The dialysis bag was placed into a beaker and was subjected to dialysis with 1,000 mL PBS, with the beaker temperature maintained constant at 37°C in the oil bath with stirring. At the predesigned time 0,1, 2, 4, 6, 12, 24, and 36 h, 100 μL of the micelle solution was removed from the dialysis bag. Simultaneously, about 100 μL PBS was added to the DAPP micelles solution inside membrane and 100 μL acetonitrile was added to the collected micelles solution to break the micelles and release DOX. The solution was then analyzed by UV-VIS spectrophotometer. The DOX release was calculated using the following equation:

$$Drug_{release} = \frac{M_T - M_R}{M_T} \times 100\% \quad (1)$$

Where M_R is the DOX concentration, and M_T the initial DOX concentration of DAPP micelles.

Endocytosis

B16F10 cells were seeded into a confocal culture dish (5×10^3cells/dish) with 2.0 mL DMEM medium and cultured for 24 h. Next, the cells were treated with DOX, DAPP, and DAPP with NIR-light and incubated for 2 h at 37°C. The culture medium of B16F10 cells was aspirated, and cells were rinsed with PBS twice, fixed for 10 min with 1.0 mL paraformaldehyde solution, followed by rinsing with PBS three times. The nuclei of the B16F10 cells were stained with DAPI working solution for 10 min, and the B16F10 cells were visualized by inverted fluorescence microscope (Han et al., 2017b).

In-vitro Cytotoxicity

The growth inhibitory effect of DOX, GNRs exposed to NIR-light, and DAPP exposed to NIR-light on B16F10 tumor cells *in vitro* was determined using the CCK-8 assay. B16F10 cells were digested and seeded onto 96-well plates (5×10^4 cells/mL, 0.1 mL/well) and incubated overnight till the cells reached confluence. The samples of DOX, GNRs, and DAPP were diluted by DMEM with concentration of 2, 4, 6, 8, and 10 μg/mL, the medium was removed, and the diluted sample solution of different concentrations were added to the 96-well plates and incubated for an additional 24 h. The GNR and DAPP groups were exposed to 1,200 mV NIR for 5 min, while other groups were without NIR. The medium was incubated with 10% CCK-8 at 37°C for about 0.5–1 h. The optical density (OD) value of 96-well plates was measured at the wavelength of 450 nm by an enzyme-labeling instrument (Kinoh et al., 2020; Mi et al., 2020). The cell viability was calculated using the following equation:

$$Cell_{viability}\ \% = \frac{A_S - A_B}{A_C - A_B} \times 100\% \quad (2)$$

Where A_S, A_B, and A_C were the absorption values of the drug treatment groups, culture medium, and cells without drug, respectively.

In-vivo Distribution and Antitumor Effects of DAPP in BALB/c Nude Mice

BALB/c nude mice (4 weeks) were allowed to acclimate for 1 week in the animal facility to reduce stress. The melanoma-bearing murine model was established by subcutaneously implanting 1×10^7 B16F10 cells into the right back (Cao P. et al., 2015; Han et al., 2018). After 10 days, the mice were divided randomly into three treatment groups (three nude mice per group) for *in-vivo* distribution experiment: free fluorescein isothiocyanate (FITC), DAPP, and DAPP with NIR-light, and *in-vivo* anti-tumor effect experiment: PBS, DAPP, and DAPP with NIR-light. As the tumor volume (following equation 3) reached about 100 mm^3, the mice were injected with FITC and DAPP by tail vein, then the DAPP-treated group was illuminated with NIR-light for 5 min at the laser irradiation of 1,200 mV while the others were not exposed to NIR-light. After 4 h, the mice were anesthetized by isoflurane, and *in-vivo* tumor accumulation was tested by IVIS® Lumina II Imaging System (Xenogen) at an excitation wavelength of 474 nm. For the anti-tumor experiment, mice were injected with PBS and DAPP (0.1 mg/mL) at the dose of 50 mg/kg from the tail vein, and the DAPP group was irradiated by NIR with power of 1,200 mV for 5 min every 2 days. The volume of tumor tissue was measured every 2 days using a digital vernier from the first day of injection to the last day, and the relative tumor volume was calculated according to the following equation:

$$V_{tumor} = Width^2 \times Length/2 \quad (3)$$

$$V_{relative} = V_{tumor}/V_{initial} \quad (4)$$

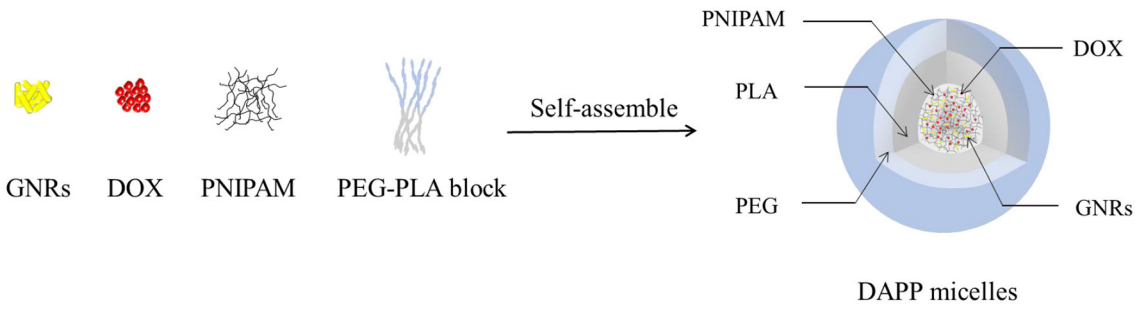

FIGURE 1 | The scheme illustrates the structure of DAPP with temperature and light dual-function.

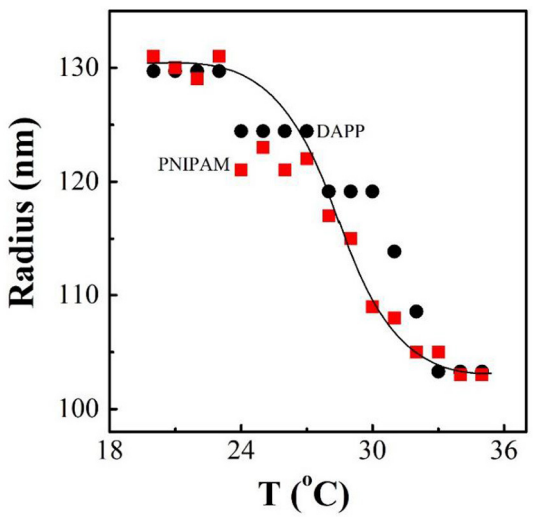

FIGURE 2 | The temperature dependence of radius for PNIPAM and DAPP micelles in aqueous solutions at same concentration as tested by the dynamic laser light scattering (DLS).

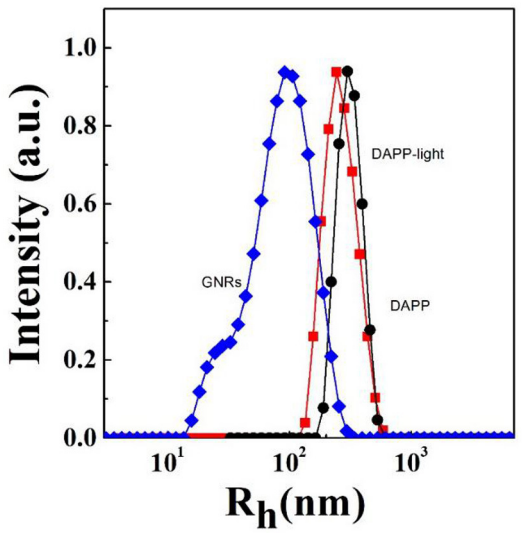

FIGURE 3 | The hydrodynamic radius (R_h) and size distribution of GNRs, DAPP with NIR-light, and DAPP as measured by DLS.

Where *width* and *length* were the longest and shortest diameters of tumor tissue. $V_{initial}$ is the volume of first day injection therapy drug. The tumor progression was evaluated in terms of relative tumor volume (Equation 4), and the body weight of all mice was also recorded to analyze the systemic toxicity of treatment.

All mice were purchased from the Shanghai Experimental Animal Center of Chinese Academic of Sciences (Shanghai, China). The animals were maintained in a pathogen-free environment and allowed to acclimate for at least one week before tumor implantation. The animal study was reviewed and approved by the Institutional Review Board of the Second Military Medical University.

Statistical Analysis

Statistical analysis was performed by Student's *t*-test or one-way ANOVA to identify significant differences. A $p < 0.05$ was considered statistically significant.

RESULTS AND DISCUSSION

Preparation and Characterization of DAPP

The structure and composition of DAPP are illustrated in **Figure 1**. The GNRs and DOX were first mixed with PNIPAM. The mixture was then encapsulated into the core of the PEG-PLA micelles by adding them to the amphiphilic polymer PEG-PLA solution, and then blended and stirred. The physicochemical properties of the DAPP were adjusted by fine-tuning the composition of GNRs and PNIPAM during the process of self-assembly to form nanoparticles with shell-core structure.

It is well-known that the lower critical solution temperature (LCST) of PNIPAM is about 32°C, but it can be modified by different methods of polymerization. In this study, the thermosensitive homopolymer PNIPAM was physically entrapped inside the core of the micelles. The volume phase transition temperature (VPTT) of the DAPP sample was similar to the LCST of the PNIPAM, indicating that the polymer synthesized after loading GNRs and DOX still exhibited a good

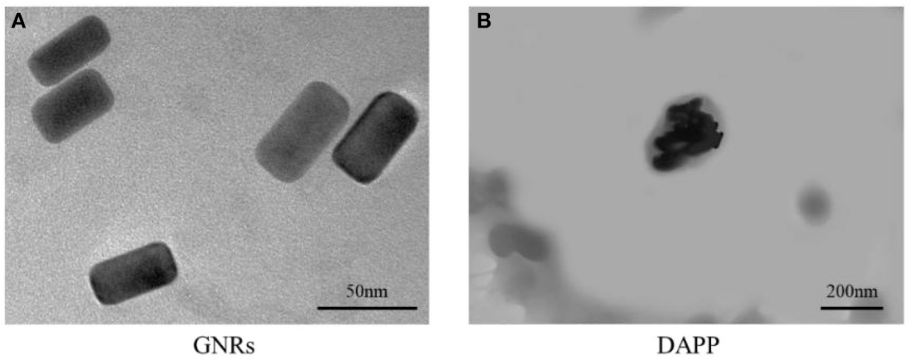

FIGURE 4 | TEM image of GNRs **(A)** and DAPP micelles **(B)**.

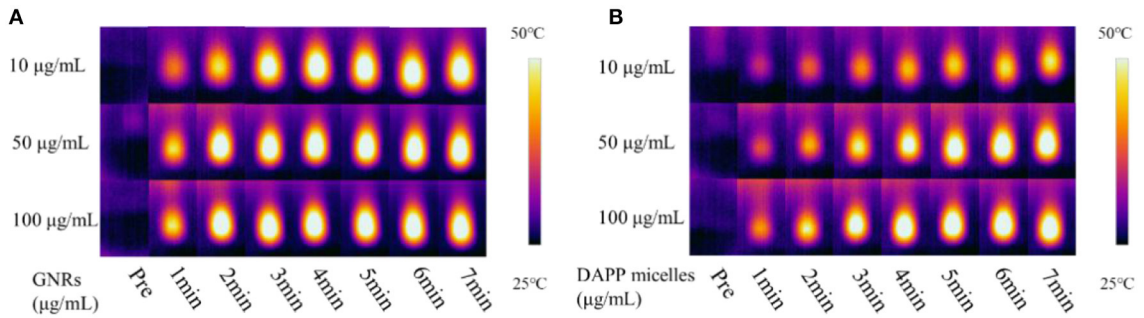

FIGURE 5 | The photothermal transition efficiency of GNRs **(A)** and DAPP **(B)**.

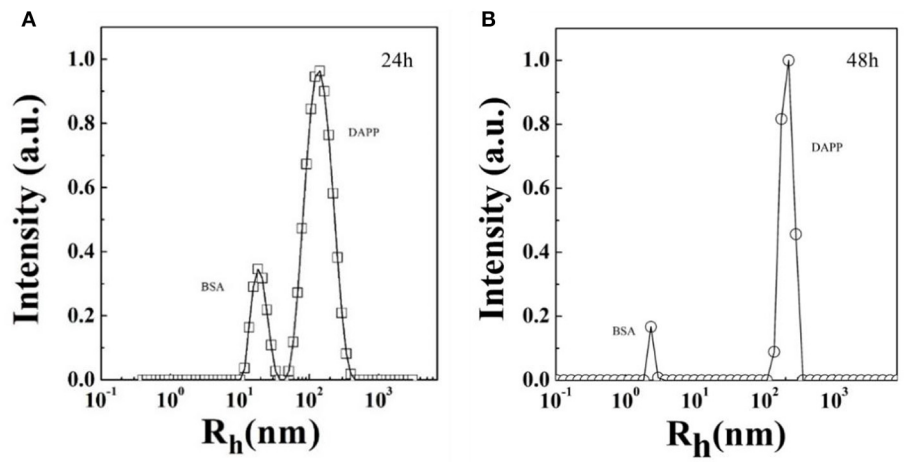

FIGURE 6 | (A,B) The serum stability of DAPP micelles as tested by the blend of BSA with DAPP at 24 h and 48 h.

temperature response (**Figure 2**). The size and size distribution of GNRs, DAPP, and DAPP with NIR-light were evaluated by DLS as shown in **Figure 3**. It was clear that the GNRs were entrapped into the micelles, and the size was shifted to the right with a hydrodynamic radius in the range of 200 to 300 nm. However, as the DAPP was irradiated by the NIR light, and the size of the DAPP became smaller. The size changes indicated that photothermal transition and PNIPAM shrinking had occurred, and ultimately indicated the successful composition and structure construction. This photothermal transformation

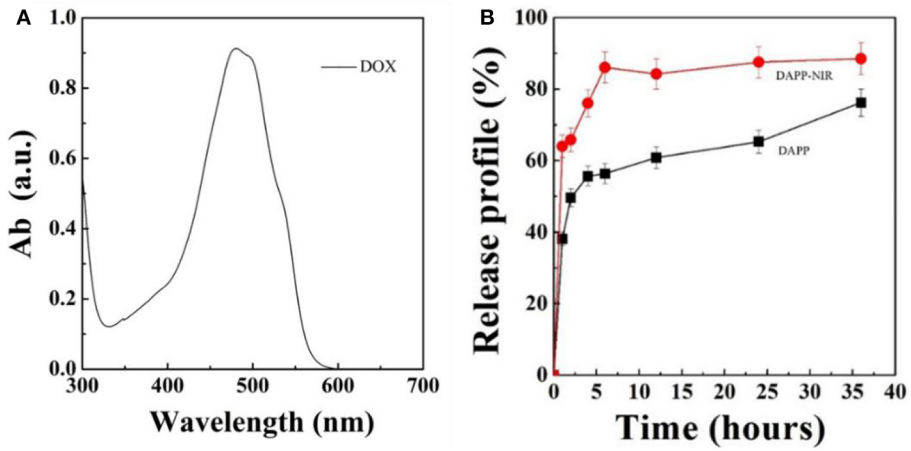

FIGURE 7 | Optical absorption curve of DOX **(A)** and *in-vitro* DOX releasing profile of DAPP and DAPP with NIR-light at 37°C **(B)**.

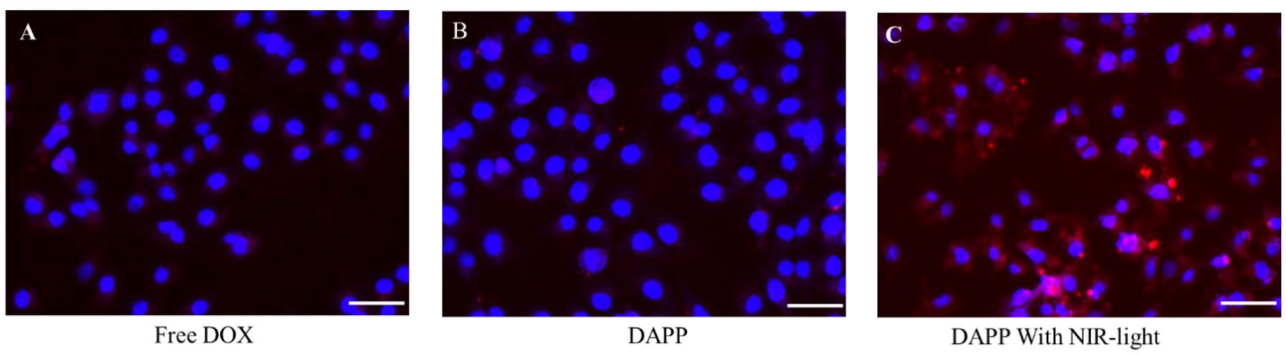

FIGURE 8 | The B16F10 cellular uptake evaluation. Free DOX **(A)**, DAPP **(B),** and DAPP with NIR-light **(C)**, the scale bar:100 μm.

of GNRs can be effectively used to promote the shrinking of PNIPAM inside of DAPP and to further control the DOX release inside the tumor lesion.

The TEM morphology of GNRs and DAPP are shown in **Figures 4A,B**. The particle sizes of GNRs and DAPP obtained from TEM were similar to that of DLS. The photothermal conductivity efficiencies of GNRs and DAPP at the same concentration but at different times are shown in **Figure 5**. Both the temperature of the GNRs solution (left panel) and DAPP solution (right panel) increased with the time and concentration exposed to light. The excellent photothermal conversion efficiency could be used to regulate the PNIPAM phase transition and drug release inside tumors. Overall, the preceding evidence indicated that the temperature and light-sensitive dual-functional DAPP was successfully constructed.

Serum Stability and Release Profile of DAPP

Serum stability and successful intratumoral drug release are two key factors strongly affecting drug accumulation. Here, the serum stability of DAPP was tested by checking the size and size distribution of DAPP and its blending with serum protein BSA, which was carefully checked by the DLS as shown in **Figure 6**. It is clear that there were two well-separated peaks with sizes about 10 and 200 nm. The small peak was similar to that of BSA, which is in the range of 1–10 nm. Conversely, the larger peak was about 200–300 nm. As mentioned above, the size of the DAPP obtained both in the DLS and on TEM analyses was about 200 nm. Thus, the larger peak in **Figure 6** reflected the size of the DAPP. In DLS, the peaks can be utilized to analyze the interaction between particles. Theoretically, the size of BSA and DAPP will merge together if there is an interaction between BSA and DAPP, which includes the absorption of BSA onto DAPP, the charge neutralization, and chain entanglement. The size will increase markedly with a broad distribution. Both **Figures 6A,B** shows that the two peaks were well-defined at different detecting time 24 and 48 h, which indicates that the DAPP holds high serum stability.

Figure 7 shows the DOX release profile. As mentioned above, intratumoral drug-release plays an important role in the therapeutic efficiency when the DAPP accumulates in the tumor. In this study, we used NIR-light as a sensor to trigger the photothermal transition through the GNRs. The collapse of the

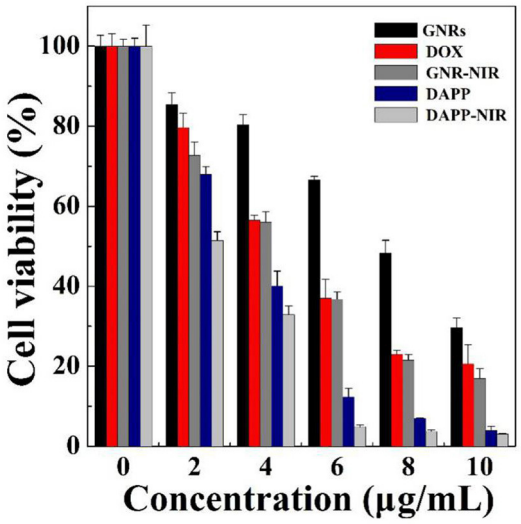

FIGURE 9 | *In-vitro* evaluation of the cytotoxicity of DAPP against B16F10 cells.

PNIPAM was triggered by the heat generated and was followed by an increase in DOX release. The *in-vitro* release profile of DOX from DAPP was then regulated intratumorally. **Figure 7** shows that the maximum absorption wavelength of DOX is 480 nm and the DOX concentration increased after NIR-light because the drug release rate of the DAPP with NIR-light was significantly higher than that of DAPP without NIR. Compared with the DAPP (non-NIR), about 90% of DOX was released within 10 h, which indicated that GNRs and PNIPAN loaded in the core of the DAPP had performed as expected and was suitable for promoting intratumoral drug accumulation.

In-vitro Cellular Internalization and Cytotoxicity

After intratumoral accumulation and drug release, tumor cell capture and cytotoxicity are the next most important issues for tumor inhibition. Herein, the cellular internalization was monitored by inverted fluorescence microscopy as shown in **Figure 8**. The blue fluorescence indicates the nucleus stained by DAPI and red fluorescence is from DOX. The image clearly shows that the cellular uptake of DAPP with NIR-light (**Figure 8C**) was much higher than of free-DOX (**Figure 8A**) and DAPP without the NIR-light trigger (**Figure 8B**). Therefore, it can be easily concluded that DAPP could deliver the drug to tumor cells. Moreover, the drug could be stimulated to be released in tumor cells by exposure to NIR-light and produced a high intratumoral accumulation of DOX.

The *in-vitro* cytotoxicity of GNRs, DOX, and DAPP against B16F10 melanoma cells was further evaluated by the CCK-8 assay as shown in **Figure 9**. The cytotoxicity assay was conducted under NIR-light. At the same concentrations and time points, the cytotoxicity of DAPP with NIR-light was much higher than that of free-DOX or free-GNR. The higher temperature generated by GNRs under the NIR-light could also kill cancer cells, which also resulted in higher cytotoxicity by GNRs. This indirectly suggested that GNRs had a good photothermal conversion effect. This cytotoxicity results were similar to our previous studies, in which the intracellular mechanism of GNRs to selectively kill cancer cells under the conditions of NIR-light was systemically investigated (Zhang et al., 2017). Therefore, the cytotoxicity of the temperature/light dual-functional DAPP micelles correlated with the increased cellular uptake and enhanced intracellular drug release shown in **Figure 8**.

In-vivo Biodistribution and Antitumor Effects of DAPP

The *in-vivo* distribution of DAPP micelles monitored by the florescent marker FITC in the melanoma tumor-bearing nude mice is shown in **Figure 10**. From the living animal images, the red fluorescent area of DAPP detected for the NIR light-treated group was obviously higher than that of DAPP without NIR-light treatment and FITC-free groups, which indicated that the DAPP could significantly promote drug accumulation at the tumor site. This enhanced tumor accumulation of FITC is partly due to the EPR effect, which is dominated by the PEG chain surrounding the DAPP. Meanwhile, the high fluorescent intensity of DAPP with NIR-light is mainly attributable to the GNRs photothermo transition, which promotes the release of on-site fluorescent molecule release at the same site as intratumor accumulation of DAPP. Therefore, the DAPP with NIR-light treated group promoted the concentration of DOX at the tumor sites, which was significantly improved by NIR-light. Noted here, the experiments about biodistribution and biosafety of DAPP were conducted while the data was not shown here, which was analyzed and used in our other work.

Figure 11 shows the *in-vivo* antitumor effects evaluated in melanoma tumor-bearing nude mice. When the tumor grew to around 100 mm^3, the mice were divided into three treatment groups: PBS, DAPP, and DAPP with NIR-light. Compared with DAPP without NIR-light exposure, the relative tumor volume was much smaller. This clearly indicated that the intratumor drug release was successfully enhanced by the NIR exposure due to the photothermal transition followed by the thermo-regulated drug release. **Figure 11** shows that the relative tumor volume of the PBS-treated group, that is, the control group, was the largest, which indicated that the EPR effect of the nano-sized DAPP was promoted by both the size and the PEG chain (**Figure 10**). Consequently, the tumor volume of the control group was about 6-times larger than that of DAPP-NIR light-treated group, which is attributed to both the EPR effect and the photothermo transition of GNRs inside of DAPP of the treatment groups. It may be concluded that the concentration of DOX release as delivered by the DAPP micelles at the tumor site was regulated by physical stimuli represented by the NIR-light. In addition, as shown in **Figure 11B**, the therapeutic effects were also clearly reflected in the tumor tissue harvested from the corresponding groups. Moreover, both our's and other's previous works confirmed that GNRs exposed specific toxicity to tumor

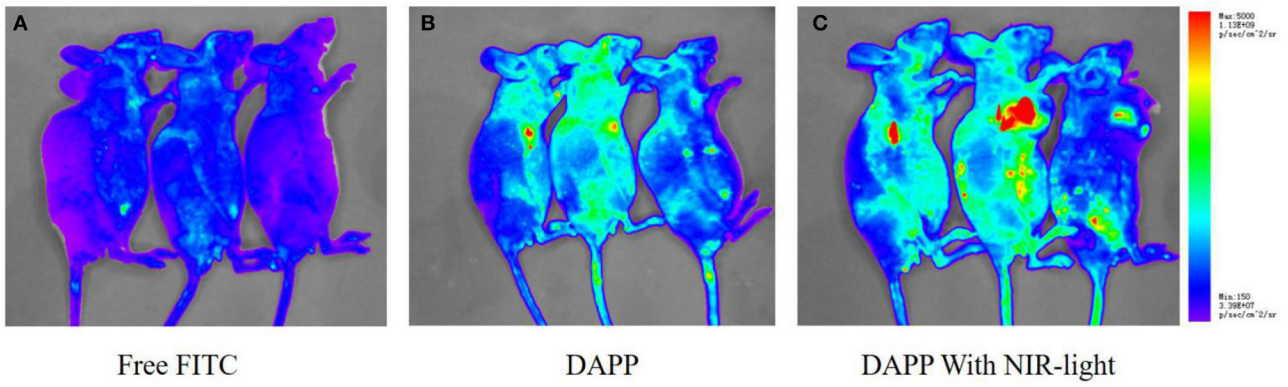

FIGURE 10 | The *in-vivo* biodistribution evaluation. The biodistribution of free FITC **(A)**, DAPP **(B),** and DAPP with NIR-light **(C)**.

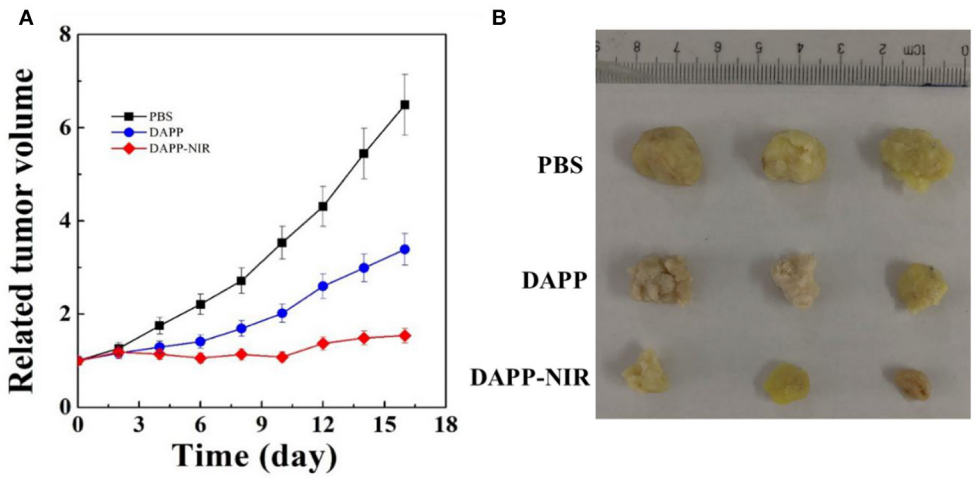

FIGURE 11 | The *in-vivo* antitumor effect of PBS, DAPP, and DAPP-NIR **(A)** and the volume of solid tumor harvested from different groups **(B)**.

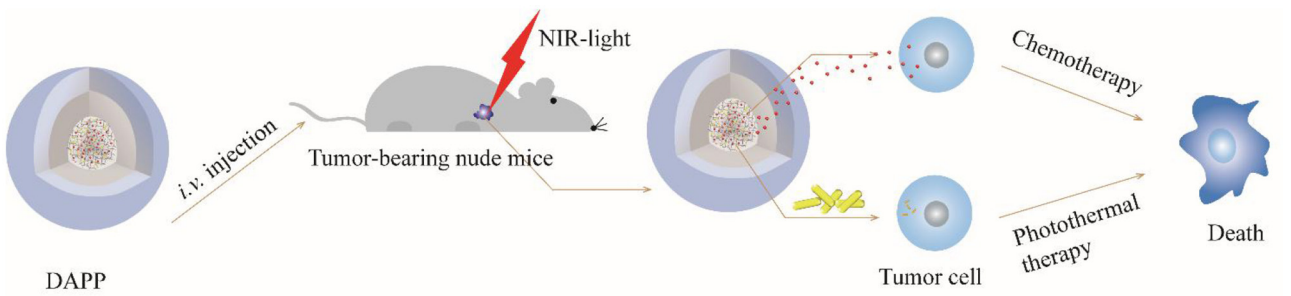

FIGURE 12 | This scheme illustrates the *in-vitro/in-vivo* mechanism of the DAPP.

cells, while there was little cytotoxicity to non-tumor cells (Wang et al., 2011; Zhang et al., 2017).

Taken together, the overall mechanism of DAPP activity is illustrated in **Figure 12**. DOX and GNRs are combined with PNIPAM, and then loaded in photo- and thermo-sensitive micelles, which act as dual-function DAPP. These bifunctional nanomicelles were successfully prepared by fine-tuning physical properties as described in our previous study (Su et al., 2017). The particle size of the DAPP was about 220 nm and presented a spherical shape, and its construction was tailored

to exhibit dual-functions, good biocompatibility, excellent photo and thermal sensitivity, and good serum stability. The release of DOX in DAPP micelles showed a greater dependency on the GNRs photothermal conversion effect and on the temperature responsiveness of PNIPAM, which strongly influenced its therapeutic activity against melanoma. The *in-vitro* cytotoxicity assay showed that the GNRs and the chemotherapeutic drug DOX exhibited a synergistic effect on the killing of B16F10 cells. The results of the *in-vivo* distribution and tumor inhibition assay showed that DAPP micelles were more highly enriched at tumor sites, which was partly due to the EPR effects of DAPP. In addition, the tumor inhibition effect of DAPP under NIR-light-treatment was even superior to that of other groups, because the DAPP micelles system can control PNIPAM shrinkage and lead to higher in-site tumor cellular drug release and thus promote a stronger chemotherapeutic effect.

CONCLUSION

In summary, temperature and light-sensitive dual-functional DAPP micelles were successfully prepared by a fine-tuned physical-chemical self-assembly and exhibit a well-defined shell-core structure and excellent biocompatibility. First, the EPR effect of DAPP promoted the accumulation of micelles at the tumor site. Then, the photothermal effect of GNRs in the DAPP core further enhanced the drug release in tumor cells regulated by the PNIPAM collapse, which in turn was regulated by the NIR-light-induced photothermal transition, which triggered the release of a high concentration of DOX at the tumor site. In addition, the advantages of this dual functional DAPP included the sparing of normal tissue as compared with previous strategy by *in-vivo* tissue ablation. The experimental results showed that DAPP induced excellent antimelanoma effects both *in vitro* and *in vivo* under NIR-light-triggered drug release. Consequently, this study supports the use of the DAPP micelles construct as an effective nanodrug delivery system with high treatment potential against melanoma through a physical stimuli-responsive cargo release, and may represent a novel approach to the clinical therapy of melanoma.

DATA AVAILABILITY STATEMENT

The original contributions presented in the study are included in the article/supplementary materials, further inquiries can be directed to the corresponding author/s.

ETHICS STATEMENT

The animal study was reviewed and approved by the Institutional Review Board of the Second Military Medical University.

AUTHOR CONTRIBUTIONS

All authors listed have made a substantial, direct and intellectual contribution to the work, and approved it for publication.

FUNDING

This work was financially supported by the National Natural Science Foundation of China (31470964), the National Key New Drug Creation and Manufacturing Program, and the Ministry of Science and Technology (2018ZX09J18107-4).

REFERENCES

Cabral, H., Miyata, K., Osada, K., and Kataoka, K. (2018). Block copolymer micelles in nanomedicine applications. *Chem. Rev.* 118, 6844–6892. doi: 10.1021/acs.chemrev.8b00199

Cao, M., Wang, P., Kou, Y., Wang, J., Liu, J., Li, Y., et al. (2015). Gadolinium(III)-chelated silica nanospheres integrating chemotherapy and photothermal therapy for cancer treatment and magnetic resonance imaging. *ACS Appl. Mater. Interfaces* 7, 25014–25023. doi: 10.1021/acsami.5b06938

Cao, P., Sun, X., Liang, Y., Gao, X., Li, X., Li, W., et al. (2015). Gene delivery by a cationic and thermosensitive nanogel promoted established tumor growth inhibition. *Nanomedicine* 10, 1585–1597. doi: 10.2217/nnm.15.20

Chen, C. Y., Kim, T. H., Wu, W. C., Huang, C. M., Wei, H., Mount, C. W., et al. (2013). pH-dependent, thermosensitive polymeric nanocarriers for drug delivery to solid tumors. *Biomaterials* 34, 4501–4509. doi: 10.1016/j.biomaterials.2013.02.049

Chen, D., Zhu, X., Tao, W., Kong, Y., Huag, Y., Zhang, Y., et al. (2020). Regulation of pancreatic cancer microenvironment by an intelligent gemcitabine@nanogel system via *in vitro* 3D model for promoting therapeutic efficiency. *J. Control. Release* 324, 545–559. doi: 10.1016/j.jconrel.2020.06.001

Deng, C., Zhang, Q., Fu, Y., Sun, X., Gong, T., and Zhang, Z. (2017). Coadministration of oligomeric hyaluronic acid-modified liposomes with tumor-penetrating peptide-iRGD enhances the antitumor efficacy of doxorubicin against melanoma. *ACS Appl. Mater. Interfaces* 9, 1280–1292. doi: 10.1021/acsami.6b13738

Gong, J., Zhang, Y., Huang, Y., Zhang, T., Liang, B., Hu, S., et al. (2019). The effects of the surface properties of a gold nanorod on its *in vitro/vivo* toxicity against cancer cells. *J. Biomed. Nanotechnol.* 15, 2262–2270. doi: 10.1166/jbn.2019.2851

Han, K., Ma, Z., Dai, X., Zhang, J., and Han, H. (2018). Steric shielding protected and acidity-activated pop-up of ligand for tumor enhanced photodynamic therapy. *J. Control. Release* 279, 198–207. doi: 10.1016/j.jconrel.2018.04.033

Han, K., Zhang, J., Zhang, W., Wang, S., Xu, L., Zhang, C., et al. (2017a). Tumor-triggered geometrical shape switch of chimeric peptide for enhanced *in vivo* tumor internalization and photodynamic therapy. *ACS Nano* 11, 3178–3188. doi: 10.1021/acsnano.7b00216

Han, K., Zhang, W. Y., Ma, Z. Y., Wang, S. B., Xu, L. M., Liu, J., et al. (2017b). Acidity-triggered tumor retention/internalization of chimeric peptide for enhanced photodynamic therapy and real-time monitoring of therapeutic effects. *ACS Appl. Mater. Interfaces* 9, 16043–16053. doi: 10.1021/acsami.7b04447

Hou, Y., Zhou, J., Gao, Z., Sun, X., Liu, C., Shangguan, D., et al. (2015). Protease-activated ratiometric fluorescent probe for pH mapping of malignant tumors. *ACS Nano* 9, 3199–3205. doi: 10.1021/acsnano.5b00276

Kinoh, H., Shibasaki, H., Liu, X., Yamasoba, T., Cabral, H., and Kataoka, K. (2020). Nanomedicines blocking adaptive signals in cancer cells overcome tumor TKI resistance. *J. Control. Release* 321, 132–144. doi: 10.1016/j.jconrel.2020.02.008

Li, S., Zhang, Y., Wang, J., Zhao, Y., Ji, T., Zhao, X., et al. (2017). Nanoparticle-mediated local depletion of tumour-associated platelets disrupts vascular barriers and augments drug accumulation in tumours. *Nat. Biomed. Eng.* 1, 667–679. doi: 10.1038/s41551-017-0115-8

Li, W., Feng, S., and Guo, Y. (2012b). Tailoring polymeric micelles to optimize delivery to solid tumors. *Nanomedicine* 7, 1235–1252. doi: 10.2217/nnm.12.88

Li, W., Feng, S.-S., and Guo, Y. (2012a). Block copolymer micelles for nanomedicine. *Nanomedicine* 7, 169–172. doi: 10.2217/nnm.11.182

Li, W., Guo, Q., Zhao, H., Li, P., Li, J., Gao, J., et al. (2012c). Novel dual-control poly(N -isopropylacrylamide- co -chlorophyllin) nanogels for improving drug release. *Nanomedicine* 7, 383–392. doi: 10.2217/nnm.11.100

Li, W., Li, J., Gao, J., Li, B., Xia, Y., Meng, Y., et al. (2011a). The fine-tuning of thermosensitive and degradable polymer micelles for enhancing intracellular uptake and drug release in tumors. *Biomaterials* 32, 3832–3844. doi: 10.1016/j.biomaterials.2011.01.075

Li, W., Nakayama, M., Akimoto, J., and Okano, T. (2011b). Effect of block compositions of amphiphilic block copolymers on the physicochemical properties of polymeric micelles. *Polymer* 52, 3783–3790. doi: 10.1016/j.polymer.2011.06.026

Li, W., Zhao, H., Qian, W., Li, H., Zhang, L., Ye, Z., et al. (2012d). Chemotherapy for gastric cancer by finely tailoring anti-Her2 anchored dual targeting immunomicelles. *Biomaterials* 33, 5349–5362. doi: 10.1016/j.biomaterials.2012.04.016

Long, Y., Lu, Z., Mei, L., Li, M., Ren, K., Wang, X., et al. (2018). Enhanced melanoma-targeted therapy by "Fru-Blocked" phenyboronic acid-modified multiphase antimetastatic micellar nanoparticles. *Adv. Sci.* 5:1800229. doi: 10.1002/advs.201800229

Ma, T., Zhang, P., Hou, Y., Ning, H., Wang, Z., Huang, J., et al. (2018). "Smart" nanoprobes for visualization of tumor microenvironments. *Adv. Healthc. Mater.* 7:e1800391. doi: 10.1002/adhm.201800391

Mi, P., Cabral, H., and Kataoka, K. (2020). Ligand-installed nanocarriers toward precision therapy. *Adv. Mater.* 32:e1902604. doi: 10.1002/adma.201902604

Pautu, V., Leonetti, D., Lepeltier, E., Clere, N., and Passirani, C. (2017). Nanomedicine as a potent strategy in melanoma tumor microenvironment. *Pharmacol. Res.* 126, 31–53. doi: 10.1016/j.phrs.2017.02.014

Pinho, J., Matias, M., and Gaspar, M. (2019). Emergent nanotechnological strategies for systemic chemotherapy against melanoma. *Nanomaterials* 9:1455. doi: 10.3390/nano9101455

Siegel, R. L., Miller, K. D., and Jemal, A. (2019). Cancer statistics, 2019. *CA Cancer J. Clin.* 69, 7–34. doi: 10.3322/caac.21551

Smith, M. J. F., Smith, H. G., Joshi, K., Gore, M., Strauss, D. C., Hayes, A. J., et al. (2018). The impact of effective systemic therapies on surgery for stage IV melanoma. *Eur. J. Cancer* 103, 24–31. doi: 10.1016/j.ejca.2018.08.008

Su, Y., Huang, N., Chen, D., Zhang, L., Dong, X., Sun, Y., et al. (2017). Successful *in vivo* hyperthermal therapy toward breast cancer by Chinese medicine shikonin-loaded thermosensitive micelle. *Int. J. Nanomed.* 12, 4019–4035. doi: 10.2147/ijn.S132639

Wang, L., Liu, Y., Li, W., Jiang, X., Ji, Y., Wu, X., et al. (2011). Selective targeting of gold nanorods at the mitochondria of cancer cells: implications for cancer therapy. *Nano Lett.* 11, 772–780. doi: 10.1021/nl103992v

Wilhelm, S., Tavares, A. J., Dai, Q., Ohta, S., Audet, J., Dvorak, H. F., et al. (2016). Analysis of nanoparticle delivery to tumours. *Nat. Rev. Mater.* 1:16014. doi: 10.1038/natrevmats.2016.14

Yang, S., and Gao, H. (2017). Nanoparticles for modulating tumor microenvironment to improve drug delivery and tumor therapy. *Pharmacol. Res.* 126, 97–108. doi: 10.1016/j.phrs.2017.05.004

Yang, Y., Tai, X., Kairong, S., Ruan, S., Qiu, Y., Zhang, Z.-R., et al. (2016). A new concept of enhancing immuno-chemotherapeutic effects against B16F10 tumor via systemic administration by taking advantages of the limitation of EPR effect. *Theranostics* 6, 2141–2160. doi: 10.7150/thno.16184

Zhang, D., Wu, T., Qin, X., Qiao, Q., Shang, L., Song, Q., et al. (2019a). Intracellularly generated immunological gold nanoparticles for combinatorial photothermal therapy and immunotherapy against tumor. *Nano Lett* 19. doi: 10.1021/acs.nanolett.9b02903

Zhang, F., Chen, D., Wang, Y., Zhang, L., Dong, W., Dai, J., et al. (2017). Lysosome-dependent necrosis specifically evoked in cancer cells by gold nanorods. *Nanomedicine* 12, 1575–1589. doi: 10.2217/nnm-2017-0126

Zhang, F., Zhu, X., Gong, J., Sun, Y., Chen, D., Wang, J., et al. (2016). Lysosome-mitochondria-mediated apoptosis specifically evoked in cancer cells induced by gold nanorods. *Nanomedicine* 11, 1993–2006. doi: 10.2217/nnm-2016-0139

Zhang, P., Hou, Y., Zeng, J., Yingying, L., Wang, Z., Zhu, R., et al. (2019b). Coordinatively unsaturated Fe3+ based activable probes for enhanced MRI and therapy of tumors. *Angewandte Chem. Int. Edn.* 58, 11088–11096. doi: 10.1002/anie.201904880

Zhu, X., Sun, Y., Chen, D., Li, J., Dong, X., Wang, J., et al. (2017). Mastocarcinoma therapy synergistically promoted by lysosome dependent apoptosis specifically evoked by 5-Fu@nanogel system with passive targeting and pH activatable dual function. *J. Control. Release* 254, 107–118. doi: 10.1016/j.jconrel.2017.03.038

Conflict of Interest: The authors declare that the research was conducted in the absence of any commercial or financial relationships that could be construed as a potential conflict of interest.

frontiers in Chemistry

REVIEW
published: 12 April 2021
doi: 10.3389/fchem.2020.572471

Activable Multi-Modal Nanoprobes for Imaging Diagnosis and Therapy of Tumors

Yan Yang[1†], Saisai Yue[1†], Yuanyuan Qiao[1†], Peisen Zhang[2,3], Ni Jiang[1], Zhenbo Ning[1], Chunyan Liu[4] and Yi Hou[1,2]**

[1]College of Life Science and Technology, Beijing University of Chemical Technology, Beijing, China, [2]Key Laboratory of Colloid, Interface and Chemical Thermodynamics, Institute of Chemistry, Chinese Academy of Sciences, Beijing, China, [3]School of Chemistry and Chemical Engineering, University of Chinese Academy of Sciences, Beijing, China, [4]Institute of Atmospheric Physics, Chinese Academy of Sciences, Beijing, China

Malignant tumors have become one of the major causes of human death, but there remains a lack of effective methods for tiny tumor diagnosis, metastasis warning, clinical efficacy prediction, and effective treatment. In this context, localizing tiny tumors via imaging and non-invasively extracting molecular information related to tumor proliferation, invasion, metastasis, and drug resistance from the tumor microenvironment have become the most fundamental tasks faced by cancer researchers. Tumor-associated microenvironmental physiological parameters, such as hypoxia, acidic extracellular pH, protease, reducing conditions, and so forth, have much to do with prognostic indicators for cancer progression, and impact therapeutic administrations. By combining with various novel nanoparticle-based activatable probes, molecular imaging technologies can provide a feasible approach to visualize tumor-associated microenvironment parameters noninvasively and realize accurate treatment of tumors. This review focuses on the recent achievements in the design of "smart" nanomedicine responding to the tumor microenvironment-related features and highlights state-of- the-art technology in tumor imaging diagnosis and therapy.

Keywords: tumor theranostics, microenvironment, target-triggering, multi-modal probe, nanomedicine

OPEN ACCESS

Edited by:
Zoe Pikramenou, University of Birmingham, United Kingdom

Reviewed by:
Raghvendra Ashok Bohara, National University of Ireland Galway, Ireland
Jinzhi Du, South China University of Technology, China

****Correspondence:***
Peisen Zhang
zhangps@iccas.ac.cn
Yi Hou
houyi@iccas.ac.cn

†These authors have contributed equally to this work

Specialty section:
This article was submitted to Nanoscience, a section of the journal Frontiers in Chemistry

Received: *14 June 2020*
Accepted: *18 December 2020*
Published: *12 April 2021*

Citation:
Yang Y, Yue S, Qiao Y, Zhang P, Jiang N, Ning Z, Liu C and Hou Y (2021) Activable Multi-Modal Nanoprobes for Imaging Diagnosis and Therapy of Tumors. Front. Chem. 8:572471. doi: 10.3389/fchem.2020.572471

INTRODUCTION

Effective precision cancer diagnosis and therapy remain as critical challenges in current tumor studies and clinics. The prognostic factors of malignant tumors, including proliferation, invasion, and metastasis, are closely associated with variations in physiological parameters, such as hypoxia, low extracellular pH, enzymes, and reducing conditions (Ma et al., 2018b). For instance, the lowered extracellular pH induced by the enhanced glucose uptake and altered glucose metabolism of tumor cells is deemed to be a hallmark of cancer, because it can promote angiogenesis in tumor tissue, and accelerate the degradation of the extratumoral matrix by affecting proteolytic enzymes (Ma et al., 2018a). Thus, monitoring the parameters and clarifying their relationship is critical not only for tumor diagnostics, but also for therapeutic administrations.

The current characterizations of tumor-associated microenvironments mostly rely on *in vitro* analysis of the secreted proteins and gene expression, or invasive methods such as microelectrodes (Anh-Nguyen et al., 2016; Zhang et al., 2018; Song Y. et al., 2019). Although these methods can provide accurate molecular information, they are not able to provide complete information on the

tumor microenvironment due to its complexity and spatiotemporal heterogeneity. In this context, tumor microenvironment analysis still needs advanced diagnostic techniques to offer exhaustive information on the tumor progression.

The development of noninvasive molecular imaging techniques and probes provides new insights into this area by providing versatile engineered molecular imaging probes for noninvasively monitoring the tumor microenvironment (Mi et al., 2016; Zhang P. et al., 2019b; Wang et al., 2020). In principle, molecular imaging can adopt different imaging techniques such as computed tomography (CT), magnetic resonance imaging (MRI), nuclear imaging, optical imaging, and so forth. The molecular imaging based on recognition between the exogenous probes and molecular marks associated with tumors can provide spatiotemporal information of the tumor at a cellular or even molecular level (Weissleder, 1999; Weissleder and Ntziachristos, 2003). The tumor microenvironment physiological parameters are important hallmarks, thus rendering them attractive targets to design target-triggering probes that can respond to stimuli in the tumor microenvironment based on novel chemical designing (Mura et al., 2013; Gao et al., 2017; Ma et al., 2018b).

A series of molecular imaging probes, especially nanoparticle (NP)-based probes, have been emerging rapidly as potential precision tumor theranostic agents, as they are able to not only serve as imaging agents to improve the diagnosis' accuracy, but also provide a platform for innovative tumor therapies (Janib et al., 2010; Kelkar and Reineke, 2011; Omidi, 2011). Regarding the therapeutics of tumors, current clinical cancer therapies mainly rely on surgical resection, chemotherapy, and radiotherapy. However, it remains a challenge to remove tumors precisely and completely through oncological surgery, due to the extreme difficulty in identifying the tumor boundary (Chen Q. et al., 2019), while chemo drugs and radiation would lead to serious side effects (Oun et al., 2018). In order to improve therapeutic efficacy and minimize the side-effects, several innovative nano-based tumor therapies are being developed, including targeted chemotherapy with controlled release of anti-cancer agents, chemodynamic therapy (CDT), nanovaccine-based immunotherapy, gene therapy mediated by nanocarriers, and nano-enhanced physical therapy such as photothermal therapy (PTT), photodynamic therapy (PDT), magnetic hyperthermia (MHT), and radiotherapy.

This review focuses on the state-of-the art of target-triggered nanoprobes for tumor theranostics; we will summarize the preparation strategies, response mechanisms, and theranostic applications of state-of-the art activable theranostic nanoprobes.

CANCER THERANOSTIC PROBES FOR CONTROLLED RELEASE OF CHEMICAL ANTICANCER AGENTS

To endow the tumor imaging nanoprobes with the abilities of loading and controlling the release of anticancer chemicals is one of the most basic and widely used approaches for designing cancer theranostics nanoprobes (Chen et al., 2018; Gu et al., 2019). On the one hand, nanomaterials can be employed as excellent signal carriers due to their various intrinsic optical and magnetic properties to sensitively detect the tumors (Jing et al., 2020). One the other hand, nano-delivery systems can overcome the limitations of rapid nonspecific clearance and poor biodistribution of conventional low-molecular-weight antitumor drugs by packaging the chemical agents within sterically stabilized, long-circulating nanoformulations, which can be further surface-modified with ligands to actively target cellular/molecular components of the tumors (Sumer and Gao, 2008; Saha, 2009; Tee et al., 2019).

Using Nanocarriers to Improve Conventional Chemotherapy Drugs for Tumor Theranostics

As is well known, the clinical application of chemotherapy is impeded by its unsatisfactory efficacy and severe side effects (Rezaee et al., 2017; Peters, 1994). In this regard, several cancer nanomedicines have been developed through loading the chemotherapeutics on nanoagents aimed at reducing side effects, and are currently used in clinic (Bobo et al., 2016). For example, the FDA has approved anticancer nanodrugs including Doxil (PEGylated liposomal encapsulation of the anticancer drug doxorubicin) for ovarian cancer treatment (1995) and Abraxane (albumin-bounded paclitaxel nanoparticles) for breast cancer treatment (2005), metastatic non-small-cell lung cancer (2012), and metastatic pancreatic cancer (2013), which significantly alleviate the adverse effects of patients in clinical trials (Barenholz, 2012). However, even though the delivery of cytotoxic chemotherapeutics through nanocarriers can enhance drug tolerability in patients as compared to the conventional formulations, the survival benefit of them are still modest (Petersen et al., 2016). In addition, long-term side effects associated with nanomedicines should be considered (Schottler et al., 2016). A large proportion of intravenously administered nanoparticles will be finally captured by the immune system of an organism and then retained in the reticuloendothelial system (RES, e.g., liver and spleen), which could cause potential risks of toxicity due to long-term retention if they are difficult to metabolize, largely hampering their practical application (De Jong et al., 2008; Poon et al., 2019).

To overcome these limitations, nano-systems incorporating stimuli-responsive materials have been designed to selectively release anticancer agents within tumor regions, and can keep silent in normal tissue to greatly avoid off-target side effects. In addition, due to the properties of nanocarriers, these controlled drug release systems can be further combined with tumor imaging to accurately track the drug delivery routes. Based on this concept, fabricating the imaging moiety and the anticancer prodrug together is the most commonly used design strategy for these probes. For example, Luo and coworkers prepared a stimuli-responsive polymeric nano-prodrug for tumor theranostics through imaging moieties (gadolinium-chelates) and therapeutic moieties (PTX). Such branched polymeric PTX-Gd-based nanoparticles (BP-PTX-Gd NPs) exhibit good

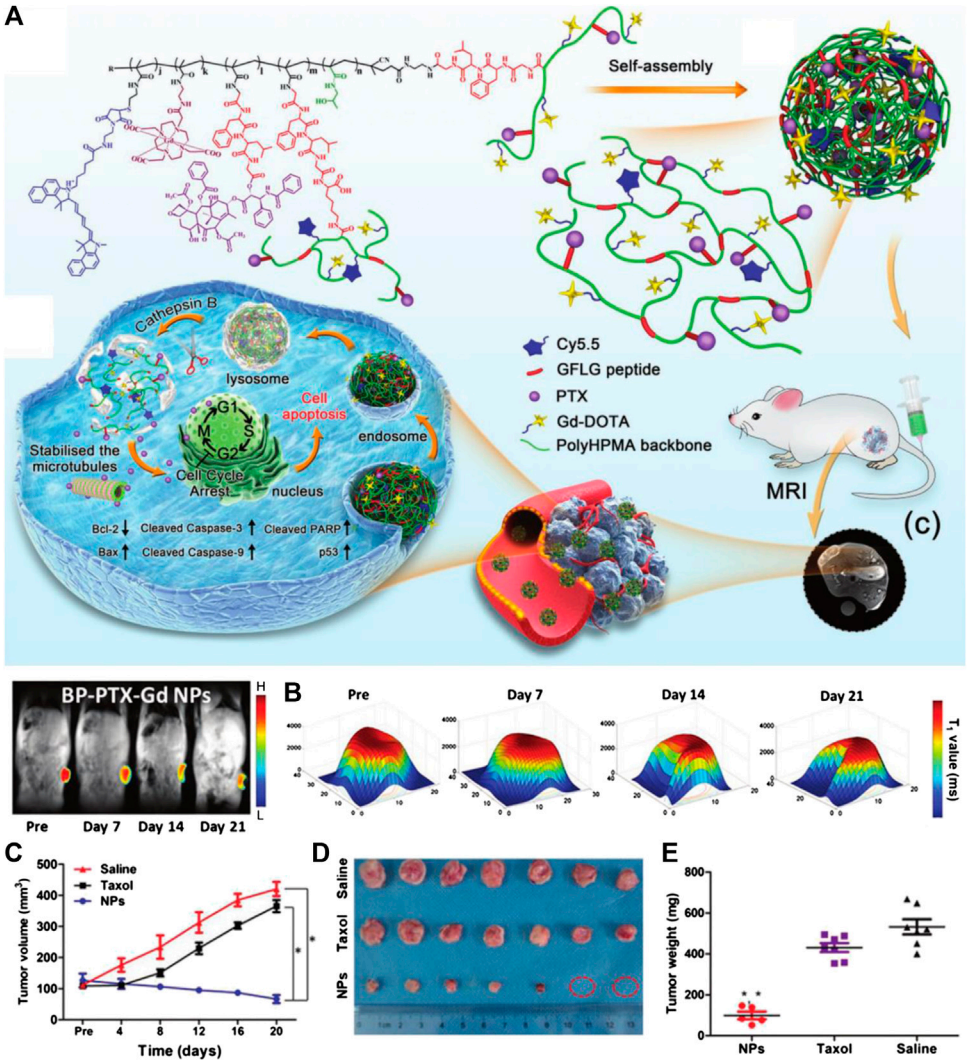

FIGURE 1 | (A) Schematic illustration of cathepsin B-responsive biodegradable theranostic nanomedicine derived from branched pHPMA. **(B)** Distribution of T_1 value of tumor at different time points after injection. **(C)** Quantitative tumor volume changes of mice obtained by MRI after being treated with saline, Taxol, and BP-PTX-Gd NPs ($n = 7$, $^*p < 0.001$ vs. saline, $^*p < 0.001$ vs. Taxol). **(D)** Images of the tumors harvested from the mice 21 days after the treatment. **(E)** The tumor weight of tumor-bearing mice after treatment ($^*p < 0.001$ vs. saline, $^*p < 0.001$ vs. Taxol). Reproduced with permission from Cai H. et al. (2020). Copyright 2020 Wiley-VCH Verlag GmbH & Co. KgaA.

biocompatibility and high stability under physiological conditions, but can be triggered to degrade in the tumor microenvironment and release PTX. On an animal level, BP-PTX-Gd NPs can not only significantly improve the MRI contrast of tumors due to the high r_1 value (8.6 mM^{-1} s^{-1}), but also possess a satisfying therapeutic effect on tumors, which is much better than that of Taxol, a clinical anticancer drug (**Figure 1**) (Cai H. et al., 2020). In another work, Song and coworkers reported a sequential pH and reduction-responsive hybrid assembly composed of polymer and gold nanorod (AuNR) to overcome the biological barriers via a two-stage size decrease and disassembly through responding to the specified tumor microenvironment. After tumor uptake, the ultrasmall AuNRs with polymerized reduction-responsive DOX prodrug on their surface will disassemble, and then penetrate into the deep area of solid tumors and realize the release of DOX. In the meantime, these hybrid nanoparticles can be employed as satisfactory deep-tissue PA and surface-enhanced Raman scattering imaging agents for real-time monitoring of physiological behaviors of tumors during nano-based treatments (Liu T. et al., 2019).

Another interesting strategy is to make the imaging signal also capable of responding to stimuli (Han et al., 2020). As the probe reaches the tumor regions, the prodrug and the imaging module can be simultaneously activated, thereby realizing the specific diagnosis and treatment of the tumor (Mura et al., 2013; Lu et al., 2016). Through this approach, the probes can not only realize the theranostics of tumor, but also readily monitor drug release by the activated imaging signal enhancement in a spatiotemporally

concurrent manner, which makes imaging the activity and intratumoral distribution of drugs easier, thus enhancing the therapeutic efficacy and prognostic evaluation. Huang and coworkers report a manganese-iron layered double hydroxide (MnFe-LDH) to serve as a pH-responsive nanoplatform for cancer theranostics. Such a platelet-like nanoplatform can be successfully triggered by the lower pH in the microenvironment of a solid tumor to release paramagnetic Mn^{2+} and Fe^{3+} ions, thereby enhancing the T_1 MR signal of T_1 of tumor sites. More importantly, the layered structure endows MnFe-LDH with pH-controlled chemotherapeutic drug methotrexate (MTX) loading capacity, which can effectively kill the tumor cells (Huang et al., 2017). Similarly, manganese dioxide (MnO_2) nanoparticles were prepared and stabilized by bovine serum albumin (BSA), which was further coated with a nanoscale coordination polymers (NCP)-shell composed of a high atomic number of Hf ions and cisplatin prodrug c,c,t- (diamminedichlorodisuccinato)Pt (IV) (DSP). After further protection from polyethylene glycol (PEG), the formed BM@NCP(DSP)-PEG can not only diagnose the tumor through MRI by Mn^{2+} release in an acidic tumor microenvironment, but also serve as a radio-sensitizer due to the strong X-ray attenuation ability of Hf to realize radiotherapy, together with a chemotherapeutic drug attributed to the release of cisplatin. Meanwhile, the excess O_2 will be generated by the tumor endogenous H_2O_2 *in situ* under the MnO_2 catalysis, which can overcome the radio-resistance caused by hypoxia to enhance the efficacy (Liu et al., 2017). In another work, Chen and coworkers reported a kind of GSH-responsive nanovesicles with a yolk-shell structure, in which both therapeutic drugs (DOX) and MRI contrast agents were both encapsulated inside the nanovesicles. The obtained nanovesicles with restrained drug activity and quenched T_1 MRI contrast ability can respond to GSH in a tumor microenvironment and lead to both T_1 contrast activation and DOX release, thereby monitoring drug release by activated T_1 MRI signal (Liu D. et al., 2020).

Tumor Probe Integrated With Imaging and Chemodynamic Therapy

The Fenton reaction, which can be simply defined as the formation of hydroxide (OH^-) and highly oxidative hydroxyl (•OH) radical by a reaction between ferrous ion (Fe^{2+}) and hydrogen peroxide (H_2O_2), has been widely used to degrade the organic pollutant (Gupta et al., 2016).

$$Fe^{2+} + H_2O_2 \rightarrow Fe^{3+} + OH^- + \bullet OH$$

Apart from the catalytic effect of Fe ions, other transition metal ions, such as Mn^{2+}, Ti^{3+}, Cu^{2+}, or Co^{2+} ions, can also be employed as catalytic ions of the reaction to generate •OH from H_2O_2, which is known as the Fenton-like reaction. Based on this mechanism, chemodynamic therapy (CDT), a kind of *in situ* tumor treatment approach, is proposed to kill cancer cells through excessive •OH produced by Fenton or Fenton-like reaction in tumor sites (Tang et al., 2018). Specifically, transition metal ions contain nanomaterials that can be designed to release these ions under the specific tumor microenvironment and initiate the Fenton or Fenton-like reaction to decompose the tumor endogenous H_2O_2, thus accumulating the •OH to trigger apoptosis of tumor cells (Zhang et al., 2016). Notably, Fenton or Fenton-like reaction will be significantly inhibited in the weak alkaline physiological conditions or in the normal tissues with insufficient H_2O_2. Therefore, compared with general radiotherapy and chemotherapy, CDT shows better tumor selectivity and thus avoids off-target side effects.

Based on this tumor therapy, one feasible strategy to design theranostic nanoprobes is to combine CDT with MRI. The paramagnetic ions, such as Mn^{2+}, Fe^{3+}, or Cu^{2+}, are not only the reactants or products of Fenton or Fenton-like reactions, but also excellent T_1-MRI contrast agents owing to their long electron spin relaxation times and high magnetic moments, providing a natural bridge between tumor diagnosis and treatment.

Iron ion is the first reported ion that can trigger the Fenton reaction within a tumor area. Due to the existence of various redox molecules, such as ROS an GSH, in the tumor microenvironment, Fe^{3+} and Fe^{2+} can readily transform to each other, thus leading to a stronger catalytic effect on H_2O_2, and causing a large accumulation of ROS in cancer cells, which is also known as Ferroptosis (Dixon et al., 2012; Schoenfeld et al., 2017; Zheng et al., 2017). However, as a kind of paramagnetic ion, Fe^{3+} can significantly reduce the relaxation time of 1H protons of surrounding water molecules, thereby selectively lightening the tumor in T_1-weighted MR images. Accordingly, several Fe-based nanoprobes, which are able to release Fe^{3+} in the tumor area, have been widely studied as Fenton reagents and tumor CDT initiators (Huo et al., 2019; Zhao P. et al., 2019; Du et al., 2020). However, the harsh reaction requirement of a low pH (~3–4) and the slow reaction rate (63 m^{-1} s^{-1}) still limits their practical application in tumor theranostics. To overcome this problem, Bu and coworkers successfully accelerated the intratumoral Fenton process with the help of a temperature increase generated by photothermal treatment to improve the therapeutic effect of CDT. They prepared an antiferromagnetic pyrite polyethylene glycol (FeS_2-PEG) nanocube, which was activated by peroxide, and formed a valence-variable elemental Fe layer on the surface through self-oxidation, inducing both the self-enhanced MRI and photothermal enhanced CDT. Such a designed FeS_2-PEG can catalyze H_2O_2 disproportionately to efficiently generate •OH, leading to a specific CDT. The Fe^{3+} on the surface layer of the nanocube after self-oxidation can enhance the T_1 and T_2 relaxation and reports the H_2O_2 content in tumor through MR signal enhancement. (Tang et al., 2017). On the basis of this study, Gao and coworkers proposed another approach to further improve the CDT efficacy under the premise of heating. They found that the coordinatively unsaturated complex formed by gallic acid and Fe^{3+} will become less stable in an acidic pH range, and can be readily triggered by a weak acid microenvironment to slowly decompose, thus releasing Fe^{3+}. Based on this approach, they designed coordinatively unsaturated Fe(III) complex-based activatable nanoprobes toward activable tumor MR imaging and therapy (**Figure 2**). Through coating upconversion luminescence (UCL) nanoparticles with the coordinatively unsaturated GA-Fe(III) complex, the release of Fe^{3+} can be triggered by the low pH of

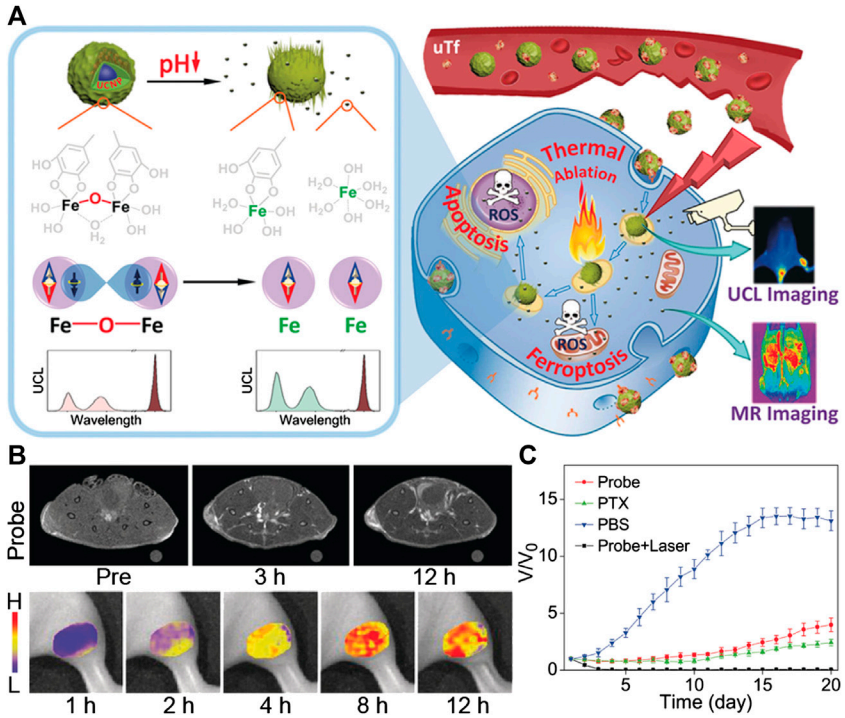

FIGURE 2 | (A) Illustration to demonstrate the activatable function of UCNP@GA-FeIII probe for MRI and its therapeutic function involving multiple pathways. **(B)** T_1-weighted MR images of tumor-bearing mice acquired at different time points pre- and post-injection of UCNP@GA-FeIII probe **(upper)**, and mapping of Fe^{3+} release based on I_{475}/I_{800} ratio of upconversion luminescence **(bottom)**. **(C)** the tumor growth curves in different groups of mice after treatment. Reproduced with permission from Zhang P. et al. (2019a). Copyright 2019 Wiley-VCH Verlag GmbH & Co. KgaA.

the microenvironment and can be monitored by UCL at different wavelengths. Through the comparison of optical and MR imaging of the tumor area, it was confirmed that the release of Fe^{3+} within the tumor area can significantly boost the T_1 contrast of tumors. Apart from this activable MRI capacity, the released Fe^{3+} in tumor can also generate free radicals in tumor cells through catalyzing the Fenton reaction, while the remaining GA-Fe(III) complex on the surface of the nanoprobe can still realize the photothermal conversion for PTT to further enhance the therapeutic effect of the tumor. This work thus provides a novel design integrating the activable MRI ability and tumor treatment with multiple pathways of Fe-based PTT/CDT (Zhang P. et al., 2019a).

Similar to Fe^{3+}, a number of other ions-based nanomaterials have been developed to serve as Fenton reagents and MRI contrast agents, which also exhibited great potential for CDT because of their ROS generation and T_1-weighted MRI signal enhanced abilities in tumor sites because of ion release. For example, Cu (I)-based nanomaterials are more adaptable to the slightly acidic tumor microenvironment with high •OH production. The reaction rate of the Cu-induced Fenton-like reaction is much greater ($1 \times 10^4\ M^{-1}\ s^{-1}$) than that of a Fe-based Fenton reaction in the microenvironment (Cai et al., 2019; Hu R. et al., 2019). Liu and coworkers fabricated a highly efficient Cu-based Fenton-like reagent Cu_3P nanocrystal for tumor theranostics. Such nanocrystals could respond to over-expressed H_2O_2 in tumor sites and generate a large amount of toxic •OH through Fenton-like reaction through Cu (I) catalysis. The Cu_3P nanocrystal also possess considerable photothermal conversion effects in the NIR II region, which can not only serve as a PAI agent to detect the tumor, but also significantly improve the efficiency of Fenton-like reaction, achieving good synergistic therapeutic effects of PTT and CDT. In addition, the product of the Fenton-like reaction, paramagnetic Cu(II), can be employed as a satisfactory T_1 contrast agent for *in situ* self-generation MRI (Liu Y. et al., 2019b).

More recently, Li and coworkers reported a biomimetic CS-GOD@CM nanocatalyst for breast cancer CDT. Such nanomaterials, which contain $Cu_{2-x}Se$ nanoparticles, glucose oxidase, and tumor cell membrane, can effectively improve the Fenton reaction through increasing the H_2O_2 concentration within tumors. With the monitoring of PAI, as the amount of H_2O_2 in the tumor reaches its peak value, the second near-infrared (NIR-II) light irradiation was employed to further boost the efficacy of tumor treatment at the maximum concentration, which is monitored by photoacoustic imaging. The magnified Fenton-like reaction can produce a large amount of radicals and exhibits an excellent therapeutic efficacy of breast cancer (Wang T. et al., 2019).

As mentioned before, although the tumor microenvironment exhibits the characteristics of a low pH and H_2O_2 overproduction, it also has a higher concentration of GSH (up to 10×10^{-3} M) with •OH scavenging ability, which largely limits the CDT effect. To address this problem, Chen and coworkers developed self-reinforcing CDT nano-agents MS@MnO_2 through encapsulating

mesoporous SiO_2 with MnO_2, which possesses both Mn^{2+} release and GSH consumption properties. Such nano-agents can be employed to design a tumor-microenvironment- triggered theranostic platform for MRI-monitored cancer therapy. In the presence of HCO^{3-} in physiological conditions, Mn^{2+} can accelerate Fenton-like reaction to generate •OH from endogenous H_2O_2 in a tumor microenvironment. The GSH depletion properties of MnO_2 renders cancer cells more vulnerable to •OH, which further ensures the effective CDT of MS@MnO_2 NPs. On the other hand, MS@MnO_2 NPs can also be used as activable MRI contrast agents owing to the GSH-triggered generation of paramagnetic Mn^{2+} T_1, which is suitable for monitoring the CDT process of a tumor (Lin et al., 2018).

To further enhance the therapeutic effect on tumors, CDT can be combined with chemotherapy, as discussed in the previous section, to fight against tumors through both reactive oxygen species (ROS) and chemotherapeutic drugs (Liu et al., 2019). Chen and coworkers developed a nanomedicine (LaCIONPs) for cancer chemo/chemodynamic combination therapy, which can realize microenvironment-triggered tumor-specific chemotherapeutic drug release and ROS production. The LaCIONPs are prepared through assembling and encapsulating the iron oxide nanoparticles (IONPs) and lapachone (La) in a nanostructure via H_2O_2-responsive polyprodrug and pH-responsive polymer, which can be further labeled by radionuclide to identify the tumor and trace the biodistribution of nanoagents *in vivo* through PET imaging. Once the LaCIONPs are ingested by tumor cells, their structure will be decomposed in acidic lysosomes, leading to the rapid release of both La and iron ions, in which La can generate H_2O_2 through tumor specific catalysis to react with Fe ions and generate highly toxic •OH for CDT. In addition, H_2O_2 also activates the release of chemotherapeutic drug camptothecin for chemotherapy (Wang S. et al., 2019). In another work, an organic theranostic nanomedicine (PTCG NPs) is constructed through the coordination chemistry between Fe^{3+} ion and epigallocatechin-3-gallate (EGCG), phenolic platinum (IV) prodrug (Pt-OH), and polyphenol modified block copolymer (PEG-b-PPOH). Such PTCG NPs possess high stability in the blood stream due to their stable metal-polyphenol coordination, but can efficiently release cisplatin after ingestion by tumor cells. Meanwhile, the released Fe^{3+} can catalyze H_2O_2 to produce free radicals to kill cancer cells. Interestingly, apart from the chemotherapeutic effect, cisplatin can also serve as an artificial enzyme to generate H_2O_2 as the reactant of CDT through cascade reactions, which remarkably enhances the anticancer effect of nanomedicine. The imaging function of nanomedicine can also be successfully introduced by doping PTCG NPs with Gd to trace the delivery route and drug release behaviors of nanomedicine, achieving precise diagnosis and treatment of cancer (Ren et al., 2020).

CANCER THERANOSTIC PROBES FOR GENE THERAPY

Gene therapy has enormous potential for the treatment of various diseases due to its highly specific and effective regulation of gene and protein expression, which introduce exogenous nucleic acids such as genes, gene segments, oligonucleotides, miRNAs, or siRNAs into targeted tumor cells, correcting the abnormally expressed genes and restoring their normal biological function, so as to achieve the purpose of treating diseases (Shu et al., 2014; Wang et al., 2016; Zhou et al., 2017; Jiang et al., 2019; Boumahdi and De Sauvage, 2020; Wang and Yu, 2020). This treatment approach is apparently more suitable for cancer since the successful transfected cancer cells have a proliferative advantage and can further amplify the gene therapy effect through division process. In the case of systemic and presystemic deliveries, the administration of naked nucleic acids is largely hindered by biological barriers, nuclease decomposition, renal clearance, or immune response (Han et al., 2013; Kim et al., 2016). To overcome these limitations, nano-carriers/vectors that can protect the nucleic acid cargo from damage and ensure the efficient targeting of these therapeutic nucleic acid into the tumor cells to carry out the desired clinical results and decrease side effects are used (Yang et al., 2014). In combination with the imaging ability of the nanoformulations, the theranostic probe can not only accurately detect the tumor, but also reflect the process of *in vivo* behavior of target gene such as pairing, silencing, or transfection in the treatment process, enabling visual assessment of efficacy (Wolfbeis, 2015).

Nanotechnology Improves Viral Mediated Gene Delivery for Tumor Theranostics

Viral systems, the earliest gene carriers, are widely accepted as efficient gene delivery tools and have an excellent transfection efficiency (Kotterman et al., 2015; Ni et al., 2016). Viruses have the innate ability to break through the biological barriers in the body and specifically target the host cells and begin replicating, which enables them to protect their genes from nuclease attack to safely enter the nucleus and effectively integrate into the host genome and realize a high gene expression (Lundstrom, 2003; Liu and Deisseroth, 2006; Waehler et al., 2007; Wu and Zhou, 2011). Using these properties, viruses are utilized to selectively target tumor cells and deliver the gene with higher efficiency (Koppers-Lalic et al., 2013). However, viruses have crucial setbacks that largely limit the *in vivo* applications. The randomness and uncontrollability of viruses to re-combinate the tumor may lead to severe side effects, which has aroused certain solemn concerns (Santiago-Ortiz and Schaffer, 2016; Tian Y. et al., 2018; High and Roncarolo, 2019). Thus, nanotechnology has attempted to address these problems in different ways.

Liu and coworkers developed an oncolytic adenovirus (OA) delivery platform that can be employed for accurate virotherapy of tumors. Such a platform is constructed by coating OA with bioengineered cell membrane nanovesicles (BCMNs), which is useful for the specific targeting of tumor cells and decreases the antiviral immune response of the body. The tumor targeting ligands can be inserted into the BCMNs, which not only endow the nano-platform with the ability of tumor targeting, but also provides a stealth effect under immune surveillance. In addition, this targeted delivery process can be monitored by *in vivo* fluorescence imaging. Through these features, OA can offer

systemic delivery efficiently with immune escape ability and few side effects (Lv et al., 2019). In another study, Xie and coworkers proposed an approach to protect viruses from removal by the host immune system and prolong their *in vivo* retention to enhance the tumor targeting. They developed an engineered OA by enwrapping them with a calcium and manganese carbonates (MnCaCs) biomineral shell. After arriving at the tumor sites, MnCaCs will dissolve under the acidic condition and release Mn^{2+}, which can not only catalyze the endogenous H_2O_2 into O_2 to accelerate the replication of OA, but also enhance the signal of both MRI and PAI, providing real-time monitoring for the therapy. This theranostic approach demonstrated the promise for visualized oncolytic virotherapy with high efficacy by systemic administration (Huang et al., 2019).

Nanotechnology can offer new avenues in virus-based gene therapy; nevertheless, the size limitation of the transgene that can be packaged into a viral vector and the technical problems faced by the large-scale production of viral vectors still make it difficult for viral-mediated gene delivery to achieve clinical translation.

Nano-Based Nonviral Gene Delivery for Tumor Theranostics

Owing to the safety concerns of viral-mediated gene delivery, currently, several other carriers have been implemented as an alternative to viral vectors, especially for engineered nano-vectors that could mimic the features of viral vectors as a type of novel gene carrier (Fenton et al., 2018; Yuan et al., 2019).

Liposome-based materials have been studied extensively for the delivery of nucleic acids, as they can carry various types of nucleic acids, such as mRNA and siRNA, within a hydrophilic cavity (Ozpolat et al., 2014; Mangraviti et al., 2015; Duro-Castano et al., 2017; Kuang et al., 2017). For example, Anderson and coworkers developed a combinatorial library of ionizable lipid-like materials by using a three-dimensional multi-component reaction system to construct mRNA delivery vehicles that carry mRNA to the desired area *in vivo* and trigger an immune reaction. They found that several formulations of this library can successfully induce a strong immune response, and can suppress the tumor growth, thereby prolonging the survival rate of tumor-bearing mice through mRNA delivery (Miao et al., 2019). The liposomes can be modified with targeting molecules to endow them with the ability to recognize the lesions specifically. For example, Zhao and coworkers developed a PEGylated liposome loaded with pcDNA3.1-CSF1-mES for gene therapy of vascular endothelial cell and tumor imaging, which conjugated with anti-CD105 mAb to obtain targeting ability. With this targeting moiety, the liposomes can successfully recognize the tumor-derived endothelial cells *in vivo*, monitored by fluorescence imaging of tumor-bearing mice, which can significantly improve the gene expression and thereby inhibit the tumor growth (Zhuo et al., 2018). Such results demonstrate the advantages of the liposomes to enhance tumor targeting, imaging, and gene transfer applications.

One another advantages of using liposomes to deliver nucleic acid is that they facilitate cellular uptake through interaction with lipids in the cell membrane to induce membrane fusion, which can directly release the nucleic acid in the cytoplasm to avoid trapping in endosomes, or by inserting the targeting molecules that enhance the specific binding ability to cell receptors (Alex and Sharma, 2013). Kim and coworkers employed porous silicon nanoparticles as the siRNA host, which were then encapsulated by the fusogenic lipid with the targeting peptide modified on the surface for selective tissue homing. Importantly, the fusogenic lipid coatings can induce the membrane fusion between the liposomes and the cellular membrane, which efficiently deliver the siRNA into the cytoplasm to avoid endocytosis. In an ovarian-cancer- tumor-bearing mouse, this liposome can successfully target the tumor area shown by *ex vivo* fluorescence imaging, efficiently silence the Rev3l subunit of polymerase Pol ζ to inhibit DNA repair in combination with cisplatin, and reprogram tumor-associated macrophages (TAMs) into a proinflammatory state (Kim et al., 2019).

However, liposome carriers still face some problems. The interactions between lipid and cell membrane help the nucleic acid enter the cells, but also has potential toxicity (Xue et al., 2014), and some liposomes have been found to cause an immune response that leads to immunotoxicity (Vangasseri et al., 2009; Ni et al., 2016). Thus, the biochemical studies of these liposomes should be considered more carefully when they are used as carriers.

In addition to liposomes, other types of nanomaterials have been employed to serve as carriers of nucleic acids, which can realize the theranostic treatment of tumors (Guo and Huang, 2014; Tsouris et al., 2014). For example, Tang and coworkers designed a series of Ag@AIE core@shell nanocarriers with tunable and uniform morphology by employing of aggregation-induced emission luminogen (AIEgen). This nanocarrier successfully facilitated the delivery efficiency of siRNA, which endowed this nanocarrier with excellent capabilities in specific mRNA interference and tumor growth suppression. In addition, the cellular uptake, endosomal escape of siRNA, and tumor area can be visualized real-time by the unique AIE fluorescence signal of nanocarriers *in vivo*. Compared to the commercial transfection reagents, the biocompatibility, delivery efficiency, and reproducibility of such nanocarriers are significantly improved, which represent a promising future in RNAi-related cancer therapy (He et al., 2019). In another study, Nie's group reported a novel peptide-based nanoparticle that can specifically deliver and release the small interfering RNA (siRNA) into the solid tumor to silence the expression of tumor-associated TF, a major initiator of blood coagulation that played a critical role in the hematogenous metastasis of tumors (**Figure 3**). With the ability of tumor targeting and prohibition of tumoral TF expression, such nano-systems can effectively inhibit the interactions of circulating tumor cells with platelets and reverse the tumor coagulant state. Furthermore, the nano-system can also prevent the spreading of tumors, which significantly inhibits metastasis to the lung in a mouse breast cancer model through attenuating TF expression of tumor cells. In addition, after labeling the siRNA of nanosystems with Cy5, the *in vivo* fluorescence imaging indicated that it can efficiently accumulate in the tumor region, which ensures the local

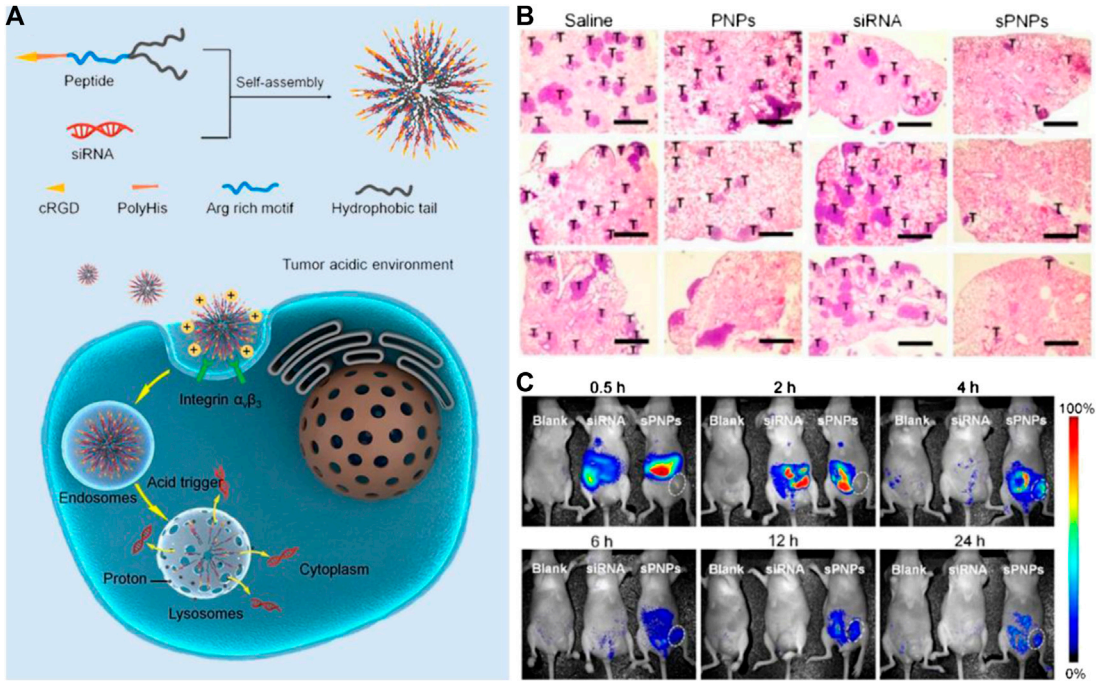

FIGURE 3 | (A) Schematic of the self-assembly of the sPNPs nanoparticles and their antitumor mechanism. **(B)** Effects of PNP, free TF siRNA, and sPNPs on metastasis in 4T1 tumor bearing mice. **(C)** *In vivo* fluorescence imaging of MDA-MB-231 tumors bearing mice after administration of nothing **(left)**, free Cy5-siRNA **(middle)**, or Cy5-sPNPs **(right)**. Reproduced with permission from Liu S. et al. (2019). Copyright 2019 American Chemical Society.

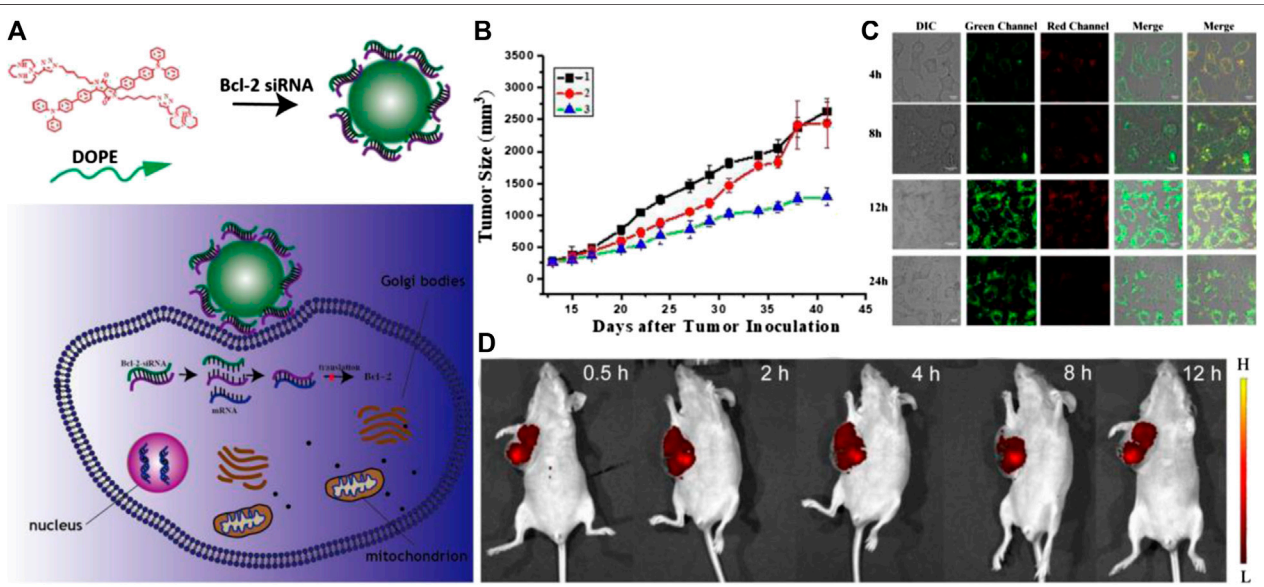

FIGURE 4 | (A) The scheme of tumor targeting gene vectors for visual tracking of Bcl-2 siRNA transfection and anti-tumor therapy. **(B)** Body weight changes of the nude mice of different groups over 41 days; **(C)** Fluorescent confocal laser scanning microscopic images of Hela cells after treatment with DPL/siRNA under different incubation time. The siRNA was labeled with fluorescein amidite (FITC). The embedded scale bars correspond to 10 μm. **(D)** Fluorescence imaging of tumor-bearing mice *in vivo* after DPL/siRNA injection via tail vein. Reproduced with permission from Sun et al. (2020). Copyright 2020 American Chemical Society.

concentration of siRNA to improve the efficacy. This nano-system displays a novel approach to safely and precisely knock down tumor-associated TF for preventing metastasis and may offer a new form of tumor gene therapy (Liu S. et al., 2019). Sun and coworkers designed and synthesized a tumor-targeting fluorescent gene vector (DPL), which was derived from

diketopyrrolopyrrole (DPP) via the modification with aneN_3 and TPA units (**Figure 4**). Owing to the siRNA condensation capabilities, DPL can successfully in real-time display the process of cellular uptake and siRNA release *in vitro* and can kill the cancer cells by carrying a small amount of siRNA. On an animal level, DPL can recognize tumor regions in mice through the EPR effect after intravenous injection and deliver the Bcl-2 siRNA for tumor treatment, which can be monitored by fluorescence imaging *in vivo*. This work provides a new non-viral gene vector for achieving real-time tracking of the therapeutic siRNA delivery process as well as cancer therapy (Sun et al., 2020).

Polymers can also be employed as a class of potential carriers to load nucleic acid. Wang and coworkers designed a multifunctional diblock copolymer and constructed it into heterogenous membrane polymersomes with "boarding" and "debarkation" gates, which can act as gene vectors for encapsulating nucleic acid in an aqueous solution through opening the "boarding" gate, and then releases them by triggering the "debarkation gate" using the proton sponge effect within the target cells. The encapsulated plasmid DNA exhibit better transfection ability than the adsorbed plasmid DNA due to the more excellent protection for plasmid DNA available inside the polymersomes. Through the fluorescent imaging *in vivo*, the signal of GFP-encoding plasmid DNA can be seen 6 days post-injection, confirming that the polymersomes increase the transfection and expression of pDNA in animals (Wang et al., 2018). Lee and coworkers developed a biocompatible poly (D, L-lactide-glycolide) (PLG) nanoparticle with imaging function and therapeutic genes, which was modified with rabies virus glycoprotein (RVG) peptide (RVG-PNPs) to target neuroblastoma. As a result, RVG-PNPs had great potential and can be used as cancer detection tools for molecular imaging in a neuroblastoma-bearing mouse model. Compared with unmodified nanoparticles (PNPs), the RVG-PNPs can significantly enhance cell uptake and gene silencing of N2a cells *in vitro* and can effectively fight against neuroblastomas specifically through a therapeutic gene cocktail (siMyc, siBcl-2, and siVEGF) *in vivo*. With fluorescence imaging, these nanoparticles precisely detect the neuroblastoma of mice (Lee et al., 2016).

These above works show the great potential of a plenty of nano-agents to serve as carriers to deliver nucleic acids, including various DNA, siRNA, or mRNA, with tumor visualization function, which provides a new avenue for tumor diagnosis and treatment.

THERANOSTIC PROBES FOR CANCER IMMUNOTHERAPY

Immunotherapy is a kind of treatment approach based on the natural function of the immune system in protecting the host. Its cardinal features including potency, specificity, and memory. In recent years, cancer immunotherapy has made great success in clinic, with chimeric antigen receptor (CAR) T-cell therapies and checkpoint blockade treatment with immunomodulatory agents that block the inhibitory receptors cytotoxic T lymphocyte antigen-4 (CTLA-4) or programmed death-1 (PD-1) (Fridman et al., 2012; Bakos et al., 2018) the most common options. However, as the immune drugs activate the immune system, they may also lead to severe nonspecific systemic inflammation and autoimmune side effects, resulting in a series of adverse reactions from the body, including significant weight loss, systemic cytokine storms, and even death (Grahnert et al., 2011; Weber et al., 2015).

Currently, several formulations based on nanotechnology are being explored to prepare anti-tumor immune preparation, which possess some degree of intrinsic adjuvant or immunostimulant properties compared with conventional low-molecular-weight immune agents and should also be able to co-encapsulate multiple antigenic epitopes, targeting ligands and external adjuvants into a single carrier. These nano-based anti-tumor immune agents are expected to not only protect the structural integrity of the antigens, effectively deliver them to the desired sites, and make these substances synergistic to induce an immune response, but also reduce the systematic side effects owing to their specific targeting ability (Liu et al., 2014; Song W. et al., 2019).

Based on the different targets of nano-based immune agents and distinct pathways of immune response they induced to kill tumor cells, in this section, two major targeting directions are being explored, in which nanomedicines are designed to directly target the tumor immune microenvironment or to target the peripheral immune system. Meanwhile, the imaging function of nano-agents endows them with the powerful ability to track and monitor the immunotherapy process, which not only ensures the accuracy of treatment, but also provides more guidance information for prognosis evaluation to avoid immune side effects to the greatest extent (Torrente-Rodríguez et al., 2020).

Target Peripheral Immune Cells for Tumor Theranostics

Peripheral immune cells are a class of immune cells including lymphocytes, antigen presenting cells (APCs), mast cells, and other immune cells, which reside in the peripheral immune organs, and are mainly responsible for recognizing antigens and participating in the immune response. Within the peripheral immune organs, the induction of anti-tumor immunity is a multi-step process, which includes the recognition and presentation of tumor antigen by APCs, activation of antigen-specific T cells, and attacking of the tumor cells by effector T cells (Song Q. et al., 2019). However, tumor cells can usually escape immunosurveillance through a number of special mechanisms, which largely reduce the body's immune response and ensures the survival of cancer cells (Mohme et al., 2017). In order to enhance the specific tumor cell immune response, nanoformulations have been designed as regulators to promote the maturation of dendritic cells and the activation of T cells.

Compared with the conventional low-molecular -weight immunoregulators, the well-engineered nanomaterials can not only enhance the power of immune response via intrinsic

immunogenicity, but can also track the migration routes of immune cells after activation. Liu's group loaded ovalbumin (OVA) antigen on the upconversion nanoparticles (UCNPs), which can be efficiently engulfed by dendritic cells (DCs), to label them with upconversion luminescence (UCL) and induce the maturity of DCs *in vitro* as an artificial DCs vaccine. After intradermal administration at the right footpad of such an artificial DCs vaccine, their homing behavior to draining lymph nodes can be monitored *in vivo* through UCL imaging. Importantly, the strong antigen-specific immune responses of such a nanovaccine, including enhanced T cell proliferation, interferon gamma (IFN-γ) production, and cytotoxic T lymphocyte (CTL)-mediated responses, are induced by this nanoparticle-pulsed DCs vaccine, which effectively suppresses the tumor growth (Xiang et al., 2015).

Apart from the artificially modified APCs *ex vivo*, several nano-agents have been designed to directly activate the APCs *in vivo* to reduce production costs, simplify the preparation procedure, and make large-scale production easier. To enhance the activation efficiency of APCs *in vivo*, antigens and adjuvants (mainly a class of receptors agonists) are usually co-delivered by nano-systems. For example, Liu and coworkers reported a kind of cancer nanovaccine synthesized using nanoscale coordination polymer (NCP) composed of Mn^{2+} ions and a nucleotide oligomerization binding domain one agonist, meso-2,6-diaminopimelic acid (DAP), as the organic ligand, to load OVA antigen. The obtained OVA@Mn-DAP nanovaccine could actively migrate into lymph nodes after local administration, as monitored by MR and optical imaging *in vivo*. Therefore, such a nanovaccine can be used as an effective tumor vaccine to accelerate the maturation of dendritic cells (DCs) via stimulating the Nod1 pathway with DAP, thereby promoting the cross-presentation of antigens (Zhao H. et al., 2019).

Due to the strong escape mechanism of cancer cells, the tumor suppressive ability of effector T cells activated by a single antigen is still insufficient. Tumor vaccines are expected to contain a variety of effective tumor antigens to activate multiple antigen-specific T cells through more APCs to achieve better tumor treatment effects (Chang et al., 2020). In this regard, tumor cell membranes, which express multiple tumor-associated antigens, are becoming a potential candidate to construct nanovaccines with multi-antigens. Li and coworkers have developed a novel class of magnetosomes through coating TLR agonist CpG-ODN and Fe_3O_4 nanoparticles with anti-CD205 mAb modified cancer cell membranes. The Fe_3O_4 nanoparticles endow the magnetosomes with magnetic retention ability in the lymph nodes, as revealed by MRI, which prolong the time period for antigen uptake by DCs. Moreover, the cancer cell membrane provides various cancer specific antigens for subsequent multi-antigenic responses. In addition, the anti-CD205 mAb can promote the uptake of $CD8^+$ DCs, thus facilitating MHC I cross-presentation. Through tail base subcutaneously injection of the nanovaccine and attraction of the magnetic field at inguinal lymph nodes, the *in vivo* T cells can be activated with satisfied clonal diversity and superior cytotoxic activity, leading to great prophylactic and therapeutic effects of cancer (Li et al., 2019) (**Figure 5**). Du and Li developed an intelligent clustering nanoparticle delivery system, iCluster, whose size can change from ~100 to ~5 nm in the acidic tumor microenvironment, thereby improving the implantation of particles in the interstitium of the primary tumor. Furthermore, the resultant smaller nanoparticles could drain into lymph nodes through tumor lymphatics, thus inhibiting tumor metastasis (Liu J. et al., 2019). In another work, Grippin designed a kind of multifunctional magnetic liposome loaded with RNA to trigger the antitumor immune response as an early biomarker of cancer treatment. These particles can induce the maturity of DCs more effectively than electroporation, thereby successfully suppressing the tumor growth in mice treatment models. In addition, the iron oxide nanoparticles have been proven to promote the transfection of DCs, and trace the migration path of DCs through MRI (Grippin et al., 2019). Tan's group developed a novel intratumoral nano-agents delivery system for long-term suppression of tumors through apoptotic bodies (AB) of cancer cells as the drug carriers. Specifically, CpG immunoadjuvant-modified gold-silver nanorods (AuNR-CpG) was encapsulated by AB to construct the nanomedicine. After intravenous injection, these nano-agents can be selectively ingested by inflammatory Ly-$6C^+$ monocytes, which then actively penetrate into the deep solid tumor via their natural tumor-homing ability, which can be indicated by the fluorescent imaging. In addition, AuNR-CpG/AB could effectively induce the maturity of DCs *in vivo* under NIR irradiation, thereby promoting the secretion of the proinflammatory cytokine by DCs to activate effector T cells, thus eliciting a potent immune response to fight against the tumors. Such cell-mediated delivery systems can not only successfully inhibit the primary tumors, but also elicit a great immunity to prevent tumor metastasis and recurrence (Zheng et al., 2020).

The above pre-clinical studies demonstrated the great potential of nano-agents in cancer immunotherapy through initiating an effective and durable antitumor response. However, the limitations of antigen identification, APC activation efficiency, and weak immune response still limit the practice of cancer nanovaccines (Bol et al., 2016; Milling et al., 2017; Sprooten et al., 2019). Larger animal models and larger amounts of validation results are required to promote the clinical translation, which will also help to further determine the precise modalities of the application.

Target the Tumor Immune Microenvironment for Tumor Theranostics

The clinical successes in immunotherapy have been astounding, but also unsatisfactory. Immune-checkpoint blockade approaches, such as CTLA-4 and PD-1, which are commonly used in clinical trials, are unfortunately ineffective for a large number of patients, who do not respond to the triggers. Recently, several pieces of research have shown that the tumor microenvironment is one of the major barriers to effective treatment of carcinoma through immunotherapy (Fu et al., 2020). Within the tumor microenvironment, a class of immune or non-immune cells are found, which can secrete

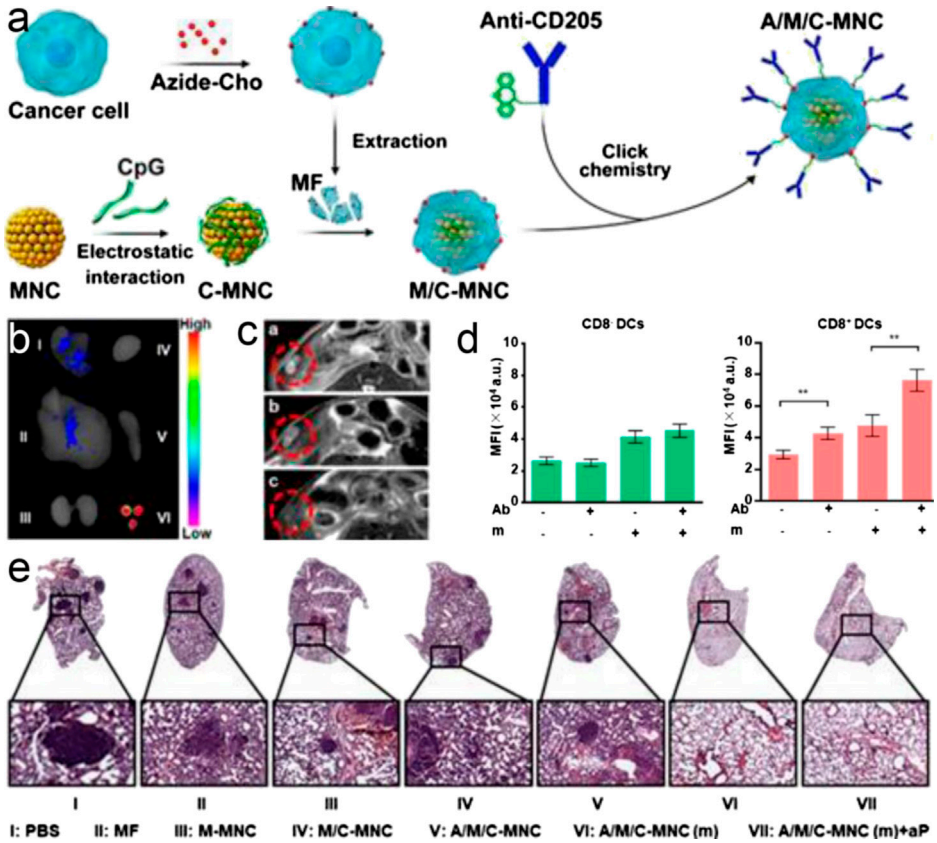

FIGURE 5 | (A) Fabrication process of A/M/C-MNC. **(B)** Fluorescence imaging of excised lymph nodes and visceral organs two days after vaccination with A/M/C-MNC. I-VI were lung, liver, kidneys, heart, spleen, and lymph nodes, respectively. **(C)** *In vivo* T_2-weighted MR imaging of mice vaccinated with different formulations. The red circles outline the lymph nodes. **(D)** MFI of DCs in the lymph nodes after vaccination with different DiD-labeled formulations. Ab, anti-CD205 conjugation; m, magnetic field retention in the lymph nodes. **(F)** H&E-stained lung sections of different groups. All data represent the mean ± SD (n = 6). Reproduced with permission from Liu S. et al. (2019). Copyright 2019 American Chemical Society.

various factors, leading to a chronic inflammatory and immunosuppressive environment, in which cancer cells can adapt and proliferate comfortably without eradication by host immunosurveillance (Gajewski et al., 2006; Binnewies et al., 2018). To overcome this obstacle, a nano-based immunomodulatory agent that can directly target the immune microenvironment in solid tumors has been developed, which can monitor and mediate the immunosupressive state, or even remodel the microenvironment to improve the tumor immunotherapy.

Enhance the Killing Effect of Immune Cells for Tumor Theranostics

NK cells and T lymphocytes have the ability to fight against tumors, however, they are usually suppressed by the tumor immune microenvironment (Whiteside, 2008). Based on this phenomenon, several nano-agents have been designed to help these immune cells break through the barriers and recover the ability to kill tumors.

Chen and coworkers reported an inherently therapeutic fucoidan-dextran-based magnetic Nanomedicine (IO@FuDex3) connected with antibodies, including checkpoint inhibitors (anti-PD-L1) and T-cell activators (anti-CD3 and anti-CD28). Such IO@FuDex3 can remodel the immunosuppressive tumor microenvironment by directly inducing T-cell activation and block the immunosuppressive PD-L1 pathways via intravenous medication. Moreover, the magnetic navigation effectively amplified the accumulation of IO@FuDex3 at the tumor site and minimized the systemic exposure, which can be clearly visualized by single-photon emission computed tomography imaging, minimizing the off-target side effects (Chiang et al., 2018). In another work, Nie prepared magnetic nanoclusters (NCs) modified with responsive PD-1 antibody by using a pH-sensitive benzoic–imine bond and inverse electron-demand Diels-Alder cycloaddition. Owing to the high magnetization and superparamagnetism of NCs, the T cells, together with PD-1 antibody, can be magnetically attracted within the tumor area under the monitoring of MRI. Arriving at the tumor sites with a lower pH, the benzoic–imine can be hydrolyzed, causing the release of PD-1 antibody, which can therefore be coupled with the adoptive T cells to activate their therapeutic effects. This study successfully combined the immune cytotoxicity and checkpoint blockade together in a synergistic manner (Nie et al., 2019).

However, owing to the diversity of immunosuppressive factors in the tumor microenvironment (TME), the immunosuppression of solid tumors is too strong to overcome and the amount of antigen-specific T cells in the microenvironment is not enough. These limitations largely weaken the effect of tumor treatment, and hinder the clinical application of this strategy of immunotherapy (Song C. et al., 2019). It may be possible to consider the possibility of combining this approach with other therapies in the future.

Attenuate the Inhibition of Immune Cells for Tumor Theranostics

Tumor-associated macrophages (TAMs) are a class of major immunosuppressive players in the tumor immune microenvironment, which can mainly be polarized into anti-tumor M1 type and pro-tumor M2 type under the action of different stimulating factors (Ovais et al., 2019). Although M1 phenotypes can inhibit the tumor growth and can be seen as a good hallmark of prognosis, they are usually suppressed in the microenvironment. On the other hand, M2 phenotypes of TAMs support the tumor growth via secreting a variety of cytokines, such as IL-10, and are usually active in the tumor microenvironment due to tumor stimulations (Hattermann et al., 2014). They also promote angiogenesis by secreting corresponding hormones, promote the formation of an immunosuppressive microenvironment, and accelerate the growth of tumors. In established human progressive tumors, TAM usually expresses an M2 phenotype, thereby promoting tumor progression, metastasis, and resistance to chemotherapy (Sousa et al., 2015). For this reason, a nano-based immunomodulator that can inhibit or modify the TAMs has been designed to increase the efficacy of cancer immune therapy. For example, Fan and coworkers developed an elaborate ferrimagnetic vortex-domain iron oxide nanoring and graphene oxide (FVIOs-GO) hybrid nanoparticle, which exhibited high thermal conversion efficiency under alternating magnetic field (AMF) and could generate a large amount of ROS under alternating magnetic field, inducing a potent immune response in a hypoxic tumor microenvironment. In addition, the in-situ heat can be generated at a physiological tolerable temperature through magnetothermodynamic therapy, which can be guided by T_2-weight MR imaging *in vivo*. Importantly, such nanoparticles can promote the macrophages' polarization to pro-inflammatory M1 phenotypes, and further elevate the tumor-infiltrating T lymphocytes to kill tumor cells (Liu X. et al., 2020). In another work, Weissleder and coworkers prepared R848-loaded β-cyclodextrin nanoparticles (CDNP-R848), which can successfully deliver the drug to TAMs effectively. Such nanoparticles can remodel the tumor immunosuppressive microenvironment toward an M1 phenotype, in order to prohibit the tumor growth and prevent the metastasis and recurrence of the tumor. With the *in vivo* imaging of an orthotopic lung adenocarcinoma mice model, R848 and the CDNP carrier can be co-localized *in vivo* at the subcellular level within TAMs, which confirmed that the CDNPs successfully deliver R848 to TAMs. By combining with the immune checkpoint inhibitor anti-PD-1, the strength of the immunotherapy response can be further increased. This study displayed the satisfactory ability and efficacy of nano-agents designed for TAMs remodeling for cancer immunotherapy (Rodell et al., 2018).

In addition to TAM, myeloid-derived suppressor cells (MDSCs) are another kind of immunosuppressive cells involved in the formation of the tumor immune microenvironment, which have also been seen as an available targeting marker for alleviation of the immunosuppression state of a tumor microenvironment. MDSCs often suppress the immune function of T cells and NK cells in a tumor microenvironment, and establish the pre-metastasis microenvironment via promoting angiogenesis and recruiting and interacting with other immunosuppressive cells such as M2 phenotype TAMs and Tregs (Uhel et al., 2017; Han et al., 2018). In order to inhibit the activity of MDSCs, Yu and coworkers developed a BSA-based nano-regulator incorporating MnO_2 and PI3K γ inhibitor IPI549 to reshape the tumor immune microenvironment to unleash the immune system. The intravenously injected nano-regulators effectively accumulated within the tumor tissue to relieve hypoxia via oxygen generated by MnO_2, and down-regulated the expression of immunosuppressive PD-L1. The binding of released IPI549 to PI3K γ on MDSCs can successfully cause the M1-polarization of TAMs and re-activate the tumor-suppressive T-lymphocytes to kill tumor cells. This process can be visualized by the tumor-specific MRI induced by local generation of Mn^{2+} in the tumor microenvironment (Yu et al., 2019).

Directly Target Cancer Cells for Tumor Theranostics

As the tumor cells are suffering from apoptosis, they will over-express several membrane proteins, which can change their state from non-immunogenic to immunogenic, and consequently stimulate the anti-tumor immune effect in the body, known as the immunogenic death (ICD) of tumors (Yatim et al., 2017; Irvine and Dane, 2020). Interestingly, this strategy of tumor treatment leads to a "chain reaction" of tumor death, that is, the first apoptotic tumor cell initiates the chain initiation step of cell death, which can provide the antigens to APCs, and then these antigens will be presented to the cytotoxic T lymphocytes to further induce more tumor cells apoptosis, as in the propagation step. Nano-agents can be designed to be the initiator of this chain reaction and/or the promotor to magnify the immune response. For example, Na developed the biocompatibility controllable immuno-sensitizer (BCI) based on polyethylene imine with optical imaging function and pH response ability, which was successfully used in tumor theranostics. After arriving at tumor sites, BCI can induce the necrosis of tumor cells, which subsequently leads to the release of a variety of tumor antigens. Such antigens will then be recognized by antigen presenting cells such as DCs in tumor draining lymph nodes and be presented to recruite cytotoxic T cells to attack the tumors (Shin and Na, 2019). Similarly, Xie and coworkers constructed magnetosomes by coating both Fe_3O_4 nanoclusters (NCs) and TGF-β inhibitors with artificially engineered leukocyte

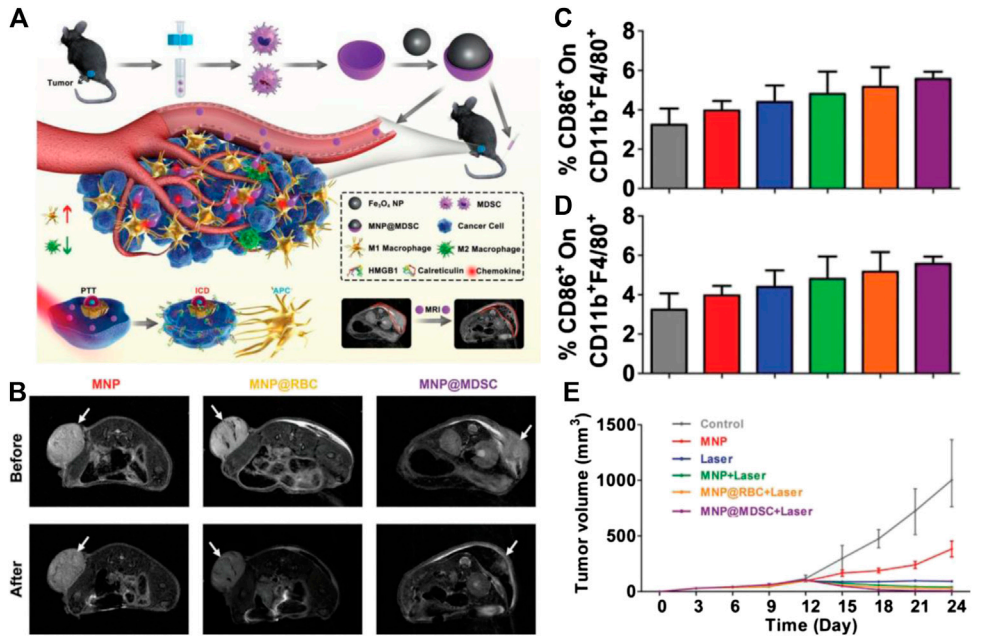

FIGURE 6 | (A) Schematic illustration of the synthesis of MNP@MDSC and its application in cancer theranostics **(B)** T_2-weighted MR images of B16/F10-tumor-bearing mice taken before and after injection of the nanoparticles. **(C)** Percentage of CD86 $^+$ cells within the CD11 b + F4/80 + population of suspension cells from the mouse spleen after different treatments. **(D)** Percentage of CD206 + cells within the CD11b + F4/80 + population of suspension cells from the mouse spleen after different treatments. **(E)** Growth (in volume) curves of mouse tumors in different treatment groups. Reproduced with permission from Zhang F. et al. (2019). Copyright 2018 Wiley-VCH Verlag GmbH & Co. KgaA.

membranes, in which PD-1 antibodies are employed to anchor on the surface of leukocyte membranes. Through intravenous medication, the camouflage of the leukocyte membrane can prolong the blood half-live of this nanostructure, and the NCs core within the membrane endow the magnetosomes with enhanced MRI ability. Upon arriving at the tumor sites, PD-1 antibodies and TGF-β inhibitors synergistically create an immunogenic microenvironment, thereby increasing the percentage of M1 macrophages to produce H_2O_2 and simultaneously initiate the Fenton reaction through the catalysis of Fe^{3+} released from NCs. The accumulated ROS will subsequently activate the ferroptosis process of cancer cells, which can then produce a large amount of tumor antigens and increase the immunogenicity of the tumor microenvironment to amplify the immune response. As a result, such synergistic immunomodulation and ferroptosis leads to more satisfactory tumor therapeutic effects (Zhang F. et al., 2019). In addition, Yu and coworkers extracted the cell membrane of MDSCs to coat the iron oxide nanoparticles, which displayed a superior ability to escape immune surveillance, precisely detect the tumor through MRI, and treat the tumor by PTT. In comparison with the red blood cell membrane-coated nanoparticles (MNPs@RBC) or naked MNPs, MNP@MDSCs possess high selectivity in tumor targeting. Upon arriving at the tumor regions, MNP@MDSC can first act as a PTT agent to initiate the antitumor immune response through inducing ICD of the tumor, then they reprogram the TAM to reduce the tumor metabolic activity, further promoting the immunotherapy of the tumor (Yu et al., 2018) (**Figure 6**).

In addition to inducing tumor cell death to express immunogenic protein molecules, theranostic nanoprobes are also enabled to directly enhance the expression of the immunogenic protein of tumor cells. Dravid and coworkers reported a high-density lipoprotein (HDL) mimicking magnetic nanostructures (HDL-MNSs), which can selectively bind with the HDL receptor, scavenger receptor type B1 (SR-B1), thereby causing cellular cholesterol depletion via hindering the cholesterol secretion in SR-B1 receptor positive lymphoma cells. In addition, the thermal activation of MNS core under an external radio frequency field can lead to antitumor immune responses by increasing the heat shock proteins' expression to promote the maturity of APCs and realize lymphocyte trafficking. Besides, HDL-MNS with T_2 enhanced ability and specificity toward the SRB1 receptor cause a distinguishable contrast between SR-B1 positive and negative cells, which highlight its capability in molecular imaging (Singh et al., 2019).

Although the above studies show the promising effect on tumor theranostics, the immunosuppressive microenvironment of solid tumors is still a big obstacle limiting tumor immunotherapy. Considering that tumors can assimilate the surrounding immune cells, which subsequently facilitates the proliferation and invasion of cancer cells, more strategies should be proposed to suppress and even reverse these behaviors.

THERANOSTIC PROBES FOR PHYSICAL THERAPY OF TUMORS

In addition to chemotherapy, immunotherapy, and gene therapy, physical therapy is another class of treatment method to deal with cancer in clinical application. Compared with other treatment approaches, physical therapy that treats the disease through physical means such as thermotherapy, photodynamic therapy, or radionuclide therapy, can not only kill the tumor cell with high efficiency, but also minimize the side effects through reducing systematic exposure, thereby improving the quality of life of patients (Dougherty et al., 1998; Agostinis et al., 2011). The rich intrinsic physical and chemical properties of nanomaterials have made them potential candidates for the tumor theranostic probes involved in physical therapy. Compared with traditional physical therapy, nano-based physical therapy can not only significantly improve the efficiency of tumor therapy via passive targeting ability through EPR effect, but can also provide highly specific, robust detection of tumors in high contrast images to guide the physical stimuli.

Photothermal Nanoprobes for Tumor Theranostics

Photothermal therapy (PTT) is a kind of non-invasive treatment which relies on an external laser source to make the photothermal agents absorb photon energy and convert it into heat energy, and thereby cause thermal ablation of tumor cells (Pan et al., 2019). This technique of thermotherapy of tumors has been widely adopted in clinical treatments (Liu Y. et al., 2019a). But the efficiency is not so ideal in treating the tumor tissues growing deep in the body due to the limitation of light penetration depth. In comparison with conventional clinical photothermal agents, the wavelength of the excitation source of nanomaterials with NIR absorption can be adjusted in the NIR region, which largely increases tissue penetration. At the same time, through combining with imaging functions such as fluorescence/photoacoustic/MR imaging, highly specific, robust detection of tumors can be realized for precise treatment. Owing to these excellent properties of nano-agents, they are worthy candidates for constructing tumor specific theranostic probes.

Through EPR effect, the nano-agents are able to passively target the tumor cells, thus showing a higher concentration at the tumor site (Fang et al., 2011; Lammers et al., 2012). Under irradiation, the temperature in the tumor site increases much more significantly in comparison with normal tissues, which realize the selective treatment of the tumor. For example, Li and coworkers prepared subminiature magnetic $CuFeSe_2$ ternary nanocrystals, which have a wide near infrared absorption and high photothermal conversion efficiency of 500–1,100 nm (82%). These characteristics make them ideal nanotherapeutics for tumor photothermal therapy guided by multimodal imaging (such as PAI, MRI, and CT). Animal experiments show that the invasive metastasis of tumor cells can be significantly inhibited after 30 days of treatment, which proves that the imaging guided PTT of tumors assisted by $CuFeSe_2$ nanocrystals has good efficacy (Jiang et al., 2017). Similarly, Zeng and coworkers prepared a kind of mixed gold nanostructure for optical/PA imaging, drug-controlled release, and PTT of tumors. The epidermal growth factor receptor (EGFR) inhibitor EB was loaded with this gold nanostructure to obtain the nano-drug EA-AB. Upon entering the cell, EB can be released via lysosomal protease and partial acid pH, meanwhile restoring the fluorescence imaging performance of AuCluster. The irradiation of NIR light will further promote the release of drugs and produce PTT effect, achieving significant inhibition of tumor growth. In addition, the biodistribution and metabolic process of nanostructures can be successfully screened by the whole-body and 3D MSOT imaging (Zhan et al., 2019). These above studies display the high efficiency of theranostic probes with NIR absorption to fight against tumors. To further improve the specificity of treatment for tumors, Shi and his coworkers developed a hydrogen sulfide (H_2S) responsive nanoplatinum probe (Nano-PT) for NIR-II fluorescence-guided PTT of colorectal cancer (CRC). The over-expressed H_2S in colon cancer can activate the Nano-PT to serve as a photothermal agent with high photothermal conversion efficiency, which largely improves the specificity of theranostics (Shi et al., 2018).

Photodynamic Nanoprobes for Tumor Theranostics

Similar to photothermal therapy, photodynamic therapy (PDT), as another non-invasive and selective physical therapy, has been widely used for tumor treatment in clinic. Based on the employment of photosensitizers (PSs), which can be activated by light to generate ROS such as singlet-oxygen, PDT can destroy the tumor cells, especially mitochondria and nucleic acid (Chan et al., 2018). However, tumor cells can adapt to ROS attack by launching DNA damage repair to mitigate the damages, which could greatly decrease the therapeutic efficiency of current oxidation therapy (Juarranz et al., 2008). To amplify the tumor killing ability of PDT, Zhang's group proposed an enhanced oxidative damage strategy for PDT, which was focused not only on the increase of ROS production but also on the simultaneous inhibition of the activity of MTH1 enzyme with DNA protection ability. Specifically, the actionable nano-system, which is a stimuli-responsive nano-system based on mesoporous silica-coated Prussian blue (PMPT) for enhanced oxidative stress of the tumor, was constructed by relieving the hypoxia-resistant situation, elevating ROS generation of PDT, and inhibiting the MTH1-regulated DNA damage repair pathway. Such PMPT could decompose the H_2O_2 in the tumor area to provide sufficient oxygen as the reactant of PDT. Under light irradiation, photodynamic reaction produced sufficient ROS, while the DNA repairing process can be inhibited by acid-responsive released TH287, magnifying the oxidative damage of tumor cells. In addition, the accumulation process of PMPT can be visualized by fluorescence and PA imaging, which guided the orientation of light and ensured the PDT efficiency (Hu J.-J. et al., 2019). In another work, Liu's group prepared a kind of hollow $CaCO_3$-PDA composite nanoparticle as a multi-functional treatment and diagnosis nanoplatform. The

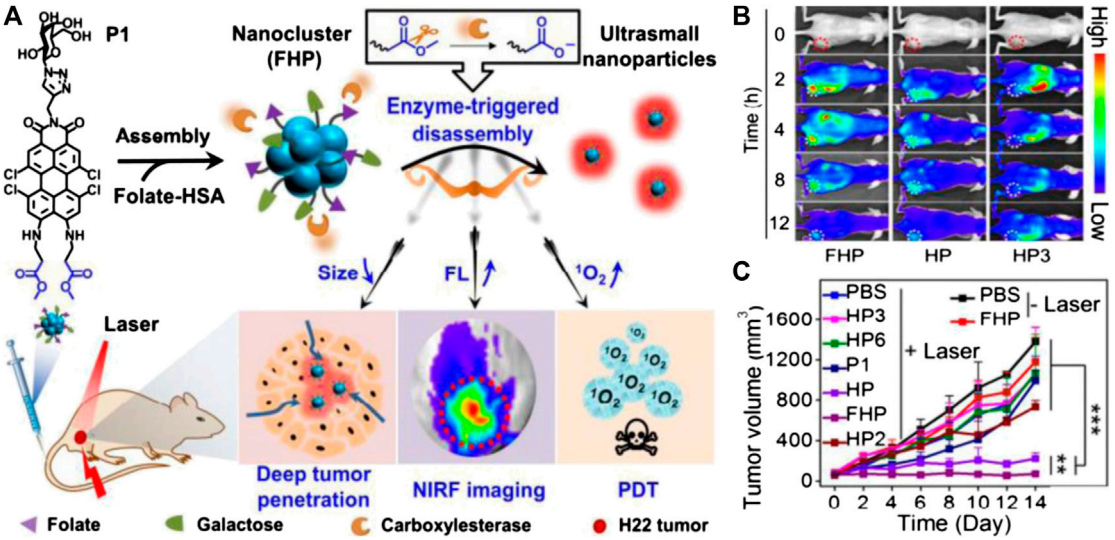

FIGURE 7 | (A) Schematic illustrations of FHP nanocluster fabrication (assembly of P1 and folate-modified human serum albumin (HSA)), enzyme-triggered disassembly of FHP with size shrinkage for deep tumor penetration, and activatable photoactivity for near-infrared fluorescence (NIRF) imaging-guided deep PDT. **(B)** Real-time monitoring of fluorescence images *in vivo* of tumor-bearing mice after intravenous injection of FHP, HP, and HP3 (3.75 mg kg^{-1} per injection). **(C)** Tumor growth curves of H22 tumor-bearing mice treated with various agents. Reproduced with permission from Tang et al. (2019). Copyright 2020 Wiley-VCH Verlag GmbH & Co. KgaA.

nanoparticles have high sensitivity to pH and can be rapidly degraded in the acidic microenvironment of the tumor. Therefore, the photoactivity of the loaded dihydroporphyrin E6 (CE6) photosensitizer, which was quenched by PDA in its original state, can be activated in tumor, showing recoverable fluorescence and more ROS production. In addition, due to the stable coordination between metal ions and PDA, nanoparticles can be combined with various types of metal ions, which endow them with multimodal imaging ability to guide the PDT therapy (Dong et al., 2018).

At present, the most commonly used PSs in clinic are porphyrin and its derivatives, of which the excitation bands usually range from UV to visible wavelength. However, the light in such a band can be largely absorbed by tissues and scatter to lose accuracy, thereby reducing the PDT therapeutic effects in deep tumors (Rajora et al., 2017). Nano-based photosensitizers can overcome this limitation through sophisticated design. Gao's group chemically conjugated the protoporphyrin IX molecules with jeffamines molecules to improve the hydrophilicity and biocompatibility of porphyrin, and the obtained water-soluble porphyrin-jeffamine (PJ) was further modified on the surface of PEGylated upconversion nanoparticles (UCNPs) via "click" reaction, which can construct the FRET couple between UCNP and PJs. As a result, the probes can be successfully photosensitized to generate ROS under the irradiation of 980 nm NIR light, which paves a new way to enhance the photoactivation efficiency of tumors located in deep tissues (Sun et al., 2019). Zhang and coworkers prepared an UCNP with the core-shell structure of $NaErF_4$:Yb/Tm@$NaYF_4$:Yb@$NaNdF_4$:Yb that can be excited by two different near infrared light (NIR) at 808 and 980 nm. Through precise control of the energy transfer process, the red emission light under 980 nm excitation can trigger PDT, while the green emission under 808 nm light excitation can used for diagnosis to monitor the treatment. Using these nanoparticles as PTT agents, the tissue penetration depth has been significantly improved (Tang et al., 2019). In addition to adjusting the excitation band, the poor active penetration of the photosensitizer can be further enhanced by a well-designed responsive strategy of nanoprobes. Yi and coworkers reported a smart perylene monoimide-based nanocluster, which can be triggered by enzymes in the microenvironment to disassemble and penetrate in the deeper area of the tumor, realizing deep PDT (**Figure 7**). Specifically, tetrachloroperylene monoimide (P1) with the carboxylesterase (CE)-responsive ability can be further fabricated with folate-decorated albumins to construct nanostructure (FHP) with an approximate size of 100 nm. After arriving at the tumor area, P1 will be hydrolyzed by the overexpressed CE, leading to the disassembly of FHP to form ultrasmall nanoparticles of only ~10 nm, which significantly increased their penetration depth in tumor tissue. Furthermore, during enzyme-triggered disassembly of FHP, the fluorescence intensity of this nanostructure can be largely enhanced with the elevation of ROS production, enabling the self-enhanced *in situ* NIR optical imaging as well as enhanced PDT. As a result, FHP exhibit remarkable tumor suppression ability *in vivo* with satisfied biosafety through precise imaging-guided, enzyme-triggered PDT with deep penetration (Cai Y. et al., 2020).

Although PDT is a promising strategy against tumors, the PSs will be inevitably distributed in normal tissues, especially in the skin, which may induce phototoxicity when the body is exposed to light. To address this problem, Li and Wang jointly developed an AIE type of PSs, which were loaded into liposomes to improve the stability to construct AIE-PS@liposomes. The AIE-PSs did

not exhibit photosensitivity when entrapped in liposomes. After entering tumor regions, the AIE-PSs will be released from liposomes and immediately aggregate in a targeted area, which can trigger the photosensitivity of AIE-PSs at a turn-on state and induce cytotoxicity. Therefore, the AIE-PS@liposomes can significantly minimize the phototoxicity of PSs to normal tissues and organs, thereby avoiding the side effects (Yang et al., 2019).

Magnetic Hyperthermia Nanoprobes for Tumor Theranostics

Magnetic hyperthermia (MHT) has been proposed as an alternative therapy for cancer treatment, as it can kill tumor cells with heat produced by magnetothermal agents under a strong alternating magnetic field (AMF). Unlike the aforementioned commonly developed PTT, which heats up tumors through light irradiation, MHT is able to treat deeper tumors in bodies owing to the excellent tissue penetration ability of AMF. It may also stimulate the immune function of the body itself (Mai et al., 2019), which significantly improves the therapeutic effect of tumors.

Although MHT has been shown to be an extremely powerful anti-cancer approach, the potential of this therapy is still hindered by a number of limitations, such as the non-homogeneous distribution of temperature over the tumor tissue, insufficient selectivity, and unsatisfactory patient compliance. Currently, new and high-efficiency magnetic nanomaterials, which possess not only excellent tumor targeting and penetration ability to identify the tumor tissues, realizing the selectively heated of the tumor area only under the AMF, but also possess high saturation magnetization to boost magnetothermal conversion efficiency, are being developed, promoting the application of this therapy in tumor treatment (Yavuz et al., 2006; Lacroix et al., 2010; Yoo et al., 2011; Cheng et al., 2019).

Superparamagnetic iron oxide nanoparticles, with satisfied saturation magnetization and biocompatibility, are widely employed as materials in MHT agents. Usually, these agents can also be employed as MRI or magnetic particle imaging (MPI) contrast agents to provide high resolution tumor images to monitor the process of the treatment. For example, Tian and Liang jointly developed a nano-system for active targeting tumor MHT with dual-modalities MRI/MPI capabilities. In order to improve the uniformity of its delivery, 18 nm iron oxide nanoparticles were modified by tumor targeting peptide CREKA to target tumors. With the improvement of MRI/MPI imaging, the targeting agent could significantly improve the uniformity of nanomaterials' distribution within the tumor tissues. Through this property, MHT efficiency of tumor can be significantly improved (Du et al., 2019). Similarly, Wang and coworkers prepared ultrasmall superparamagnetic Fe_3O_4 nanoparticles (ES-MIONs) with a size of 3.5 nm, which can serve as a T_1 contrast agent of MRI. After entering into the tumor tissue, these nanoparticles can be triggered to assemble into large-scale nanoclusters, which will largely enhance the T_2 signal in MRI and simultaneously realize the MHT (Wang et al., 2017).

In another work, Fan's group successfully prepared Uniform wüstite $Fe_{0.6}Mn_{0.4}O$ nanoflowers as an innovative theranostic agent for dual-modal MRI sensitivity. After the medication of the $Fe_{0.6}Mn_{0.4}O$ nanoflowers, the orthotopic glioma in a mouse model can be clearly delineated in both T_1-and T_2-weighted MRI. In addition, the $Fe_{0.6}Mn_{0.4}O$ nanoflowers can also be employed as HMT agents, which can successfully cause the apoptosis of MCF-7 breast cancer cells and remarkably shrink the tumor with negligible side effects (Liu et al., 2016). These results have confirmed that this nano-agent could be a satisfactory magnetic theranostic platform with the capabilities of T_1-T_2 dual-modalities MRI for tumor imaging and MHT for tumor treatment.

However, the magnetothermal conversion efficiency determined by the specific absorption rate (SAR) of iron oxide nanoparticles is still not very high, owing to the inadequate inherent saturation magnetization (Ms) of approximately 60 emu/g. Therefore, the high local concentrations, together with high-power AMF, is required for effective MHT ablation of tumors, which is usually difficult to achieve. To address this problem, nanoparticles using pure iron or its alloys have been employed as MHT agents, as the Ms of these particles are much higher than that of iron oxide (Chao et al., 2019). For instance, very recently, Rao and Dai developed graphitic carbon-coated FeCo nanoparticles (FeCo@C), which exhibited high saturation magnetization of the FeCo core as well as strong NIR absorbance of the carbon shell, and showed a strong enhancement of MPI, high r_2 MRI relaxivity, together with NIR-I and NIR-II PA imaging capability (Song et al., 2020). Such probes with magnetothermal and photothermal properties can therefore be used for tumor ablation in mice, and their high optical absorbance in a band NIR region spectral range makes them suitable as tracers for PAI.

Nanoparticle-Enhanced Radiotherapy for Tumor Theranostics

External beam-based cancer radiotherapy is a commonly used cancer treatment strategy that has been extensively used in clinic to treat 65–75% of primary solid tumors at different stages, and employs local ionizing radiation beams, such as high-energy X-ray, γ-ray, or electron beams, to kill cancer cells (Barnett et al., 2009; Hainfeld et al., 2013; Robert et al., 2011). However, as a type of local treatment, conventional radiotherapy is not able to kill distantly spreading tumors and thus is ineffective to control tumor metastases. Unlike external beam radiotherapy, another kind of radiotherapy, which relies on the tumor-targeted systematic delivery of radioactive substances, known as radionuclide therapy, and has displayed excellent capability for the treatment of spreading tumors and lymphomas (Eroglu and Ribas, 2016). In recent years, nano-agents have been widely studied as tumor-targeting carriers of radionuclide owing to their plentitude of labeling sites.

For example, Herth and coworkers exploited a targeting agent based on polymers that can be used for pre-targeted imaging and can divide the tumor from the imaging step timely to minimize

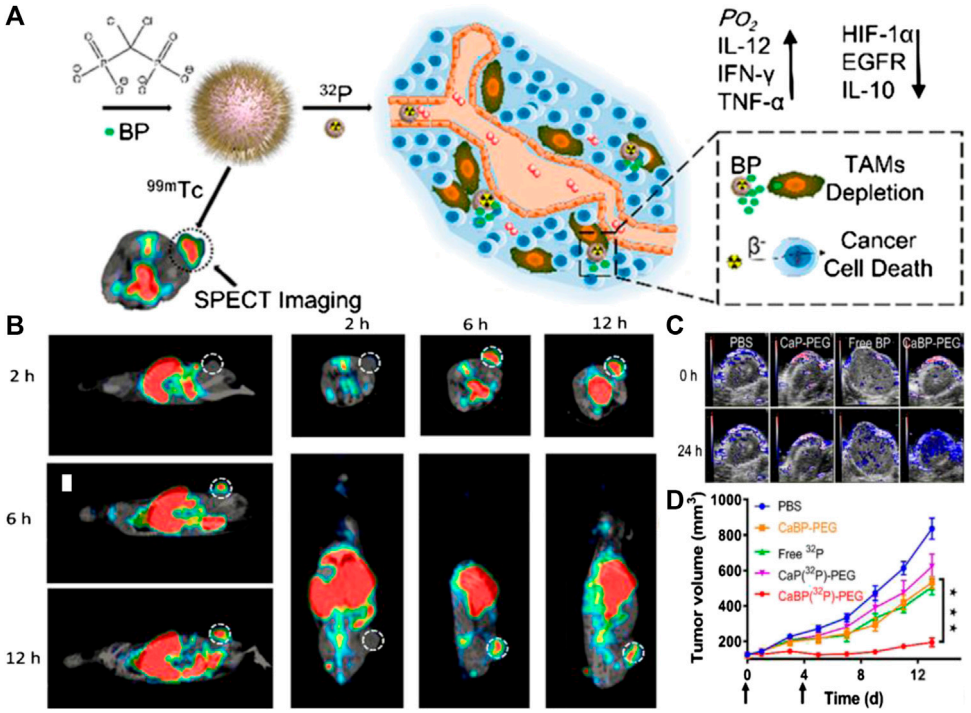

FIGURE 8 | (A) Calcium bisphosphonate (CaBP-PEG) nanoparticles for chelator-free radiolabeling chemistry, effective *in vivo* depletion of TAMs, and imaging-guided enhanced cancerradioisotope therapy (RIT). **(B)** SPECT images of mice at 2, 6, and 12 h after intravenous injection of CaBP(^{99m}Tc)-PEG nanoparticles. Tumors of mice are highlighted by the dotted circles. **(C)** Photoacoustic imaging showing tumor saturated O_2 levels of mice after i.v. injection of PBS, CaP-PEG, free BP, or CaBP-PEG nanoparticles. **(D)** Tumor volume curves of mice with various treatments. Doses for each injection: 100 μCi of 32P, 200 μg of BP. The mice were treated twice at day 0 and 4 (black arrows). Reproduced with permission from Chen J. et al. (2019). Copyright 2018 American Chemical Society.

side effects during nuclear imaging and targeted radionuclide therapy. Specifically, *trans*-cyclooctene (TCO) is employed to modify the polypeptide-graftpolypeptoid polymers (PeptoBrushes) to form the targeting moiety, while the ^{111}In-labeled 1,2,4,5-tetrazine derivative serves as an imaging agent to connect with TCO-modified PeptoBrushes. The sufficient contrast of the tumor can be observed 2 h post-injection of the tetrazine imaging agent, which further increases to 22 h to clearly depict the morphology of CT-26 tumors in mouse models (Steen et al., 2020). Such results demonstrate that PeptoBrushes have great potential to serve as a pre-targeting agent. In another work, Quinn and coworkers developed Lutetium-177 (^{177}Lu) radiolabeled ultrasmall fluorescent silica nanoparticles (C′ dots) for effective tumor radiotherapy. Such PEGylated C′ dots with alpha melanocyte stimulating hormone (αMSH) cyclic peptide analogs on their surface can successfully recognize the melanoma tumor cells which over-expressed melanocortin-1 receptor (MC1-R). With the radiochemical stability, biological activity, and high affinity cellular binding properties of ^{177}Lu-DOTA-αMSH-PEG-C′ dots, efficient tumor uptake and safe metabolic behavior were revealed through SPECT imaging in mice melanoma models. Such C′ dots successfully prolonged the survival period of mice with satisfactory biosafety, paving a new road for nuclear imaging and targeted radionuclide therapy (Zhang et al., 2020).

Radiotherapy efficacy is also severely impaired by the hypoxia of the tumor microenvironment. Recently, a variety of approaches employing nano-agents with unique physiochemical properties have been demonstrated to efficiently alleviate the hypoxic state of tumors and thus significantly promote radiotherapy. Chen and coworkers developed a biocompatible hybrid protein nanoreactor (HSA-CAT NRs) based on human serum albumin (HSA) and catalase (CAT) molecules through glutaraldehyde-mediated crosslinking, which can be further labeled with therapeutic ^{131}I. Such HSA-CAT NRs can well protect the stability of enzymes, and thus can efficiently catalyze the decomposition of H_2O_2. HSA-CAT NRs can also accumulate with the tumor area successfully, which can be visualized under the fluorescence imaging system and gamma camera after being intravenously injected into tumor-bearing mice. More importantly, HSA-CAT NRs can significantly attenuate tumor hypoxia by decomposing endogenous H_2O_2 in a tumor microenvironment to produce oxygen, and thereby largely increase the therapeutic efficacy of radionuclide ^{131}I (Chen J. et al., 2019). In another work, Tian and coworkers reported a biocompatible and biodegradable nanoplatform based on calcium bisphosphonate (CaBP-PEG) nanoparticles for chelator-free radiolabeling chemistry, effective *in vivo* depletion of TAMs,

and imaging-guided enhanced cancer radioisotope therapy (**Figure 8**). After administration, CaBP(^{99m}Tc)-PEG nanoparticles can actively find the tumor through the tumor homing effect, as was clearly confirmed by SPECT imaging. Due to the inhibition effect of clinical drugs to TAMs, the immunosuppression of the tumor microenvironment will be relieved. This remodeling of the microenvironment creates a favorable condition for cancer radioisotope therapy through using CaBP(^{32}P)-PEG as the radio-therapeutic agent, which displayed an appropriate synergistic therapeutic effect in suppression of the tumor growth (Tian L. et al., 2018).

SUMMARY AND OUTLOOK

In this review, recently developed target-triggered tumor theranostic nanoprobes were summarized, which were successfully associated with various imaging modalities with distinct treatment approaches including improved chemotherapy, chemodynamic therapy, gene therapy, immunotherapy, and physical therapy. Owing to the integration of both diagnosis and treatment of cancer, these nanoprobes are obviously superior to the conventional probes with only one property, and possess powerful abilities to not only monitor and trace *in vivo* behavior themselves, but also give immediate feedback on the treatment outcome without time consumption, thereby evaluating the prognosis in real-time. This approach is helpful to customize specific treatment strategies for different patients as early as possible through a deeper understanding of the interaction between nanomedicine and tumors, and enables the establishment of patient-specific "personalized medicine" under the precision medicine plan in the near future.

Although the clinical translation of these promising multi-functional nanomaterials is highly expected, it remains challenging. The major challenges in the road map of translation include large-scale production and modification of a given nanoparticle with high reproducibility, and evaluation of safe pharmacology. As regards the production of nanoprobes on an industrial scale, the performance and pharmacokinetic behaviors of nanoprobes from different research labs, or even from different batches prepared by the same research lab, might be highly different due to the tiny variations in multiple properties. Therefore, the large-scale production of high-quality nanoprobes is the primary factor for the clinical translation of nanoprobes. Apart from that, the practical biomedical application of a newly designed theranostic nanoprobe not only depends on the imaging effect and therapeutic efficacy, but is also largely determined by its biosafety profile. In this regard, the absorption, distribution, metabolism, and excretion of nanoprobes must be studied carefully, especially for the intravenous administrated nano-formulations, which can be easily captured by the reticuloendothelial system and be retained long-term in the body. However, on the other hand, owing to the myriad variations of these sophisticated nanoprobes, the biosafety assessment becomes much more difficult compared with conventional anti-cancer drugs (Fadeel et al., 2018). Therefore, it is also very urgent to establish a decent evaluation system for these nanomedicines.

Despite the biosafety concerns and difficulties in toxicity assessment, target-triggered tumor theranostic nanoprobes, with excellent tumor diagnosis and treatment properties, will offer more viable treatment options for cancer patients in the foreseeable future.

AUTHOR CONTRIBUTIONS

All authors listed have made a substantial, direct, and intellectual contribution to the work and approved it for publication.

FUNDING

The authors acknowledge the support from Fundamental Research Funds for the Central Universities of China (12060094038), NSFC (81671754, 81771902, 81801766).

ACKNOWLEDGMENTS

The authors are grateful to Man Xu from Beijing Institute of Fashion Technology (BIFT) for graphic design.

REFERENCES

Agostinis, P., Berg, K., Cengel, K. A., Foster, T. H., Girotti, A. W., Gollnick, S. O., et al. (2011). Photodynamic therapy of cancer: an update. *CA Cancer J. Clin.* 61, 250–281. doi:10.3322/caac.20114

Alex, S. M., and Sharma, C. P. (2013). Nanomedicine for gene therapy. *Drug Deliv. Transl. Res.* 3, 437–445. doi:10.1007/s13346-012-0120-0

Anh-Nguyen, T., Tiberius, B., Pliquett, U., and Urban, G. A. (2016). An impedance biosensor for monitoring cancer cell attachment, spreading and drug-induced apoptosis. *Sensors Actuators A: Phys.* 241, 231–237. doi:10.1016/j.sna.2016.02.035

Bakos, O., Lawson, C., Rouleau, S., and Tai, L.-H. (2018). Combining surgery and immunotherapy: turning an immunosuppressive effect into a therapeutic opportunity. *J. Immunotherapy Cancer* 6, 86. doi:10.1186/s40425-018-0398-7

Barenholz, Y. (2012). Doxil - the first FDA-approved nano-drug: lessons learned. *J. Controlled Release* 160, 117–134. doi:10.1016/j.jconrel.2012.03.020

Barnett, G. C., West, C. M. L., Dunning, A. M., Elliott, R. M., Coles, C. E., Pharoah, P. D. P., et al. (2009). Normal tissue reactions to radiotherapy: towards tailoring treatment dose by genotype. *Nat. Rev. Cancer* 9, 134–142. doi:10.1038/nrc2587

Binnewies, M., Roberts, E. W., Kersten, K., Chan, V., Fearon, D. F., Merad, M., et al. (2018). Understanding the tumor immune microenvironment (TIME) for effective therapy. *Nat. Med.* 24, 541–550. doi:10.1038/s41591-018-0014-x

Bobo, D., Robinson, K. J., Islam, J., Thurecht, K. J., and Corrie, S. R. (2016). Nanoparticle-based medicines: a review of FDA-approved materials and clinical trials to date. *Pharm. Res.* 33, 2373–2387. doi:10.1007/s11095-016-1958-5

Bol, K. F., Schreibelt, G., Gerritsen, W. R., De Vries, I. J. M., and Figdor, C. G. (2016). Dendritic cell-based immunotherapy: state of the art and beyond. *Clin. Cancer Res.* 22, 1897–1906. doi:10.1158/1078-0432.CCR-15-1399

Boumahdi, S., and De Sauvage, F. J. (2020). The great escape: tumour cell plasticity in resistance to targeted therapy. *Nat. Rev. Drug Discov.* 19, 39–56. doi:10.1038/s41573-019-0044-1

Cai, H., Dai, X., Wang, X., Tan, P., Gu, L., Luo, Q., et al. (2020). A nanostrategy for efficient imaging-guided antitumor therapy through a stimuli-responsive branched polymeric prodrug. *Adv. Sci.* 7, 1903243. doi:10.1002/advs.201903243

Cai, X., Xie, Z., Ding, B., Shao, S., Liang, S., Pang, M., et al. (2019). Monodispersed copper(I)-Based nano metal-organic framework as a biodegradable drug carrier with enhanced photodynamic therapy efficacy. *Adv. Sci.* 6, 1900848. doi:10.1002/advs.201900848

Cai, Y., Ni, D., Cheng, W., Ji, C., Wang, Y., Müllen, K., et al. (2020). Enzyme-triggered disassembly of perylene monoimide-based nanoclusters for activatable and deep photodynamic therapy. *Angew. Chem. Int. Ed.*, 59, 14014. doi:10.1002/anie.202001107

Chan, M.-H., Pan, Y.-T., Chan, Y.-C., Hsiao, M., Chen, C.-H., Sun, L., et al. (2018). Nanobubble-embedded inorganic 808 nm excited upconversion nanocomposites for tumor multiple imaging and treatment. *Chem. Sci.* 9, 3141–3151. doi:10.1039/c8sc00108a

Chang, H. C., Zou, Z. Z., Wang, Q. H., Li, J., Jin, H., Yin, Q. X., et al. (2020). Targeting and specific activation of antigen-presenting cells by endogenous antigen-loaded nanoparticles elicits tumor-specific immunity. *Adv. Sci.* 7, 1900069. doi:10.1002/advs.201900069

Chao, Y., Chen, G., Liang, C., Xu, J., Dong, Z., Han, X., et al. (2019). Iron nanoparticles for low-power local magnetic hyperthermia in combination with immune checkpoint blockade for systemic antitumor therapy. *Nano Lett.* 19, 4287–4296. doi:10.1021/acs.nanolett.9b00579

Chen, H., Gu, Z., An, H., Chen, C., Chen, J., Cui, R., et al. (2018). Precise nanomedicine for intelligent therapy of cancer. *Sci. China Chem.* 61, 1503–1552. doi:10.1007/s11426-018-9397-5

Chen, J., Liang, C., Song, X., Yi, X., Yang, K., Feng, L., et al. (2019). Hybrid protein nano-reactors enable simultaneous increments of tumor oxygenation and iodine-131 delivery for enhanced radionuclide therapy. *Small* 15, e1903628. doi:10.1002/smll.201903628

Chen, Q., Wang, C., Zhang, X., Chen, G., Hu, Q., Li, H., et al. (2019). *In situ* sprayed bioresponsive immunotherapeutic gel for post-surgical cancer treatment. *Nat. Nanotech.* 14, 89–97. doi:10.1038/s41565-018-0319-4

Cheng, X., Sun, R., Xia, H., Ding, J., Yin, L., Chai, Z., et al. (2019). Light-triggered crosslinking of gold nanoparticles for remarkably improved radiation therapy and computed tomography imaging of tumors. *Nanomedicine* 14, 2941–2955. doi:10.2217/nnm-2019-0015

Chiang, C.-S., Lin, Y.-J., Lee, R., Lai, Y.-H., Cheng, H.-W., Hsieh, C.-H., et al. (2018). Combination of fucoidan-based magnetic nanoparticles and immunomodulators enhances tumour-localized immunotherapy. *Nat. Nanotech.* 13, 746–754. doi:10.1038/s41565-018-0146-7

De Jong, W. H., Hagens, W. I., Krystek, P., Burger, M. C., Sips, A. J. A. M., and Geertsma, R. E. (2008). Particle size-dependent organ distribution of gold nanoparticles after intravenous administration. *Biomaterials* 29, 1912–1919. doi:10.1016/j.biomaterials.2007.12.037

Dixon, S. J., Lemberg, K. M., Lamprecht, M. R., Skouta, R., Zaitsev, E. M., Gleason, C. E., et al. (2012). Ferroptosis: an iron-dependent form of nonapoptotic cell death. *Cell* 149, 1060–1072. doi:10.1016/j.cell.2012.03.042

Dong, Z., Feng, L., Hao, Y., Chen, M., Gao, M., Chao, Y., et al. (2018). Synthesis of hollow biomineralized CaCO3-polydopamine nanoparticles for multimodal imaging-guided cancer photodynamic therapy with reduced skin photosensitivity. *J. Am. Chem. Soc.* 140, 2165–2178. doi:10.1021/jacs.7b11036

Dougherty, T. J., Gomer, C. J., Henderson, B. W., Jori, G., Kessel, D., Korbelik, M., et al. (1998). Photodynamic therapy. *JNCI J. Natl. Cancer Inst.* 90, 889–905. doi:10.1093/jnci/90.12.889

Du, K., Liu, Q., Liu, M., Lv, R., He, N., and Wang, Z. (2020). Encapsulation of glucose oxidase in Fe(III)/tannic acid nanocomposites for effective tumor ablation via Fenton reaction. *Nanotechnology* 31, 015101. doi:10.1088/1361-6528/ab44f9

Du, Y., Liu, X., Liang, Q., Liang, X.-J., and Tian, J. (2019). Optimization and design of magnetic ferrite nanoparticles with uniform tumor distribution for highly sensitive MRI/MPI performance and improved magnetic hyperthermia therapy. *Nano Lett.* 19, 3618–3626. doi:10.1021/acs.nanolett.9b00630

Duro-Castano, A., Gallon, E., Decker, C., and Vicent, M. J. (2017). Modulating angiogenesis with integrin-targeted nanomedicines. *Adv. Drug Deliv. Rev.* 119, 101–119. doi:10.1016/j.addr.2017.05.008

Eroglu, Z., and Ribas, A. (2016). Combination therapy with BRAF and MEK inhibitors for melanoma: latest evidence and place in therapy. *Ther. Adv. Med. Oncol.* 8, 48–56. doi:10.1177/1758834015616934

Fadeel, B., Farcal, L., Hardy, B., Vázquez-Campos, S., Hristozov, D., Marcomini, A., et al. (2018). Advanced tools for the safety assessment of nanomaterials. *Nat. Nanotech.* 13, 537–543. doi:10.1038/s41565-018-0185-0

Fang, J., Nakamura, H., and Maeda, H. (2011). The EPR effect: unique features of tumor blood vessels for drug delivery, factors involved, and limitations and augmentation of the effect. *Adv. Drug Deliv. Rev.* 63, 136–151. doi:10.1016/j.addr.2010.04.009

Fenton, O. S., Kauffman, K. J., Mcclellan, R. L., Kaczmarek, J. C., Zeng, M. D., Andresen, J. L., et al. (2018). Customizable lipid nanoparticle materials for the delivery of siRNAs and mRNAs. *Angew. Chem. Int. Ed.* 57, 13582–13586. doi:10.1002/anie.201809056

Fridman, W. H., Pagès, F., Sautès-Fridman, C., and Galon, J. (2012). The immune contexture in human tumours: impact on clinical outcome. *Nat. Rev. Cancer* 12, 298–306. doi:10.1038/nrc3245

Fu, J., Li, K., Zhang, W., Wan, C., Zhang, J., Jiang, P., et al. (2020). Large-scale public data reuse to model immunotherapy response and resistance. *Genome Med.* 12. doi:10.1186/s13073-020-0721-z

Gajewski, T. F., Meng, Y., Blank, C., Brown, I., Kacha, A., Kline, J., et al. (2006). Immune resistance orchestrated by the tumor microenvironment. *Immunol. Rev.* 213, 131–145. doi:10.1111/j.1600-065X.2006.00442.x

Gao, Z., Hou, Y., Zeng, J., Chen, L., Liu, C., Yang, W., et al. (2017). Tumor microenvironment-triggered aggregation of antiphagocytosis 99m Tc-labeled Fe3 O4 nanoprobes for enhanced tumor imaging in vivo. *Adv. Mater.* 29, 1701095. doi:10.1002/adma.201701095

Grahnert, A., Grahnert, A., Klein, C., Schilling, E., Wehrhahn, J., and Hauschildt, S. (2011). Review: NAD+: a modulator of immune functions. *Innate Immun.* 17, 212–233. doi:10.1177/1753425910361989

Grippin, A. J., Wummer, B., Wildes, T., Dyson, K., Trivedi, V., Yang, C., et al. (2019). Dendritic cell-activating magnetic nanoparticles enable early prediction of antitumor response with magnetic resonance imaging. *ACS Nano* 13, 13884–13898. doi:10.1021/acsnano.9b05037

Gu, Z., Zhu, S., Yan, L., Zhao, F., and Zhao, Y. (2019). Graphene-based smart platforms for combined cancer therapy. *Adv. Mater.* 31, 1800662. doi:10.1002/adma.201800662

Guo, S., and Huang, L. (2014). Nanoparticles containing insoluble drug for cancer therapy. *Biotechnol. Adv.* 32, 778–788. doi:10.1016/j.biotechadv.2013.10.002

Gupta, P., Lakes, A., and Dziubla, T. (2016). A free radical primer. *Oxidative Stress Biomater.* 2016, 1–33. doi:10.1016/b978-0-12-803269-5.00001-2

Hainfeld, J. F., Smilowitz, H. M., O'Connor, M. J., Dilmanian, F. A., and Slatkin, D. N. (2013). Gold nanoparticle imaging and radiotherapy of brain tumors in mice. *Nanomedicine* 8, 1601–1609. doi:10.2217/nnm.12.165

Han, B., Mao, F.-Y., Zhao, Y.-L., Lv, Y.-P., Teng, Y.-S., Duan, M., et al. (2018). Altered NKp30, NKp46, NKG2D, and DNAM-1 expression on circulating NK cells is associated with tumor progression in human gastric cancer. *J. Immunol. Res.* 2018, 1. doi:10.1155/2018/6248590

Han, H., Hou, Y., Chen, X., Zhang, P., Kang, M., Jin, Q., et al. (2020). Metformin-induced stromal depletion to enhance the penetration of gemcitabine-loaded magnetic nanoparticles for pancreatic cancer targeted therapy. *J. Am. Chem. Soc.* 142, 4944–4954. doi:10.1021/jacs.0c00650

Han, K., Chen, S., Chen, W.-H., Lei, Q., Liu, Y., Zhuo, R.-X., et al. (2013). Synergistic gene and drug tumor therapy using a chimeric peptide. *Biomaterials* 34, 4680–4689. doi:10.1016/j.biomaterials.2013.03.010

Hattermann, K., Sebens, S., Helm, O., Schmitt, A. D., Mentlein, R., Mehdorn, H. M., et al. (2014). Chemokine expression profile of freshly isolated human glioblastoma-associated macrophages/microglia. *Oncol. Rep.* 32, 270–276. doi:10.3892/or.2014.3214

He, X., Yin, F., Wang, D., Xiong, L.-H., Kwok, R. T. K., Gao, P. F., et al. (2019). AIE featured inorganic-organic Core@Shell nanoparticles for high-efficiency siRNA delivery and real-time monitoring. *Nano Lett.* 19, 2272–2279. doi:10.1021/acs.nanolett.8b04677

High, K. A., and Roncarolo, M. G. (2019). Gene therapy. *N. Engl. J. Med.* 381, 455–464. doi:10.1056/NEJMra1706910

Hu, J.-J., Chen, Y., Li, Z.-H., Peng, S.-Y., Sun, Y., and Zhang, X.-Z. (2019). Augment of oxidative damage with enhanced photodynamic process and MTH1 inhibition for tumor therapy. *Nano Lett.* 19, 5568–5576. doi:10.1021/acs.nanolett.9b02112

Hu, R., Fang, Y., Huo, M., Yao, H., Wang, C., Chen, Y., et al. (2019). Ultrasmall Cu2-xS nanodots as photothermal-enhanced Fenton nanocatalysts for synergistic tumor therapy at NIR-II biowindow. *Biomaterials* 206, 101–114. doi:10.1016/j.biomaterials.2019.03.014

Huang, G., Zhang, K.-L., Chen, S., Li, S.-H., Wang, L.-L., Wang, L.-P., et al. (2017). Manganese-iron layered double hydroxide: a theranostic nanoplatform with pH-responsive MRI contrast enhancement and drug release. *J. Mater. Chem. B* 5, 3629–3633. doi:10.1039/c7tb00794a

Huang, L.-L., Li, X., Zhang, J., Zhao, Q. R., Zhang, M. J., Liu, A.-A., et al. (2019). MnCaCs-biomineralized oncolytic virus for bimodal imaging-guided and synergistically enhanced anticancer therapy. *Nano Lett.* 19, 8002–8009. doi:10.1021/acs.nanolett.9b03193

Huo, M., Wang, L., Wang, Y., Chen, Y., and Shi, J. (2019). Nanocatalytic tumor therapy by single-atom catalysts. *ACS Nano* 13, 2643–2653. doi:10.1021/acsnano.9b00457

Irvine, D. J., and Dane, E. L. (2020). Enhancing cancer immunotherapy with nanomedicine. *Nat. Rev. Immunol.* 20, 321–334. doi:10.1038/s41577-019-0269-6

Janib, S. M., Moses, A. S., and Mackay, J. A. (2010). Imaging and drug delivery using theranostic nanoparticles. *Adv. Drug Deliv. Rev.* 62, 1052–1063. doi:10.1016/j.addr.2010.08.004

Jiang, Q., Zhao, S., Liu, J., Song, L., Wang, Z.-G., and Ding, B. (2019). Rationally designed DNA-based nanocarriers. *Adv. Drug Deliv. Rev.* 147, 2–21. doi:10.1016/j.addr.2019.02.003

Jiang, X., Zhang, S., Ren, F., Chen, L., Zeng, J., Zhu, M., et al. (2017). Ultrasmall magnetic CuFeSe2 ternary nanocrystals for multimodal imaging guided photothermal therapy of cancer. *ACS Nano* 11, 5633–5645. doi:10.1021/acsnano.7b01032

Jing, L., Yang, C., Zhang, P., Zeng, J., Li, Z., and Gao, M. (2020). Nanoparticles weaponized with built-in functions for imaging-guided cancer therapy. *View*, 1, e19. doi:10.1002/viw2.19

Juarranz, Á., Jaén, P., Sanz-Rodríguez, F., Cuevas, J., and González, S. (2008). Photodynamic therapy of cancer. Basic principles and applications. *Clin. Transl Oncol.* 10, 148–154. doi:10.1007/s12094-008-0172-2

Kelkar, S. S., and Reineke, T. M. (2011). Theranostics: combining imaging and therapy. *Bioconjug. Chem.* 22, 1879–1903. doi:10.1021/bc200151q

Kim, B., Sun, S., Varner, J. A., Howell, S. B., Ruoslahti, E., and Sailor, M. J. (2019). Securing the payload, finding the cell, and avoiding the endosome: peptide-targeted, fusogenic porous silicon nanoparticles for delivery of siRNA. *Adv. Mater.* 31, 1902952. doi:10.1002/adma.201902952

Kim, J., Lee, Y. M., Kim, H., Park, D., Kim, J., and Kim, W. J. (2016). Phenylboronic acid-sugar grafted polymer architecture as a dual stimuli-responsive gene carrier for targeted anti-angiogenic tumor therapy. *Biomaterials* 75, 102–111. doi:10.1016/j.biomaterials.2015.10.022

Koppers-Lalic, D., Hogenboom, M. M., Middeldorp, J. M., and Pegtel, D. M. (2013). Virus-modified exosomes for targeted RNA delivery; a new approach in nanomedicine. *Adv. Drug Deliv. Rev.* 65, 348–356. doi:10.1016/j.addr.2012.07.006

Kotterman, M. A., Chalberg, T. W., and Schaffer, D. V. (2015). Viral vectors for gene therapy: translational and clinical outlook. *Annu. Rev. Biomed. Eng.* 17, 63–89. doi:10.1146/annurev-bioeng-071813-104938

Kuang, H., Ku, S. H., and Kokkoli, E. (2017). The design of peptide-amphiphiles as functional ligands for liposomal anticancer drug and gene delivery. *Adv. Drug Deliv. Rev.* 110-111, 80–101. doi:10.1016/j.addr.2016.08.005

Lacroix, L.-M., Ho, D., and Sun, S. (2010). Magnetic nanoparticles as both imaging probes and therapeutic agents. *Ctmc* 10, 1184–1197. doi:10.2174/156802610791384207

Lammers, T., Kiessling, F., Hennink, W. E., and Storm, G. (2012). Drug targeting to tumors: principles, pitfalls and (pre-) clinical progress. *J. Controlled Release* 161, 175–187. doi:10.1016/j.jconrel.2011.09.063

Lee, J., Jeong, E. J., Lee, Y. K., Kim, K., Kwon, I. C., and Lee, K. Y. (2016). Optical imaging and gene therapy with neuroblastoma-targeting polymeric nanoparticles for potential theranostic applications. *Small* 12, 1201–1211. doi:10.1002/smll.201501913

Li, F., Nie, W., Zhang, F., Lu, G., Lv, C., Lv, Y., et al. (2019). Engineering magnetosomes for high-performance cancer vaccination. *ACS Cent. Sci.* 5, 796–807. doi:10.1021/acscentsci.9b00060

Lin, L.-S., Song, J., Song, L., Ke, K., Liu, Y., Zhou, Z., et al. (2018). Simultaneous fenton-like ion delivery and glutathione depletion by MnO2 -based nanoagent to enhance chemodynamic therapy. *Angew. Chem. Int. Ed.* 57, 4902–4906. doi:10.1002/anie.201712027

Liu, B., Hu, F., Zhang, J., Wang, C., and Li, L. (2019). A biomimetic coordination nanoplatform for controlled encapsulation and delivery of drug-gene combinations. *Angew. Chem. Int. Ed.* 58, 8804–8808. doi:10.1002/anie.201903417

Liu, D., Zhou, Z., Wang, X., Deng, H., Sun, L., Lin, H., et al. (2020). Yolk-shell nanovesicles endow glutathione-responsive concurrent drug release and T1 MRI activation for cancer theranostics. *Biomaterials* 244, 119979. doi:10.1016/j.biomaterials.2020.119979

Liu, H., Moynihan, K. D., Zheng, Y., Szeto, G. L., Li, A. V., Huang, B., et al. (2014). Structure-based programming of lymph-node targeting in molecular vaccines. *Nature* 507, 519–522. doi:10.1038/nature12978

Liu, J., Chen, Q., Zhu, W., Yi, X., Yang, Y., Dong, Z., et al. (2017). Nanoscale-coordination-polymer-shelled manganese dioxide composite nanoparticles: a multistage redox/pH/H2O2-responsive cancer theranostic nanoplatform. *Adv. Funct. Mater.* 27, 1605926. doi:10.1002/adfm.201605926

Liu, J., Li, H.-J., Luo, Y.-L., Xu, C.-F., Du, X.-J., Du, J.-Z., et al. (2019). Enhanced primary tumor penetration facilitates nanoparticle draining into lymph nodes after systemic injection for tumor metastasis inhibition. *ACS Nano* 13, 8648–8658. doi:10.1021/acsnano.9b03472

Liu, S., Zhang, Y., Zhao, X., Wang, J., Di, C., Zhao, Y., et al. (2019). Tumor-specific silencing of tissue factor suppresses metastasis and prevents cancer-associated hypercoagulability. *Nano Lett.* 19, 4721–4730. doi:10.1021/acs.nanolett.9b01785

Liu, T., Tong, L., Lv, N., Ge, X., Fu, Q., Gao, S., et al. (2019). Two-stage size decrease and enhanced photoacoustic performance of stimuli-responsive polymer-gold nanorod assembly for increased tumor penetration. *Adv. Funct. Mater.* 29, 1806429. doi:10.1002/adfm.201806429

Liu, X. L., Ng, C. T., Chandrasekharan, P., Yang, H. T., Zhao, L. Y., Peng, E., et al. (2016). Synthesis of ferromagnetic Fe0.6Mn0.4O nanoflowers as a new class of magnetic theranostic platform for in vivo T1-T2Dual-mode magnetic resonance imaging and magnetic hyperthermia therapy. *Adv. Health Mater.* 5, 2092–2104. doi:10.1002/adhm.201600357

Liu, X., Yan, B., Li, Y., Ma, X., Jiao, W., Shi, K., et al. (2020). Graphene oxide-grafted magnetic nanorings mediated magnetothermodynamic therapy favoring reactive oxygen species-related immune response for enhanced antitumor efficacy. *ACS Nano* 14, 1936–1950. doi:10.1021/acsnano.9b08320

Liu, Y., Bhattarai, P., Dai, Z., and Chen, X. (2019a). Photothermal therapy and photoacoustic imaging via nanotheranostics in fighting cancer. *Chem. Soc. Rev.* 48, 2053–2108. doi:10.1039/c8cs00618k

Liu, Y., Wu, J., Jin, Y., Zhen, W., Wang, Y., Liu, J., et al. (2019b). Copper(I) phosphide nanocrystals for in situ self-generation magnetic resonance imaging-guided photothermal-enhanced chemodynamic synergetic therapy resisting deep-seated tumor. *Adv. Funct. Mater.* 29, 1904678. doi:10.1002/adfm.201904678

Liu, Y., and Deisseroth, A. (2006). Tumor vascular targeting therapy with viral vectors. *Blood* 107, 3027–3033. doi:10.1182/blood-2005-10-4114

Lu, Y., Aimetti, A. A., Langer, R., and Gu, Z. (2016). Bioresponsive materials. *Nat. Rev. Mater.* 2, 16075. doi:10.1038/natrevmats.2016.75

Lundstrom, K. (2003). Latest development in viral vectors for gene therapy. *Trends Biotechnol.* 21, 117–122. doi:10.1016/s0167-7799(02)00042-2

Lv, P., Liu, X., Chen, X., Liu, C., Zhang, Y., Chu, C., et al. (2019). Genetically engineered cell membrane nanovesicles for oncolytic adenovirus delivery: a versatile platform for cancer virotherapy. *Nano Lett.* 19, 2993–3001. doi:10.1021/acs.nanolett.9b00145

Ma, T., Hou, Y., Zeng, J., Liu, C., Zhang, P., Jing, L., et al. (2018). Dual-ratiometric target-triggered fluorescent probe for simultaneous quantitative visualization of tumor microenvironment protease activity and pH *in vivo*. *J. Am. Chem. Soc.* 140, 211–218. doi:10.1021/jacs.7b08900

Ma, T., Zhang, P., Hou, Y., Ning, H., Wang, Z., Huang, J., et al. (2018). "Smart" nanoprobes for visualization of tumor microenvironments. *Adv. Health Mater.* 7, 1800391. doi:10.1002/adhm.201800391

Mai, B. T., Balakrishnan, P. B., Barthel, M. J., Piccardi, F., Niculaes, D., Marinaro, F., et al. (2019). Thermoresponsive iron oxide nanocubes for an effective clinical translation of magnetic hyperthermia and heat-mediated chemotherapy. *ACS Appl. Mater. Inter.* 11, 5727–5739. doi:10.1021/acsami.8b16226

Mangraviti, A., Tzeng, S. Y., Kozielski, K. L., Wang, Y., Jin, Y., Gullotti, D., et al. (2015). Polymeric nanoparticles for nonviral gene therapy extend brain tumor survival *in vivo*. *ACS Nano* 9, 1236–1249. doi:10.1021/nn504905q

Mi, P., Kokuryo, D., Cabral, H., Wu, H., Terada, Y., Saga, T., et al. (2016). A pH-activatable nanoparticle with signal-amplification capabilities for non-invasive imaging of tumour malignancy. *Nat. Nanotech* 11, 724–730. doi:10.1038/nnano.2016.72

Miao, L., Li, L., Huang, Y., Delcassian, D., Chahal, J., Han, J., et al. (2019). Delivery of mRNA vaccines with heterocyclic lipids increases anti-tumor efficacy by STING-mediated immune cell activation. *Nat. Biotechnol.* 37, 1174–1185. doi:10.1038/s41587-019-0247-3

Milling, L., Zhang, Y., and Irvine, D. J. (2017). Delivering safer immunotherapies for cancer. *Adv. Drug Deliv. Rev.* 114, 79–101. doi:10.1016/j.addr.2017.05.011

Mohme, M., Riethdorf, S., and Pantel, K. (2017). Circulating and disseminated tumour cells - mechanisms of immune surveillance and escape. *Nat. Rev. Clin. Oncol.* 14, 155–167. doi:10.1038/nrclinonc.2016.144

Mura, S., Nicolas, J., and Couvreur, P. (2013). Stimuli-responsive nanocarriers for drug delivery. *Nat. Mater* 12, 991–1003. doi:10.1038/nmat3776

Ni, R., Zhou, J., Hossain, N., and Chau, Y. (2016). Virus-inspired nucleic acid delivery system: linking virus and viral mimicry. *Adv. Drug Deliv. Rev.* 106, 3–26. doi:10.1016/j.addr.2016.07.005

Nie, W., Wei, W., Zuo, L., Lv, C., Zhang, F., Lu, G.-H., et al. (2019). Magnetic nanoclusters armed with responsive PD-1 antibody synergistically improved adoptive T-cell therapy for solid tumors. *ACS Nano* 13, 1469–1478. doi:10.1021/acsnano.8b07141

Omidi, Y. (2011). Smart multifunctional theranostics: simultaneous diagnosis and therapy of cancer. *Bioimpacts* 1, 145–147. doi:10.5681/bi.2011.019

Oun, R., Moussa, Y. E., and Wheate, N. J. (2018). The side effects of platinum-based chemotherapy drugs: a review for chemists. *Dalton Trans.* 47, 6645–6653. doi:10.1039/c8dt00838h

Ovais, M., Guo, M., and Chen, C. (2019). Tailoring nanomaterials for targeting tumor-associated macrophages. *Adv. Mater.* 31, 1808303. doi:10.1002/adma.201808303

Ozpolat, B., Sood, A. K., and Lopez-Berestein, G. (2014). Liposomal siRNA nanocarriers for cancer therapy. *Adv. Drug Deliv. Rev.* 66, 110–116. doi:10.1016/j.addr.2013.12.008

Pan, Y.-B., Wang, S., He, X., Tang, W., Wang, J., Shao, A., et al. (2019). A combination of glioma *in vivo* imaging and *in vivo* drug delivery by metal-organic framework based composite nanoparticles. *J. Mater. Chem. B* 7, 7683–7689. doi:10.1039/c9tb01651a

Peters, B. G. (1994). An overview of chemotherapy toxicities. *Top. Hosp. Pharm. Manage.* 14, 59–88.

Petersen, G. H., Alzghari, S. K., Chee, W., Sankari, S. S., and La-Beck, N. M. (2016). Meta-analysis of clinical and preclinical studies comparing the anticancer efficacy of liposomal versus conventional non-liposomal doxorubicin. *J. Controlled Release* 232, 255–264. doi:10.1016/j.jconrel.2016.04.028

Poon, W., Zhang, Y.-N., Ouyang, B., Kingston, B. R., Wu, J. L. Y., Wilhelm, S., et al. (2019). Elimination pathways of nanoparticles. *ACS nano* 13, 5785–5798. doi:10.1021/acsnano.9b01383

Rajora, M. A., Lou, J. W. H., and Zheng, G. (2017). Advancing porphyrin's biomedical utility via supramolecular chemistry. *Chem. Soc. Rev.* 46, 6433–6469. doi:10.1039/c7cs00525c

Ren, Z., Sun, S., Sun, R., Cui, G., Hong, L., Rao, B., et al. (2020). A metal-polyphenol-coordinated nanomedicine for synergistic cascade cancer chemotherapy and chemodynamic therapy. *Adv. Mater.* 32, 1906024. doi:10.1002/adma.201906024

Rezaee, R., Momtazi, A. A., Monemi, A., and Sahebkar, A. (2017). Curcumin: a potentially powerful tool to reverse cisplatin-induced toxicity. *Pharmacol. Res.* 117, 218–227. doi:10.1016/j.phrs.2016.12.037

Robert, C., Thomas, L., Bondarenko, I., O'day, S., Weber, J., Garbe, C., et al. (2011). Ipilimumab plus dacarbazine for previously untreated metastatic melanoma. *N. Engl. J. Med.* 364, 2517–2526. doi:10.1056/NEJMoa1104621

Rodell, C. B., Arlauckas, S. P., Cuccarese, M. F., Garris, C. S., Li, R., Ahmed, M. S., et al. (2018). TLR7/8-agonist-loaded nanoparticles promote the polarization of tumour-associated macrophages to enhance cancer immunotherapy. *Nat. Biomed. Eng.* 2, 578–588. doi:10.1038/s41551-018-0236-8

Saha, M. (2009). Nanomedicine: promising tiny machine for the healthcare in future-a review. *Omj* 24, 242–247. doi:10.5001/omj.2009.50

Santiago-Ortiz, J. L., and Schaffer, D. V. (2016). Adeno-associated virus (AAV) vectors in cancer gene therapy. *J. Controlled Release* 240, 287–301. doi:10.1016/j.jconrel.2016.01.001

Schoenfeld, J. D., Sibenaller, Z. A., Mapuskar, K. A., Wagner, B. A., Cramer-Morales, K. L., Furqan, M., et al. (2017). O_2−and H_2O2 -mediated disruption of Fe metabolism causes the differential susceptibility of NSCLC and GBM cancer cells to pharmacological ascorbate. *Cancer cell* 31, 487–500. doi:10.1016/j.ccell.2017.02.018

Schöttler, S., Landfester, K., and Mailänder, V. (2016). Controlling the stealth effect of nanocarriers through understanding the protein corona. *Angew. Chem. Int. Ed.* 55, 8806–8815. doi:10.1002/anie.201602233

Shi, B., Yan, Q., Tang, J., Xin, K., Zhang, J., Zhu, Y., et al. (2018). Hydrogen sulfide-activatable second near-infrared fluorescent nanoassemblies for targeted photothermal cancer therapy. *Nano Lett.* 18, 6411–6416. doi:10.1021/acs.nanolett.8b02767

Shin, H., and Na, K. (2019). *In situ* vaccination with biocompatibility controllable immuno-sensitizer inducing antitumor immunity. *Biomaterials* 197, 32–40. doi:10.1016/j.biomaterials.2019.01.015

Shu, Y., Pi, F., Sharma, A., Rajabi, M., Haque, F., Shu, D., et al. (2014). Stable RNA nanoparticles as potential new generation drugs for cancer therapy. *Adv. Drug Deliv. Rev.* 66, 74–89. doi:10.1016/j.addr.2013.11.006

Singh, A., Nandwana, V., Rink, J. S., Ryoo, S.-R., Chen, T. H., Allen, S. D., et al. (2019). Biomimetic magnetic nanostructures: a theranostic platform targeting lipid metabolism and immune response in lymphoma. *ACS Nano* 13, 10301–10311. doi:10.1021/acsnano.9b03727

Song, C., Phuengkham, H., Kim, Y. S., Dinh, V. V., Lee, I., Shin, I. W., et al. (2019). Syringeable immunotherapeutic nanogel reshapes tumor microenvironment and prevents tumor metastasis and recurrence. *Nat. Commun.* 10, 3745. doi:10.1038/s41467-019-11730-8

Song, G., Kenney, M., Chen, Y.-S., Zheng, X., Deng, Y., Chen, Z., et al. (2020). Carbon-coated FeCo nanoparticles as sensitive magnetic-particle-imaging tracers with photothermal and magnetothermal properties. *Nat. Biomed. Eng.* 4, 325–334. doi:10.1038/s41551-019-0506-0

Song, Q., Zheng, C., Jia, J., Zhao, H., Feng, Q., Zhang, H., et al. (2019). A probiotic spore-based oral autonomous nanoparticles generator for cancer therapy. *Adv. Mater.* 31, 1903793. doi:10.1002/adma.201903793

Song, W., Das, M., Xu, Y., Si, X., Zhang, Y., Tang, Z., et al. (2019). Leveraging biomaterials for cancer immunotherapy: targeting pattern recognition receptors. *Mater. Today Nano* 5, 100029. doi:10.1016/j.mtnano.2019.100029

Song, Y., Shi, Y., Huang, M., Wang, W., Wang, Y., Cheng, J., et al. (2019). Bioinspired engineering of a multivalent aptamer-functionalized nanointerface to enhance the capture and release of circulating tumor cells. *Angew. Chem. Int. Ed.* 58, 2236–2240. doi:10.1002/anie.201809337

Sousa, S., Brion, R., Lintunen, M., Kronqvist, P., Sandholm, J., Mönkkönen, J., et al. (2015). Human breast cancer cells educate macrophages toward the M2 activation status. *Breast Cancer Res.* 17, 101. doi:10.1186/s13058-015-0621-0

Sprooten, J., Ceusters, J., Coosemans, A., Agostinis, P., De Vleeschouwer, S., Zitvogel, L., et al. (2019). Trial watch: dendritic cell vaccination for cancer immunotherapy. *Oncoimmunology* 8, 1638212. doi:10.1080/2162402X.2019.1638212

Stéen, E. J. L., Jørgensen, J. T., Johann, K., Nørregaard, K., Sohr, B., Svatunek, D., et al. (2020). Trans-cyclooctene-Functionalized PeptoBrushes with improved reaction kinetics of the tetrazine ligation for pretargeted nuclear imaging. *ACS Nano* 14, 568–584. doi:10.1021/acsnano.9b06905

Sumer, B., and Gao, J. (2008). Theranostic nanomedicine for cancer. *Nanomedicine* 3, 137–140. doi:10.2217/17435889.3.2.137

Sun, W., Liu, X.-Y., Ma, L.-L., and Lu, Z.-L. (2020). Tumor targeting gene vector for visual tracking of bcl-2 siRNA transfection and anti-tumor therapy. *ACS Appl. Mater. Inter.* 12, 10193–10201. doi:10.1021/acsami.0c00652

Sun, X., Zhang, P., Hou, Y., Li, Y., Huang, X., Wang, Z., et al. (2019). Upconversion luminescence mediated photodynamic therapy through hydrophilically engineered porphyrin. *Chem. Eng. Process* 142, 107551. doi:10.1016/j.cep.2019.107551

Tang, M., Zhu, X., Zhang, Y., Zhang, Z., Zhang, Z., Mei, Q., et al. (2019). Near-infrared excited orthogonal emissive upconversion nanoparticles for imaging-guided on-demand therapy. *ACS Nano* 13, 10405–10418. doi:10.1021/acsnano.9b04200

Tang, Z., Liu, Y., He, M., and Bu, W. (2018). Chemodynamic therapy: tumour microenvironment-mediated fenton and fenton-like reactions. *Angew. Chem.* 131, 958–968. doi:10.1002/ange.201805664

Tang, Z., Zhang, H., Liu, Y., Ni, D., Zhang, H., Zhang, J., et al. (2017). Antiferromagnetic pyrite as the tumor microenvironment-mediated nanoplatform for self-enhanced tumor imaging and therapy. *Adv. Mater.* 29, 1701683. doi:10.1002/adma.201701683

Tee, J. K., Yip, L. X., Tan, E. S., Santitewagun, S., Prasath, A., Ke, P. C., et al. (2019). Nanoparticles' interactions with vasculature in diseases. *Chem. Soc. Rev.* 48, 5381–5407. doi:10.1039/c9cs00309f

Tian, L., Yi, X., Dong, Z., Xu, J., Liang, C., Chao, Y., et al. (2018). Calcium bisphosphonate nanoparticles with chelator-free radiolabeling to deplete tumor-associated macrophages for enhanced cancer radioisotope therapy. *ACS Nano* 12, 11541–11551. doi:10.1021/acsnano.8b06699

Tian, Y., Zhou, M., Shi, H., Gao, S., Xie, G., Zhu, M., et al. 2018). Integration of cell-penetrating peptides with rod-like bionanoparticles: virus-inspired gene-silencing technology. *Nano Lett.* 18, 5453–5460. doi:10.1021/acs.nanolett.8b01805

Torrente-Rodríguez, R. M., Tu, J., Yang, Y., Min, J., Wang, M., Song, Y., et al. (2020). Investigation of cortisol dynamics in human sweat using a graphene-based wireless mHealth system. *Matter*, 2, 921. doi:10.1016/j.matt.2020.01.021

Tsouris, V., Joo, M. K., Kim, S. H., Kwon, I. C., and Won, Y.-Y. (2014). Nano carriers that enable co-delivery of chemotherapy and RNAi agents for treatment of drug-resistant cancers. *Biotechnol. Adv.* 32, 1037–1050. doi:10.1016/j.biotechadv.2014.05.006

Uhel, F., Azzaoui, I., Grégoire, M., Pangault, C., Dulong, J., Tadié, J.-M., et al. (2017). Early expansion of circulating granulocytic myeloid-derived suppressor cells predicts development of nosocomial infections in patients with sepsis. *Am. J. Respir. Crit. Care Med.* 196, 315–327. doi:10.1164/rccm.201606-1143OC

Vangasseri, D. P., Cui, Z., Chen, W., Hokey, D. A., Falo, L. D., and Huang, L. (2009). Immunostimulation of dendritic cells by cationic liposomes. *Mol. Membr. Biol.* 23, 385–395. doi:10.1080/09687860600790537

Waehler, R., Russell, S. J., and Curiel, D. T. (2007). Engineering targeted viral vectors for gene therapy. *Nat. Rev. Genet.* 8, 573–587. doi:10.1038/nrg2141

Wang, F., Gao, J., Xiao, J., and Du, J. (2018). Dually gated polymersomes for gene delivery. *Nano Lett.* 18, 5562–5568. doi:10.1021/acs.nanolett.8b01985

Wang, J., Mi, P., Lin, G., Wáng, Y. X. J., Liu, G., and Chen, X. (2016). Imaging-guided delivery of RNAi for anticancer treatment. *Adv. Drug Deliv. Rev.* 104, 44–60. doi:10.1016/j.addr.2016.01.008

Wang, L., Huang, J., Chen, H., Wu, H., Xu, Y., Li, Y., et al. (2017). Exerting enhanced permeability and retention effect driven delivery by ultrafine iron oxide nanoparticles with T1-T2 switchable magnetic resonance imaging contrast. *ACS Nano* 11, 4582–4592. doi:10.1021/acsnano.7b00038

Wang, S., Wang, Z., Yu, G., Zhou, Z., Jacobson, O., Liu, Y., et al. (2019). Tumor-specific drug release and reactive oxygen species generation for cancer chemo/chemodynamic combination therapy. *Adv. Sci.* 6, 1801986. doi:10.1002/advs.201801986

Wang, T., Zhang, H., Liu, H., Yuan, Q., Ren, F., Han, Y., et al. (2019). Boosting H 2 O 2 -guided chemodynamic therapy of cancer by enhancing reaction kinetics through versatile biomimetic fenton nanocatalysts and the second near-infrared light irradiation. *Adv. Funct. Mater.* 30, 1906128. doi:10.1002/adfm.201906128

Wang, Y., and Yu, C. (2020). Emerging concepts of nanobiotechnology in mRNA delivery. *Angew. Chem. Int. Ed.*, 59, 23374. doi:10.1002/anie.202003545

Wang, Z., Xue, X., Lu, H., He, Y., Lu, Z., Chen, Z., et al. (2020). Two-way magnetic resonance tuning and enhanced subtraction imaging for non-invasive and quantitative biological imaging. *Nat. Nanotechnol.*, 15, 482. doi:10.1038/s41565-020-0678-5

Weber, J. S., Yang, J. C., Atkins, M. B., and Disis, M. L. (2015). Toxicities of immunotherapy for the practitioner. *Jco* 33, 2092–2099. doi:10.1200/JCO.2014.60.0379

Weissleder, R. (1999). Molecular imaging: exploring the next Frontier. *Radiology* 212, 609–614. doi:10.1148/radiology.212.3.r99se18609

Weissleder, R., and Ntziachristos, V. (2003). Shedding light onto live molecular targets. *Nat. Med.* 9, 123–128. doi:10.1038/nm0103-123

Whiteside, T. L. (2008). "Immune effector cells in the tumor microenvironment: their role in regulation of tumor progression," in *Innate and adaptive immunity in the tumor microenvironment* (Dordrecht, The Netherlands: Springer), 1–33.

Wolfbeis, O. S. (2015). An overview of nanoparticles commonly used in fluorescent bioimaging. *Chem. Soc. Rev.* 44, 4743–4768. doi:10.1039/c4cs00392f

Wu, T.-L., and Zhou, D. (2011). Viral delivery for gene therapy against cell movement in cancer. *Adv. Drug Deliv. Rev.* 63, 671–677. doi:10.1016/j.addr.2011.05.005

Xiang, J., Xu, L., Gong, H., Zhu, W., Wang, C., Xu, J., et al. (2015). Antigen-loaded upconversion nanoparticles for dendritic cell stimulation, tracking, and vaccination in dendritic cell-based immunotherapy. *ACS Nano* 9, 6401–6411. doi:10.1021/acsnano.5b02014

Xue, H. Y., Liu, S., and Wong, H. L. (2014). Nanotoxicity: a key obstacle to clinical translation of siRNA-based nanomedicine. *Nanomedicine* 9, 295–312. doi:10.2217/nnm.13.204

Yang, J., Liu, H., and Zhang, X. (2014). Design, preparation and application of nucleic acid delivery carriers. *Biotechnol. Adv.* 32, 804–817. doi:10.1016/j.biotechadv.2013.11.004

Yang, Y., Wang, L., Cao, H., Li, Q., Li, Y., Han, M., et al. (2019). Photodynamic therapy with liposomes encapsulating photosensitizers with aggregation-induced emission. *Nano Lett.* 19, 1821–1826. doi:10.1021/acs.nanolett.8b04875

Yatim, N., Cullen, S., and Albert, M. L. (2017). Dying cells actively regulate adaptive immune responses. *Nat. Rev. Immunol.* 17, 262–275. doi:10.1038/nri.2017.9

Yavuz, C. T., Mayo, J. T., Yu, W. W., Prakash, A., Falkner, J. C., Yean, S., et al. (2006). Low-field magnetic separation of monodisperse Fe3O4 nanocrystals. *Science* 314, 964–967. doi:10.1126/science.1131475

Yoo, D., Lee, J.-H., Shin, T.-H., and Cheon, J. (2011). Theranostic magnetic nanoparticles. *Acc. Chem. Res.* 44, 863–874. doi:10.1021/ar200085c

Yu, G.-T., Rao, L., Wu, H., Yang, L.-L., Bu, L.-L., Deng, W.-W., et al. (2018). Myeloid-derived suppressor cell membrane-coated magnetic nanoparticles for cancer theranostics by inducing macrophage polarization and synergizing immunogenic cell death. *Adv. Funct. Mater.* 28, 1801389. doi:10.1002/adfm.201801389

Yu, M., Duan, X., Cai, Y., Zhang, F., Jiang, S., Han, S., et al. (2019). Multifunctional nanoregulator reshapes immune microenvironment and enhances immune memory for tumor immunotherapy. *Adv. Sci.* 6, 1900037. doi:10.1002/advs.201900037

Yuan, Y., Gu, Z., Yao, C., Luo, D., and Yang, D. (2019). Nucleic acid-based functional nanomaterials as advanced cancer therapeutics. *Small* 15, 1900172. doi:10.1002/smll.201900172

Zhan, C., Huang, Y., Lin, G., Huang, S., Zeng, F., and Wu, S. (2019). A gold nanocage/cluster hybrid structure for whole-body multispectral optoacoustic tomography imaging, EGFR inhibitor delivery, and photothermal therapy. *Small* 15, 1900309. doi:10.1002/smll.201900309

Zhang, C., Bu, W., Ni, D., Zhang, S., Li, Q., Yao, Z., et al. (2016). Synthesis of iron nanometallic glasses and their application in cancer therapy by a localized fenton reaction. *Angew. Chem. Int. Ed.* 55, 2101–2106. doi:10.1002/anie.201510031

Zhang, F., Li, F., Lu, G.-H., Nie, W., Zhang, L., Lv, Y., et al. (2019). Engineering magnetosomes for ferroptosis/immunomodulation synergism in cancer. *ACS Nano* 13, 5662–5673. doi:10.1021/acsnano.9b00892

Zhang, P., Hou, Y., Zeng, J., Li, Y., Wang, Z., Zhu, R., et al. (2019a). Coordinatively unsaturated Fe 3+ based activatable probes for enhanced MRI and therapy of tumors. *Angew. Chem. Int. Ed.* 58, 11088–11096. doi:10.1002/anie.201904880

Zhang, P., Meng, J., Li, Y., Wang, Z., and Hou, Y. (2019b). pH-sensitive ratiometric fluorescent probe for evaluation of tumor treatments. *Materials* 12, 1632. doi:10.3390/ma12101632

Zhang, X., Chen, F., Turker, M. Z., Ma, K., Zanzonico, P., Gallazzi, F., et al. (2020). Targeted melanoma radiotherapy using ultrasmall 177Lu-labeled α-melanocyte stimulating hormone-functionalized core-shell silica nanoparticles. *Biomaterials* 241, 119858. doi:10.1016/j.biomaterials.2020.119858

Zhang, Y., Xiao, J., Sun, Y., Wang, L., Dong, X., Ren, J., et al. (2018). Flexible nanohybrid microelectrode based on carbon fiber wrapped by gold nanoparticles decorated nitrogen doped carbon nanotube arrays: in situ electrochemical detection in live cancer cells. *Biosens. Bioelectron.* 100, 453–461. doi:10.1016/j.bios.2017.09.038

Zhao, H., Xu, J., Li, Y., Guan, X., Han, X., Xu, Y., et al. (2019). Nanoscale coordination polymer based nanovaccine for tumor immunotherapy. *ACS Nano* 13, 13127–13135. doi:10.1021/acsnano.9b05974

Zhao, P., Tang, Z., Chen, X., He, Z., He, X., Zhang, M., et al. (2019). Ferrous-cysteine-phosphotungstate nanoagent with neutral pH fenton reaction activity for enhanced cancer chemodynamic therapy. *Mater. Horiz.* 6, 369–374. doi:10.1039/c8mh01176a

Zheng, D.-W., Lei, Q., Zhu, J.-Y., Fan, J.-X., Li, C.-X., Li, C., et al. (2017). Switching apoptosis to ferroptosis: metal-organic network for high-efficiency anticancer therapy. *Nano Lett.* 17, 284–291. doi:10.1021/acs.nanolett.6b04060

Zheng, L., Hu, X., Wu, H., Mo, L., Xie, S., Li, J., et al. (2020). *In vivo* monocyte/macrophage-hitchhiked intratumoral accumulation of nanomedicines for enhanced tumor therapy. *J. Am. Chem. Soc.* 142, 382–391. doi:10.1021/jacs.9b11046

Zhou, Z., Liu, X., Zhu, D., Wang, Y., Zhang, Z., Zhou, X., et al. (2017). Nonviral cancer gene therapy: delivery cascade and vector nanoproperty integration. *Adv. Drug Deliv. Rev.* 115, 115–154. doi:10.1016/j.addr.2017.07.021

Zhuo, H., Zheng, B., Liu, J., Huang, Y., Wang, H., Zheng, D., et al. (2018). Efficient targeted tumor imaging and secreted endostatin gene delivery by anti-CD105 immunoliposomes. *J. Exp. Clin. Cancer Res.* 37, 42. doi:10.1186/s13046-018-0712-8

Conflict of Interest: The authors declare that the research was conducted in the absence of any commercial or financial relationships that could be construed as a potential conflict of interest.

Advantages of publishing in Frontiers

OPEN ACCESS
Articles are free to read for greatest visibility and readership

FAST PUBLICATION
Around 90 days from submission to decision

HIGH QUALITY PEER-REVIEW
Rigorous, collaborative, and constructive peer-review

TRANSPARENT PEER-REVIEW
Editors and reviewers acknowledged by name on published articles

Frontiers
Avenue du Tribunal-Fédéral 34
1005 Lausanne | Switzerland

Visit us: www.frontiersin.org
Contact us: frontiersin.org/about/contact

REPRODUCIBILITY OF RESEARCH
Support open data and methods to enhance research reproducibility

DIGITAL PUBLISHING
Articles designed for optimal readership across devices

FOLLOW US
@frontiersin

IMPACT METRICS
Advanced article metrics track visibility across digital media

EXTENSIVE PROMOTION
Marketing and promotion of impactful research

LOOP RESEARCH NETWORK
Our network increases your article's readership